Universiteit
Leiden
The Netherlands

Dynamics of TNFalpha signaling and drug-related toxicity

Huppelschoten, S.

Citation

Huppelschoten, S. (2017, December 6). *Dynamics of TNFalpha signaling and drug-related toxicity*. Retrieved from https://hdl.handle.net/1887/59476

Version:	Not Applicable (or Unknown)
License:	Licence agreement concerning inclusion of doctoral thesis in the Institutional Repository of the University of Leiden
Downloaded from:	https://hdl.handle.net/1887/59476

Note: To cite this publication please use the final published version (if applicable).

Cover Page

Universiteit Leiden

The following handle holds various files of this Leiden University dissertation:
http://hdl.handle.net/1887/59476

Author: Huppelschoten, S.
Title: Dynamics of TNFalpha signaling and drug-related toxicity
Issue Date: 2017-12-06

Dynamics of TNFalpha signaling and drug-related liver toxicity

Suzanna Huppelschoten

Dynamics of TNFalpha signaling and drug-related liver toxicity

Suzanna Huppelschoten
December 2017

ISBN: 978-94-028-0823-0

Cover design: Hjalmar Haagsman, *www.dachtikhetniet.nl*

Printing: Ipskamp Printing, Amsterdam

© 2017 Suzanna Huppelschoten
All rights reserved. No part of this thesis may be reproduced, stored in a retrieval system, translated, or transmitted in any form or by any means now or hereafter known, electronic or mechanical, without permission in writing from the author.

Dynamics of TNFalpha signaling and drug-related liver toxicity

Proefschrift

ter verkrijging van
de graad van Doctor aan de Universiteit Leiden
op gezag van de Rector Magnificus, prof. mr. C.J.J.M Stolker
volgens besluit van het College voor Promoties
te verdedigen op woensdag 6 december 2017 klokke 16:15

door

Suzanna Huppelschoten

geboren op 8 december 1987 te Zeist, Nederland

Promotor

Prof. dr. B. van de Water	Toxicology, LACDR, Universiteit Leiden

Promotion committee:

Prof. dr. H. Irth	Biomolecular Analysis, LACDR, Universiteit Leiden, *voorzitter*
Prof. dr. J.A. Bouwstra	Drug Delivery, LACDR, Universiteit Leiden, *secretaris*
Prof. dr. J. Kuiper	Therapeutic immunomodulation, LACDR, Universiteit Leiden
Prof. dr. C.E.P. Goldring	Molecular and Clinical Pharmacology, Institute of Translational Medicine, Universitiy of Liverpool
Prof. dr. P. Jennings	ADMET and Molecular Toxicology, Department of Chemistry and Pharmaceutical Science, Vrije Universiteit Amsterdam

This research was conducted at the Division of Toxicology of the Leiden Academic Centre for Drug Research, Leiden University, Leiden, The Netherlands

Table of contents

Chapter 1 **1**
Introduction, aim and scope of thesis
Chapter 2 **11**
TNFα signaling: From *in vivo* understanding to *in vitro* testing approaches
Chapter 3 **25**
Phenotypic screen of TNFα-mediated NF-κB nuclear translocation dynamics reveals CDK12 as suppressor of anti-apoptotic signaling and A20 expression
Chapter 4 **49**
Drugs with liver toxicity liability enhance both TNFα-induced and intrinsically drug-induced inflammatory target gene expression
Chapter 5 **77**
Identification of TNF receptor signaling pathway components that regulate hepatotoxic drug/TNFα-induced synergistic apoptosis
Chapter 6 **103**
High content live cell imaging of dynamics of multiple adaptive stress response pathways enables assessment of drug-induced liver injury liabilities
Chapter 7 **131**
Discussion and future perspective

Appendix

References 142

Abbreviations 153

Nederlandse samenvatting 155

List of publications 159

About the author 161

Chapter 1

Introduction, aim and scope of thesis

Highlights

- Idiosyncratic drug-induced liver injury remains a major problem in drug discovery, safety assesment and clinical practice
- Host factors, including immune system activation, play an increasingly recognized role in the etiology of idiosyncratic drug-induced liver injury
- In this thesis, we asses hepatocyte proinflammatory TNFα signaling mechanistically and in applied *in vitro* testing systems

Idiosyncratic drug-induced liver injury (DILI) remains one of the major challenges in drug development, safety assessment and clinical practice. Increased mechanistic understanding and improved toxicity testing strategies are essential to predict DILI hazard for specific compounds and patients. In this thesis, we studied possible mechanisms of drug-induced liver toxicity, with a focus on TNFα signaling in hepatocytes. Furthermore, we developed a model to monitor drug-induced cellular stress responses and predicted DILI hazard of a set of compounds. Here we will introduce the liver, liver specific immune regulation and the role of TNFα in DILI. Furthermore, we will discuss how immune signaling currently can be assessed with recent liver toxicity models.

The liver

The liver is an essential organ in maintaining both metabolic and immunological homeostasis in the human body. In agreement with this diverse function, the structure of the liver is very complex. The functional units of the liver are the hexagonal liver lobules (Fig. 1A). Oxygen-rich blood enters the liver via the hepatic artery. Nutrient-rich blood arrives via the portal vein, together with the bile duct situated in the portal triad. The portal vein collects blood from both spleen and intestines, making the blood rich in antigens from food, toxic substances and pathogens. Blood from the artery and vein mix inside the sinusoids, and is relatively long exposed to and detoxified by hepatocytes. Due to this process the amount of specific molecules, including metabolites, toxic substances and oxygen, differ over the length of the sinusoidal axis (Fig. 1C). Among other mechanisms, oxygen responsive transcription factors mediate the expression of specific metabolic enzymes, thereby regulating the metabolic zonation. Toxicity is most seen in the periportal region, warranting a different classification of liver regions in periportal, pericentral and midlobular zones (Fig. 1A)[1,2].

In general, fenestral liver sinusoidal cells (LSEC) surrounded by stellate cells line up between the sinusoid and the hepatocytes, forming the perisinusoidal space (Fig. 1B). The diffusion rate into the perisinusoidal space is regulated by the hepatic stellate cells, which also store the body's main stock of vitamin A[3]. To facilitate the clearance and efficient transport of specific molecules to the hepatocytes, LSECs are specialized in endocytosis and transcytosis[4]. The liver resident macrophages, Kupffer cells (KCs), travel through the liver sinusoids and eliminate large antigens. Together with a relatively large fraction of natural killer cells they form the resident liver immune cell population. When activated, the Kupffer cells can differentiate into the proinflammatory M1 phenotype or in the alternative M2 phenotype. In contrast to the M2 phenotype, M1 macrophages express high proinflammatory cytokines, including TNFα, and low IL10 levels. This differentiation process depends on the activation signal, the environmental context and the genetic background of the individual[5]. However, not only the immune cells affect inflammation. Also the stellate and LSEC have recognized immunomodulatory functions, which have recently been reviewed[3,6]. Hepatocytes are the most abundant cell type in the liver, responsible for most metabolic and homeostatic functions. These parenchymal cells produce bile to aid in the digestion, which is transported via the bile canaliculi and collected in bile ducts, lined by

cholangiocytes. Logically, liver failure is in the end always a result of malfunctioning hepatocytes. However, the interplay between hepatocytes and non-parenchymal cell populations plays a very important and increasingly recognized role on the path to hepatotoxicity.

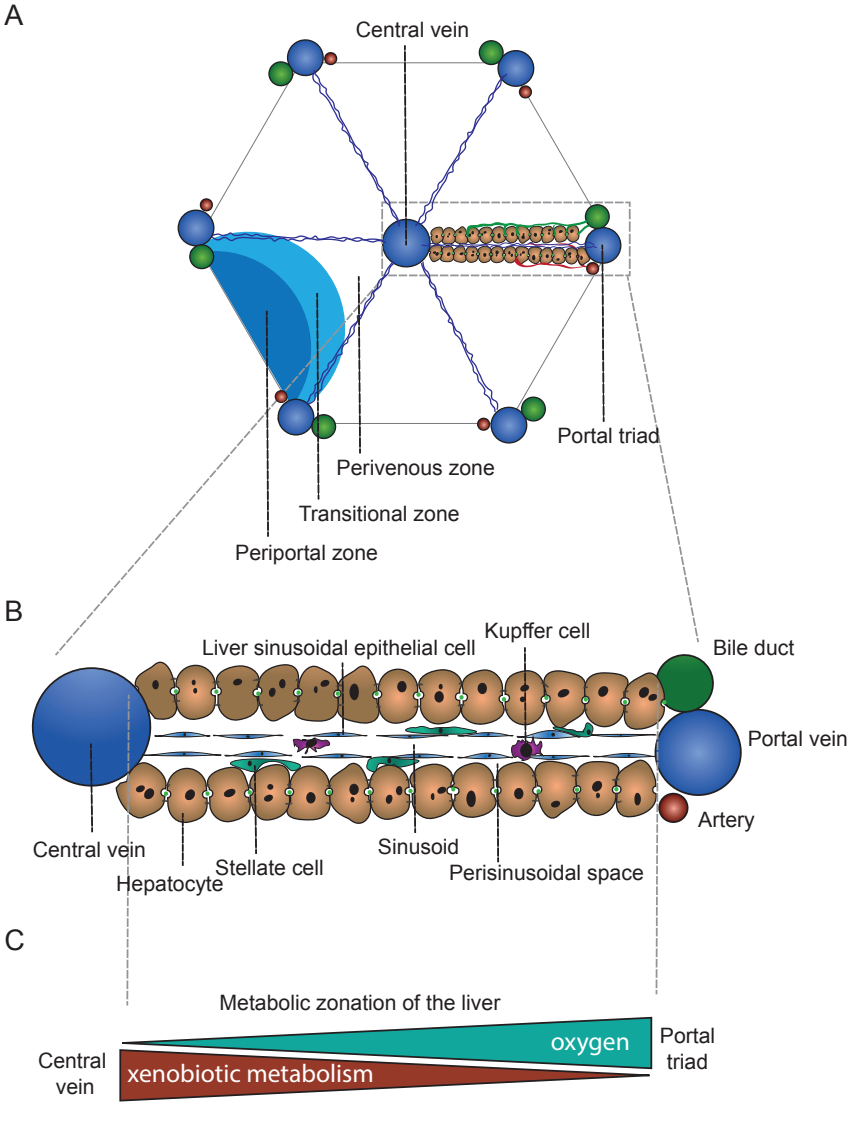

Fig 1. **Structure of the liver** A) The liver lobule is schematically represented. The different zones are indicated. The portal triad consists of a bile duct, hepatic vein and a hepatic artery. The bile duct and bile canaliculi are indicated in green, the arterial blood flow is indicated in red and the venal blood flow in blue. B) An enlargement of A, the sinusoid lined with hepatocytes. The different cell types are indicated and the bile canaliculi are visualized in green. C) Part of B, the metabolic zonation. Oxygen and xenobiotic levels are indicated by the relative height of the triangles.

Drug-induced liver injury and inflammatory stress

Drug-induced hepatotoxicity is a common adverse drug reaction, raising problems in drug development and clinical practice. The unpredictability and low incidence of idiosyncratic DILI (iDILI) makes it difficult to detect in expensive clinical trials. Furthermore, the risk on iDILI for few patients leads to black box warnings and inhibits prescription of an, for most patients, effective drug therapy.

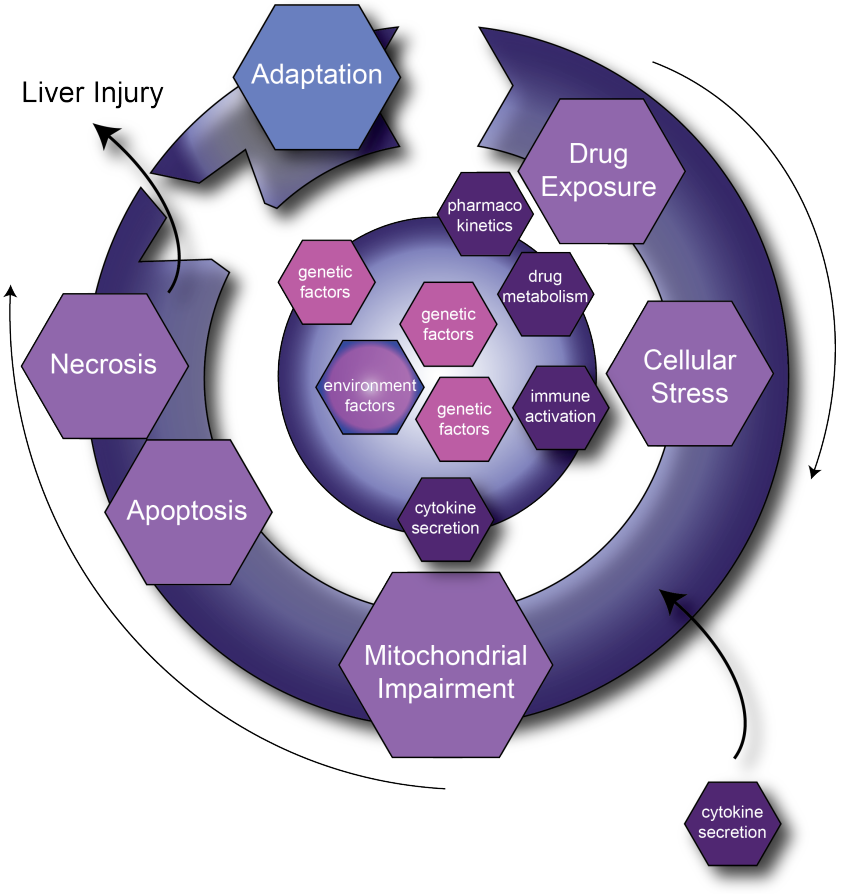

Fig 2. **Etiology of idiosyncratic drug-induced liver injury in hepatocytes** Different processes and factors are represented in this overview of risk factors for idiosyncratic drug-induced liver injury. Host factors are visualized in the inner circle and cellular processes in hepatocytes in the outer circle. Going clockwise, drug exposure will lead to cellular stress. Host factors as pharmacokinetics and drug metabolisms can diverge between individuals due to genetic variability, and thereby modulate DILI liability in a specific individual. Upon cellular stress, immune activation and mitochondrial impairment can be regulated by genetic and environmental factors (including concurrent therapies and diseases). Combined, these processes can lead to apoptosis or necrosis of the hepatocyte. The liver can restore after some injury, called clinical adaptation. However, in some cases hepatotoxicity levels will increase and lead to liver failure. In this thesis, cytokine secretion is mimicked by manual addition of proinflammatory cytokines.

To predict which drugs are going to induce iDILI in specific people from *in vitro* and *in vivo* studies, we have to understand the interaction of drug properties with both general and drug-induced cellular signaling. One reoccurring host factor involved in DILI is activation of the innate immune system (Fig. 2).

In vivo, mimicking viral or bacterial infection, for example by poly I:C or LPS exposure, concurrent to exposure of a non-toxic dose of certain drugs lead to synergistically increased hepatotoxicity[7–10]. For trovafloxacin toxicity upon LPS exposure, this synergism has been proven to be dependent on TNF receptor and TNFα expression[11]. TNFα is a proinflammatory cytokine, in the liver mainly produced by KCs or invading immune cells upon damage or inflammation-induced chemotaxis. Drug-induced signaling in the KC itself can lead to proinflammatory cytokine production, including TNFα production[12]. However, recognition of pathogen-associated molecular patterns or damage-associated molecular patterns secreted by drug-treated liver cells can evoke KC activation and cytokine production as well. TNFα produced by KCs can signal to hepatocytes via the TNF receptor (TNFR). Healthy hepatocytes are not sensitive for TNFα-induced cell death. However, excessive and long-term hepatic inflammation characterized by chronic high levels of TNFα, can lead to massive hepatotoxicity and is associated with several hepatic diseases[13]. Currently, it is unknown how TNFα stimulation together with drug exposure can induce synergistic cell death in hepatocytes in only few individuals. The role of MAP kinases and cellular stress response pathways have been studied before[14–16]. In **chapter 5** we detect several known regulators of the TNF receptor signaling pathway that play important roles in drug/TNFα synergistic apoptosis.

TNFα signaling pathway

Upon binding of TNFα, trimerization of the TNFR leads to recruitment of the TNFR signaling complex. The TNFR signaling complex activates the IKK kinase complex and subsequently induces NF-κB transcriptional activity. NF-κB activation protects hepatocytes from TNFα-induced cytotoxicity[17]. Besides NF-κB activation, also MAPK pathways JNK and p38 are activated via the TNFR signaling complex. The induction of antioxidant proteins via NF-κB transcriptional activity prevents prolonged JNK activation and cell death[18,19]. Furthermore, NF-κB induces general anti-apoptotic protein expression and these dissociate the TNFR signaling complex. Without NF-κB activity induced anti-apoptotic protein expression, the TNFR signaling complex progresses into complex II, inducing cytotoxicity[17]. TNFα-induced apoptosis is characterized by caspase 8 activation and necroptosis by RIPK3 activation. The exact TNFα-induced cell death mechanisms have recently been reviewed by Brenner *et al.*[20].

The NF-κB transcription factor family consists of 5 proteins: RelA (p65), RelB, cREL, p50/p105 and p52/p100. All proteins share a Rel homology domain for dimerization and DNA binding, but only RelA, RelB and cREL have a c-terminal transactivation domain. RelB forms the core of the non-canonical NF-κB pathway. This pathway is activated by cytokines including CD40 and lymphotoxin beta, and characterized by stabilization of NIK (MAP3K14) and IKKα activity[21]. Precursors p105 and p100 need processing, before taking

their active DNA binding form. For p100, this process is regulated by phosphorylation by active IKKα, while p105 is constantly processed. Several different homo- and hetero-dimers can be formed. Homodimers from p50 and p52 are thought to be transcriptionally inactive and inhibit active NF-κB dimer DNA binding by competitive binding[22]. The best-characterized NF-κB signaling heterodimer is RelA-p50, which becomes transcriptionally active upon TNFα signaling.

Upon TNFα stimulation, NF-κB translocates into the nucleus and transcribes its own inhibitors IκBα and A20 (TNFAIP3). By this negative feedback loop NF-κB itself regulates its oscillatory nuclear phenotype upon stimulation[23,24]. The reason behind and physiological result of this oscillatory phenotype is largely unknown. Currently, the major belief is that this oscillatory phenotype translates into differentially regulated functional gene transcription patterns[25–27]. However, the function of this relation between transcription factor oscillations and subsequent transcription profiles is not well understood. NF-κB regulates the transcription of around 600 target genes. These genes are expressed in many functional and three temporally differentiated groups; early, middle and late[28]. NF-κB target genes function in many cellular processes, including inflammation, cell growth, cell cycle and cell survival[29]. In **chapter 3** and **chapter 4**, we studied the regulation of TNFα-induced NF-κB nuclear oscillation and the effect of drug exposure on its target gene induction, respectively.

Drug toxicity hepatocyte models

Cell death of hepatocytes is the hallmark feature of hepatotoxicity. Therefore, most hepatic drug safety testing systems include hepatocytes at the core of their model. However, as all models do, they limit the complexity of the human liver. For example, metabolic zonation of the liver forms a factor not often reflected. Interactions between hepatocytes themselves, the different cell types and the extracellular matrix and blood stream is another feature that is difficult to capture in *in vitro* models. The attempts to reflect all these layers of complexity in 3D models and artificial liver 'on a chip' approaches have been extensively reviewed elsewhere[2,30].

Reliable co-culture, or co-exposure methods of hepatocytes and KCs have recently been developed and increase the predictive power for specific immune related toxicants[12,31,32]. However, the need for glucocorticoids to stabilize CYP expression in the hepatocytes has a clear anti-inflammatory effect on the Kuppfer cell[31]. Besides some of these technical drawbacks, co-culture models using donor-specific Kupffer cells and hepatocytes can add major mechanistic insight into the role of the innate immune system and the individual susceptibility of certain patients herein. Furthermore, once optimized and validated, they can form a testing platform for early detection of possible immune-related DILI. Trovafloxacin-mediated toxicity can be detected in Kupffer cell and hepatocyte co-culture[31]. Interestingly, this increased hepatocyte toxicity can also be detected in a hepatocyte only model with the manual addition of TNFα[33].

Separate hepatocyte and immune cell culture methods can provide mechanistic understanding, distinguishing between hepatocyte and Kupffer cell signaling in the process

of developing DILI. For example, IκBα phosphorylation in 7 day old mice is regulated by TRAF2 expression in liver and spleen, but not in lung and muscle[34]. Also, ketoconazole treatment did lead to NF-κB pathway activation in HepG2 cells, but not in the macrophage cell line THP-1[35]. These studies underline that the specific cellular background is of major importance for mechanistic research and the design of fit-for-purpose studies, especially concerning immune signaling.

The golden standard in hepatocyte toxicity screening are currently freshly isolated primary human hepatocytes (PHH). The variety of PHH models, including 3D culture, co-culture and precision-cut liver slices have been reviewed extensively by Godoy *et al.*[1]. As fresh hepatocytes are difficult to use due to their unpredictable availability, cryopreservation is a good alternative. None of the hepatocyte cell lines HepG2, Upcyte or HepaRG, are currently able to mimic PHHs in metabolic enzyme expression and activity[36]. However, also PHHs quickly lose their metabolic capacity upon isolation and culturing[37]. Adjusting the culture methods to low glucose medium, 3D cultures or co-culture systems can improve hepatic function[1].

One of the difficulties in using PHHs for hepatocyte inflammatory signaling research is the possible contamination with a minority of immune cells during the isolation procedure. These few immune cells can excrete massive amounts of signaling mediators when activated, shifting the homeostasis within a “hepatocyte only” culture massively. However, even pure hepatocyte cultures seem to activate an inflammatory disease phenotype[37]. In addition, the preferred PHH culture medium includes a glucocorticoid, both inducer of CYP enzyme expression and NF-κB inhibitor. This could inhibit the inflammatory response in primary hepatocyte cultures. However, as hormones as hydrocortisone are also present in the human body, it is unknown if these additives result in non-physiological behavior of hepatocytes. A final consideration on the use of PHH cultures is that donor differences can be major. As some donors are not plateable, we probably underestimate the donor variability based upon available data[1,38].

For early toxicity screening in the pharmaceutical industry, the HepG2 cell line is still routinely used. HepG2 cells have retained many hepatocyte specific functions, but have in general very low expression of drug and bile transporter proteins and phase I metabolic enzymes. These levels can differ between separate batches[39]. Simple endpoint studies performed with the same clone at different companies showed stark differences in outcome, although HepG2 cells are generally viewed as a very stable cell line[40]. Both in PHHs and HepG2 cells co-exposure of drug and cytokines, including TNFα, can lead to synergistic apoptosis[33,41]. To increase the fit-for-purpose applicability of the easy-to-handle HepG2 cell in toxicity screening, their relation to primary human hepatocytes should be more precisely determined. Including cytokines as co-stimulation would also increase usability. In **chapter 6**, we predicted DILI liabilities of marketed compounds using a HepG2 stress response reporter platform, including TNFα-induced NF-κB target gene ICAM1.

Aim and scope of this thesis

In previous studies at our laboratory it was demonstrated that drug exposure of HepG2 cells can lead to an altered TNFα-induced NF-κB oscillatory phenotype, concurrent with a synergistically increased sensitivity for TNFα-induced apoptosis[42]. We have also shown that synergistic drug/ TNFα-induced cell death is dependent on concurrent cellular stress responses[16,43]. To monitor these stress responses, we have developed a fluorescent protein stress response reporter platform, feasible for high throughput approaches[44]. In this thesis, we focus on an *in vitro* HepG2 cell model, in which the addition of TNFα reflects inflammatory stress (Fig.2). We studied inflammatory signaling, both for use in improved *in vitro* testing approaches and to gain mechanistic understanding of TNFα-induced signaling in hepatocytes. In **Chapter 2**, the current knowledge on the role of TNFα signaling during iDILI and several models in which TNFα signaling could be reflected *in vitro* have been summarized. In **Chapter 3**, we used a siRNA-mediated screen approach, detecting regulators of the TNFα-induced RelA oscillatory phenotype. We studied their regulation of A20 expression and synergistic drug/TNFα cytotoxicity. We revealed CDK12 (CRK7) as a novel regulator of TNFα-induced RelA oscillation, A20 expression and synergism. In **Chapter 4,** we systematically evaluated drug effects on TNFα-induced NF-κB nuclear translocation and target gene induction. Interestingly, drug exposure by itself induced TNFα target gene induction, including RelB, CCL5 and IL8. RelB expression showed strong correlation with oxidative stress response induction and was independent of RelA transcriptional activity. The drug-induced expression of chemokines CCL5 and IL8 was RelA-dependent, but also negatively regulated by NF-κB family members RelB and cRel. In **Chapter 5**, we studied known TNF receptor pathway components and their role in carbamazepine/TNFα synergism towards apoptosis by a siRNA-mediated approach, revealing 24 candidate genes. We determined 3 out of 124 drugs that acted synergistically towards apoptosis with TNFα (colchicine, griseofulvin and valproic acid). The candidate genes consisted of both specific and generic drug/TNFα synergism regulators (e.g. A20, PHF5A) The effect of candidate gene knockdowns on drug/TNFα synergism were correlated with drug-induced cellular stress responses. We detected two separate branches of the oxidative stress and DNA damage response pathways that were strongly correlated with certain candidate gene effects. For **Chapter 6**, a HepG2 cell line harboring a fluorescent TNFα responsive ICAM1 gene has been generated and used as part of the stress response fluorescent reporter platform to predict DILI potential in humans. We predicted DILI hazard with a sensitivity of 60% and a specificity of 75%. Finally, in **Chapter 7** I summarize all findings in this thesis and provide an overview and future perspective on the implications of these studies.

Chapter 2

Drug-induced liver injury and TNFα signaling: from *in vivo* understanding to *in vitro* testing approaches

---

Highlights

- Idiosyncratic drug-induced liver injury, including diclofenac-induced liver injury, is associated with derailed proinflamamtory (TNFα) signaling
- *In vitro* testing methods for liver toxicity liability do not often include immune-related tests
- Fit-for-purpose approaches could include a range of *in vitro* models to better predict DILI liability

This chapter has been published as:

Huppelschoten, S[1]. & van de Water, B[1].

Drug-Induced Liver Injury and TNFα Signaling:
From In Vivo Understanding to In Vitro Testing Approaches

Appl. Vitr. Toxicol. 2;4 1–10 (2016).
[1]*Division of Toxicology, Leiden Academic Centre for Drug Research, Leiden University, Leiden, The Netherlands*

For new candidate drugs the liability towards idiosyncratic drug-induced liver injury (DILI) remains difficult to predict from preclinical *in vitro* and *in vivo* studies. The DILI-inducing potential of a drug is generally only detected in the clinical testing phase or once on the market. In the last decades, research on the interaction of host factors and drug-dependent processes has produced valuable insights into the mechanisms of idiosyncratic DILI. Continued development of screening methods and prediction models has led to improved prediction of DILI. However, the immune component involved in many drug-induced toxicities is notoriously difficult to characterize. In this review, we will discuss the interaction of innate inflammatory signaling, thereby focusing on TNFα-signaling, and drug-induced processes leading to hepatotoxicity. In general, there is a clear interaction between liver-resident innate immune cells and hepatocytes during the onset of DILI. At a mechanistic, intracellular level this involves interaction of drug-induced general adaptive stress response activation and cytokine-mediated signaling, and this interaction provides a basis for hepatocyte cytotoxicity. Understanding of these complex mechanistic interactions in human idiosyncratic DILI will allow development of tailored *in vitro* screening approaches.

Keywords: diclofenac, drug-induced liver injury, hepatotoxicity, in vitro models, LPS, stress response, TNFα

Introduction to drug-induced liver injury

Drug-induced Liver Injury (DILI) is a complex condition with difficult diagnosis and prediction, since it displays a broad array of symptoms that resemble other chronic or acute liver conditions. In the most recent prospective studies in the US and Iceland, it was found that around 11 % of all idiosyncratic acute liver failure cases were caused by drugs[45] and that the incidence rate of DILI in the general population was 19.1 cases per 100.000 inhabitants per year[46]. Currently, DILI remains one of the major concerns in both clinical and drug developmental practices. Since 1997, no drugs were approved by the Food and Drug Administration that had to be withdrawn later due to DILI, indicating raised awareness and improved detection of DILI in clinical trials[47]. However, to prevent the enormous costs that accompany clinical studies for a drug with DILI-potential, the emphasis of current research lies with better prediction of DILI from animal and *in vitro* approaches.

Over the last decade, the over-simplified classification of DILI in intrinsic and idiosyncratic has developed in a less distinctive mapping. Acetaminophen, the classical example of intrinsic DILI, causes most acute liver failure cases in the U.S. in a predominantly dose-dependent fashion. However, the prognosis for acetaminophen-toxicity outcome seems to be dose-independent, pointing to general mechanisms starting to act the moment the threshold for toxicity is reached[48]. Furthermore, a study in the U.S. published in 2005 found around 8% of the cases developed by therapeutic dosing, suggesting mechanistic explanations that are rather associated with idiosyncratic DILI[49]. In this review,

idiosyncratic mechanisms of toxicity are defined as involvement of specific host factors interacting with the drug, its metabolites or responses induced by either, inducing hepatotoxicity in a few individuals.

Even when excluding acetaminophen hospitalization, drug treatment remains the major cause for acute liver failure in the U.S. Of these drug-induced cases of hepatotoxicity, most are considered idiosyncratic being relatively dose-independent and occurring in a yet unpredictable minority of people treated with the culprit drugs[50]. Risk factors include a high daily dose and drug-characteristics, including lipophilicity and metabolism, but more importantly the personal environmental factors like age, pre-existing liver disease, obesity and ethnicity, all of which has been summarized in a recent review[51]. One reoccurring and very interesting risk factor is gender. Although on first glance the ratio of DILI incidence might seem similar for females and males, the percentage of patients that develops severe acute liver failure is significantly higher for women[45,51]. Furthermore, genetic association studies have identified various defined HLA allele variants that are associated with idiosyncratic DILI[52,53]. The fact that gender background and in particular the HLA genotype are regarded as risk factors for DILI might point towards the immune system as one of the causal factors of DILI, since there are differences in immune reactions between males and females in various fields, as described in this review[54]. Observations that strengthen this hypothesis are that autoimmune hepatitis upon drug exposure is rarely seen in males and that the injury pattern of DILI seems to change in females above 60 compared to younger women. However, gender has not been detected as a risk factor for DILI in all studies and has been suggested to be drug-specific[51]. In mice, both halothane-induced injury and Con A-induced liver injury were more severe in females. This was regulated by sex hormones inducing an altered cytokine response and thereby modulating the subsequent adaptive immune response[55,56]. Taken all together, these data suggest that the modulation of the immune system is a critical factor in developing DILI and progression to severe hepatotoxicity.

This review will discuss the role of the innate immune system in the onset and progress of idiosyncratic DILI. The central part of this review will discuss the archetypical idiosyncratic drug diclofenac and the involvement of lipopolysaccharide (LPS) and tumor necrosis factor alpha (TNFα) signaling in DILI. This will be followed by an overview of the progress in the application of *in vitro* cell systems for the mechanistic understanding and prediction of DILI that involve innate immune signaling.

Liver immunology and drug-induced inflammatory response

Immune system in the liver

The liver has a unique immunological build-up; this is essential since it is situated at the portal vein with continuous exposure to gut-derived antigens and cellular debris from the blood stream. As peripheral immunotolerant organ, it contains a population of liver resident immune cells as Kupffer cells (KC), natural killer cells (NK) and dendritic cells (DC) that are skewed to inducing tolerance, therefore called tolerogenic[6,57]. Together with hepatocytes, liver sinusoidal endothelial cells (LSEC) and stellate cells, they form an environment in

which it is difficult to invoke a tissue-damaging pro-inflammatory response (see for details[3,4,58]). To sustain this tolerogenic environment, antigen presentation, clonal deletion of antigen-specific T cells and the shift from a Th2 favored response to a Th1 response must be strictly controlled by direct and paracrine signaling (reviewed by[59,60]). Many of the signaling pathways in the liver that lead to tolerance mechanisms are altered and skewed towards inflammation by exposure to DILI drugs. One of the main pathways leading to activation of the innate immune system is the Toll-like receptor 4 (TLR4) signaling pathway, driven by LPS, an endotoxin from the outer membrane of Gram-negative bacteria.

Toll-like receptor signaling in drug-induced liver injury

In the liver, TLR4 is expressed on KCs, hepatic DCs, NK cells, LSECs, stellate cells and hepatocytes[61,62]. Signaling by TLR4 is remarkably inhibited in a healthy liver, sustaining the tolerogenic environment. The continuous low exposure to LPS is essential for maintaining tolerance by affecting KCs and LSECs in a negative feedback-loop regulating expression of several proteins, miRNAs and IL10 signaling[61,63–65]. Indeed, administering low doses of LPS protects against D-galactosamine/LPS and ischemia-reperfusion liver injury by downregulation of TLR4-mediated signaling[66,67]. Interestingly, in many chronic liver diseases and obesity, often named risk factors for DILI, TLR4 signaling is upregulated[61,68]. Furthermore, it is generally accepted that antimicrobials are amongst the drugs that most frequently and severely induce DILI[69]. Altered TLR signaling might explain this DILI inducing potential. Antimicrobials change the gut microbiome, thereby increasing the transfer of commensal bacteria across the gut epithelium. Translocated bacteria can induce inflammatory responses via TLR signaling[70]. Increased LPS translocation together with inflammatory signaling from the gut environment could lead to increased pro-inflammatory signaling in the liver. Combined, these data suggest a role of the gut environment and altered LPS leakage to the liver as an possible mechanism in the development of antimicrobial-induced hepatotoxicity. Finally, TLR4 signaling is involved in the several rodent models that show a synergistic increase in hepatotoxicity with co-exposure of LPS with well-known DILI drugs including diclofenac, trovafloxacin, sulindac, and chlorpromazine. In these studies, LPS was administered at different time points ranging from 2 hours pre-treatment to 16 hours post-treatment[8,9,71–73]. It would be relevant to determine whether repeated low-dose LPS exposure would be able to prevent hepatotoxicity of the combined LPS/drug exposures in these animal models, as it would confirm the importance of inhibition of TLR4 signaling in the protection against aberrant inflammation during drug exposure.

The function and signaling cascades induced by TLR4 activation in the different cell types in the liver are much debated. Here, we will discuss the effects of LPS on KCs and hepatocytes. TLR4 signaling in other liver cell types is reviewed in these publications[62,65]. Via the portal vein the blood enters the liver, rich in nutrients, metabolites and potentially toxic compounds. From the hepatic artery, oxygen rich blood joins this mixture. This blood mixture contains many antigens that have to be cleared from the blood before it enters the systemic circulation. The clearance of gut-derived LPS from the blood

stream in non-inflammatory conditions depends on both hepatocytes and KCs[74,75] and is based on receptor-dependent endocytosis and phagocytosis, respectively[76]. In hepatocytes, binding of LPS and subsequent clearance seems to induce TLR4-induced signaling, although not via the classical MyD88 pathway but via p38/MAPK signaling[77]. Furthermore, TLR4-mediated LPS clearance activates adaptive stress response pathways, like p62-regulated autophagy and the Nrf2-mediated oxidative stress response[78]. Non-endocytosed LPS on the other hand, signals via the classical TLR signaling pathway, inducing NF-κB and MAPK signaling. This leads to low levels of pro-inflammatory cytokine production and induction of metabolic activity by regulation of CYP enzyme expression in hepatocytes[79,80]. The induction of CYP enzyme expression upon TLR4 stimulation contradicts many studies that show an LPS-induced decrease of CYP enzyme expression and metabolic activity, both *in vivo* and *in vitro*[81,82]. This downregulation of CYP enzymes seems to be dependent on LPS-induced cytokine production, amongst which are IL6 and TNFα. The function of down-regulated CYP enzyme expression during inflammation is currently much debated, as is discussed in this review[83].

In a recent elegant mouse study, cell-type specific TLR4 knockouts were used in a model for sepsis. TLR4 expression in the myeloid cell population (KCs and neutrophils) is essential for efficient bacterial clearance and determines the level of inflammation and liver injury in a high bacterial load model. However, in a low bacterial load model, TLR4 expression on the hepatocytes was essential to prevent LPS-induced pro-inflammatory cytokine production by KCs and hepatotoxicity, measured by increased plasma ALT levels[84]. This data shows that both hepatocyte and KC TLR4 signaling is essential in clearance of LPS during sepsis. This might suggest a role for hepatocytes in LPS clearance in healthy, steady state liver as well.

LPS is not the only TLR4 ligand present upon hepatocyte dysfunction. High mobility group box-1 (HMBG1), a nuclear factor that is released from sites of hepatocellular stress, activates TLR4 signaling in the liver[85]. HMBG1 resembles LPS in that pre-conditioning with repeated low levels of HMBG1 can protect against ischemia/reperfusion (I/R)-induced liver injury[86]. TLR4-dependency of different cell type specific knockouts in mice was studied in a model of sterile inflammation caused by I/R as well. In this model, no LPS was present to stimulate TLR4 signaling.. However, liver injury was dependent on effective TLR4 signaling in both KC and hepatocyte population, while the TLR4 signaling in the DC population was protective based on IL10 secretion. Furthermore, TLR4 signaling in hepatocytes was necessary for neutrophil recruitment, and via c-Jun N-terminal kinase (JNK) activation also for the excretion of HMBG1[87]. Altogether these studies point to a cooperative mechanism of activated KCs and hepatocytes in the induction of both endotoxin-mediated and sterile inflammation, which could lead to liver injury.

Activated KCs upregulate the secretion of pro-inflammatory cytokines (TNFα, IL1), eicosanoids, and chemokines (e.g. CCL3, CCL4, CCL5, and CCL12)[88–90]. While the exact effect of individually upregulated cytokines and chemokines on different liver cell types and hepatotoxicity is unclear, they are involved in pro-inflammatory processes as for example recruitment of immune cells, the acute phase response and increased cell death, as well as

in repair processes[91]. For instance TNFα, as is described below, induces hepatocyte apoptosis when drugs interfere with TNFα-induced cytoprotective signaling. In contrast, the expression of the TNFα receptor and in some cases TNFα itself, are required for liver regeneration[92].

Drug-induced idiosyncratic liver injury

Diclofenac-induced idiosyncratic liver injury

An archetypical drug that can induce idiosyncratic DILI is the common anti-inflammatory painkiller diclofenac. Currently, diclofenac is still prescribed and even sold without prescription in the UK and Europe as nonsteroidal anti-inflammatory drug (NSAID). Among the class of NSAIDs, diclofenac is one of the drugs with the highest risk on DILI[93]. In the most recent study on NSAID-induced liver injury with data from the Drug-Induced Liver Injury Network in the U.S., diclofenac-induced liver injury was most frequent and most severe[94]. Diclofenac-induced liver injury is in most cases hepatocellular, and in a minority of the cases cholestatic[95]. This correlates with the genetic variants found in drug excretion proteins, for example in MRP2 (ABCC2), that were associated with diclofenac-induced liver injury[96]. Latency times range from 6 days to a year, and the disease can present itself in some cases with an immunoallergic phenotype with symptoms like fever and rash or with the production of autoimmune antibodies[94,95].

Diclofenac metabolism

Diclofenac-induced liver injury is slightly dose dependent, the risk increasing by daily doses higher than 150 mg[97]. The major diclofenac metabolites are 4′-OH diclofenac mainly formed by CYP2C9, 5-OH diclofenac by CYP3A4, CYP2C8 and CYP2C19 and diclofenac acyl-glucuronide mainly by UGT2B7[93]. Of these, especially the reactive 5-OH diclofenac-derived quinone imines and acyl-glucuronides are implicated in diclofenac-induced toxicity. Genetic variants of UGT2B7 and CYP2C8 have been correlated to diclofenac-induced hepatotoxicity[96]. Furthermore, comparison between metabolically active HepaRG cells and metabolically less active HepG2 cells showed less toxicity in the HepaRG cells, pointing towards protection by increased detoxifying processes in HepaRG cells. In both cell types, TNFα stimulation was able to increase cytotoxicity[98]. Interestingly, the exposure of HepG2 cells to 4′-OH diclofenac in combination with TNFα showed increased cytotoxicity, in contrast to the 5-OH diclofenac and diclofenac acyl-glucuronide[99]. In conclusion, it is still unclear if drug metabolism actually protects against synergistic induction of cell death or plays a role in the induction of TNFα-induced cytotoxicity.

Diclofenac-induced immune activation

Autoimmune and immunoallergic presentation of diclofenac-induced liver injury as stated earlier, points to the activation of the adaptive immune system. The question how drug-induced activation of the immune response can occur has inspired many theories, including the hapten hypothesis, the p-i concept, and the danger hypothesis. The hapten hypothesis states that a drug on itself cannot induce an adaptive immune response unless covalently

bound to proteins in plasma or liver. Diclofenac-derived acyl-glucuronides can form metabolite adducts by binding to target proteins. These adducts can act as haptens and are mainly found in liver zone 3.In diclofenac-induced liver injury, zone 3 necrosis is a common finding[94], although the relation between these two observation is unclear. Indeed, acyl-glucuronide and acyl-glucuronide-induced adduct formation are found in human plasma in diclofenac users[100,101]. However, antibodies recognizing diclofenac-induced protein adducts were detected in the majority of the diclofenac users that did not demonstrate DILI[102]. This finding implicates adaptive immune responses towards acyl-glucuronide-induced protein adducts are not the single causative reason for idiosyncratic diclofenac-induced liver injury. The p-i concept states that drugs by itself can be recognized as antigens by specific T cell clones. Although shown for several drugs including carbamazepine[103], this seems not to be the case for diclofenac[104]. The danger hypothesis claims that absence of danger-related signals will lead to tolerance by hapten-presentation. The danger signals necessary to mount a full immune response are the interaction of the processed hapten with the T-cell receptor, an independent interaction of co-receptor with a stimulatory molecule and polarizing cytokine signaling[105]. The timing and ratio of danger signals likely determines the activation profile of cytotoxic T cells[106]. Since polymorphisms in the tolerance-inducing cytokines IL10 and IL4 were associated with diclofenac hepatotoxicity [102] and activated cytotoxic CD8+ T cells seems to be mainly involved in DILI[107], it is likely this theory is at least partially applicable on diclofenac-induced liver injury.

Animal models of inflammation in drug-induced liver injury

Immune-dependent latency in a mice model

An interesting observation in clinical studies is the apparent clinical adaptation of patients with mild DILI under continuation of the drug. In these cases, patients that take the drug develop mildy abnormal liver function values. However, these abnormalities disappear while the patients continue taking the culprit drug. Very few of these patients progress towards severe DILI. This suggests that the cases of severe DILI have disturbed clinical adaptation processes, leading to severe hepatotoxicity[59]. A mouse model in which this adaptation process is reflected has been generated by Methusi et al., in which amodiaquine treatment in PD1-/- mice induced mild liver injury, resolving despite continuous treatment. However, co-treatment with CTLA4 antibody, blocking the tolerogenic signaling induced by CTLA4, induced severe liver injury[108]. Although CD8+ T cells were the most abundant in this model of severe injury, NK cells seem to play a more important role in the development of the mild injury upon treatment in PD1 knockout mice[109]. This points to a role for the innate immune system in the early processes in drug-induced liver injury. It would be interesting to see the effect of treatment with diclofenac or other idiosyncratic DILI drugs in this model. This mice model nicely shows the cumulative effect of several signaling cascades that is necessary to break the tolerance and develop severe liver injury instead of adaptation. However, how these mechanisms relate to human idiosyncratic DILI remains unclear.

Animal models on the inflammatory response in diclofenac-induced liver injury

The application of rodents to understand the mechanisms of immune-related mechanisms of diclofenac toxicity shows that small non-toxic doses of LPS can greatly enhance diclofenac-induced hepatotoxicity[8,99]. Although neutrophils are recruited and correlated to injury, they seem to play a minor causative role in the hepatotoxicity in LPS/diclofenac-induced injury[110]. To mimic human treatment, Ramm et al. treated rats with very low doses of diclofenac for seven days. On the seventh day, a small non-toxic dose of LPS was administered. Significant toxicity of combined LPS/diclofenac treatment was seen compared to diclofenac or LPS treated rats. Glutathione depletion and drug metabolism were not enhance by LPS/diclofenac treatment compared to diclofenac treatment.However, combined diclofenac/LPS treatment induced upregulation of cellular stress responses, including the oxidative stress response, the NF-κB response and hypoxic stress response. Taken together with an upregulation of pro-inflammatory cytokines and danger-associated molecules, this could lead to the hepatotoxicity seen in diclofenac-induced liver injury[99,111]. Interestingly, the highest upregulation of stress responses and protein production of TNFα and HMGB1 was detected in the only two animals that died from co-treatment of LPS and diclofenac[99].

In vivo studies into other DILI-inducing drugs, trovafloxacin and sulindac, have showed the importance of TNFα-signaling in LPS/drug-induced liver injury. The replacement of LPS with TNFα showed a similar pattern of hepatic injury. In both cases, the increased hepatotoxicity was dependent on prolonged elevated plasma TNFα levels and altered TNFα-receptor (TNFR) signaling[10,11]. Moreover, the neutralizing TNFα antibody Etanercept clearly diminished LPS-induced trovafloxin- or sulindac-mediated liver injury in rodents[9,72]. However, in both human and mouse precision-cut liver slices, diclofenac downregulated LPS-induced TNFα production upon co-exposure[112,113], contradicting the trovafloxin/sulindac research. What this downregulation of LPS-induced TNFα exactly means in the context of diclofenac-induced toxicity is not clear.

Role of TNFα signaling in diclofenac-induced liver injury

Upon LPS stimulation in the liver, TNFα is mainly produced by KCs and less by other liver resident cells[114]. In acetaminophen-induced liver injury in mice, the removal of KCs abolished the TLR4-dependent upregulation of TNFα, and led to significantly less liver injury[115].However, it should be noticed that the removal of KCs and their role in acetaminophen-induced liver injury has revealed contradictory results, as described in this review[116]. Signaling by the pleiotropic cytokine TNFα regulates many processes in target cells, including proliferation, production of pro-inflammatory cytokines, cell death and cell survival. These contradictory processes are regulated by an intricate web of signaling proteins and post-translational modifications, leading to well-known key players as the transcription factors NF-κB, c-Jun, AP-1 and cell death modulators like RIP1, RIP3 and caspase-8. These complex signaling pathways leading to cell death or survival are quite recently discussed in this review by Brenner et al[20], and the role of these pathways in inflammatory processes by Wallach[117]. In short, TNFα stimulation leads to conformational

changes of the TNFR, assembling an receptor signaling complex. This complex contains TAK1, a kinase that can activate MAPK signaling cascades including JNK, and the IKK complex. The IKK complex phosphorylates IκBα, the cytoplasmic inhibitor of NF-κB. Upon subsequent proteosomal breakdown of IκBα, NF-κB translocates into the nucleus and induces signaling. Maturation of the TNFR complex based on the status of RIP1 ubiquitination can lead to formation of cell death complexes, inducingapoptosis, necrosis or necroptosis[20].

In *in vitro* cell culture models using HepG2 cells, primary human or rat hepatocytes, diclofenac synergizes with TNFα to induce apoptosis[41,42]. This synergism has been shown to be dependent on JNK activation, inhibition of NF-κB nuclear translocation and an activated mitochondrial apoptotic pathway[42]. In addition, diclofenac/TNFα-induced synergism has been shown to be increased by concomitant IFNγ exposure. This increased synergism is dependent on ERK-dependent STAT1 activation[14]. Activation of the endoplasmic reticulum (ER) stress response is essential for induction of diclofenac-mediated TNFα-induced cytotoxicity. Expression of ER-stress response-related genes including transcription factor CHOP is enhanced upon diclofenac exposure alone in HepG2 cells, primary human hepatocytes (PHH) and human precision-cut liver slices. Subsequent siRNA-mediated knockdown of CHOP and its upstream translational regulator EIF4A1 in HepG2 cells confirmed the role of ER-stress in TNFα-induced hepatotoxicity[16].

The role of the ER-stress response in different liver diseases has recently been reviewed[118]. In HepG2 cells, diclofenac-induced increase in intracellular calcium was increased by both TNFα and IFNγ, leading to activation of JNK and ERK and subsequent cytotoxicity[15]. Interestingly, ER-stress in HepG2 cells seems to induce ER-stress in THP-1 macrophages via both soluble and insoluble factors. ER stress in macrophages leads to a reduction in pro-inflammatory cytokine secretion and is thereby providing a negative feedback loop for drug-induced inflammation[119]. Also trovafloxacin-mediated TNFα-induced cell-death was characterized by ERK activation and prolonged JNK activation. However, in this case activation of these signaling pathways was mediated by DNA replication stress[33,120]. Furthermore, oxidative stress and heat shock responses have been shown to interact with TLR4 and TNFα-induced signaling and NF-κB activation[121]. Several DILI-inducing drugs that synergize with TNFα activate oxidative stress responses by themselves[43]. Inhibition or aberrant activation of these oxidative stress responses in HepG2 cells by siRNA-mediated knockdown enhances or inhibits this TNFα-induced cytotoxicity, respectively[16]. Together, these data suggest that several drug-induced adaptive stress response pathways can interfere with TNFα-induced hepatotoxicity.

Idiosyncratic drug-induced liver injury prediction by *in vitro* approaches

It is clear that the cause of idiosyncratic DILI is in all cases multifactorial. Drug-specific responses make it difficult to predict the effect of novel drug-candidates on the many host factors involved in the development of DILI. However, using improved prediction models on clinical trial results led to majorly improved prediction of DILI hazard[47]. Currently used *in*

vitro methods have been extensively reviewed[1,122,123]. In this review, we will focus on the incorporation of inflammatory signaling in *in vitro* models.

DILI is characterized by massive hepatocyte cell death. Therefore, hepatocyte only models are much-used in the pharmaceutical industry to test for the hepatotoxic potential of novel compounds. For these models, PHHs are the golden standard, besides having some serious drawbacks in for example donor variability and low availability. The quite recently established hepatoma cell line HepaRG forms hepatocyte-like cells surrounded by biliary epithelial-like cells upon differentiation. This cell line is relatively easy to handle and shows enhanced metabolic capacity and hepatic transporter function, giving better prediction of especially drug-induced cholestasis[124]. Immortalized cell lines, for instance HepG2, are much used for their easy handling, high availability and stable phenotype. However, severely decreased drug-metabolism capacity makes this model less applicable in cases of drug metabolite-induced toxicity. Functionality and phenotypes of these cell lines for toxicity research have been frequently compared and the results are not conclusive[125,126], introducing the pragmatic "fit for purpose" approach[1,127,128]. PHHs, HepaRG cells and HepG2 cells have all been shown to greatly improve their hepatocyte phenotype by sandwich culture or 3D culture, together with prolonged sustainability and the possibility of repeated dosing. However, high-throughput screening, especially with other than endpoint measurements, remains difficult with this culture method[1], although some progress has been made (unpublished data;[129]). Mimicking activated liver immune cells in hepatocyte only cultures occurs mainly by manual addition of effector proteins or cytokines. This approach can be used in high-throughput screening methods and in prediction models (unpublished data;[41,130]).

Co-culture models with non-parenchymal cell types in 2D and 3D systems greatly improve hepatocyte function and phenotype[1]. In 2D, KC and hepatocyte co-culture showed in general upregulated hepatocyte CYP enzyme expression and drug metabolism in hepatocytes, and increased KC cytokine production and concurrent hepatotoxicity[12,31,32,35].

***Fig. 1*. The applicability of experimental model systems for hepatotoxicity screening and understanding cytokine-induced hepatocyte toxicity** Model systems used to detect immune signaling in human idiosyncratic drug-induced liver injury are assessed, both on the reflection of the human immune response in the model system and the possibility to detect specific hepatocyte signaling on immune activation. All depicted cell model systems can be implemented with either cell lines or pri- mary cells. The models are evaluated on the complexity level of immune signaling that is possible, the hepatocyte phenotype, the donor variability, the possibility of hepatocyte-specific measurements, the possibility of genomic interference, the availability of the model for high-throughput approaches, the sustainability of the cell culture model over time, and the possibility of interfer- ence of the system (in, for instance, measuring or adding a specific cytokine). Specifically mentioned is the possibility to use fluorescent reporter cell lines in complex models as 3D models and cocultures of cell lines. The use of these fluorescent reporters is extensively reviewed in Wink *et al.* (2014); the use of these reporter cell lines confers the possibility to detect hepatocyte-specific immune signaling on the mentioned models, increasing model value for mechanistic and predictive toxicity research. LPS, lipopolysaccharide; PHHs, primary human hepatocytes. Color images available online at www.liebertpub.com/aivt

The applicability of research models for screening and understanding cytokine-induced hepatotoxicity

Human

+ best immune/non parenchymal cell environment
+ best functional liver phenotype
+/- high donor variability
- hepatocyte measurements not possible
- genomic interference techniques not possible
- need of reliable biomarkers
- low controllability of the system interferences during research

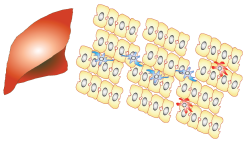

Human liver *ex vivo* and human precision-cut liver slices

+ good immune/non parenchymal cell environment
- no recruited immune cells
+ good functional liver phenotype
+/- high donor variability
- no interaction with body-derived input (e.g. gut-derived LPS)
- hepatocyte measurements not possible
- genomic interference techniques not possible
- low/medium availability
- low sustainability
+/- higher controllability of the system interferences during research

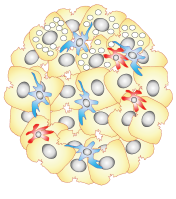

Human 3D spheroids/sandwich co-culture

+/- relatively good immune environment
- no recruited immune cells
- artifical ratio hepatocytes/immune cells
+/- relatively high-differentiated hepatocyte phenotype
+/- less donor variability (applicable for cell lines and PHHs)
- direct hepatocyte measurements not possible
+ genomic interference techniques possible in cell lines
+ medium availability
+ high sustainability
+/- higher controllability of the system interferences during research

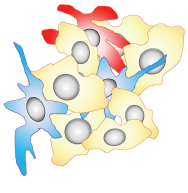

Human 2D co-culture/micropatterned culture

+/- medium level immune environment
- no recruited immune cells
- artifical ratio hepatocytes/immune cells
+/- medium differentiated hepatocyte phenotype
+/- less donor variabiliaty (applicable for cell lines and PHHs)
- direct hepatocyte measurements not possible
+ genomic interference techniques possible
+ high availability
+/- relatively low sustainability
+/- higher controllability of the system interferences during research

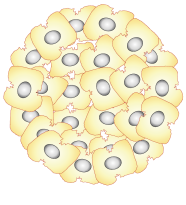

Human 3D hepatocyte spheroids/sandwich culture

- no representative immune environment
+/- relatively low differentiated hepatocyte phenotype
+/- less donor variability (applicable for cell lines and PHHs)
+ direct hepatocyte measurements possible
+ genomic interference techniques possible
+/- medium availability
+/- medium sustainability
+ high controllability of the system interferences during research

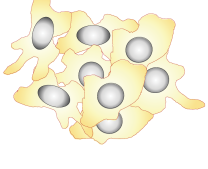

Human 2D hepatocyte culture

- no representative immune environment
- low differentiated hepatocyte phenotype
+/- less donor variability (applicable for cell lines and PHHs)
+ direct hepatocyte measurements possible
+ genomic interference techniques possible
+ high availability
- low sustainability
+ high controllability of the system interferences during research

fluorescent reporter cell lines are applicable ↓

complete & complex ↓

controllable & simplified ↓

Culture systems in which the proximity of KCs and hepatocytes can be controlled, as is the case in micropatterned culturing methods, have demonstrated an increased hepatocyte function compared to random co-culture[1]. Furthermore, it has been shown that the ratio of KCs to hepatocytes, cell-cell contact and the relative proximity between these cell types determine the functionality of hepatocytes[131]. However, to our best knowledge, no co-exposure experiments with LPS and drugs have been performed in this model. However, co-culture of KCs with hepatocytes in a 3D culture model, shows that KC activation by LPS decreased the cytotoxicity threshold for trovafloxacin threefold compared to only trovafloxacin treatment[132]. Taken together, these co-culture models show promising results for the assessment of inflammatory stress in high throughput approaches.

Another, more complex, multicellular approach eventually feasible for low/medium throughput purposes are human precision-cut liver slices. This model can show LPS-induced synergistic cytotoxicity and can be used to classify hepatotoxicants, although it has to be further developed for screening purposes[112,113,133]. A general overview of the most-used cell culture methods in toxicity screening and their applicability for the detection of inflammation-induced signaling and hepatotoxicity is displayed in figure 1. Advantages and disadvantages of each model are listed, clearly showing that these models have their own restricted values. The advantages and shortcomings of each model make serious consideration of the purpose of the screening or mechanistic study essential in choosing a fitting model system. Currently, the most exciting progress in model development in the idiosyncratic DILI research field is made with human-induced pluripotent stem cells. These cells can be developed into donor-specific hepatocytes, enabling the research on donor-specific cells from DILI-susceptible donors[1,134]. Once the induction of stem cells into hepatocytes and especially in non-parenchymal cells is optimized, this model will revolutionize toxicity research.

The models described above can be used not only for screening and prediction purposes, but also to gain mechanistic understanding. Fluorescent HepG2 reporter cell lines allow the quantitative, time-resolved detection of adaptive stress response activation on a single-cell basis[135]. These data, in combination with phosphoproteomics[130], genomics approaches[16], and co-culture system proteomics[35] point towards the important role of adaptive stress responses interfering with cytokine-induced signaling. These insights in cytokine-induced toxicity from *in vitro* models might help unravel human DILI. They also show how immune/cytokine signaling is reflected, or lacks, in *in vitro* high throughput predictive models when compared to human and animal *in vivo* data..

Summary and future perspective

Idiosyncratic DILI remains one of the most unpredictable adverse drug reactions, often leading to discontinuation of drug development or restricted use of effective drugs. In this review, the inflammatory signaling as a host factor that increases DILI potential has been discussed, highlighting the recent progress in this field. This with a main focus on the role of TNFα signaling, TLR4 signaling, and diclofenac. Taken together, these data suggest that drug-induced adaptive stress response pathways in hepatocytes and non-parenchymal

cells could sensitize cells to drug-independent host factors. It would explain the idiosyncratic nature of many drug-induced liver injury, since a critical amount of host factors would be involved in both drug-dependent and -independent cellular adaptive processes. The typically unpredictable length of latency time suggests that many processes are involved in the adaptive processes before the threshold is reached for induction of hepatotoxicity. Furthermore, the clinical adaptation of most of the mild DILI cases despite continuation of drug treatment implies inherent negative feedback signaling. Finally, understanding idiosyncratic DILI in human, together with the understanding of the potential and limitations of our *in vitro* screening approaches will lead to improved prediction of idiosyncratic DILI in an early drug development stage.

Acknowledgements

This work was supported by the Innovative Medicine Initiative MIP-DILI project (grant agreement no 115336) and the European Horizon2020 EU-ToxRisk project (grant agreement no. 681002).

Disclosure Statement

No competing financial interests exist.

Chapter 3

Phenotypic screen of TNFα-mediated NF-κB nuclear translocation dynamics reveals CDK12 as suppressor of anti-apoptotic signaling and A20 expression

Highlights

- siRNA-mediated screening of TNFα-induced nuclear NF-κB oscillation identified 46 regulators
- Several of these regulators modulate A20 expression and drug/TNFα synergistic cytotoxicity
- CDK12 is revealed as a novel modulator of TNFα-induced NF-κB oscillation, synergistic apoptosis signaling and A20 expression

This chapter is based on a manuscript in preparation:

Bram Herpers[1,2], Lisa Fredriksson[1,2], Suzanna Huppelschoten[1,2], Giulia Benedetti[1], Zi Di[1], Matthijs Vlasveld[1], Janna Klip[1], Sylvia Lé Dévedec[1], Hans de Bont[1], John Meerman[1], Marjo de Graauw[1] and Bob van de Water[1]

Phenotypic screen of TNFα-mediated NF-κB nuclear translocation dynamics reveals CDK12 as suppressor of anti-apoptotic signaling and A20 expression

[1]Division of Toxicology, Leiden Academic Centre for Drug Research, Leiden University, Leiden, The Netherlands
[2]These authors contributed equally

NF-κB signaling is critical in normal homeostasis and disease progression. Tumor necrosis factor-alpha (TNFα) triggers nuclear oscillation of the dimeric transcription factor NF-kappaB (NF-κB). In the nucleus, NF-κB directs transcription of target genes involved in diverse biological programs and its own response inhibitors, IkappaBalpha (IκBα) and the ubiquitin-editing enzyme A20. To unravel the signaling programs that regulate the TNFα-induced NF-κB oscillatory response, we applied a live-cell imaging-based siRNA screen to identify individual kinases, (de)ubiquitinases and sumoylases that control the temporal NF-κB oscillatory response using liver HepG2 cells as a model. We identified 46 candidate genes that either positively or negatively regulate the oscillatory behavior of NF-κB. These include a majority of previous uncharacterized NF-κB regulators, for instance the kinases CDK12, ADCK2, TTK, MAPK4 and AATK, and (de)ubiquitinases USP8, FBXW5 and TRIM50. A characteristic delay in TNFα-induced NF-κB oscillation generally protected against TNFα-induced cytotoxicity in combination with drugs with established liability for hepatotoxicity. For several candidate regulators the cytotoxicity protection was associated with enhanced expression of A20, a negative regulator of TNFα-mediated apoptotic signaling. Depletion of the cellular stress-related kinase CDK12 delayed TNFα-induced NF-κB oscillation, which was concurrent to upregulation of TNFα-induced A20 expression. Moreover, CDK12-depleted cells are partially protected against drug/TNFα-dependent cytotoxicity, suggesting a relationship between these effects of CDK12 knockdown. Overall the work provides a refined repository of TNFα signaling components that control the TNFα-induced spatio-temporal activity of NF-κB and A20 expression. These signaling components may contribute to novel therapeutic strategies to modulate disease status involving TNFα-mediated NF-κB activation.

Keywords: NF-κB signaling, RNAi screening, systems microscopy, apoptosis, CDK12, A20

Introduction

The dimeric transcription factor nuclear factor-κB (NF-κB) plays a central role in normal physiological homeostasis as well as disease onset and progression[136,137]. Transcriptionally active NF-κB is crucial in the host-pathogen response by inducing pro-inflammatory gene expression and thereby activating the innate and adaptive immune response[138]. In addition, erroneous regulation of NF-κB has been associated with disease states such as cancer, chronic inflammatory, autoimmune diseases and adverse drug reactions[13,29].

The best-characterized proinflammatory cytokine that induces NF-κB transcriptional activity is tumor necrosis factor-α (TNFα). Targeting TNFα-signaling with TNFα and TNF-receptor specific antibodies has become a regular therapy for NF-κB-related inflammatory auto-immune diseases such as arthritis and psoriasis, but can also induce unexpected and remarkably severe side effects[20,139]. TNFα exerts pleiotropic effects upon effector cells, including cell survival or cell death. These effects are dependent on cell

type and homeostatic status of these cells[20]. The transcriptional activity of NF-κB seems crucial in prevention of TNFα-induced hepatocyte cell death, by inducing anti-apoptotic gene expression[17]. These anti-apoptotic NF-κB target genes block the progression of the initial TNF receptor complex to the so-called TNF receptor complex II. As TNF receptor complex II is formed this leads to cell death, including apoptosis[20,140]. Post-translational modification, including phosphorylation but specifically ubiquitination, are the most important regulators of signaling from both TNF receptor complexes[141]. Genetic mice and biochemical studies all underline the importance of the enigmatic ubiquitin-editing enzyme A20 (or TNFAIP3) in inflammatory and auto-immune diseases[142,143]. A20 exhibits E3 ligase, ubiquitin-binding and de-ubiquitinases (DUB) function and its expression is induced by NF-κB transcriptional activity. Upon induction, A20 also inhibits NF-κB activation, functioning as a negative feedback loop. Furthermore, A20 activity forms a switch between NF-κB signaling and cell death complex formation by ubiquitination and deubiquitination of TNFR complex subunits[142,144].

The TNFα-induced signaling pathways that control the transcriptional activity of NF-κB have been well-studied. Recent gain- and loss-of-function screens based on NF-κB luciferase reporter constructs or fixed immunostaining of NF-κB, were performed using cDNA[145], RNA-interference[146–150], or miRNA screens[151]. While these screens unraveled many upstream regulators, these primarily focused on TNFα-induced NF-κB translocation or transcriptional activity on a specific time point, and the luciferase constructs determine one particular NF-κB target gene response. Since NF-κB has many target genes (http://www.bu.edu/nf-kb/gene-resources/target-genes) with very distinctive temporal patterns of activation[152,153], the coverage of signaling modalities that modulate NF-κB signaling are likely incomplete.

To avoid the specificities of a particular target gene and time point, we examined a general feature of NF-κB transcriptional activation: nuclear translocation. Nuclear translocation of NF-κB is a key characteristic of activation and has been linked to NF-κB induced target gene expression on single cell level[27,154]. Translocation detection has been previously used for screening purposes, however this was on fixed time points[150]. The nuclear translocation of NF-κB is an oscillatory response that is controlled by negative feedback mechanisms and varies between individual cells and different cell types[24,155].This oscillatory phenotype might determine NF-κB target gene expression levels and kinetics[25–27].

To discover novel regulators of critical NF-κB transcriptional activity in survival signaling pathways, we established an automated high-throughput assay to follow TNFα-induced NF-κB oscillation over time[156]. We and others demonstrated that the anti-inflammatory liver toxic drug diclofenac disturbed the cytokine-induced NF-κB nuclear oscillation and amplified the TNFα-induced cytotoxicity in liver cells[42]. Here, we used diclofenac to facilitate the RNAi-based discovery of novel positive and negative regulators of the TNFα-induced dynamics of the nuclear translocation of NF-κB subunit RelA. We then determined the role and mechanism of several of these regulators in the regulation of TNFα signaling and the onset of liver TNFα/drug-induced cytotoxicity. We identified, for the first

time, a key role for CDK12 in modulation of TNFα-induced A20 expression, NF-κB oscillation and cytotoxicity.

Material and Methods

Reagents and antibodies

Human recombinant TNFα was acquired from R&D Systems (Abingdon, UK). Diclofenac sodium, carbamazepine, and the antibody against tubulin were from Sigma-Aldrich (Zwijndrecht, The Netherlands). AnnexinV-Alexa633 and AnnexinV-Alexa561 were in house generated as previously described (20). The antibody against IκBα was from Cell Signaling (Bioké, Leiden, The Netherlands), A20 was from Santa Cruz (Tebu-Bio, Heerhugowaard, The Netherlands), UFD1L was from BD Transduction Laboratories (Breda, the Netherlands), caspase-8 was from Cell Signaling (Bioké, Leiden, The Netherlands) and cleaved-PARP was from BioLabs (Ipswich, UK). The bromo phenol blue lysis buffer was from Merck (Merck Millipore, Amsterdam, The Netherlands).

Cell culture

Human hepatoma HepG2 cells were obtained from American Type Culture Collection (clone HB-8065, ATCC, Wesel, Germany). HepG2 cells stably expressing GFP-p65 (NF-κB subunit RelA) were created by 400 µg/ml G418 selection upon pEGFP-C1-p65 transfection using Lipofectamine™ 2000 (Invitrogen, Breda, Netherlands). HepG2 BAC A20-GFP cells were generated by bacterial artificial chromosome (BAC) recombineering[44,157]. Upon validation of correct C-terminal integration of the GFP-cassette by PCR, the BAC-GFP construct was transfected using Lipofectamine™ 2000. Stable HepG2 BAC A20-GFP cells were obtained by 500 µg/ml G418 selection. For all experiments the cells were cultured in Dulbecco's modified Eagle's medium (DMEM) supplemented with 10% (v/v) fetal bovine serum (FBS), 25 U/ml penicillin, and 25 µg/ml streptomycin between passages 5 and 25.

RNA interference experiments

Transient knockdowns of individual target genes were achieved using siGENOME SMARTpool siRNA reagents in the primary screen or single siRNA sequences in the secondary deconvolution screen (50 nM; Dharmacon GE Healthcare, Landsmeer, Netherlands) and other experiments. HepG2 cells were transfected using INTERFERin siRNA transfection reagent according to the manufacturer's procedures (Polyplus transfection, Leusden, Netherlands) and medium was refreshed after 16 hours of incubation. The cells were used at 72 hours after siRNA transfection to achieve maximal knockdown before treatment. The negative controls used were mock transfection of INTERFERin without siRNA, siGENOME non-targeting pool #1 and siGFP, all from Dharmacon (GE Healthcare, Landsmeer, Netherlands).

Exposures and live cell imaging of GFP-p65 and A20-GFP in HepG2 Cells

Prior to imaging, nuclei were stained with 100 ng/ml Hoechst 33342 in complete DMEM for 45 minutes or overnight. The cells were exposed to diclofenac 500 µM, carbamazepine 500

μM, or DMSO 0.2% for 8 hours. The cells were then challenged with human TNFα (10 ng/ml) addition to the compound medium.The GFP-p65 nuclear translocation response upon 10 ng/ml human TNFα challenge was followed for a period of 6 hours by automated confocal imaging every 6 minutes (Nikon TiE2000, Nikon, Amstelveen, Netherlands). Quantification of the nuclear/cytoplasmic ratio of GFPp65 intensity in individual cells was performed using an algorithm for ImageJ [156]. A20-GFP accumulation was measured in live cells using automated confocal imaging every hour (Nikon TiE2000, Nikon, Amstelveen, Netherlands). Quantitative analysis was performed with Cell Profiler version 2.1.1[158] with an in house developed segmentation module[159]. Data analysis was performed with an in house developed data analysis package H5CellProfiler (Wink *et al.,* manuscript in preparation) using R.

Translocation response class definition and hit definition statistics

For the primary screen, the amplitudes of the individual translocation response tracks were normalized to their intrinsic response maxima (=1) and minima (=0) to be able to compare the timing of the nuclear translocation events versus the plate average. For the secondary screen, non-normalized data were used. Four different classes were defined according to the type of nuclear p65 oscillation response: increased, no oscillation, decreased and different compared to the oscillation observed with control siRNA. Each class used a different set of five specific parameters (Fig. 1A). For each targeted gene, a Pearson's chi-squared cumulative statistic was calculated from the set of five parameters of each class and p-values were obtained by comparing the value of the statistic to a chi-squared distribution. Targeted genes obtaining a p-value lower than or equal to 0.001 were considered as hits.

Apoptosis measurements

Apoptosis was determined by the live cell apoptosis assay previously described[160]. The relative Annexin V fluorescence intensity per image was quantified using Image Pro (Media Cybernetics, Bethesda, MD) and normalized to the number of nuclei.

Western Blot

Cells were harvested in sample buffer (6 times diluted bromophenol blue solution, with β-mercaptoethanol). The samples were subjected to protein separation, blotted on Immobilon-P (Millipore, Amsterdam, The Netherlands). Phosphorylated IκBα was detected using the Tropix Western-Star kit™ (Applied Biosystems) following manufacturer's protocol. For tubulin, A20, UFD1L and IκBα, the membranes were blocked for 1h at room temperature in milk powder 5% (w/v) in Tris-buffered saline/Tween 20 (TBS-T). Primary antibody incubation was done overnight at 4°C followed by incubation with cy5-labeled secondary or horseradish peroxidase-conjugated antibodies (Jackson Immunoresearch, Newmarket, UK) in 1% BSA in TBS-T for 1 h at room temperature. Protein signals were detected with ECL (GE Healthcare Diegem, Belgium) followed by film detection, by

visualization on the Typhoon 9400 imager (GE Healthcare, Diegem, Belgium), or by detection on an ImageQuant LAS 4000 (GE Healthcare, Diegem, Belgium).

Statistical procedures

All numerical results are expressed as mean ± standard error of the mean (SEM). Statistical significance was determined by GraphPad Prism/R using an unpaired t-test, * P≤0.05, ** P≤0.01, *** P≤0.001. Heatmap representations and hierarchical clustering (using Pearson correlation) were performed using the Multiple Experiment Viewer (MeV) software. For statistical analysis of the screen results, see above.

Results

NF-κB nuclear oscillation phenotype siRNA screening in HepG2 cells

Stimulation with TNFα initiates oscillatory nuclear translocation of NF-κB in various cell types, including HepG2 cells[42,155]. We established HepG2 cells with GFP-tagged RelA to follow the dynamics of NF-κB using time-lapse confocal microscopy. TNFα stimulation induced transient nuclear translocation of RelA-GFP, followed by a dampened oscillation at defined time intervals. Under control conditions the translocation peaks at 30 minutes after TNFα stimulation, followed by a second and third peak at 150 and 270 minutes, respectively (Fig. 1A, top). The maximum oscillation response was seen at 10 ng/mL TNFα[135]. For unbiased hit detection we required the quantitative classification of the four oscillatory phenotypes: normal oscillation, increased oscillation, decreased oscillation and no oscillation. Normal oscillation was determined as the DMSO, mock-transfected control condition. The ubiquitin editing enzyme A20 (TNFAIP3) has a negative feedback on the activity of the IKK complex and suppresses NF-κB activation[161]. Knockdown of A20 slightly decreased the time-interval between oscillations, leading to faster oscillation (increased oscillation). In contrast, knockdown of well-known NF-κB inhibitor IκBα almost completely inhibits NF-κB oscillation (no oscillation). This inhibition was associated with enhanced levels of A20 expression (Fig. 1A, middle and Suppl. Fig. S1). Treatment of hepatocytes with the hepatotoxic drug diclofenac increases the susceptibility for TNFα-induced apoptosis[41,42] and increases the time interval between NF-κB oscillation peaks (decreased oscillation) (Fig. 1A, bottom). We established a pipeline of automated image segmentation and GFP-RelA nuclear/cytoplasmic ratio quantification for all individual cells within one time-series, followed by extraction of 32 distinct oscillation features[156]. We classified the phenotypes based on the direction versus control for at least 5 oscillation features, e.g. number of peaks, time between peaks and amplitude of peaks (Fig. 1A). If more than 5 of the 32 measured oscillation features were distinct from control and the oscillation phenotype did not match any of the other categories, the response was marked as “different oscillation”.

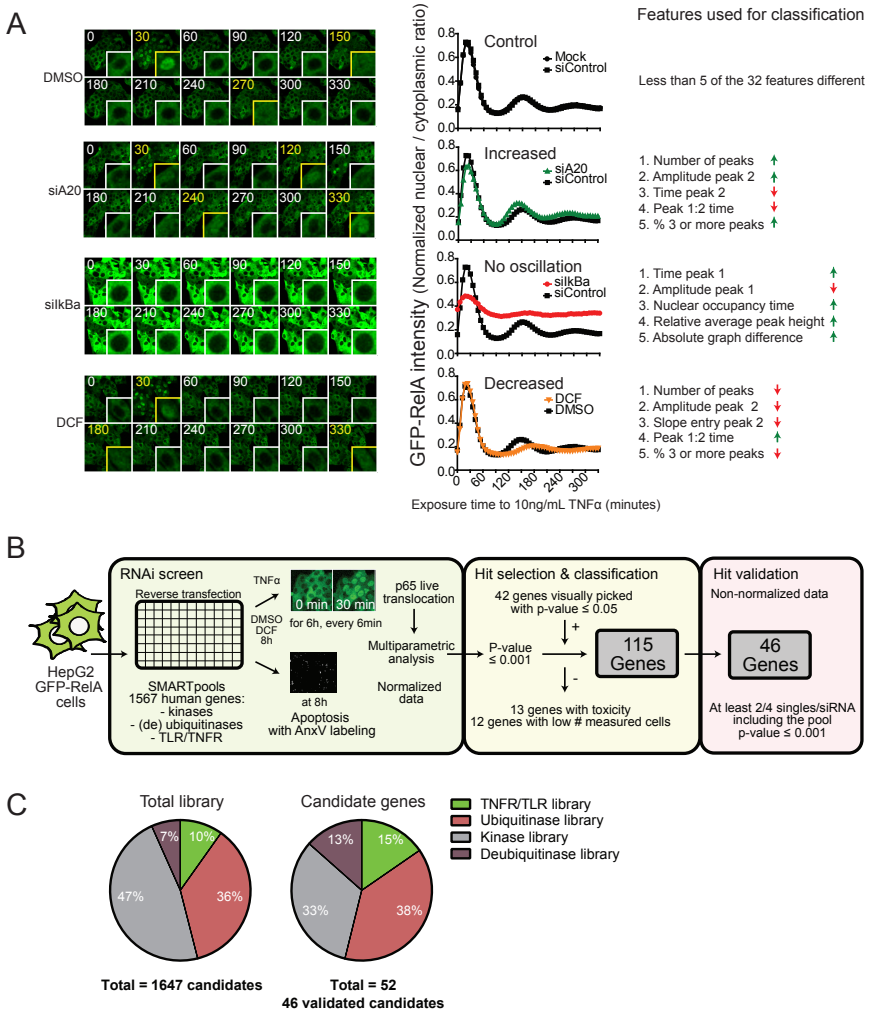

Fig. 1: **NF-κB oscillation phenotype siRNA screening in HepG2 cells** (A) Representative images of RelA-GFP translocation after TNFα (10 ng/mL) challenge in HepG2 cells by automated confocal microscopy. Insets: zooms of single cells with an average response in respect to the imaged population. The nuclear translocation events are marked by yellow boxes and the numbers indicate the time in minutes after TNFα exposure. The nuclear translocation track of each cell was quantified and normalized to its own highest nuclear-to-cytoplasmic ratio (value of 1) and its lowest ratio (0). The average response of the total cell population is presented in the middle panel. The features and their directions that define the response classes (different, increased, decreased and no oscillation) compared to control are shown in the panel to the right. (B) Flowchart of the siRNA screen. (C) Representation of the siRNA distribution between respective libraries in the primary screen compared to the final hit selection. Some candidate genes are represented in several libraries, as the TNFR/TLR library also contains kinases and (de)ubiquitinases. MAP3K14 and MAP3K8 are in both kinase and TNFR/TLR library, while CYLD is in both deubiquitinase and TNFR/TLR library. TNFAIP3(A20) is in the ubiquitinase, deubiquitinase and TNFR/TLR library.

Having established an automated system to track, segment and categorize the NF-κB oscillation pattern in individual cells, we used siRNA screening to identify genes that define the timely activity of the NF-κB response (Fig. 1B). We screened 779 kinases, 107 de-ubiquitinases and sumoylases, 580 ubiquitin ligases and 123 players in the TNFR/TLR-driven NF-κB response. We screened under control (DMSO) and 8 hr diclofenac (DCF) pre-treatment conditions. AnnexinV-Alexa633 labeling of the cells allowed identification and exclusion of genes that upon knockdown affect cell viability during screening. TNFα-induced oscillation of NF-κB was followed for 6 hours at 6 minute intervals for all individual knockdowns, directly after TNFα stimulation. Then, we normalized the nuclear/cytoplasmic GFP intensity ratio and independently analyzed the data for both treatment conditions. For each condition, we considered those genes a candidate hit at a p-value below or equal to 0.001. Within this p-value cut-off we could trace back the effect most of the A20 knockdown plate controls (76% and 92%, control and diclofenac treatment, respectively) and of the IκBα knockdown plate controls (94% and 100%, control and diclofenac, respectively) (Suppl. Fig. S2). Visual inspection of the oscillatory responses defined another 42 candidate genes, leading to in total 115 regulator genes detected from initial screening; 25 candidate genes were discarded due to limited number of cells or onset of cell death (Fig. 1). Using the same strategy, we performed a subsequent validation screen targeting the initial 115 candidate genes. For this we used 4 single siRNAs that were part of the initial smartpool siRNA mix in the primary screen. Then, 46 genes were confirmed to affect the GFP-RelA oscillation with 2 or more single siRNAs in addition to the pooled siRNAs in either or both DMSO and DCF conditions (see Supplementary movies S1-S6). We identified 17 kinases, 27 (de)ubiquitinases, and 8 genes that are known members of the TNFR/TLR signaling pathway. Knockdown of PHF5A and UCHL1[162,163] decreased oscillation; knockdown of AGTR2[164–167], MAPK4, MAPKAPK2[168], SENP2[169], TNFAIP3[142,170], RELA and TNFRSF17[171] increased oscillation; knockdown of CDK12, RBX1[172], USP8, TNFRSF18[173], ADCK2, CUL1[174], FBXW11[175], FBXW5, IKBKG[176], MAP3K14[177], MAPK8[178], RAPSN, RNF126, TNFRSF1A, TRIM27[179], TRIM50, TRIM8[180,181], TTK, UBOX5 and UFD1L[182] stopped oscillation; knockdown of TSKS, MLL2[183], AATK, CYLD[184,185], NTRK3[186], BAHD1, MVK, TTBK1, UNK, FBXW9, MAP3K8[187], OTUB2[188], UBE3A, PHF19, STRADA, MASTL and USP15[189] have a miscellaneous effect on oscillation (Fig. 1C; Table 1). Several validated candidate genes are known to affect the NF-κB signaling pathways (IKBKG, MAP3K14, CYLD), while others that showed a strong effect are novel (CDK12, PHF5A, TTK). Similar to NF-κB activity, CDK12 polymorphisms have been associated with cancer progression[190], as has TTK expression levels[191].

Candidate NF-κB signaling modifiers affect the single cell oscillation behavior

Our screening approach enabled the analysis of the dynamics of the NF-κB response at a single cell level within an entire population of cells, which allows measurement of the population dynamics upon knockdown of our candidate genes (Fig. 2A and 2B). Under control conditions 57 % of the cells showed at least three nuclear translocation events in a 6 hour period. As expected, around 70 % of the cells showed no or only one shallow

oscillation upon knockdown of genes that blocked oscillation. This is for instance true for knockdown of TNFR1 and IKKγ, that are both well-characterized as essential for NF-κB activation. (Fig. 2Bi).

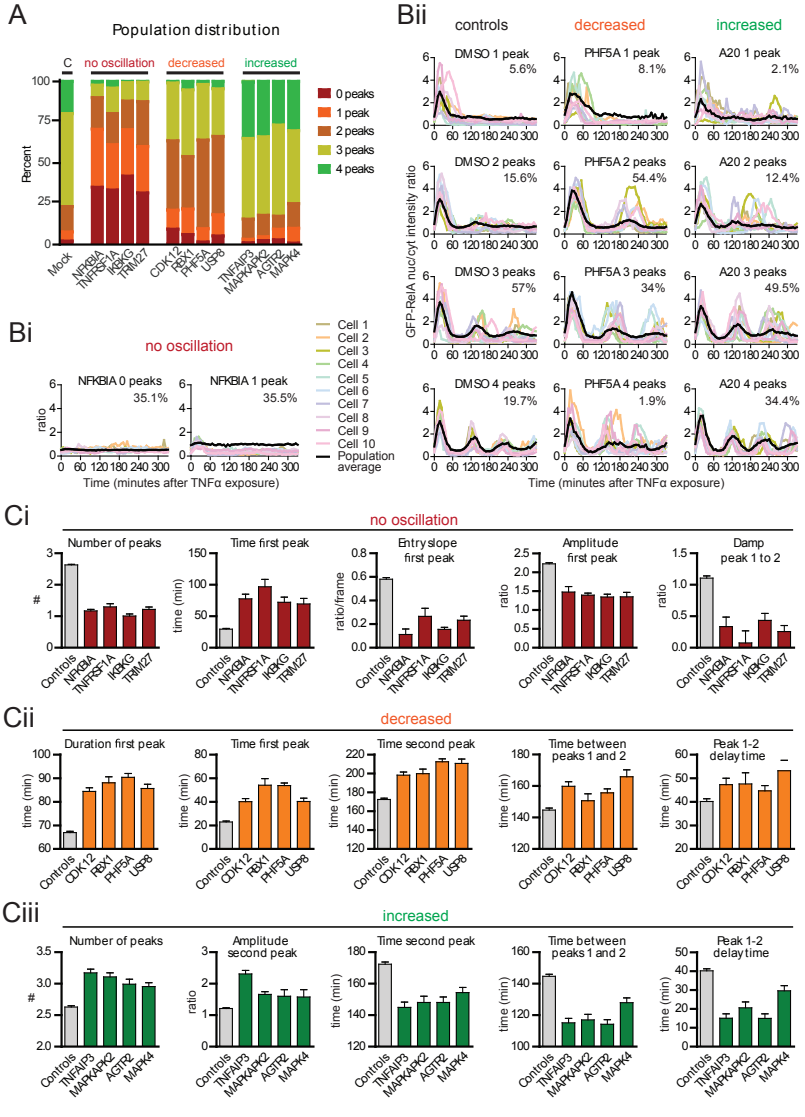

Fig. 2: **Population statistics of candidate genes** (A) The population distribution of NF-κB oscillations in HepG2 RelA-GFP cells upon indicated siRNA treatments. (B) Examples of how each phenotypic class is distributed in relation to the number of translocation peaks in single cell data. (C) The translocation features that define the different classes: “no oscillation” (Ci), “decreased” (Cii) and “increased”(Ciii) are exemplified by their representative siRNAs in the control DMSO condition.

For the decreased oscillation phenotype a drastic shift occurred for cells with 2 oscillations from 15% under control to around 50%, for example for CDK12 and PHF5A knockdown (Fig. 2Bii). The 'increased phenotype' clearly demonstrated an increase in the percentage of cells with 4 oscillations as observed for TNFAIP3 (A20) knockdown (Fig. 2Bii). Extraction of quantitative descriptors of the oscillatory response allowed further insights in the oscillatory phenotype. For the no oscillation phenotype the number of peaks was vastly reduced and any observable translocation event occurred later than in control cells, at lower amplitude and with a reduced nuclear entry slope. Within the remaining fraction of cells (~30%) that showed more than one nuclear translocation event, the peaks remained shallow, reflected by reduced dampening between the peaks and lower amplitude (Fig. 2Ci). For the candidate genes CDK12, RBX1, PHF5A and USP8 that caused a decreased oscillation phenotype upon knockdown, the overall duration and time of the first peak were extended while the second peak occurred later than in control conditions (Fig. 2Cii). Finally, knockdown of TNFAIP3 (A20), MAPKAPK2, AGTR2 and MAPK4 induced an increased oscillation phenotype, hallmarked by an increase in the number of oscillations. They showed a decreased time interval between peaks, associated with an overall increase in the amplitude of TNFα-induced NF-κB nuclear translocation (Fig. 2Ciii).

Functional and phenotypic classification of the siRNA screen hits that control NF-κB oscillation

Next, we classified our 46 validated candidate genes and defined their role in the control of NF-κB oscillatory behavior (Fig. 3A and B and summary Table 1). Under control conditions 7 genes increased the oscillation upon knockdown, including AGTR2, MAPKAP2 and MAPK4. Another 5 genes decreased the oscillation upon knockdown, including USP8, CDK12 and PHF5A. A majority of 24 genes blocked oscillation upon knockdown, including UFD1L, RNF128 and TRIM8. Furthermore, knockdown of TSKS, MLL2 and TNFRSF17 also significantly affected NF-κB oscillation based on our statistical analysis, but these did not fall within the previous three categories. Overall, diclofenac pretreatment allowed identification of the same candidate genes (Fig. 3B and 3C and Table 1). However, several additional genes were identified that enhanced the diclofenac-delayed oscillation upon knockdown, including MAP3K8, OTUB2 and UBE3A. Other genes further shifted the effect from decrease to full suppression of the oscillatory behavior upon knockdown, as observed for CDK12, RBX1 and USP8 (Fig. 3B and Table1).

Fig. 3: **Functional and phenotypic profiling of the siRNA screen candidates that control NF-κB oscillation** (A) Typical non-normalized NF-κB oscillation averages acquired in the deconvolution screen, including examples of knockdowns that led to a phenotype similar to the classification controls; siA20, diclofenac (DCF) and siIκBα. The "different" class is defined by having five or more features significantly different from the siControl. (B) Heatmap of the SMARTpool classification P-values for the hits confirmed by 2 or more single siRNAs in the deconvolution screen, clustered for their corresponding classification on the right. The overlap of the hits under DMSO and DCF conditions are additionally presented in (C). (D) Overview of functional properties of the candidate genes involved in regulation of NF-κB translocation phenotype under DMSO and DCF conditions. Candidate proteins were classified with PANTHER analysis. Statistical analysis is explained in the material and methods section.

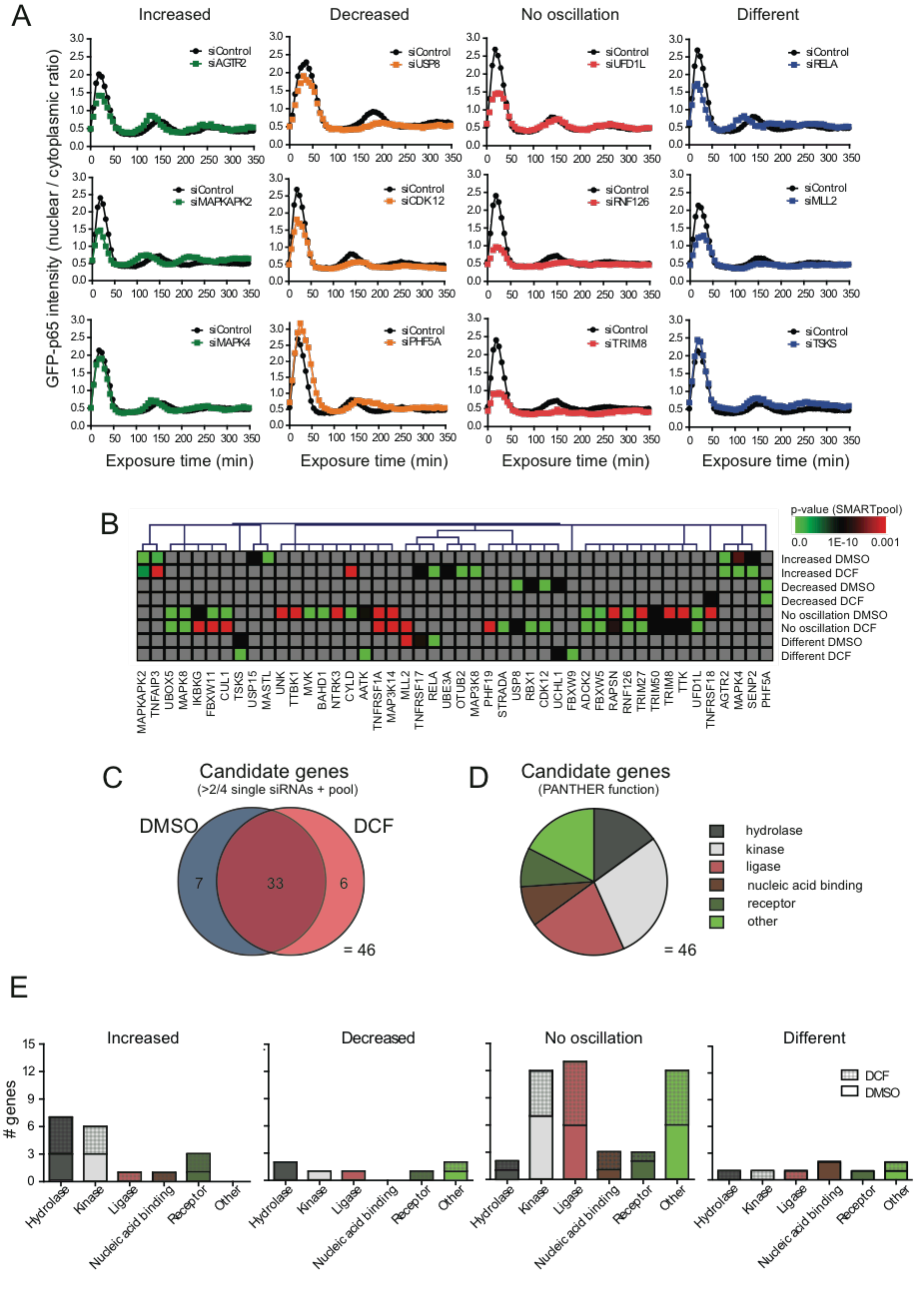
A
Increased
Decreased
No oscillation
Different
GFP-p65 intensity (nuclear / cytoplasmic ratio)
siControl
siAGTR2
siUSP8
siUFD1L
siRELA
siMAPKAPK2
siCDK12
siRNF126
siMLL2
siMAPK4
siPHF5A
siTRIM8
siTSKS
Exposure time (min)
B
p-value (SMARTpool)
0.0
1E-10
0.001
Increased DMSO
Increased DCF
Decreased DMSO
Decreased DCF
No oscillation DMSO
No oscillation DCF
Different DMSO
Different DCF
MAPKAPK2
TNFAIP3
UBOX5
MAPK8
IKBKG
FBXW11
CUL1
TSKS
USP15
MASTL
UNK
TTBK1
MYK
BAHD1
NTRK3
CYLD
AATK
TNFRSF1A
MAP3K14
MLL2
TNFRSF17
RELA
UBE3A
OTUD2
MAP3K8
PHF19
STRADA
USP8
RBX1
CDK12
UCHL1
FBXW9
ADCK2
FBXW5
RAPSN
RNF126
TRIM27
TRIM50
TRIM8
TTK
UFD1L
TNFRSF18
AGTR2
MAPK4
SENP2
PHF5A
C
Candidate genes
(>2/4 single siRNAs + pool)
DMSO
DCF
7
33
6
= 46
D
Candidate genes
(PANTHER function)
hydrolase
kinase
ligase
nucleic acid binding
receptor
other
= 46
E
Increased
Decreased
No oscillation
Different
genes
DCF
DMSO
Hydrolase
Kinase
Ligase
Nucleic acid binding
Receptor
Other

PANTHER functional analysis of the candidate genes showed that most were kinases, ubiquitin ligases and hydrolases (Fig. 3D and 3E). Knockdown of hydrolases led to a predominantly 'increased oscillation phenotype', while knockdown of kinases and ligases in general led to 'no oscillation phenotype'.

Effect of knockdown of candidate genes on drug/TNFα-mediated cell death

Transcriptional activity of NF-κB is cytoprotective against TNFα-induced apoptosis in hepatocytes [17]. Previously we hypothesized a key role for NF-κB signaling in the control of liver cell death in the context of drug-induced liver toxicity by diclofenac [42]. Here, we further explored the role of our candidate regulators of NF-κB nuclear translocation in the cytotoxic effect of drug/TNFα exposure. We focused on the 20 genes with the strongest phenotype, the ones that fully inhibited the oscillation upon knockdown (Table 1). Treatment with diclofenac or carbamazepine for 8 hours induced some cytotoxicity (Fig. 4B, 4Ci and Cii, upper, most left panel). While knockdown of most candidate genes did not affect drug-induced cytotoxicity compared to control knockdown, most remarkable, knockdown of TNFRSF1A enhanced the cell death for both diclofenac and carbamazepine conditions (Fig. 4A). Subsequent TNFα exposure vastly enhanced the cell death by diclofenac and carbamazepine (Fig.4B, lower panel). This effect was reduced by TNFR1 knockdown and strongly inhibited by caspase-8 knockdown (Fig. 4Ci and Cii, middle panel). In general, knockdown of the candidate genes caused a protection against drug/TNFα-induced cell death. Only knockdown of IKBKG increased TNFα-induced cell death significantly (Fig. 4C), demonstrating that direct and severe inhibition of NF-κB activation increases drug-induced cytotoxicity. Knockdown of CDK12 and UFD1L most strongly inhibited the TNFα-induced cytotoxic response without inducing significant changes in cytotoxicity upon diclofenac or carbamazepine treatment alone (Fig. 4A and C, Suppl.Fig.3). This indicates that CDK12 and UFD1L are strong modifiers of both TNFα-induced NF-κB nuclear translocation and drug-mediated TNFα-induced cytotoxicity.

Several candidate genes modulate both TNFα-induced NF-κB oscillation phenotype and A20 expression

Knockdown of A20 strongly increased the TNFα-induced nuclear oscillation phenotype of NF-κB (Fig. 1). A20 is a direct target gene of NF-κB and acts in a negative feedback loop to modulate TNFR1 downstream signaling and suppress NF-κB activation. Besides regulating NF-κB activity, A20 is also an important modifier of TNFα-induced apoptosis and necroptosis[20,24,141]. As such, A20 regulates tissue homeostasis[143,144,192]. Indeed, hepatocyte-specific knockdown of A20 increases TNFα-induced toxicity[192]. On the other hand, hepatocyte-specific upregulation of A20 protects against D-Gal/LPS-mediated liver injury, also under high TNFα-levels[193]. We reasoned that knockdown of our candidate genes could be modulating the expression of A20, delaying the NF-κB oscillatory phenotype and simultaneously altering the cytotoxic potential of TNFα stimulation during diclofenac and carbamazepine exposure. To monitor A20 expression using live cell imaging, we established a BAC-GFP A20 HepG2 reporter cell line.

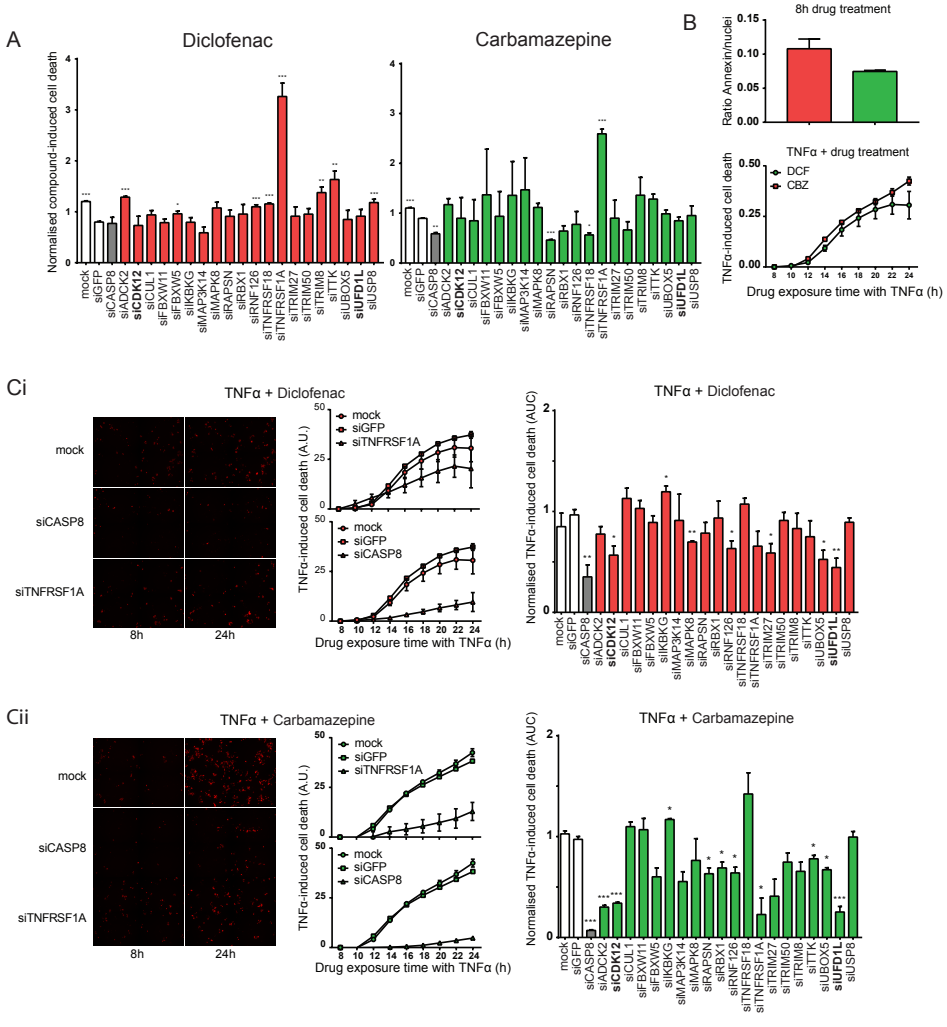

Fig. 4: **Effect of modulators of NF-κB oscillation phenotype on TNFα/drug-induced cytotoxicity** Live apoptosis imaging of parental HepG2 cells with knockdowns resulting in a "no oscillation" phenotype after 500 μM diclofenac or 500 μM carbamazepine pre-incubation for 8 hours followed by stimulation with TNFα (10 ng/mL) for 16 hours. The amount of AnV is normalized to the number of cells. A) Apoptosis after only drug-exposure of eight hours in cells with candidate knockdown, where the AUC is presented as a fold change of mock/siGFP condition. B) The upper panel reflects the ratio of AnV staining and number of nuclei after 8 hours drug exposure. The lower panel shows the increase of cell death upon TNFα-stimulation over time. C) Representative examples of AnV staining in control conditions in the left panel, quantified in the middle graphs. In the right panel, the increase of apoptosis upon TNFα with or without candidate gene knockdown has been depicted in AUC, normalized to the mock/siGFP condition. All data is represented as the mean +/- SEM. Diclofenac data are three independent experiments, carbamazepine data are two independent experiments. Significance is defined with a two-tailed student's t-test where * P≤0.05, ** P≤0.01 and ***P≤0.001.

In this cell line, we could monitor the expression of A20-GFP that is controlled by an endogenous promoter. Only carbamazepine pre-treatment suppressed A20-GFP background expression significantly (Fig.5A). We then evaluated the effect of knockdown of our 20 candidate genes that inhibit NF-κB translocation. Knockdown of CDK12 and TTK slightly increased background A20-GFP expression levels, while TRIM50 decreased A20 expression significantly; this was unaffected by diclofenac or carbamazepine treatment (Suppl. Fig. 4). Stimulation with TNFα strongly increased the expression of A20-GFP; this response was significantly inhibited by pre-treatment with either diclofenac or carbamazepine (Fig.5Aii). Importantly, KD of TNFR1 and IKBKG (NEMO/IKKγ) inhibited the A20-GFP induction by TNFα, confirming that the upregulation of A20 is likely TNFα-induced NF-κB signaling dependent. Knockdown of ADCK2, RAPSN and TRIM50 also strongly inhibited TNFα-induced A20-GFP induction. On the other hand, knockdown of CDK12, TRIM8, TTK and USP8 increased TNFα-mediated A20-GFP induction. While carbamazepine had a limited influence on the KD effects, diclofenac exposure increased the variability and in general suppressed the effect of knockdown conditions upon TNFα-induced A20-GFP expression (Fig. 5B). While both knockdown of CDK12 and UFD1L were most effective in inhibiting TNFα-induced cell death under diclofenac and carbamazepine conditions (Fig. 4), only siCDK12 and not siUFD1L enhanced TNFα-induced A20-GFP expression (Fig. 5). This effect of CDK12 knockdown was maintained in drug-treated conditions (Fig.5C).

A20 expression is essential for both delayed TNFα-induced NF-κB oscillation and the protective effect of both CDK12 and UFD1L knockdown in diclofenac pre-treated cells

Next, we investigated the functional relationship between CDK12, UFD1L and regulation of A20 expression, in the context of TNFα-induced cytotoxicity. For this purpose, we performed siRNA-mediated knockdown of A20 together with the knockdowns of CDK12 or UFD1L. Double knockdown retained robust reduction in protein expression (Suppl. Fig. 5). Single knockdown of A20 strongly enhanced the cytotoxic potential of TNFα upon diclofenac or carbamazepine pre-exposure (Fig. 6A). While knockdown of CDK12 or UFD1L alone inhibited TNFα/compound cytotoxicity, this effect was partially reversed to mock-GFP knockdown levels by additional A20 knockdown. However, knockdown of CDK12 or UFD1L did still inhibit mock/GFP + A20 knockdown toxicity (Fig. 6B). Together, these data suggest a functional dependency between UFD1L, CDK12 and A20 in TNFα/diclofenac-induced cytotoxicity. Finally, we tested whether the delayed TNFα-induced NF-κB oscillation phenotype induced by CDK12 or UFD1L knockdown was also dependent on A20 expression. For this purpose, RelA-GFP cells were transfected with siRNA leading to a double knockdown for the candidate gene and A20.

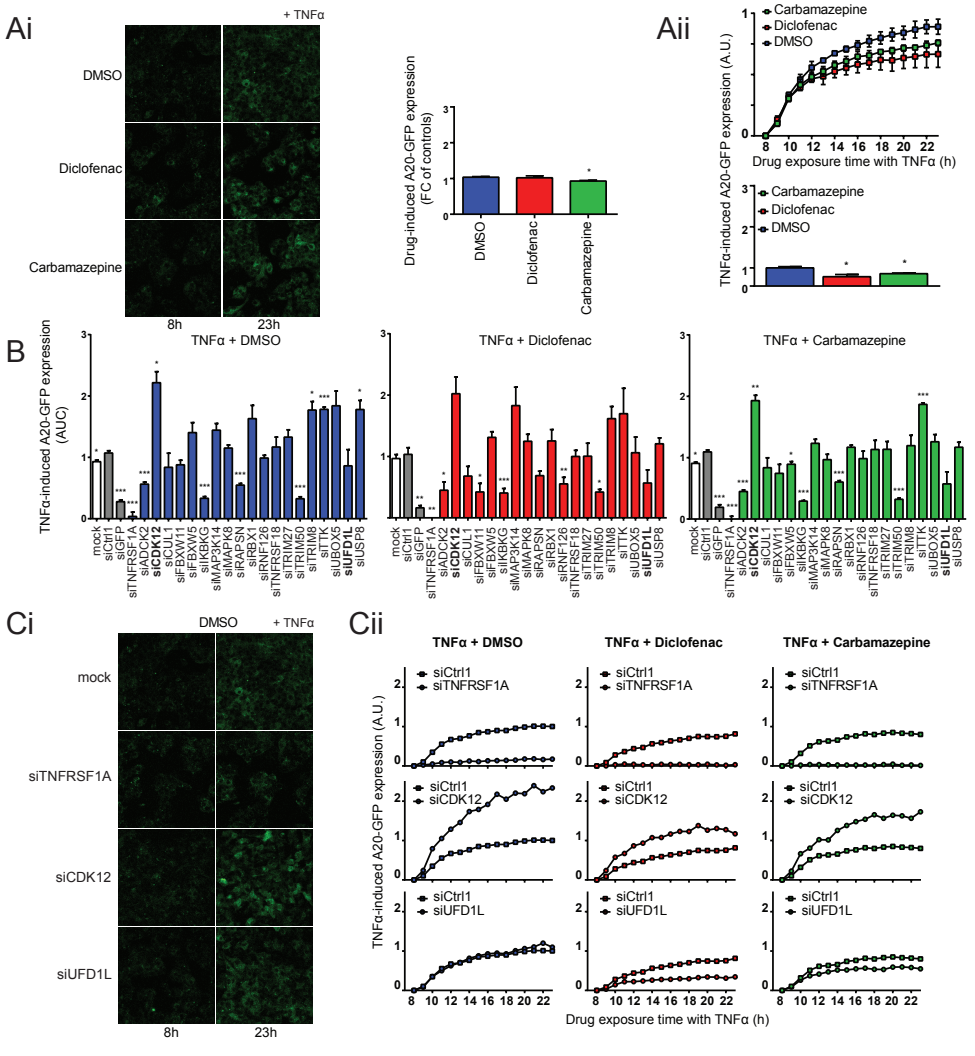

Fig. 5: **Several modulators of NF-κB oscillatory response affect A20 expression strongly** Live confocal imaging of A20-GFP BAC reporter cell line upon 500 μM diclofenac or 500 μM carbamazepine treatment followed by stimulation with TNFα (10 ng/mL) for 16 hours. Ai) Examples of TNFα-induced A20 expression under DMSO, diclofenac or carbamazepine treatment, with the 8h pre-treatment conditions quantified. Aii) Quantification of the A20-GFP time-response dynamics after TNFα-addition, and the representation in AUC values normalized to the DMSO control condition. B) AUC of the A20-GFP response after TNFα-addition, normalized to mock/siCtrl1 conditions per compound pre-treatment. Ci) Visualization of the effect of two candidate genes and controls on A20-GFP expression. Cii) Representative examples of the quantification of the response in Ci. All data is from three independent experiments, +/- SEM. Significance is defined with a two-tailed student's t-test where * P≤0.05, ** P≤0.01 and ***P≤0.001.

This was followed by stimulation with TNF and live cell imaging. The oscillation phenotype of single knockdown of A20 was similar to double knockdown of CASP8/A20. Moreover, knockdown of the TNF receptor and A20 fully abolished oscillatory NF-κB responses, thus confirming the functionality of double knockdowns in the assessment of the oscillatory response (Fig. 6C). A20 knockdown partially reversed the delay in TNFα-induced NF-κB oscillation caused by siUFD1L, and more pronouncedly reversed the delay by siCDK12 (Fig. 6C). This CDK12 knockdown reversal led to a normal population distribution of the oscillatory response, with more than 50 % of the cells demonstrating three NF-κB translocation events. This suggests that CDK12 exerts regulation of NF-κB oscillation partially via A20.

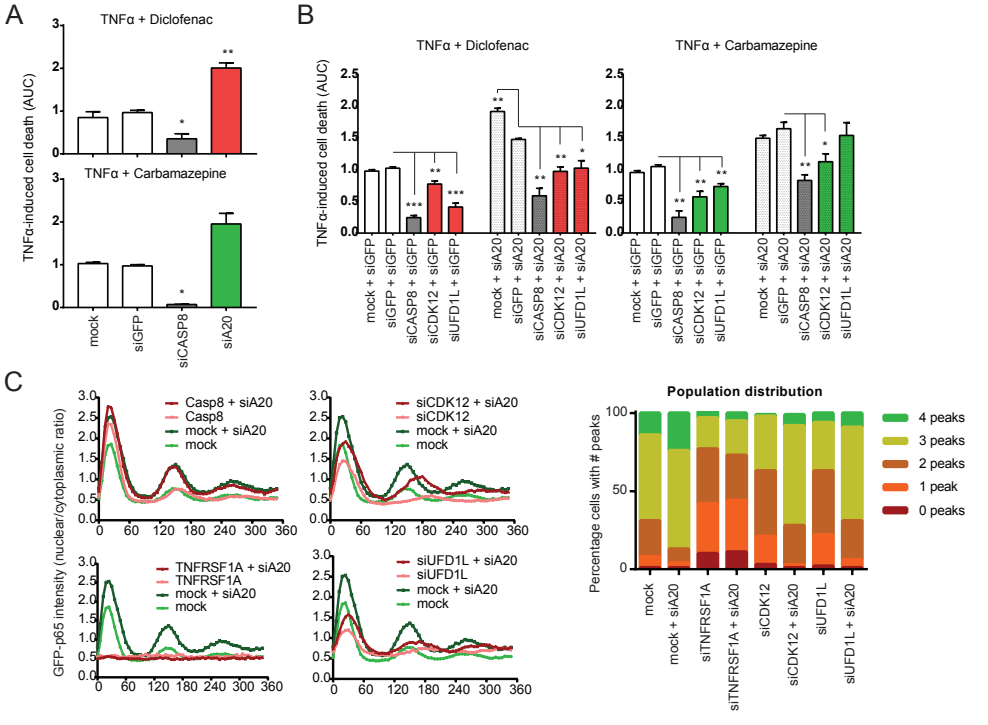

Fig. 6: **Functional interplay between CDK12, UFD1L and A20 in TNFα-induced NF-κB oscillation and cytotoxicity** (A) Live apoptosis imaging of parental HepG2 cells with an A20 knockdown after 500 µM diclofenac or 500 µM carbamazepine pre-incubation for 8 hours followed by stimulation with TNFα (10 ng/mL) for 16 hours. B) Live apoptosis imaging of wild type HepG2 with A20 or GFP knockdown together with knockdown of the candidate genes. After 500 µM diclofenac or 500 µM carbamazepine pre-incubation for 8 hours, cells were imaged upon stimulation with TNFα (10 ng/mL) for 16 hours. All data is the mean from three independent experiments +/- SEM. Significance is defined with a two-tailed student's t-test where * P≤0.05, ** P≤0.01 and ***P≤0.001. C) Live imaging of GFP-p65 cells with A20 or GFP knockdown together with knockdown of the candidate genes upon TNFα stimulation (10 ng/mL) for 6 hours. Right panel reflects the population distribution of the number of peaks of the single cell p65 oscillatory phenotype. Data is the mean from two independent experiments.

In summary, these data imply interaction of both CDK12 and UFD1L with A20 function, whereby A20 levels are partially responsible for modulating NF-κB activation as well as the apoptotic response. We anticipate that CDK12-induced regulation of TNFα-induced responses is partially due to direct modulation of A20 expression levels.

Discussion

In this study we report the systematic discovery of cell signaling components that control the TNFα-induced NF-κB nuclear translocation dynamics. From in total 1567 genes that cover kinases, (de)ubiquitinases and several mediators of TNF-receptor and Toll-like receptor signaling, we identified 46 candidate genes that modulate NF-κB oscillatory behavior. Of these, 24 genes have previously been described to affect NF-κB activity, including well- characterized components of TNFR signaling pathway IKKγ (NEMO), NIK (MAP3K14), A20 (TNFAIP3) and CYLD (Table 1). Known inhibitors of NF-κB activation indeed enhanced the oscillatory behavior upon knockdown in our screening setup. In line with the validity of our NF-κB reporter model, knockdown of previously established activators of NF-κB nuclear translocation led to a block of NF-κB oscillation. Our live cell imaging screen discovered 22 not previously described regulators of TNFα-induced NF-κB oscillation: 3 genes that increased the NF-κB oscillatory phenotype (MAKP4, UBE3A and MASTL) and 17 genes that decreased or blocked the NF-κB oscillatory phenotype (PHF5A, CDK12, USP8, ADCK2, RAPSN, RFN126, TRIM50, TTK, UBOX5, AATK, BAHD1, MVK, TTBK1, and UNK) (Table 1).

Upon TNFα stimulation, cytoplasmic NF-κB translocates to the nucleus, thereby inducing transcription of genes that are involved in cell survival and inflammatory processes. In many cell types, this translocation has been found to be oscillatory upon tonic TNF stimulation[155]. Several studies have established the relation between the oscillatory phenotype of NF-κB translocation and target gene transcription upon TNFα stimulation, both on population level and single cell level [26–28,154,194]. Very low or pulse-wise stimulation of cells increases the fraction of cells with only one initial NF-κB nuclear translocation, which affects the expression of especially late TNFα target genes, while early target gene expression remains relatively unaffected[28,194]. Several candidate genes demonstrated a reduced amount of oscillatory peaks and/or a delay of the second peak of NF-κB translocation on population level upon TNFα stimulation. We anticipate that this will affect the expression of downstream target genes, which in turn will determine the biological outcome of NF-κB activity, including the onset of apoptosis.

Inhibition of NF-κB activity enhances TNFα-induced cytotoxicity[17]. Several drugs that have a high liability for idiosyncratic drug-induced liver injury, including diclofenac and carbamazepine, delay TNFα-induced NF-κB oscillation[42,43]. Therefore, we focused on genes that inhibit TNFα-induced NF-κB oscillatory behavior upon knockdown. CDK12 and UFD1L were among the strongest effectors of TNFα/drug-induced cytotoxicity (Fig. 4C). Interestingly, CDK12 knockdown also had a strong inducing effect on TNFα-induced A20 expression; this was not observed for UFD1L knockdown (Fig. 5B and C). The moderate cytoprotective effect of CDK12 knockdown under drug exposure conditions likely depends

on this enhanced A20 upregulation, as double knockdown of CDK12/A20 reversed the cytotoxicity of drug/TNFα partially. Several other modulators of NF-κB oscillatory behavior and TNFα-induced cytotoxicity also affected A20 upregulation, albeit less pronounced than knockdown of CDK12. In summary, this study demonstrates a critical role for various signaling components in NF-κB activity and cytotoxicity, possibly via the modulation of A20 expression.

We here demonstrate for the first time that knockdown of the stress activated kinase CDK12 induces a major increase in TNFα-induced A20 expression. CDK12 interacts with many proteins involved in RNA processing, including splicing factors[195]. However, the best-characterized function of CDK12 is the phosphorylation of Ser2 on the C-terminal domain of RNA Pol II[196,197]. Interestingly, CDK12 kinase function has been implicated in cellular stress response pathways, by upregulating the transcription of specific stress-induced target genes of p53 and Nrf2[198,199]. In our system, the expression of A20 induced by diclofenac and carbamazepine was slightly enhanced by CDK12 knockdown and the TNFα-induced A20 expression was more than 2-times enhanced by CDK12 knockdown (Fig 5). Together these data indicate that CDK12 acts as a suppressor of drug-induced A20 upregulation. In general, A20 expression is quickly upregulated upon TNFα stimulation. The pre-formed transcription elongation complex containing A20-specific elongation factors ensures the rapid transcription of the gene and subsequent splicing and capping of the pre-mRNA[200,201]. Ser2 phosphorylation plays an important role in this process, as it is essential for the elongation process to proceed. Although the common Ser2 kinase CDK9 dissociates quickly after the initiation of transcriptional activity of RNA Pol II, Ser2 levels are maintained during elongation of A20 RNA transcripts[200]. We hypothesize that CDK12 suppresses TNFα-induced A20 expression through direct modulation of transcriptional activity of RNA Pol II.

Our data demonstrate that UFD1L is essential in the NF-κB oscillatory behavior and onset of TNFα/drug-induced cytotoxicity; yet, UFD1L knockdown did not enhance TNFα-induced A20 upregulation. Together with Npl4, UFD1L acts as an adaptor complex for AAA+ ATPase VCP/p97 to bind ubiquitinated proteins targeted for proteasomal degradation[202]. This complex has been reported to facilitate the degradation of the inhibitor of NF-κB, IκBα, upon TNFα stimulation[182]. However, in our hands, knockdown of UFD1L did not abolish the phosphorylation and breakdown of IκBα, indicating normal function of the IKK-complex (Suppl. Fig. 6). Other characterized functions of UFD1L in human cells converge on protection of the cellular homeostasis. UFD1L is involved in ER-associated degradation, cell cycle progression and mitosis[203,204]. Interestingly, the downregulation of endogenous UFD1L induces cell cycle arrest by upregulation of p27 in tunicamycin-induced ER stress[205]. Our previous work demonstrated a key role for ER stress in executing and modulating TNFα/drug-induced cell death[16]. We hypothesize that the depletion of UFD1L might affect ER stress and hence modulate TNFα/drug-induced cytotoxicity and NF-κB oscillation.

In the past years, the function of A20 in the regulation of TNFα-induced NF-κB activation and apoptosis has received much attention. We observed that A20 is a critical

determinant in NF-κB oscillatory behavior as well as the onset of TNFα/drug-induced cytotoxicity. Liver-specific up- or downregulation of A20 shows respectively protective or detrimental effects on TNFα-induced toxicity *in vivo*[192,193]. We anticipate that our candidate genes that affect A20 expression will also affect the susceptibility of liver cells to apoptosis onset under *in vivo* circumstances. Thus, we report here for the first time that besides CDK12 also TRIM8, TTK and USP8 strongly enhance A20 upregulation upon knockdown; reversely, knockdown of receptor-associated molecule RAPSN and E3-ligase TRIM50 strongly downregulate A20 expression (Fig. 5B). Since this involves different signaling molecules, this provides insight in the complexity of A20 modulation and hence modulation of NF-κB activity and TNFα-induced cytotoxicity.

In conclusion, our study determined novel key regulators of the TNFα response, as detected by live-cell imaging of NF-κB oscillation, A20 expression and modulation of cytotoxicity. Acute liver failure caused by drug-induced toxicity is a major challenge and its outcome is linked to an exacerbated inflammatory phenotype in patients[206]. We anticipate that our candidate genes are critical players in the regulation of inflammatory responses in the onset of idiosyncratic drug-induced liver injury.

Acknowledgements

This work was supported by the TI Pharma (grant agreement D3-201), the IMI MIP-DILI project (grant agreement 115336) and the European Union's Horizon 2020 research and innovation project EU-ToxRisk (grant agreement No 681002).

Author contributions

B.H, L.F and S.H designed, performed and analysed experiments, wrote the manuscript and designed figures. G.B, M.V and A.K performed and analysed experiments. Z.D performed analysis. H. d. B. advised on the technical microscopy setup. S.L.D advised on sustainable data repository. J.M, M. d. G and B. v. d. W advised on experimental design and performed critical reading of the manuscript.

Gene Symbol	Also known as	Name	Function	DMSO	DCF	Regulator of NF-κB	References
			Decreased				
PHF5A		PHD finger protein 5A	splicing factor	Decreased	Decreased	(-)	(-)
UCHL1		ubiquitin carboxyl-terminal esterase L1	hydrolase	Decreased	Different pattern	inhibitor	Takami, 2007; Karim 2013
			Increased				
AGTR2	AT2	angiotensin II receptor type 2	receptor	Increased	Increased	Activator/inhibitor	Guo, 2008; Rompe, 2010; Pandey, 2015; Zhu 2015
MAPK4	ERK-4	mitogen-activated protein kinase 4	kinase	Increased	Increased	(-)	(-)
MAPKAPK2	MK2	mitogen-activated protein kinase-activated protein kinase 2	kinase	Increased	Increased	Inhibitor	Gorska, 2007
SENP2		SUMO1/sentrin/SMT3 specific peptidase 2	hydrolase	Increased	Increased	Inhibitor/Activator	Lee, 2011
TNFAIP3	A20	tumor necrosis factor alpha-induced protein 3	hydrolase/ligase	Increased	Increased	Inhibitor	Shembade 2012, Ma 2012
RELA	p65	v-rel reticuloendotheliosis viral oncogene homolog A	nucleic acid binding	Different pattern	Increased	Inhibitor	
TNFRSF17	BCMA	tumor necrosis factor receptor superfamily, member 17	receptor	Different pattern	Increased	Activator	Alexaki, 2012
			Stopped				
CDK12	CRK7; CrkRS	cyclin-dependent kinase 12	kinase	Decreased	No oscillation	(-)	(-)
RBX1		ring-box 1	ligase	Decreased	No oscillation	Inhibitor	Lee, 2009
USP8		ubiquitin specific peptidase 8	hydrolase	Decreased	No oscillation	(-)	(-)
TNFRSF18	GITR	tumor necrosis factor receptor superfamily member 18	receptor	No oscillation	Decreased	Activator	Placke, 2010
ADCK2		aarF domain containing kinase 2	unclear	No oscillation	No oscillation	(-)	(-)
CUL1		cullin 1	ligase	No oscillation	No oscillation	Activator	Tan, 1999
FBXW11	BTRCP2	F-box and WD repeat domain containing 11	ligase	No oscillation	No oscillation	Activator	Suzuki, 2000
FBXW5		F-box and WD repeat domain containing 5	ligase	No oscillation	No oscillation	(-)	(-)
IKBKG	NEMO	inhibitor of kappa light polypeptide gene enhancer in B-cells kinase gamma	enzyme regulator	No oscillation	No oscillation	Activator	Israel, 2010
MAP3K14	NIK	mitogen-activated protein kinase kinase kinase 14	kinase	No oscillation	No oscillation	Activator	Zarnegar, 2008
MAPK8	JNK1	mitogen-activated protein kinase 8	kinase	No oscillation	No oscillation	Inhibitor	Tan, 2009
RAPSN	rapsyn	receptor-associated protein of the synapse	receptor adaptor protein	No oscillation	No oscillation	(-)	(-)
RNF126		ring finger protein 126	unclear	No oscillation	No oscillation	(-)	(-)
TNFRSF1A	TNFR1	tumor necrosis factor receptor superfamily member 1A	receptor	No oscillation	No oscillation	Activator	
TRIM27	RFP	tripartite motif containing 27	ligase	No oscillation	No oscillation	Inhibitor	Zha, 2006
TRIM50		tripartite motif containing 50	ligase	No oscillation	No oscillation	(-)	(-)
TRIM8		tripartite motif containing 8	ligase	No oscillation	No oscillation	Activator	Li, 2011; Tomar, 2012
TTK	PYT	TTK protein kinase	kinase	No oscillation	No oscillation	(-)	(-)
UBOX5		U-box domain containing 5	enzyme modulator	No oscillation	No oscillation	(-)	(-)
UFD1L		ubiquitin fusion degradation 1 like	enzyme modulator	No oscillation	No oscillation	Inhibitor	Li, 2014
			Micellaneous				
TSKS		testis-specific serine kinase substrate	unclear	Different pattern	Different pattern	(-)	(-)
MLL2		myeloid/lymphoid or mixed-lineage leukemia 2	nucleic acid binding	Different pattern	No oscillation	Activator	Kaikkonen, 2013
AATK	AATYK	apoptosis-associated tyrosine kinase	kinase	No oscillation	Different pattern	(-)	(-)
CYLD		cylindromatosis	hydrolase	No oscillation	Increased	Inhibitor	Kovalenka, 2003; Urbanik, 2014
NTRK3	TRKC	neurotrophic tyrosine kinase receptor type 3	kinase	No oscillation	not different	Activator	Burke, 2003
BAHD1		bromo adjacent homology domain containing 1	nucleic acid binding	No oscillation	not different	(-)	(-)
MVK		mevalonate kinase	kinase	No oscillation	not different	(-)	(-)
TTBK1		tau tubulin kinase 1	kinase	No oscillation	not different	(-)	(-)
UNK	unkempt	unkempt homolog	ligase	No oscillation	not different	(-)	(-)
FBXW9		F-box and WD repeat domain containing 9	ligase	not different	Different pattern	(-)	(-)
MAP3K8	COT, TPL2	mitogen-activated protein kinase kinase kinase 8	kinase	not different	Increased	Activator	Gewurz, 2012
OTUB2		OTU domain ubiquitin aldehyde binding 2	hydrolase	not different	Increased	Inhibitor	Li, 2010
UBE3A		ubiquitin protein ligase E3A	ligase	not different	Increased	(-)	(-)
PHF19		PHD finger protein 19	nucleic acid binding	not different	No oscillation	(-)	(-)
STRADA	STRADalpha	STE20-related kinase adaptor alpha	kinase	not different	No oscillation	(-)	(-)
MASTL	greatwall	microtubule associated serine/threonine kinase-like	kinase	Increased	not different	(-)	(-)
USP15		ubiquitin specific peptidase 15	hydrolase	Increased	not different	Inhibitor	Schweizer, 2007

Table 1

Supplementary Figures

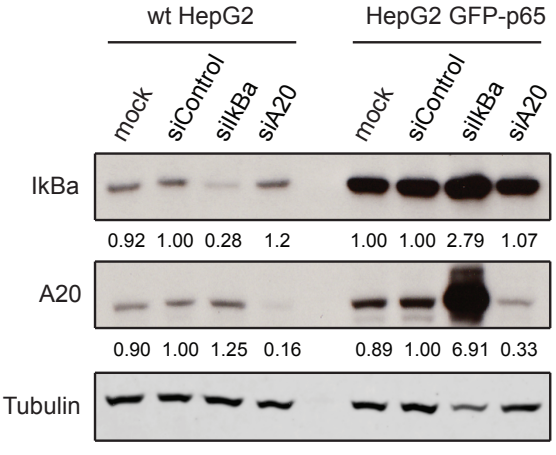

Suppl.Fig.1: **siRNA-mediated knockdown is successful in wildtype and GFP-p65 HepG2 cells** 50 nM siRNA SMARTpool transfection on positive controls, siA20 and siIκBα, results in successful knockdown using INTERFERin tranfection reagent, as determined by western blotting. In RelA-GFP cells the knockdown of IκBα results in higher IκBα levels after 72 hours of knockdown, since knockdown of this inhibitor leads to enhanced p65 activity during this period and thereby increased IκBα transcription.

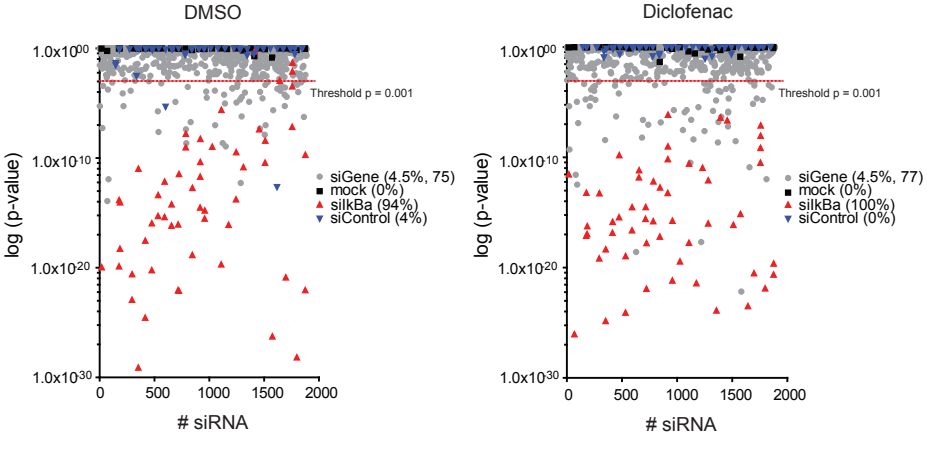

Suppl.Fig.2: **P-value distribution of the hits and the positive and negative controls** P-values of the positive control IκBα represented among all screen results. Under DMSO conditions the true discovery rate was 0.94 and 0.76 for siIκBα and siA20 respectively while the false discovery rate was 0.04. Under DCF conditions the corresponding values were, 1, 0.92 and 0 respectively. 4.5% of the screened genes were found to have an effect on the oscillation under DMSO conditions while 4.7% were determined to give a significant effect after DCF pre-exposure.

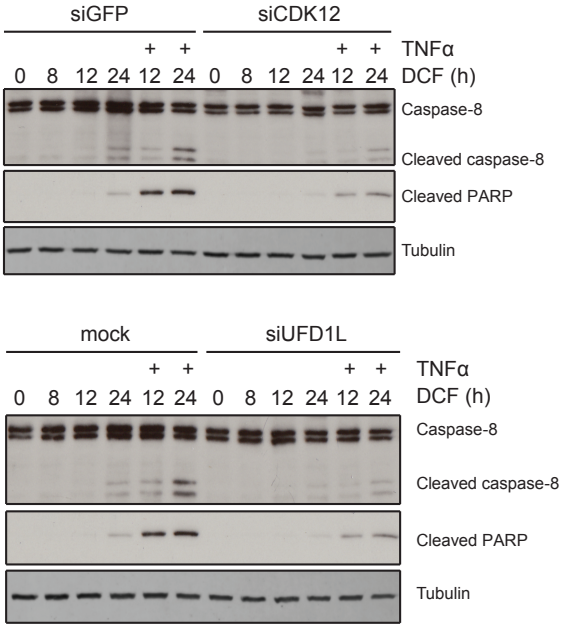

Suppl.Fig.3: **Drug/TNFα mediated caspase-8 and PARP cleavage is decreased in candidate gene knockdown conditions** Western-blot analysis of cleaved PARP and caspase-8 in wild-type HepG2 cells with indicated knockdowns of candidate genes or controls. Cells were treated with 500μM diclofenac, with or without TNFα (10 ng/mL) after 8 h pre-exposure with diclofenac as indicated.

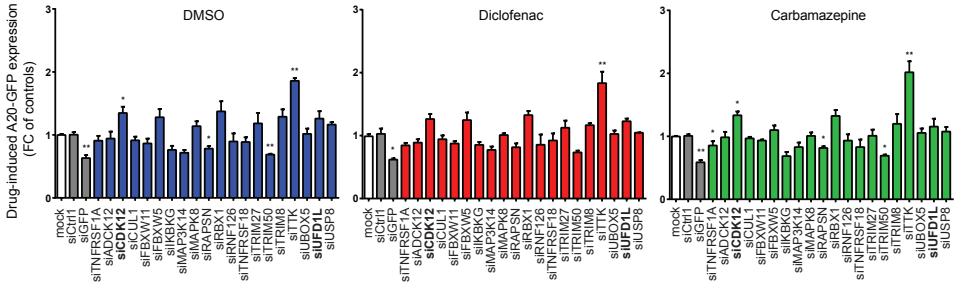

Suppl.Fig.4: **Several candidate gene knockdowns affect A20 expression** Live confocal imaging of A20-GFP BAC reporter cell line upon DMSO, 500μM diclofenac or 500μM carbamazepine treatment. AUC of over time quantification is normalized to mock/siCtrl1 condition. Data is from three independent experiments, +/- SEM. Significance is defined with a two-tailed student's t-test where * P≤0.05, ** P≤0.01 and ***P≤0.001.

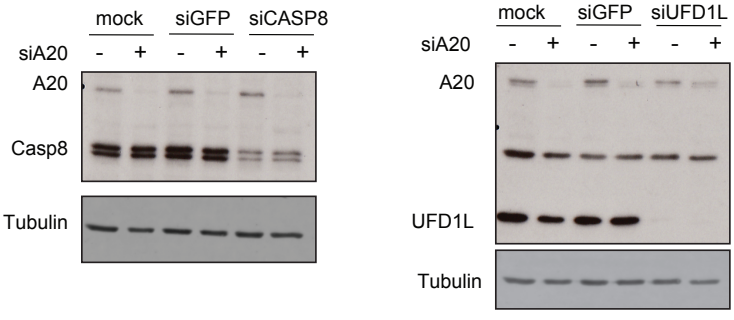

Suppl.Fig.5: **siRNA-mediated double knockdown is retains robust knockdown efficiency** Western-blot analysis of double-knockdown in wild-type HepG2 cells. A20, caspase-8 and UFD1L expression bands are indicated.

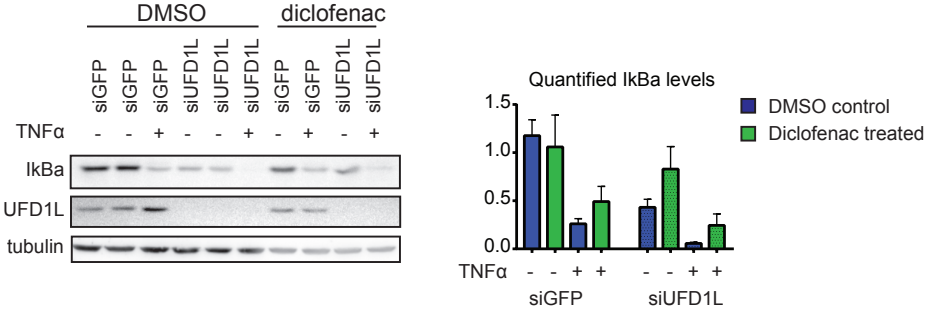

Suppl.Fig.6: **Knockdown of UFD1L does not impair TNFα-induced IκBα degradation** Western-blot analysis of IκBα and UFD1L levels of cells with UFD1L knockdown. Cells were pre-treated with 500 μM diclofenac or DMSO and stimulated with TNFα (10 ng/mL) for 15 minutes, as indicated. Quantification is the mean normalized expression of three independent experiments with error bars representing SEM. The results were not significant according to a two-tailed t-test ($p > 0.05$), compairing control and UFD1L knockdown conditions.

Chapter 4

Drugs with liver toxicity liability enhance both TNFα-induced and intrinsically drug-induced inflammatory target gene expression

Highlights

- Drug exposure enhances TNFα-induced target gene expression, independent of either kinetic gene expression profile of the target gene or liver toxicity hazard of the drug
- Drug exposure itself enhances gene expression typical for TNFα
- Drug-induced gene expression is negatively regulated by oxidative stress-induced NF-κB family members RelB and cREL, and induced by RelA

This chapter is based on a manuscript in preparation:

Suzanna Huppelschoten[1], Steven Wink[1], Wanda van der Stel[1], Anke Essing[1], Cécile Parmentier[2], Lysiane Richert[2], Bob van de Water[1]

Drugs with liver toxicity liability enhance both TNFα-induced and intrinsically drug-induced inflammatory target gene expression

[1]Division of Toxicology, Leiden Academic Centre for Drug Research, Leiden University, Leiden, The Netherlands
[2]KaLy-Cell, Research & Development, 67115 Plobsheim, France Leiden University

Drug-induced liver injury (DILI) complicates drug-development and clinical practice. Activation of the immune system has been increasingly recognized as an important host factor in the etiology of DILI. Previously, we and others showed that hepatocyte stimulation with the abundant pro-inflammatory cytokine TNFα together with drugs can culminate in synergistic hepatotoxicity. Here, we systematically evaluated the interaction of ten severe or less severe DILI drugs with the temporal TNFα-induced expression of NF-κB target genes, using high throughput transcriptomics of 44 target genes. The DILI compounds included diclofenac, carbamazepine, nefazodone, troglitazone, tolcapone, entecapone, pioglitazone, flucoxacillin, acetaminophen and metformin. TNFα caused the anticipated differential temporal induction of both early, middle and late NF-κB target genes in HepG2 cells. DILI compounds caused a significant enhancement of TNFα-induced target gene expression, with metformin, diclofenac, carbamazepine and nefazodone giving he strongest responses. Interestingly, DILI compound exposure alone also induced expression of target genes typically induced by TNFα. Drug-induced expression of several NF-κB subunits, notably RelB and NFKB2, did correlate with oxidative stress responses. Drug-induced NF-κB target gene expression was largely dependent on NF-κB subunit RelA expression, while RelB and cRel acted as suppressors. Altogether these data indicate a critical role for DILI compound-induced cellular perturbations on the modulation of the TNFα-induced inflammatory response. Such responses may have impact on the etiology and progression of DILI.

Keywords: liver toxicity, drug-induced liver injury, TNFα, NF-κB, oxidative stress

Introduction

Drug-induced liver injury (DILI) remains a major problem in both drug development and clinical practice. Most DILI responses are rare and only observed in large population settings, and often missed during clinical trials. There has been an urge to improve the mechanistic understanding of DILI and implement this knowledge in improved *in vitro* testing systems to detect the DILI liability of a novel compound in an early development phase[207].

A critical factor in DILI is the activation of both the innate and adaptive immune system[208]. Subtle immune modulations in both in vitro and *in vivo* experimental systems can invoke severe hepatotoxicity of otherwise harmless drugs[209]. For trovafloxacin, this synergism between the drug and non-toxic doses of LPS in mice is dependent on TNF-receptor signaling[11]. Also, in a repeated dose model of diclofenac in rats, the severity of hepatotoxicity upon LPS exposure is associated with the expression of TNFα[99]. We have shown that diclofenac and TNFα cause synergism in liver cells, which is directly related to a decreased NF-κB nuclear translocation behavior and transcriptional activity[42]. The current literature suggests specific interactions between DILI compounds and TNFR signaling, yet a systematic examination on NF-κB target gene activation in relation to DILI compound/TNFα co-treatment has been lacking so far.

The NF-κB transcription factor family consists of five different genes: RelA (p65), RelB and cRel as the DNA binding subunits with an activation domain, and NFKB1 (p50) and NFKB2 (p52) as DNA binding subunits without activation domain. NFKB1 and NFKB2 are first expressed as precursors p105 and p100. p105 is constantly processed. In contrast, the processing of p100 is dependent on post-translational phosphorylation. Upon extracellular cytokine stimulation (including TNFα) or internal cellular signals, NF-κB heterodimers migrate to the nucleus. This is due to the disassociation from their inhibitory binding partners. The family of inhibitory IκB proteins includes IκBα (NFKBIA), IκBε (NFKBIE) and precursors as p100 (NFKB2)[210].

TNFα binding to the TNFR induces formation of the TNF receptor complex, recruiting TRADD, TRAF2, RIP1, A20, the LUBAC complex and TAK1, among others. TAK1 activates the IKK complex and several MAP kinase signaling pathways. Activated IKK complex phosphorylates IκBα, marking it for proteosomal degradation. Dissociation of the cytoplasmic RelA-p50 causes it to translocate into the nucleus and activate gene transcription. Which target genes are activated depends on the interaction of other signaling pathways with RelA transcriptional activity and varies greatly among different (co-)stimuli and cell types[20]. Currently, the spatio-temporal nuclear translocation dynamics of NF-κB is considered as one of the critical determinants of target gene expression[26,27]. Among the critical target genes are chemokines and cytokines that modulate the inflammation responses, as well as anti-apoptotic proteins that protect cells against cell death[13,211]. However, the dynamics of TNFα-induced NF-κB target gene expression in liver hepatocytes remain unclear.

Here, we systematically characterized the TNFα-induced NF-κB signaling dynamics in the context of adverse drug reactions, using the liver hepatocyte HepG2 cell line. We used high throughput analysis of TNFα target gene expression to assess DILI drug exposure effects kinetically[16,53,212]. We detected many drug-induced changes in TNFα-induced target gene expression, which was not directly correlated to the drug-mediated delayed TNFα-induced RelA oscillatory response. Interestingly, several drug exposures induced expression of specific subsets of NF-κB target gene, including CCL5 and IL8. Their drug-induced gene expression was predominantly dependent on RelA transcriptional activity, but was inhibited by RelB and cRel expression. Drug-induced oxidative stress induction correlated strongly with drug-induced expression of RelB. This shows that drug exposure can both induce and regulate TNFα target gene expression via separate NF-κB family members. Together, these data show the complex nature of DILI compound-induced pertubations of immune signaling pathways and underlines the importance of NF-κB signaling in understanding DILI.

Material and Methods

Cell culture

Human hepatoma HepG2 cells were acquired from ATCC (clone HB8065). HepG2 RelA (p65) BAC GFP reporter cell line was generated and characterized as described previously[44]. HepG2 wild type and BAC GFP reporter were maintained and exposed to

drugs in DMEM high glucose supplemented with 10% (v/v) FBS, 25U/mL penicillin and 25µg/mL streptomycin. The cells were used between passage 5 and 25.

Reagents

Most compound chemicals were acquired through the MIP-DILI consortium (AstraZeneca). Carbamazepine was from Sigma-Aldrich (Zwijndrecht, The Netherlands). Before use, the compounds were freshly dissolved in DMSO; except for metformin and acetaminophen, that were dissolved in DMEM and subsequently spiked with DMSO. TNFα was acquired from R&D Systems (Abingdon, UK). The final treatment concentration contained 0.2% v/v DMSO. AnnexinV (AnV) was prepared in house as described before[42]. All primers were purchased from Sigma Aldrich (Zwijndrecht, The Netherlands). For the splicing experiments, primers were designed based on the FASTA sequence of the most abundant splicing variant. Criteria for the measurement of unspliced transcripts described by Hao and Baltimore[213] were met. For mRNA expression experiments KiCqStart SYBR Green primers were purchased. All primer sequences can be found in Suppl. table 2. All primers were tested for linearity and efficiency.

Live cell imaging

Accumulation and position of GFP levels and Hoechst staining was monitored using a Nikon TiE2000 confocal laser microscope (lasers: 488nm and 408nm). The microscope was equipped with an automated stage and perfect focus system at 37 degrees Celsius with humidified atmosphere and 5% CO_2/air mixture. Before imaging at 20x magnification, HepG2 cells were stained for 45 minutes with 50 ng/mL $Hoechst_{33342}$ to visualize the nuclei. The Hoechst medium was replaced with exposure medium containing the drug or control DMSO. After 8 hours pre-exposure to compound only, the medium was spiked with TNFα (1:20 dilution in 96-well-plate (RelA)) up to a final concentration of 10ng/mL . To prevent a delay in response in the oscillations of the RelA-GFP reporter, was added at the microscope per well, directly upon imaging of the first image(t=0).

Immunofluorescence of primary human hepatocytes

Three donors of cryopreserved PHH (KaLy-Cell, Plobsheim, France) (Suppl. Fig. 4) were thawed in KaLy-Cell thawing medium (KLC-TM; proprietary formulation) and next centrifuged at 168 x g for 20min at room temperature. The cell pellets were resuspended in KLC-washing medium (KLC-WM; proprietary formulation), followed by centrifugation at 100 x g for 5 minutes at room temperature. The cell pellets were resuspended and cultured in KLC- seeding medium (KLC-SM) which was composed of Williams' Medium E (Life Technologies, Paisley, UK) supplemented with 10% heat inactivated foetal calf serum (FCS, Life Technologies), 1 µM dexamethasone (Sigma-Aldrich, St Louis, Missouri), 4 µg/ml insulin (Life Technologies) and 10 U penicillin/10 mg streptomycin (Life Technologies). The attachment efficiency of cryopreserved hepatocytes varied between donors with cell densities ranging between 50000 and 70000 cells per well (96-well plate). KLC-seeding medium was replaced with exposure medium, consisting of William's Medium E and 10 U

penicillin/10 mg strepto- mycin (Life Technologies). Cells were treated with TNFα (10ng/mL) (1:20 dilution in 96 well plate) at indicated timepoints. After fixation in 4% of paraformaldehyde, samples were stained with RelA antibody (SantaCruz). Samples were measured by confocal microscopy using a Nikon TiE2000 confocal laser microscope (lasers: 488nm and 408nm).

Real-time PCR

RNA from compound-treated cells was isolated using the Machery Nagel NucleoSpin (Düren, Germany) kit according to the manufacture's protocol. cDNA synthesis was performed using the RevertAid H Minus First Strand cDNA synthesis kit from ThermoFisher Scientific (Waltham, USA). Real time PCR analysis was performed on the 7900HT Fast Real-time PCR system from Applied Biosystems (Carlsbad, USA) or QuantStudio 6 Flex Real-Time PCR System from ThermoFisher Scientific (Waltham, USA). Primer sequences can be found in Suppl. table 2. Quality control was done based on the amplification and dissociation curves.

Real-time high throughput PCR

cDNA samples were prepared as described above. High throughput Fluidigm PCR data was collected by ServiceXS (Leiden, The Netherlands). Real-Time PCR analysis was performed at ServiceXS using the 96.96 BioMark™ Dynamic Array for Real-Time PCR (Fluidigm Corporation, San Francisco, CA, U.S.A), according to the manufacturer's instructions. Before use on the BioMark array, the cDNA was first subjected to 14 cycles of Specific Target Amplification using a 0.2X mixture of all Taqman Gene Expression assays in combination with the Taqman PreAmp Master Mix (Applied Biosystems), followed by 5-fold dilution. Thermal cycling and real-time imaging of the BioMark array was done on the BioMark instrument, and Ct values were extracted using the BioMark Real-Time PCR analysis software. Quality control performed by ServiceXS was taken into account with analysis of these results, discarding flagged samples and using only Ct values within 5 -35 cycles. The Fluidigm RT-PCR array genes were selected based on previous experiments[16]. Primer sequences can be found in Suppl. table 2. Six housekeeping genes (HMBS, GAPDH, TBP, PSMB6, ACTB, MDH1) were taken along, based on their expression in HepG2 cells in literature[214–216]. The average of these genes was used to generate deltaCt values. For clustering of the HepG2 response on TNFα stimulation, timepoint 0 was substracted and responses were filtered on a fold change of 2 or higher on any timepoint compared to timepoint 0. To focus on the kinetics, responses were scaled between 0 and 1 and clustered using the *hclust* function in the package *pheatmap* with clustering method Ward2, specifying the amount of clusters as 7. The oxidative stress genes were selected upon 2 times upregulation after exposure with 100 µM diethylmaleate or 30 nM CDDO-me (bardoxolone methyl) on one of the selected time points (7 and 24 hours). The upregulated oxidative stress genes were used to rank the compounds by their average drug-induced upregulation. Linear correlation was determined by Pearson's correlation function in base

R. Annotation of protein function is based on literature and focused on liver biology (Suppl. table 1).

Fluorescence reporter image quantification and statistics

Qantitative image analysis was performed with CellProfiler version 2.1.1[158] with an in house developed module implementing the watershed masked algorithm for segmentation[159]. Image analysis results were stored as HDF5 files. Data analysis, quality control and graphics was performed using the in house developed R package H5CellProfiler (Wink *et al*., 2017, manuscript in preparation).

Data management and representation

Data was managed with R, using packages plyr, dplyr, tidyr and reshape2[217,218]. Data visualization was performed using ImageJ, GraphPad Prism and R, using the package ggplot[219].

Statistics

Unless stated otherwise, P-values were calculated using a t-test. All errorbars reflect the standard deviation (SD). For the Fluidigm PCR results, a two-way ANOVA was conducted that examined the effect of compound treatment and time of TNF treatment on gene expression levels. There were statistically significant interaction effects between the effects of time of TNF treatment and compound treatment on gene expression. Next, a Tukey post hoc test for the TNF responses over time under DMSO conditions compared to treatment conditions revealed significant differences. All analysis was done using the stats package in R[220]. P-value < 0.05 is *, P-value < 0.01 is **, P-value < 0.001 is ***.

Results

Dynamics of TNFα-induced NF-κB target gene expression

In hepatocytes, both increased NF-κB activity by knockout of A20 as well as inhibition of NF-κB activity lead to increased hepatotoxicity[17,192]. Various drugs with liver toxicity liability affect NF-κB signaling dynamics induced by TNFα; we have studied this previously in the liver hepatocyte cell line HepG2[42,43]. The dynamics of TNFα-induced target gene expression have been well characterized in mouse embryonic fibroblasts (MEFs). Here, we determined similarity of the TNFα-induced target gene kinetics between MEFs and HepG2 cells. According to literature, TNFα-induced target gene expression is temporally regulated, clustering in three well-characterized groups (early, middle and late) of gene transcription[28] (Fig. 1Ci). These kinetics are in MEFs largely defined by delayed RNA splicing kinetics and mRNA stability[152,213]. Using specific primers for non-spliced and spliced RNA transcripts of NFKBIA (IκBα; early), TNFAIP3 (A20; early), ICAM1 (middle), RELB (middle) and SLC2A6 (late), we characterized the TNFα-induced gene expression and splicing process in HepG2 cells (Fig. 1Bi).

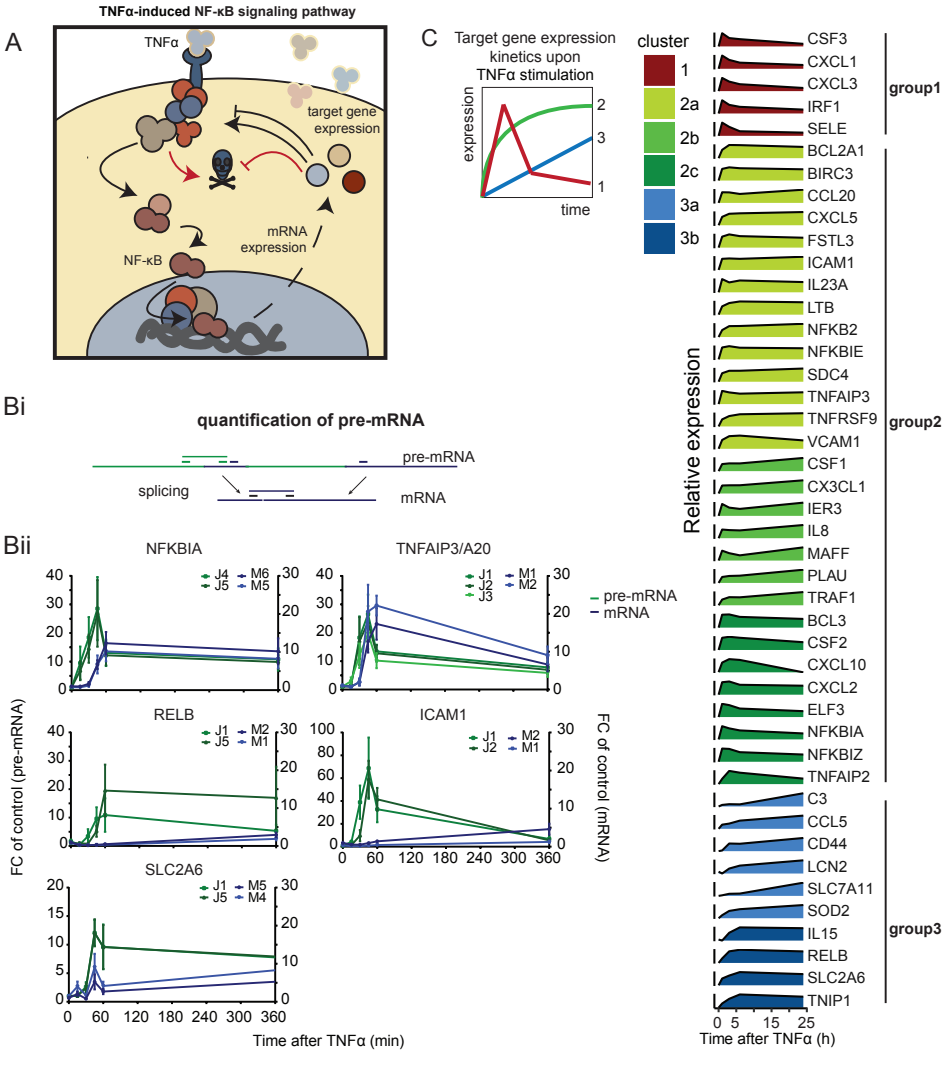

Fig. 1: **Characterization of TNFα-induced NF-κB signaling in HepG2 cells** A) Overview of TNFα-induced NF-κB signaling pathway. Bi) Schematic overview of detection of spliced transcripts. Pre-mRNA is visualized with green introns and blue exons. Pre-mRNA primers bind within an exon and within an intron (green). mRNA primers bind in exons with intermittent introns, ensuring transcription only when the gene is spliced (blue). Bii) RNA expression data of NF-κB target genes upon TNFα exposure. Pre-mRNA transcription is displayed in green and on the left y-axis, spliced mRNA is visualized in blue and on the right y-axis. Error bars represent the standard deviation over three independent experiments. C) Example of literature based TNFα-induced target gene kinetics. Clustering of target gene RNA transcription based on kinetics only (scaled between 0 and 1 and an average of three independent experiments). Cluster 1, 2, and 3 are respectively early, middle and late TNFα-induced target gene expression. Gene annotation can be found in Suppl. Table 1.

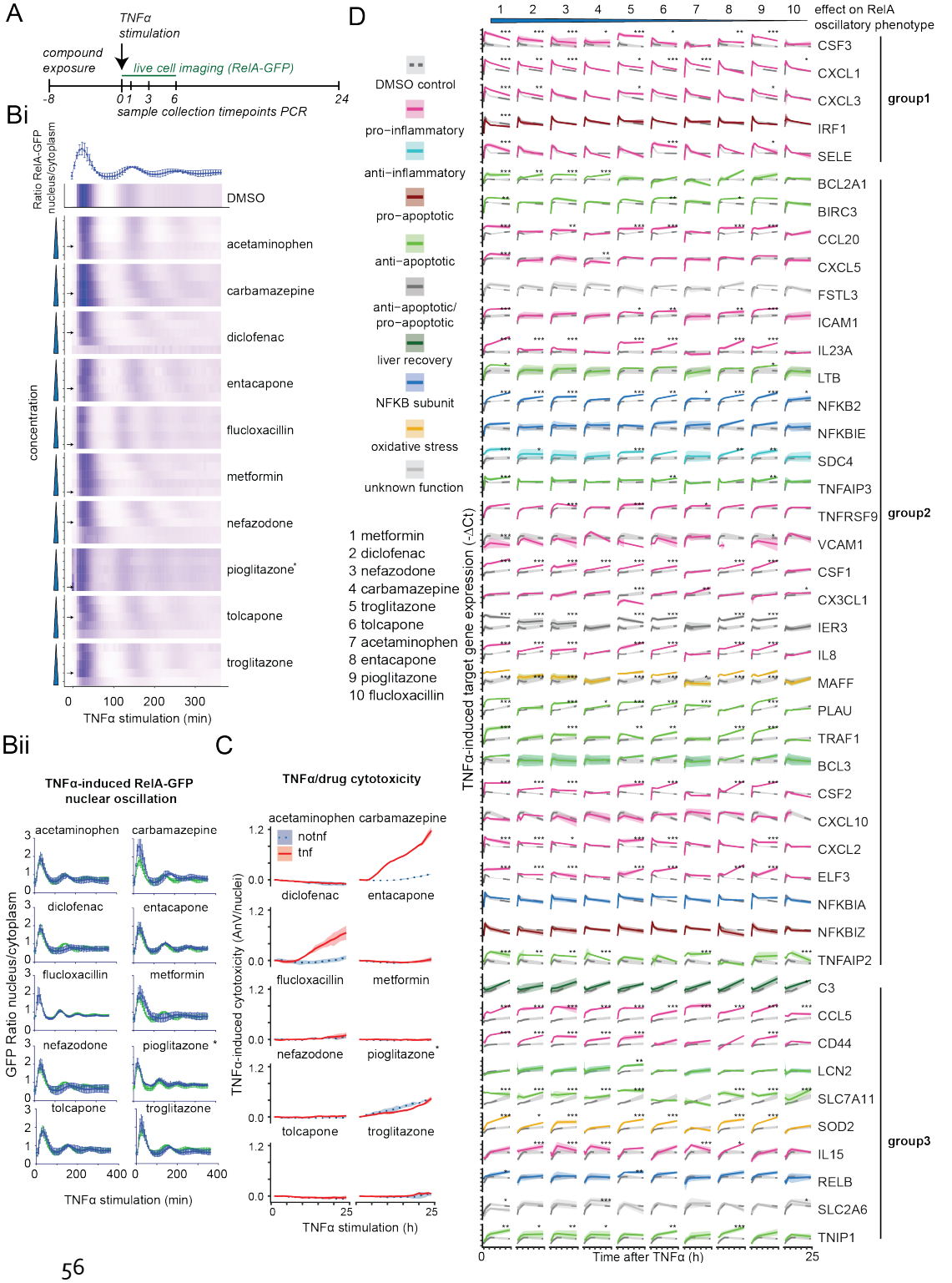
A
TNFα stimulation
compound exposure
live cell imaging (RelA-GFP)
-8
0 1
3
6
24
sample collection timepoints PCR
Bi
Ratio RelA-GFP nucleus/cytoplasm
concentration
DMSO
acetaminophen
carbamazepine
diclofenac
entacapone
flucloxacillin
metformin
nefazodone
pioglitazone*
tolcapone
troglitazone
0
100
200
300
TNFα stimulation (min)
Bii
TNFα-induced RelA-GFP nuclear oscillation
GFP Ratio nucleus/cytoplasm
TNFα stimulation (min)
C
TNFα/drug cytotoxicity
notnf
tnf
TNFα-induced cytotoxicity (AnV/nuclei)
TNFα stimulation (h)
D
effect on RelA oscillatory phenotype
DMSO control
pro−inflammatory
anti−inflammatory
pro−apoptotic
anti−apoptotic
anti−apoptotic/ pro−apoptotic
liver recovery
NFKB subunit
oxidative stress
unknown function
1 metformin
2 diclofenac
3 nefazodone
4 carbamazepine
5 troglitazone
6 tolcapone
7 acetaminophen
8 entacapone
9 pioglitazone
10 flucloxacillin
TNFα-induced target gene expression (-ΔCt)
CSF3
CXCL1
CXCL3
IRF1
SELE
group1
BCL2A1
BIRC3
CCL20
CXCL5
FSTL3
ICAM1
IL23A
LTB
NFKB2
NFKBIE
SDC4
TNFAIP3
TNFRSF9
group2
VCAM1
CSF1
CX3CL1
IER3
IL8
MAFF
PLAU
TRAF1
BCL3
CSF2
CXCL10
CXCL2
ELF3
NFKBIA
NFKBIZ
TNFAIP2
C3
CCL5
CD44
LCN2
SLC7A11
SOD2
IL15
RELB
SLC2A6
TNIP1
group3
Time after TNFα (h)

Fig. 2: **DILI compound exposure delays TNFα-induced RelA translocation and enhances NF-κB target gene expression** A) Time scale overview of experiments. Bi) HepG2 RelA-GFP oscillatory responses upon TNFα stimulation (10 ng/mL). At the top panel, the control DMSO response is visualized as both a line graph and density plot. The nuclear/cytoplasm GFP ratio data is scaled between 0 (white) and 1 (blue). Exact concentrations, and arrow-indicated concentrations used for further experiments can be found in the supplementary data (Suppl. Table 3). *Crystal precipitation of pioglitazone hampered analysis. B.ii RelA-GFP oscillatory responses with the concentration used in further experiments, non-scaled data. Green indicates DMSO treated conditions, blue drug-treated conditions. Error bars represent the standard deviation over three independent experiments. C) Cell death responses over time. Ratio of AnnexinV staining and nuclear area are depicted. Red shading is the standard deviation of two independent experiments. D) TNFα-induced target gene responses with drug exposure, depicted as negative delta Ct values. The drugs are ranked on disruptive RelA-GFP oscillation effects, the numbers correspond to the compound. Colors depict functional annotation as in suppelmentary table 1. The genes are grouped at cluster. The shaded region represents the standard deviation over three independent experiments.

All TNFα-induced genes started with a similar early peak of pre-mRNA, with NFKBIA and TNFAIP3 being slightly faster. NFKBIA and TNFAIP3 mRNA kinetics followed the unspliced transcript dynamics closely, whereas RELB, ICAM1 and SLC2A6 had a clear delay in the mRNA kinetics compared to their unspliced RNA expression (Fig.1B).

Next we applied high throughput RT-PCR to evaluate the dynamics of a larger set of TNFα-induced genes in HepG2 cells. We selected genes based on previous transcriptomics data in human primary human hepatocytes and literature[16]. Of these, 44 were upregulated more than 2-fold upon TNFα exposure. The target genes followed different temporal dynamics representing subsets of early, mid and late expression profiles (Fig. 1C). These individual profiles closely mimicked responses observed in MEFs[152,213]. Together, these data suggest that HepG2 cells present dynamics of TNFα-induced target gene expression similar to MEFs.

Effect of drugs with liver toxicity liability on NF-κB signaling

Several drugs with a liability for drug induced liver injury (DILI) act in synergy with TNFα, inducing cytotoxicity. Therefore, we studied the effect of DILI compounds on TNFα-induced NF-κB signaling. We focused on a selected panel of 10 drugs, based on the Innovative Medicine Initiative MIP-DILI project, each with a different level and mechanism of DILI liability[212]. To determine the optimal compound concentration for high throughput RT-PCR, we evaluated the effect of DILI compounds on TNFα-induced NF-κB nuclear translocation behavior. For this the RelA-GFP BAC HepG2 reporter cells were pre-treated for 8 hours with different concentrations of DILI compounds followed by stimulation with TNFα (Fig. 2A and Suppl. Fig. 5). Most DILI compounds affected the TNFα-induced oscillatory RelA-GFP response at a certain concentration, with metformin, diclofenac, nefazodone and carbamazepine being most potent (Fig. 2B). Based on disruption of RelA-GFP oscillation and toxicity, concentrations were chosen for further research (Suppl. table 3). At these concentrations not much cytotoxicity was observed for exposure to only DILI compounds. Only diclofenac and carbamazepine caused a synergistic cytotoxic response with TNFα (Fig. 1C). Next we determined the effect of pre-treatment on the TNFα-induced temporal gene expression (Fig. 2D). We observed enhanced TNFα target gene expression for most

DILI compounds; this was observed for early, middle and late target genes. Some target genes did not show enhanced induction, including TNFAIP3 and NFKBIA. There was no coherent correlation between RelA oscillatory response disruption and altered target gene expression. While metformin, diclofenac, nefazodone and carbamazepine all induce a clear disruption of TNFα-induced RelA oscillatory kinetics, each caused a different modulation of TNFα-induced target gene dynamics (Fig. 2D).

DILI compounds activate specific NF-κB target genes

DILI compounds can activate many cellular stress signaling pathways including ER stress and oxidative stress responses[16]. Oxidative stress, ER stress and DNA damage can directly modulate NF-κB signaling[13,19]. We therefore reasoned that ongoing stress responses caused by DILI compounds could affect NF-κB signaling, and thereby enhance the TNFα-induced NF-κB signaling. To study this, we compared peak TNFα responses versus the peak DILI compound-induced target gene expression. Interestingly, some TNFα target genes were induced by drug exposure itself (Fig. 3A, and see results of all DILI compounds in Suppl Fig. 1 and 2).

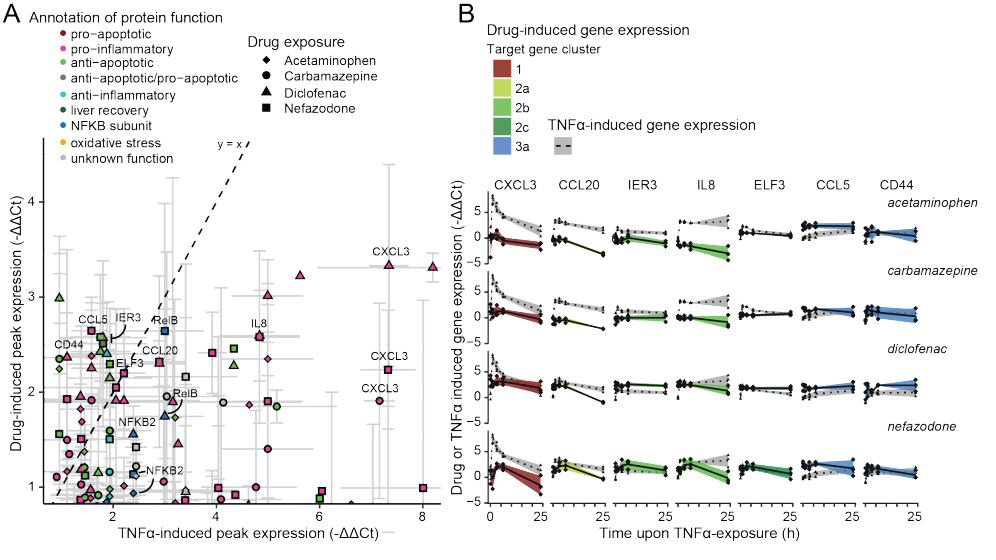

***Fig. 3:* Effect of DILI compounds on TNFα target genes expression** A) Peaks of drug-induced and TNFα-induced expression (negative deltadeltaCt values to DMSO treated control) are depicted. Shapes relate to the drug exposure and colors represent the protein function of the target genes. B) The temporal drug-induced response compared to the TNFα-induced response. The pre-exposure with drugs started 8 hours before the first timepoint (0). The data is displayed as the negative deltadelta Ct values to the DMSO-treated control. The shades or error bars represent the standard deviation over three independent experiments.

The target genes most affected by compound exposure alone included CXCL3, CCL20, IER3, IL8, ELF3, CCL5 and CD44. Diclofenac induced extensive expression of CXCL3, which was also strongly induced by TNFα. In contrast, CCL5 was strongly induced by nefazodone but only mildly induced by TNFα.

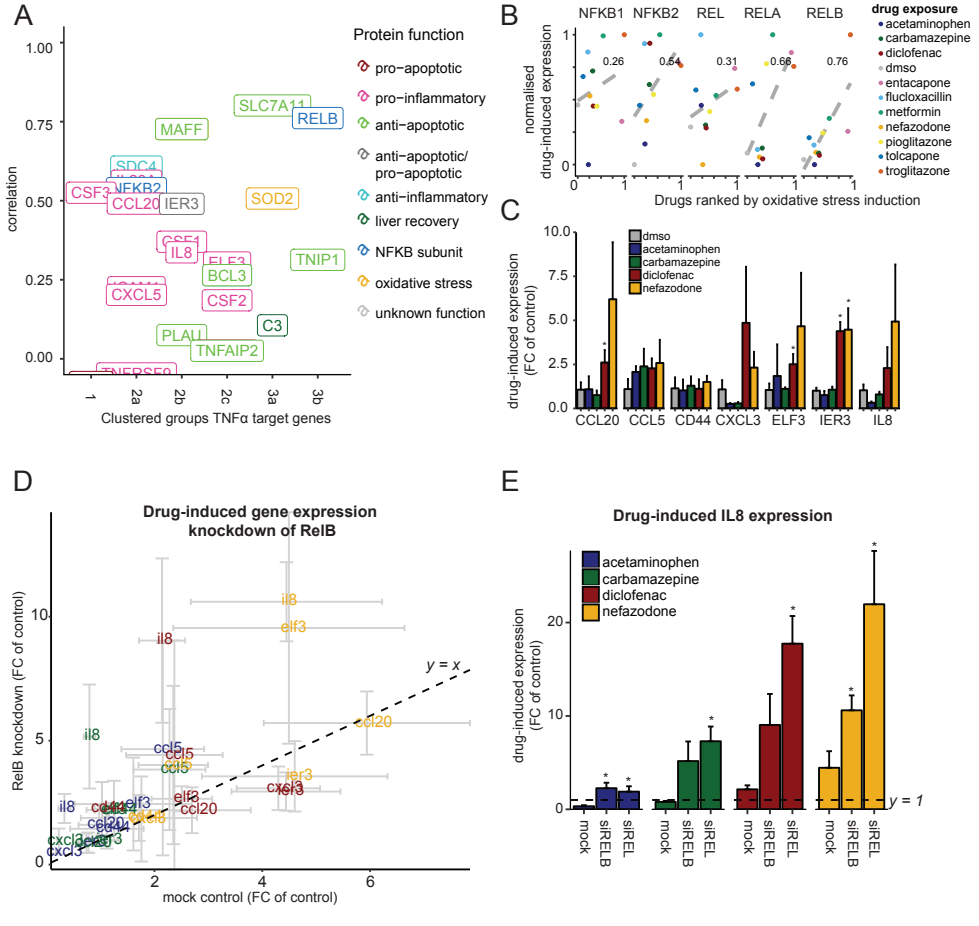

Fig. 4: **Relationship between DILI compound-induced RelB expression and oxidative stress response** A) Graph displays the genes of which the drug-induced expression correlates positively with oxidative stress. The x-axis groups the genes to their TNFα kinetic clusters. The colors depict the protein function in TNFα signaling. B) The drug-induced expression values (the fold change to the control DMSO values) are scaled between 0 and 1. The drugs are ranked based on their oxidative stress induction. The correlation is printed on the graph. Colors reflect the different drug treatments and the grey line shows the linear correlation. C) qPCR based values (Fold change to control samples) per target gene. The colors correspond to the drug exposure. The error bars show the standard deviation. D) The drug-induced expression (Fold change to control samples) is shown on the x-axis versus the drug-induced expression in RelB knockdown cells on the y-axis. The colors reflect drug exposure, data is the average of three independent experiments and the error bars show the standard deviation. Values on the y=x line are not changed upon knockdown. E) Expression of IL8 (Fold change of control) upon drug exposure and with different knockdowns. Dashed line is a fold change of one. The colors show different drug-exposures and error bars reflect the standard deviation over three independent experiments.

Visualization of the temporal expression of these genes in response to DILI compound exposure compared to the TNFα-induced response showed the induction of many typical NF-κB target genes (Fig. 3B, Suppl. Fig. 1). Overall, the drug-induced expression of TNFα-induced target genes was not associated with DILI hazard in humans, a specific kinetic cluster or protein function.

Correlation of NF-κB target gene expression and oxidative stress

Previously, we demonstrated that carbamazepine- or diclofenac-induced Nrf2 activation plays a protective role in the TNFα-mediated synergistic cell death in HepG2 cells[16] and that TNFα-induced NF-κB activation can be inhibited by DILI compounds[43]. The bidirectional interaction between ROS formation and TNF signaling has been long recognized[19]. Therefore, we evaluated the relationship between DILI compound-induced oxidative stress and compound-induced TNFα target gene expression. First, we ranked the compounds on their oxidative stress response profile. The relevance of the candidate oxidative stress genes included in the Fluidigm PCR array was assessed by treatment with two prototypical Nrf2 activators, diethylmaleate and CDDO-me (Suppl. Fig. 3A). The oxidative stress response ranking of DILI compounds was determined by the average induction of these oxidative stress genes per compound (Suppl. Fig. 3B). Next, we studied the correlation between drug-induced oxidative stress and target gene expression for each individual TNFα target gene. (Fig. 4A and Suppl. table 4). Interestingly, the NF-κB family members RelA, RelB and NFKB2 were amongst the target genes that correlated most strongly with the oxidative stress response (Fig. 4B). RelB and NFKB2 were also strongly induced by TNFα (Suppl. Fig. 3C). However, the compound-induced expression of RelB and NFKB2 was not dependent on RelA expression (Suppl Fig. 3F). RelB was induced in similar levels as by TNFα stimulation (Suppl Fig. 3F and Suppl. Fig. 2). We reasoned that RelB might contribute to DILI compound-induced target gene induction.

To assess this, we first confirmed the DILI compound-induced expression of CCL20, CCL5, CD44, CXCL3, ELF3, IER3, and IL8 by standard RT-qPCR (Fig. 4C). While neither knockdown of RelB nor cREL did affect the DILI compound-induced transcription of most genes (Fig. 5D and Suppl. Fig. 3E), compound-induced expression of IL8, CCL5 and CD44 was significantly increased by RelB and/or cREL knockdown (Fig. 4D and E, and Suppl. Fig. 3E). Together these data suggest that compound-induced RelBexpression is associated with oxidative stress responses, independently of RelA transcriptional activity. Both RelB and cREL act rather as suppressors than as enhancers of the expression of drug-induced, typical TNFα-regulated target genes.

RelA affects DILI compound-induced TNFα target gene expression

We anticipated a role for RelA during the induction of some of the TNFα-induced target genes by DILI compounds. Indeed, knockdown of RelA did decrease drug-induced expression of several TNFα target genes, most notably CCL20 and IER3 under diclofenac and nefazodone conditions, and partly CCL5 and IL8 (Fig. 5A). In contrast, siRelA knockdown enhanced ELF3 expression. While diclofenac-induced IL8 expression was

inhibited by RelA knockdown, nefazodone-induced IL8 expression was not. This role of RelA was not related to substantial nuclear translocation at the exposure concentration used in aforementioned experiments, determined by our RelA-GFP reporter. However, diclofenac itself caused significant translocation of RelA-GFP upon higher concentrations (Fig. 5B). An overview of the experimental designs and key messages of this study can be found in Suppl. Fig. 5.

Discussion

Here we demonstrate that concurring signaling events induced by various DILI compounds affect the final outcome of TNFα-induced NF-κB target gene expression. This effect is mediated through the direct compound-induced activation of NF-κB transcriptional and regulational activity. This occurs likely in close relationship to the onset of oxidative stress responses and is regulated by RelA as well as by RelB and cRel NF-κB family members. While TNFα induces an oscillatory nuclear translocation of NF-κB subunit RelA, such a spatio-temporal behavior is not observed for DILI compound-induced RelA nuclear translocation.

Cellular survival signaling in hepatocytes is critical during DILI onset and TNFα-induced NF-κB signaling is a well-characterized survival pathway. In addition, several TNFα-induced NF-κB target genes are proinflammatory cytokines or chemokines, regulating the dynamics of the inflammatory response at organ or even systemic levels. Our data demonstrate that DILI compounds impact the dynamics of TNFα-induced target gene expression substantially. As inflammation is a hallmark of DILI, these compounds might influence the inflammatory process and thereby DILI progression under *in vivo* circumstances. HepG2 cells indicates that TNFα signaling in HepG2 cells generally mimics TNFα responses in MEFs. We evaluated TNFα-induced nuclear oscillation of RelA, splicing of mRNA as an important regulator of mRNA target gene kinetics, and clustering of target genes in three similar kinetic groups[23,152,213]. Thus, we are confident that HepG2 cells represent a normal, MEF-like physiological response to TNFα.

To extend our analysis of TNFα-induced NF-κB signaling in hepatocytes, we assessed TNFα-stimulated RelA translocation in primary human hepatocytes (PHH). Unexpectedly, we were unable to induce a reproducible TNFα response in three independent cryo-preserved PHH donors (Suppl. Fig. 4). Before stimulation with TNFα, there was already RelA present inside the nucleus. The nuclear RelA levels were higher than those in unstimulated wild type HepG2 cells (Suppl. Fig. 4). These high levels made the induction of RelA translocation by TNFα less intense and the detection more difficult. To our best knowledge, the TNFα-induced translocation dynamics of RelA in PHHs have not been researched before. Furthermore, in our hands, we found that TNFα target gene transcription in cryopreserved hepatocyes was difficult to detect, had major donor differences and was in general lower than expected (data not published). These observations will be further assessed in future publications.

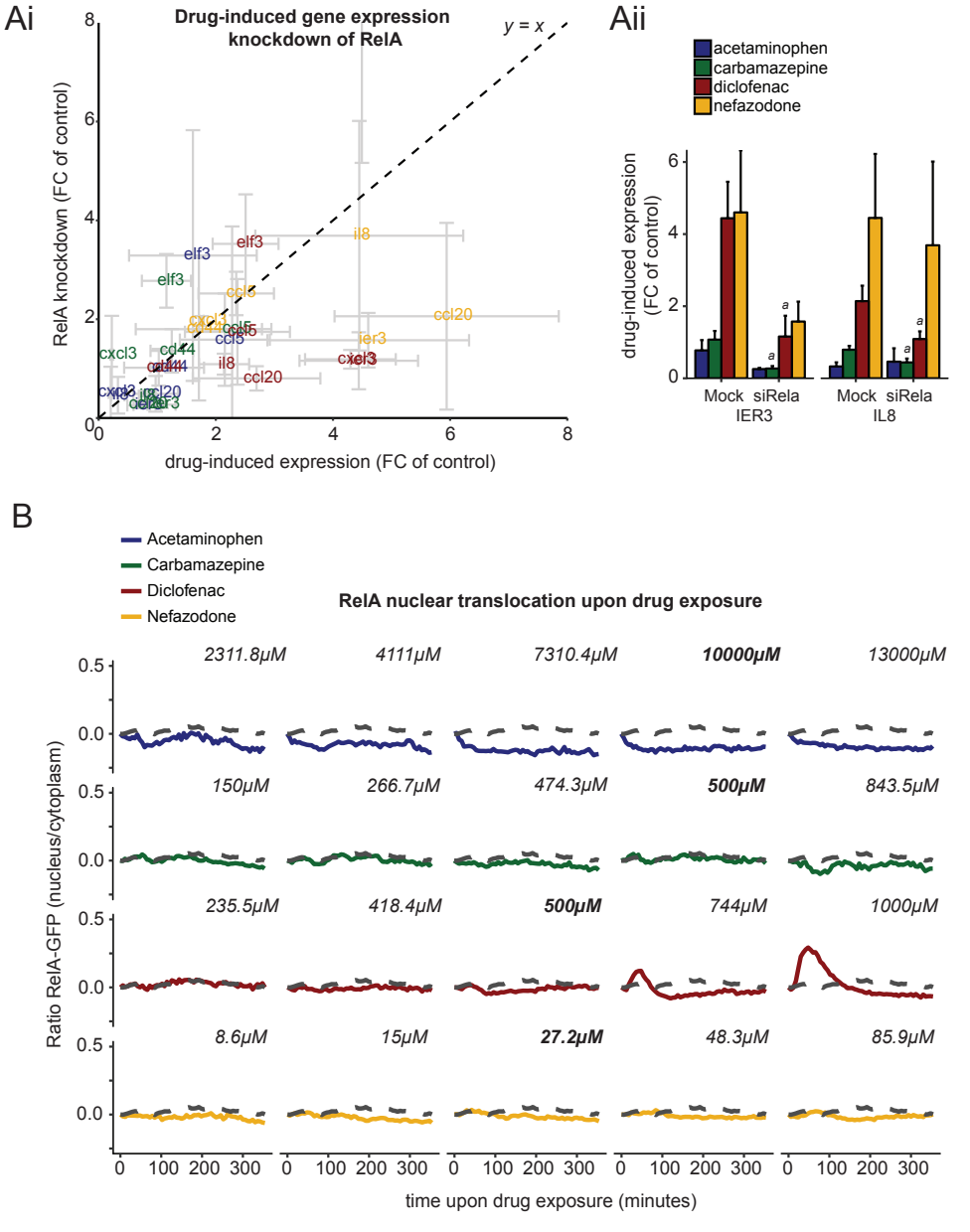

Fig. 5: **Drug-induced gene expression depends largely on RelA expression** Ai) Drug-induced gene expression (Fc to control) is plotted on the x-axis, while the drug-induced gene expression with siRNA mediated knockdown is plotted on the y-axis. The colors represent the pre-exposure drugs. The y=x line shows where the knockdown has no effect on the drug-induced gene expression. Aii) The data from Ai for IER3 and IL8 is represented in a bar graph. *a* = p-value > 0.05 compared to the mock control with the same treatment. The data is the average of three independent experiments and the error bars reflect the standard deviation. B) RelA-GFP reporter upon drug exposure. The ratio of nuclear divided by cytoplasmic GFP is shown. The bold numbers are the concentrations used in the PCR experiments in this study (see also Suppl Table 3). The data is the average of all detected cells in one independent experiment.

Previously, we have published TNFα-stimulated PHH gene expression data from the TG-GATES database, in which TNFα target gene induction was clearly seen in cryopreserved PHHs[43,221,222]. On one hand, this inconsistency could point to (polymorphic) donor differences in TNFα signaling pathways, leading to fundamentally different outcomes. On the other hand, technical issues, including hepatocyte purity levels and plating techniques, could also lead to different results. In 2016, Godoy *et al.* showed that the purity of isolation and plating procedure of PHHs is of major importance, especially for inflammation research. Inpurity, including the remains of a few KCs in the samples, induces inflammatory disease phentoypes.

They also show that improving isolation and culturing methods could diminish, but not fully prevent a disease-like inflammatory PHH phenotype[37]. Therefore, our observations in cryopreserved PHHs, but also observations and conclusions by others relating to inflammatory signaling in primary human hepatocytes should be treated with utmost care. Further research into the nature of inflammatory signaling in HepG2 cells and PHHs *in vitro* in comparison to PHHs *in vivo*, however difficult, is recommended. At last, the observed donor variations detected in our assay warrant further assessment of TNFα signaling in PHHs of different donors, as this may impact individual susceptibility to the interaction between DILI compound exposure and TNFα-induced signaling.

Our results demonstrate that the different DILI compounds show a plethora of interferences with the TNFα-induced expression of many temporally regulated genes. This underscores the complexity of interpreting single target gene responses. Some DILI compounds, including diclofenac, carbamazepine and nefazodone, demonstrate a strong effect on the RelA nuclear translocation oscillatory behavior induced by TNFα and also strong modulation of TNFα-induced target gene expression. However, these compounds did not affect the same target genes in a similar manner. Therefore, we conclude that the drug-induced delay in RelA oscillation does not directly reflect the alterations in gene expression. The relation between RelA oscillation and target gene induction is very complex. Recent data using knock-in GFP-RelA MEFs showed that pulse-wise TNFα stimulation leads to pulse-wise target gene expression, at least when the time in between pulses is sufficient. Pulse-wise gene expression reflected the pulsatile nuclear RelA localization and was much more pronounced for early genes than for middle and late TNFα-induced gene expression[27]. However, we do not detect specific early gene effects by drug-mediated TNFα-induced gene expression. In addition, other DILI compounds with limited effect on RelA oscillation also enhanced TNFα-induced target gene expression (for example entacapone). Therefore, we conclude that other drug-induced signaling pathways likely modulate TNFα-induced gene expression.

Most DILI compounds induced upregulation of TNFα target gene expression in the absence of TNFα (Suppl. Fig. 1). Of relevance, some of the compound-induced target gene inductions were correlated to the relative activation of the oxidative stress response by our compounds. As expected, these included antioxidants MAFF and SOD2. Both MAFF, exhibiting Nrf2 pathway regulation, and SOD2, exhibiting mitochondrial ROS regulation are central in diminishing the oxidative stress load upon TNFα stimulation[19,223]. Oxidative stress

is central in many types of liver injury *in vivo* and concurrent to TNFα signaling. Both oxidative stress and TNFα signaling induce JNK activation[224]. The prolonged activity of JNK is crucial in TNFα/diclofenac-induced cell death *in vitro* and in GalN/LPS induced liver failure *in vivo*[14,42,225]. Also in TNFα-stimulated mouse fibroblasts, oxidative stress inhibits MAP kinase phosphatases and thioredoxin reductase, inducing prolonged JNK activation and cell death[18]. The relationship between ROS and JNK signaling is complex, as the mutual interaction is often bidirectional, localization dependent, cell type dependent and contains many feedback loops[19,226,227]. Well-timed TNFα-induced expression of antioxidants is essential to prevent over-activation of JNK and subsequent apoptosis[19]. As our data demonstrate, TNFα-induced expression of antioxdiants is skewed upon previous drug exposure. The exact mechanistic relationship between oxidative stress, NF-κB target gene activation by DILI compounds and subsequently TNFα warrants further investigations.

Oxidative stress induction positively correlated with drug-induced RelB and NFKB2 expression as well. In recent years, the so-called non-canonical NF-κB signaling has been emerging as an important player in the regulation of RelA transcriptional activity and vice versa. Interestingly, we showed that compound-induced RelB expression is not RelA-dependent (Suppl Fig. 3F). Taken together, this suggests that drug-mediated RelB expression is mediated by oxidative stress.

Nuclear RelB can induce specific RelB target gene expression as MMP3 and p53 in non-immune cells, but is foremost known for its inhibitory effect on RelA transcriptional activity[228,229]. RelB can bind directly to, and thereby inhibit RelA. The affinity of the binding is affected by phosphorylation of both RelA and RelB[230,231]. In non-hepatic cells, Ser276 phosphorylation of RelA is inhibited by HMOX1 expression reducing oxidative stress and increased by oxidative stress induced ATM activation[232,233]. However, in our study HMOX1 expression is only minorly affected by TNFα and drug exposure (Suppl Fig. 3C). In addition, RelB together with p100 (NFKB2) can effectively capture RelA in a large complex and inhibit RelA transcriptional activity in TNFα stimulated MEFs[231,234]. Either way, inhibition of RelA transcriptional activity by RelB expression is consistent with our data. RelB knockdown did increase RelA dependent drug-induced gene expression, especially from the well-described IL8 and CCL5 (Fig. 5D).

The NF-κB target genes IL8 (also named CXCL8) and CCL5 are both chemokines that are produced in the diseased liver. IL8 recruits mainly neutrophils, CCL5 is involved in liver fibrosis, recruits monocytes and activates NK cells[235]. *In vivo*, lower expression of these chemokines would decrease proinflammatory signaling. Indeed, silencing of RelB has a protective effect on ischaemia/reperfusion-induced oxidative stress and TNFα-dependent liver injury[236]. In addition, forced activation of the non-canonical pathway in *in vivo* mouse liver (by stabilized NIK expression) induced massive hepatotoxicity. This hepatotoxicity was dependent on increased oxidative stress induction and hepatocyte-induced activation of macrophages[237]. These studies, in combination with our presented data, show the potential consequences of enhanced expression of TNFα-induced CCL5 and IL8 by DILI compounds on local inflammatory and pathological responses in the liver.

In summary, we here studied drug affected TNFα-induced NF-κB responses in HepG2 cells. We show that RelB expression was induced by compounds in a RelA-independent manner and correlated positively with oxidative stress formation. Most drug-induced TNFα target genes were RelA dependent, but well-timed and well-regulated expression of for example IL8 and CCL5 was also dependent on both RelB and cREL-mediated inhibition. Together, these results emphasize the complexity of interactions between drug and TNFα-induced NF-κB family signaling in hepatocytes.

Acknowledgements

This work was supported by the Innovative Medicine Initiative MIP-DILI project (Grant agreement No. 115336) and the European Union's Horizon 2020 EU-ToxRisk project (Grant agreement No. 681002).

Cluster	Kinetic group	variable	protein function	protein function
group		*Gene symbol*	*general*	*in TNFα signaling (focus on liver biology)*
2a	middle	CXCL5	cytokine/chemokine	pro-inflammatory[238]
2a	middle	IL23A	cytokine/chemokine	pro-inflammatory[239]
2a	middle	FSTL3	cytokine/chemokine	unknown function[240]
2a	middle	SDC4	receptor	anti-inflammatory[241]
2a	middle	NFKB2	signaling protein	NFKB subunit[22]
2a	middle	BIRC3	signaling protein	anti-apoptotic[13]
2a	middle	TNFAIP3	signaling protein	anti-apoptotic[192]
2a	middle	TNFAIP3	signaling protein	anti-inflammatory[143,242]
2a	middle	CCL20	cytokine/chemokine	pro-inflammatory[243]
2a	middle	LTB	cytokine/chemokine	anti-apoptotic[244]
2a	middle	NFKBIE	signaling protein	IkB subunit[245]
2a	middle	BCL2A1	signaling protein	anti-apoptotic[246]
2a	middle	ICAM1	adhesion molecule	pro-inflammatory[247]
2a	middle	VCAM1	adhesion molecule	pro-inflammatory[248]
2a	middle	TNFRSF9	receptor	pro-inflammatory[249]
2b	middle	IER3	transcription factor	anti-apoptotic/pro-apoptotic[250]
2b	middle	MAFF	signaling protein	oxidative stress[251]
2b	middle	MAFF	signaling protein	anti-apoptotic[252]
2b	middle	CSF1	cytokine/chemokine	pro-inflammatory[253,254]
2b	middle	CX3CL1	cytokine/chemokine	pro-inflammatory[255]
2b	middle	TRAF1	signaling protein	anti-apoptotic[256]
2b	middle	PLAU	signaling protein	anti-apoptotic[257,258]
2b	middle	IL8	cytokine/chemokine	pro-inflammatory[259]
2c	middle	NFKBIA	signaling protein	IkB subunit[245]
2c	middle	TNFAIP2	signaling protein	anti-apoptotic[260]
2c	middle	CXCL10	cytokine/chemokine	pro-inflammatory[261,262]
2c	middle	ELF3	transcription factor	pro-inflammatory[263,264]
2c	middle	NFKBIZ	signaling protein	pro-apoptotic[265]
2c	middle	CSF2	cytokine/chemokine	pro-inflammatory[266]
2c	middle	CXCL2	cytokine/chemokine	pro-inflammatory[259,267]
2c	middle	BCL3	signaling protein	anti-inflammatory[268]
2c	middle	BCL3	signaling protein	anti-apoptotic[269,270]
3a	late	CCL5	cytokine/chemokine	pro-inflammatory[271]
3a	late	SLC7A11	transporter	anti-apoptotic[272]
3a	late	C3	secretable factor	liver recovery[273,274]
3a	late	LCN2	signaling protein	anti-inflammatory[275]
3a	late	LCN2	signaling protein	anti-apoptotic[275]
3a	late	CD44	adhesion molecule	pro-inflammatory[276]
3a	late	SOD2	superoxide scavenger	oxidative stress[277]
3b	late	TNIP1	signaling protein	anti-apoptotic[278]
3b	late	SLC2A6	transporter	unkown function[279]
3b	late	RELB	transcription factor	NFKB subunit[280]
3b	late	IL15	cytokine/chemokine	pro-inflammatory[281]
1	early	CSF3	cytokine/chemokine	pro-inflammatory[282]
1	early	CXCL3	cytokine/chemokine	pro-inflammatory[283]
1	early	CXCL1	cytokine/chemokine	pro-inflammatory[267]
1	early	SELE	adhesion molecule	pro-inflammatory[284]
1	early	IRF1	transcription factor	pro-inflammatory[285]
1	early	IRF1	transcription factor	pro-apoptotic[286,287]
NA	Decreasing	INHBA	cytokine/chemokine	pro-inflammatory[288]

Suppl. Table 1

KiCq Start primers

Gene symbol	*Forward (F)/Reverse(R)*	*Sequence*
RELA	F	GCAGAAAGAGGACATTGAG
RELA	R	GTGCACATCAGCTTGC
NFKB1	F	GACAACTATGAGGTCTCTGG
NFKB1	R	ATCACTTCAATTGCTTCGG
NFKB2	F	CCATGACAGCAAATCTCC
NFKB2	R	TAAACTTCATCTCCACCCC
IL8	F	TGTAAACATGACTTCCAAGC
IL8	R	AAAACTGCACCTTCACAC
CXCL3	F	CATCAAACATAGCTCAGTCC
CXCL3	R	CCCTGTCATTTATCAAGGTG
ELF3	F	CTCTATTTAGAGCCGGGTAG
ELF3	R	GTTGCTAATCTCACAGGTTG
cREL	F	AAAGACAACTCTGCTTTTCC
cREL	R	CTTCCTTCTCCAATTGAACC
CCL20	F	TATATTGTGCGTCTCCTCAG
CCL20	R	GCTATGTCCAATTCCATTCC
TNF	F	AGGCAGTCAGATCATCTTC
TNF	R	TTATCTCTCAGCTCCACG
IER3	F	AAGTAGGAGAAGAAATGGGG
IER3	R	AGAAGATGGAAGGATCTCAC
NFKBIZ	F	CACGTTCCTTCATATTGCTG
NFKBIZ	R	AGTGCATTCATCTTTCTTGC

Splicing primers

Gene symbol	*Forward (F)/Reverse(R)*	*Sequence*	*Exon/Intron*
TNFAIP3	M1_F	AGTTTTGTCCTCAGTTTCGGG	exon
TNFAIP3	M1_R	TTCCTCAGTACCAAGTCTGTG	exon
TNFAIP3	M2_F	CAGCACGCTCAAGGAAACAGACA	exon
TNFAIP3	M2_R	GCCAGTGGAGAGGCAAGTAA	exon
TNFAIP3	J2_F	GCCAAAAGGACAGAAGAGCA	exon
TNFAIP3	J2_R	TTGGAGGTAGCATTTCGGAC	intron
TNFAIP3	J3_F	GGACGTTTCTGTCTGGGTTTT	exon
TNFAIP3	J3_R	AGACACGAAAGGAGCAAAGC	intron
NFkBIA	M5_F	TCCTCAACTTCCAGAACACC	exon
NFkBIA	M5_R	ACAGCCAGCTCCCAGAAGT	exon
NFkBIA	M6_F	CTACACCTTGCCTGTGAGCA	exon
NFkBIA	M6_R	TGACACCAGGTCAGGATTTTG	exon
NFkBIA	J4_F	GAGGATGAGGAGAGCTATGACAC	exon
NFkBIA	J4_R	TAGTTAGAGCGCCGAAGGAG	intron
NFkBIA	J5_F	ATCGTGGAGCTTTTGGTGTC	exon
NFkBIA	J5_R	GCTTATGGCTGCATTTGGAA	intron
ICAM1	M1_F	GCTGAGCTCCTCTGCTACTCA	exon
ICAM1	M1_R	GGCTATCTTCTTGCACATTGCT	exon
ICAM1	M2_F	CATAGAGACCCCGTTGCCT	exon
ICAM1	M2_R	GCAGCGTAGGGTAAGGTTCTTG	exon
ICAM1	J1_F	GCAACCTCAGCCTCGCTAT	exon
ICAM1	J1_R	TCCCATAAACAGCTACCTAAGCA	intron
ICAM1	J2_F	ATCACCATGGAGCCAATTTC	exon
ICAM1	J2_R	CATTGCAGGATACCCCACC	intron
RELB	M1_F	GACCTCTCCTCACTCTCGCTC	exon
RELB	M1_R	CCGTTCTCCTTGATGTACTCGT	exon
RELB	M2_F	TCCAGTGTGTGAGGAAGAAGG	exon
RELB	M2_R	CAGCTCTGATGTGTTTGTGGAT	exon
RELB	J1_F	AGCCACTCCCTGAGAACAGA	intron
RELB	J1_R	AGAATCACACAGCAACGGAA	intron
RELB	J5_F	CCGTCACCCCCTCAGTTTTA	intron
RELB	J5_R	CACGGAAGTCAAGGGGTTTG	exon
SLC2A6	M4_F	GTCCCTCTACGCCCTTGG	exon
SLC2A6	M4_R	AAGCTGAGCAGCAGGATCA	exon
SLC2A6	M5_F	ACCAAATCCCAGGCATCC	exon
SLC2A6	M5_R	ACGGCACAGCTGAGAACAT	exon
SLC2A6	J1_F	GCAATTTCAGCTTTGGGTATG	exon
SLC2A6	J1_R	CAAGGTGGAGAATTTGGGAG	intron
SLC2A6	J5_F	AGGCTCCCTGTTTCAAGTGC	intron
SLC2A6	J5_R	CAGGAGGTCGTTGAGGATCA	exon
CCL5	M5_F	TGCCCACATCAAGGAGTCTTT	exon
CCL5	M5_R	CGGTTCTTTCGGGTGACA	exon

Taqman Gene Expression Assays (Applied BioScience)

Gene Symbol	*Assay ID*	*Context Sequence*
ADH1A	Hs00605167_g1	ATTCTTGGTGGCTTTAAAAGTAAAG
CXCL5	Hs01099660_g1	AAATTTTGGACGGTGGAAACAAGGA
IER3	Hs04187506_g1	TCTACCCTCGAGTGGTCCGGCGCCA
NFKBIA	Hs00355671_g1	TGTCAATGCTCAGGAGCCCTGTAAT
UGT2B15	Hs00870076_s1	GAAGGAAAATGTGAACATGGAAACA
BLNK	Hs00179459_m1	ATGACTTTGACAGCGACTATGAAAA
CXCL6	Hs00605742_g1	GGAAGTGGTAGCCTCCCTGAAGAAC
IFRD1	Hs00912593_m1	ATTGGCCAGAGGAATAGAGAGTGAC
OSGIN1	Hs00203539_m1	AGAAGAAGCGAAGAGGTCTTCGCAA
CASP4	Hs01031951_m1	ATTGAAAATGGAAGCCACAAGCAGC
F3	Hs01076029_m1	TCAAATAAGCACTAAGTCAGGAGAT
IL23A	Hs00900828_g1	ACAACAGTCAGTTCTGCTTGCAAAG
REL	Hs00968440_m1	TATGACAACCGTGCTCCAAATACTG
CCL5	Hs00982282_m1	CTGCCTCCCCATATTCCTCGGACAC
FSTL3	Hs00610505_m1	GGCCGCTGCCGCAAGTCCTGTGAGC
TNFAIP2	Hs00196800_m1	CCTCTACCCCAATGACATCATCAAC
SDC4	Hs00161617_m1	GCCGAGTCGATCCGAGAGACTGAGG
CDC34	Hs00362082_m1	AGACATCATCCGGAAGCAGGTCCTG
GADD45G	Hs02566147_s1	GCAGGAGCGTGAAGGACTTAGCCGA
TNIP1	Hs00374581_m1	CCTCCATTCTGCAGACCCTGTGTGA
SLC2A6	Hs01115485_m1	CCTGCCAGTGGTGAGCACCTTCGGC
CSF3	Hs00738432_g1	ATCTGGCAGCAGATGGAAGAACTGG
GAS2	Hs01086684_m1	CATTAGGATGCTGCACAACAAACAT
MAFF	Hs00544822_m1	AAAGCTCTAAAGATCAAGCGAGAGC
FOS	Hs04194186_s1	CTACCCCGAGGCTGACTCCTTCCCC
DENND4B	Hs00208230_m1	TACTACAATAAGGCTGTGTTGGAAA
ACTB	Hs01060665_g1	CCCAGGCACCAGGGCGTGATGGTGG
MDH1	Hs00936497_g1	GGGAGAATTTGTCACGACTGTGCAG
SLC7A11	Hs00921938_m1	ATGCAGTGGCAGTGACCTTTTCTGA
CXCL10	Hs01124251_g1	CCACGTGTTGAGATCATTGCTACAA
HMBS	Hs00609296_g1	GTCCCTGCCCAGCATGAAGATGGCC
NFKB2	Hs01028901_g1	CTATCCCACTGTCAAGATCTGTAAC
ELF3	Hs00963881_m1	GCTGAGCCGGGCCATGAGGTACTAC
RELB	Hs00232399_m1	GCCCGCCATCGAGCTCCGGGATTGT
ABCA1	Hs01059118_m1	GAACAACATGAATGCCATTTTCCAA
CXCL3	Hs00171061_m1	AAAAGATACTGAACAAGGGGAGCAC
NOD2	Hs00223394_m1	TTCTTGGCATTGAGGCTGGGGAATA
CSF1	Hs00174164_m1	AGCATGACAAGGCCTGCGTCCGAAC
HAMP	Hs00221783_m1	TCCCACAACAGACGGGACAACTTGC
CFB	Hs00156060_m1	AATGATCGATGAAAGCCAGTCTCTG
GCLM	Hs00157694_m1	CGCACAGCGAGGAGCTTCATGATTG
G6PD	Hs00166169_m1	GGGTGCATCGGGTGACCTGGCCAAG
KEAP1	Hs00202227_m1	AATCTACGTCCTTGGAGGCTATGAT
CX3CL1	Hs00171086_m1	GCTGGCTGGACAGCACCACGGTGTG
PTX3	Hs00173615_m1	ACTGAGGACCCCACGCCGTGCGCCT
SLC10A1	Hs00161820_m1	GGACATGAACCTCAGCATTGTGATG
PI3	Hs00160066_m1	GCAGCTGTCACGGGAGTTCCTGTTA
CXCL1	Hs00605382_gH	GATGCTGAACAGTGACAAATCCAAC
C3	Hs00163811_m1	CAAGAAAGGGATCTGTGTGGCAGAC
BIRC2	Hs01112284_m1	GCTGACCCACCAATTATTCATTTTG
FABP1	Hs00155026_m1	AAGGCAATCGGTCTGCCGGAAGAGC
BIRC3	Hs00985031_g1	GAAGATGTTTCAGATCTACCAGTGG
SLC3A2	Hs00374243_m1	GCCCTTCCTGGACAGCCTATGGAGG
PSMB6	Hs00382586_m1	GAACAACCACTGGGTCCTACATCGC
MYLK	Hs00364926_m1	TGCAAGATTGAAGGATACCCAGACC
CFLAR	Hs00153439_m1	GCAATGAGACAGAGCTTCTTCGAGA
SRXN1	Hs00607800_m1	GACACGATCCGGGAGGACCCAGACA
BCL2L11	Hs00708019_s1	AGGTAGACAATTGCAGCCTGCGGAG
TNFAIP3	Hs00234713_m1	GAAAACGAACGGTGACGGCAATTGC
BAX	Hs00180269_m1	CTGGTGCTCAAGGCCCTGTGCACCA
PPARGC1A	Hs01016719_m1	AAGGCAATTGAAGAGCGCCGTGTGA
LCN2	Hs01008571_m1	TCGTCTTCCCTGTCCCAATCGACCA
TBP	Hs00427620_m1	GCAGCTGCAAAATATTGTATCCACA
CCL20	Hs01011368_m1	ATATTGTGCGTCTCCTCAGTAAAAA
TLR2	Hs01872448_s1	GTTGGGATCTTTATGTCACTAGTTA
TRAF1	Hs01090170_m1	CCCTTCCGGAACAAGGTCACCTTCA
STAT5A	Hs00234181_m1	TGTTCCAGGTGAAGACTCTGTCCCT
NFKBIZ	Hs00230071_m1	ATGGTGACACGTTCCTTCATATTGC
IL15	Hs01003716_m1	TCTTCTAATGGGAATGTAACAGAAT
CSF2	Hs00929873_m1	CAGAAATGTTTGACCTCCAGGAGCC
CXCL2	Hs00601975_m1	CTGAAAAATGGCAAATCCAACTGAC
CD44	Hs01075861_m1	TCGAAGAAGGTGTGGGCAGAAGAAA
CCL2	Hs00234140_m1	CGCTCAGCCAGATGCAATCAATGCC
VEGFA	Hs00900055_m1	ACATCACCATGCAGATTATGCGGAT
SELE	Hs00950401_m1	TTCAAAAGAATCAGAAACAGGTGCA
VIM	Hs00185584_m1	CTCCGGGAGAAATTGCAGGAGGAGA
LTB	Hs00242739_m1	CTGCCCACCTCATAGGCGCTCCGCT
NFKBIE	Hs00234431_m1	CGAGGACGGAGACACGCTGGTCCAC
BCL3	Hs00180403_m1	AGGACGGAGACACGCCTCTCCATAT
INHBA	Hs01081598_m1	TTGCCGAGTCAGGAACAGCCAGGAA
SOD2	Hs00167309_m1	GGAACAACAGGCCTTATTCCACTGC
NFKB1	Hs00765730_m1	ACAACTATGAGGTCTCTGGGGGTAC
HMOX1	Hs01110250_m1	TGCTCAACATCCAGCTCTTTGAGGA
PLAU	Hs01547054_m1	AACGACATTGCCTTGCTGAAGATCC
BCL2A1	Hs00187845_m1	AAAACGGAGGCTGGGAAAATGGCTT
JUNB	Hs00357891_s1	GCGGCGGTGGCGGCAGCTACTTTTC
IL1RN	Hs00893626_m1	CAGCTGGAGGCAGTTAACATCACTG
RELA	Hs00153294_m1	AGTACCTGCCAGATACAGACGATCG
ICAM1	Hs00164932_m1	CCTCACCGTGTACTGGACTCCAGAA
VCAM1	Hs01003372_m1	TCAATGTTGCCCCCAGAGATACAAC
GAPDH	Hs02758991_g1	GACTCATGACCACAGTCCATGCCAT
IL8	Hs00174103_m1	GTGTGAAGGTGCAGTTTTGCCAAGG
MMP3	Hs00968305_m1	CTTTAAAGACAGGCACTTTTGGCGC
IL6	Hs00985639_m1	TCAGCCCTGAGAAAGGAGACATGTA
IRF1	Hs00971960_m1	TCACACAGGCCGATACAAAGCAGGG
TNFRSF9	Hs00155512_m1	ACCCTGGACAAACTGTTCTTTGGAT

Suppl. Table 2

Compounds	cmax (µM)	Concentrations RelA (µM)					PCR Concentration (µM)
nefazodone	0,86	8,59	15,27	27,15	48,29	85,87	27,15
carbamazepine	15,00	150,00	266,74	474,34	500,00	843,51	500,00
diclofenac	8,10	235,27	418,38	500,00	744,00	1000,00	500,00
acetaminophen	130,00	2311,76	4110,96	7310,44	10000,00	13000,00	10000,00
flucloxacillin	31,90	319,00	567,27	1008,77	1793,87	3190,00	3190,00
metformin	116,00	652,32	1160,00	2062,80	3668,24	6523,16	6523,16
tolcapone	21,99	21,99	39,10	69,52	123,63	219,85	69,52
troglitazone	6,39	20,20	35,91	63,87	113,57	201,96	113,57
entacapone	3,93	22,10	39,30	69,89	124,28	221,00	124,28
pioglitazone	2,95	29,46	52,39	93,16	165,67	294,60	294,60

Suppl. Table 3

gene symbol	protein annotation	cluster	Pearson's correlation
SLC7A11	anti-apoptotic	3a	0,80
RELB	NFKB subunit	3b	0,76
MAFF	oxidative stress	2b	0,73
MAFF	anti-apoptotic	2b	0,73
RELA	NA	NA	0,66
SDC4	anti-inflammatory	2a	0,61
IL23A	pro-inflammatory	2a	0,56
NFKB2	NFKB subunit	2a	0,54
CSF3	pro-inflammatory	1	0,53
SOD2	oxidative stress	3a	0,51
CCL20	pro-inflammatory	2a	0,49
IER3	anti-apoptotic/pro-apoptotic	2b	0,49
CSF1	pro-inflammatory	2b	0,37
IL8	pro-inflammatory	2b	0,34
TNIP1	anti-apoptotic	3b	0,31
ELF3	pro-inflammatory	2c	0,30
BCL3	anti-inflammatory	2c	0,26
BCL3	anti-apoptotic	2c	0,26
NFKB1	NA	NA	0,26
ICAM1	pro-inflammatory	2a	0,23
CXCL5	pro-inflammatory	2a	0,20
CSF2	pro-inflammatory	2c	0,19
C3	liver recovery	3a	0,11
PLAU	anti-apoptotic	2b	0,08
CXCL2	pro-inflammatory	2c	0,03
TNFAIP2	anti-apoptotic	2c	0,03
TNFRSF9	pro-inflammatory	2a	-0,05
IRF1	pro-inflammatory	1	-0,07
IRF1	pro-apoptotic	1	-0,07
CD44	pro-inflammatory	3a	-0,10
IL15	pro-inflammatory	3b	-0,11
NFKBIE	NFKB subunit	2a	-0,15
CCL5	pro-inflammatory	3a	-0,15
LTB	anti-apoptotic	2a	-0,16
CXCL3	pro-inflammatory	1	-0,16
CXCL1	pro-inflammatory	1	-0,18
VCAM1	pro-inflammatory	2a	-0,19
TNFAIP3	anti-apoptotic	2a	-0,19
TNFAIP3	anti-inflammatory	2a	-0,19
LCN2	anti-inflammatory	3a	-0,20
LCN2	anti-apoptotic	3a	-0,20
SELE	pro-inflammatory	1	-0,20
SLC2A6	unknown function	3b	-0,22
BIRC3	anti-apoptotic	2a	-0,23
NFKBIA	NFKB subunit	2c	-0,23
BCL2A1	anti-apoptotic	2a	-0,25
CXCL10	pro-inflammatory	2c	-0,26
FSTL3	unknown function	2a	-0,29
NFKBIZ	pro-apoptotic	2c	-0,32
TRAF1	anti-apoptotic	2b	-0,35
CX3CL1	pro-inflammatory	2b	-0,44

Suppl. Table 4

Supplementary Figures

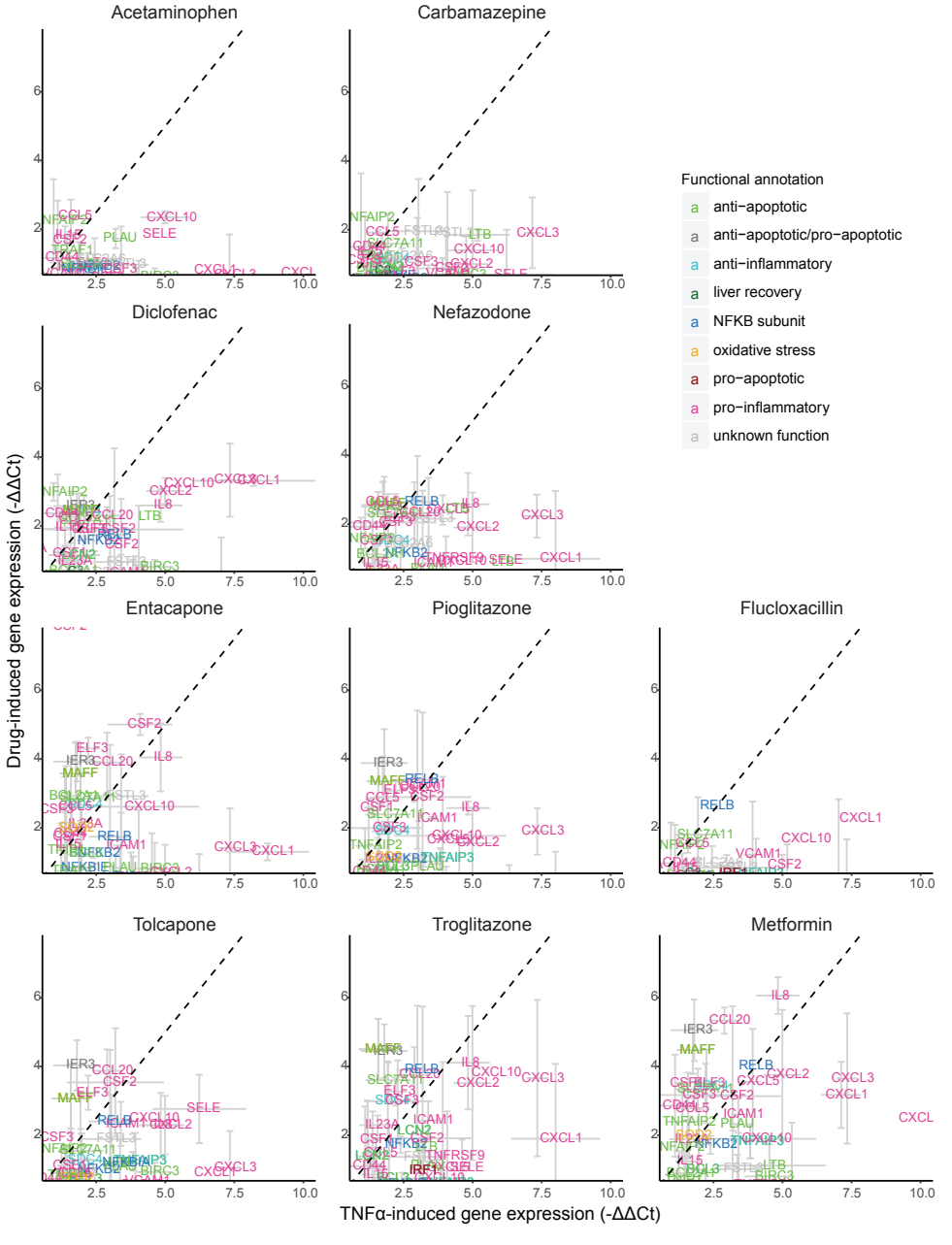

Suppl. Fig. 1: **Comparison of TNFα-induced and DILI compound-induced TNFα target gene induction** The drug-induced expression is visualized as negative deltadelta Ct to DMSO controls. The colors depict the protein function of the target genes. The data is the average of three independent experiments and the error bars reflect the standard deviation. Drug-induced negative deltadelta Ct values higher than 8 (fold change of 256) are not visualised.

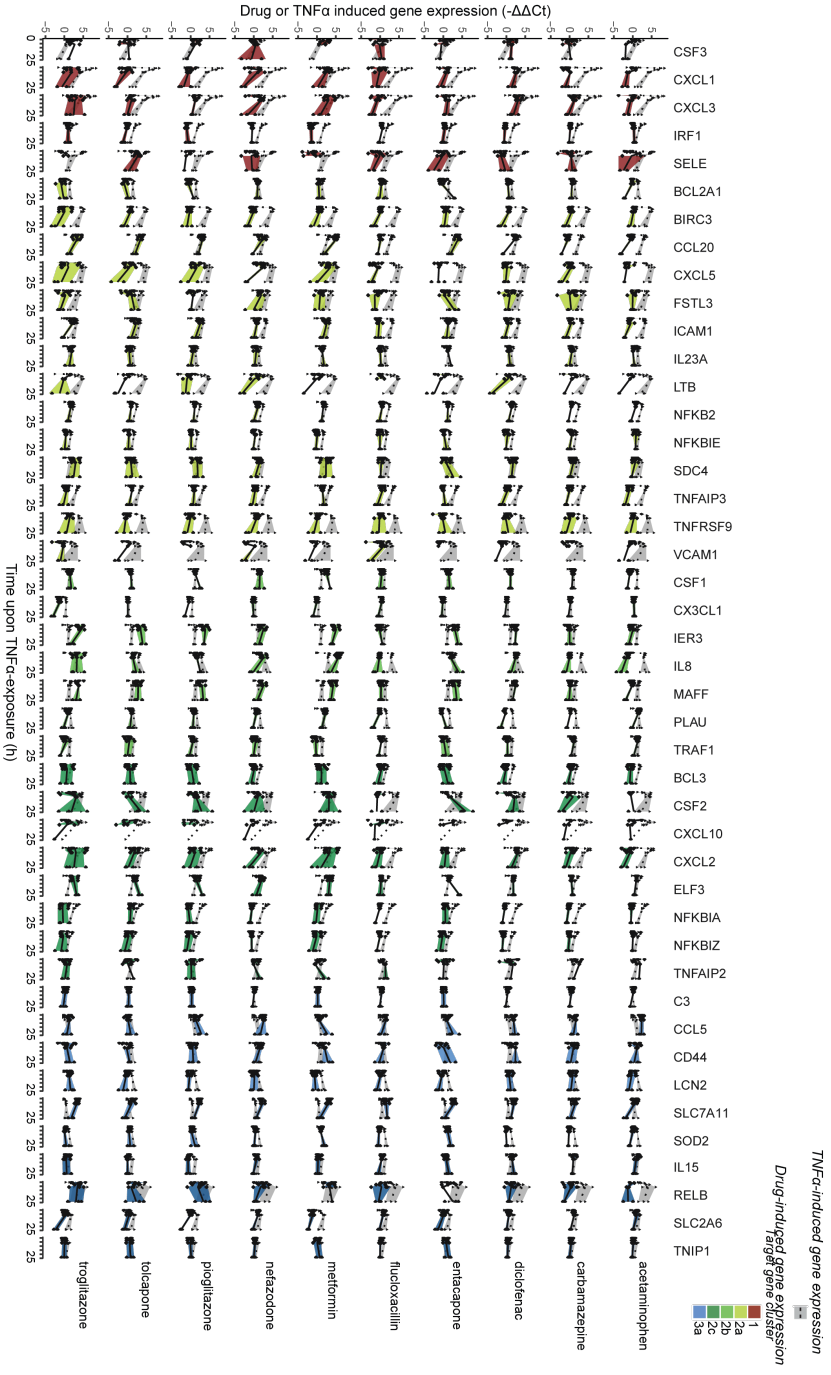

Suppl. Fig. 2: **Comparison of temporal DILI compound-induced and TNFα-induced responses** The temporal drug-induced expression is visualised as negative deltadelta Ct to DMSO controls. The grey color shows the TNFα-induced gene expression, while the colors depict the clustering of the target genes and show drug-induced gene expression. All data is the average of three independent experiments and the colored shade reflects the standard deviation.

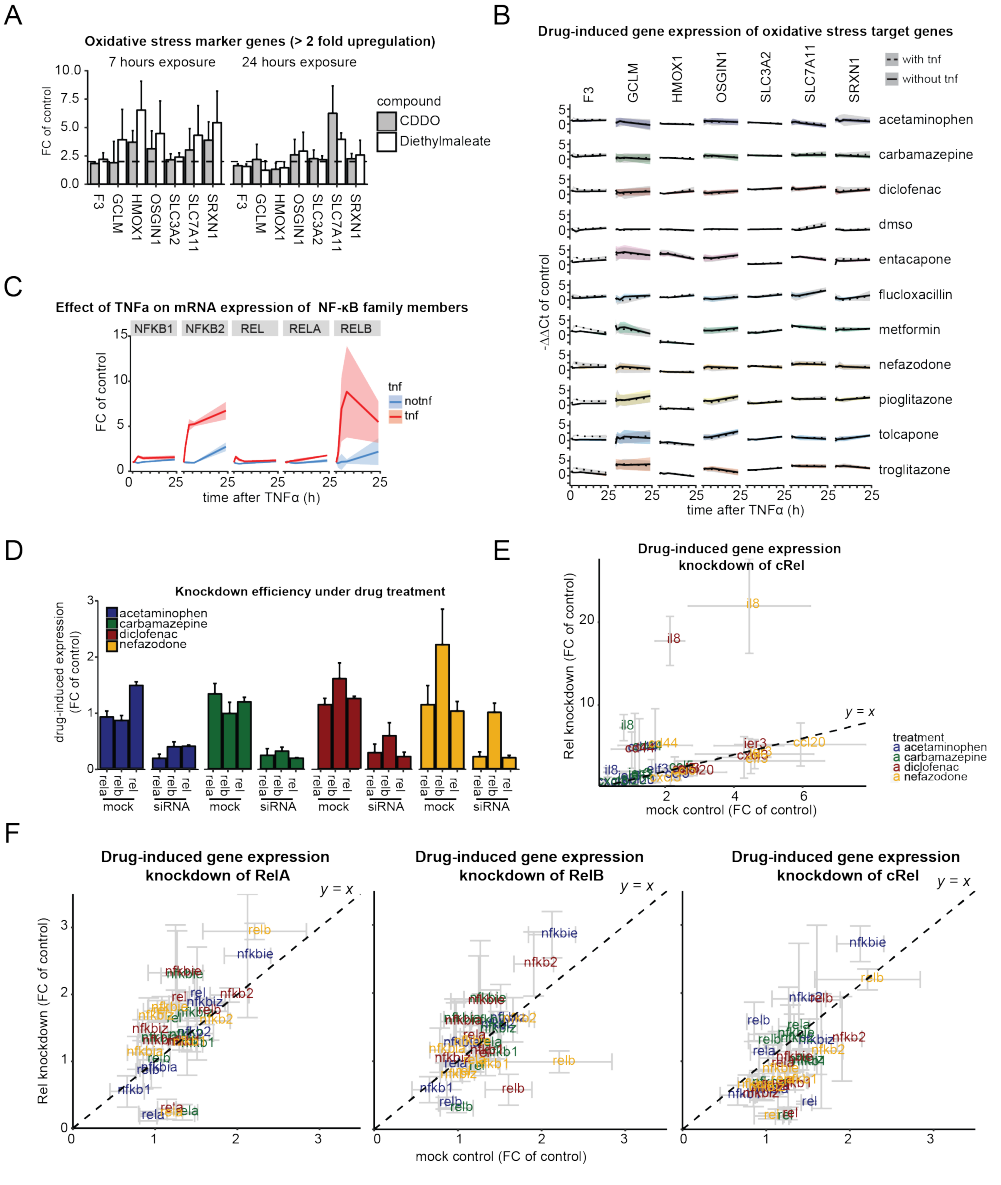

Suppl. Fig. 3: **Drug-induced oxidative stress and NF-κB family members** A) Expression (Fold change of DMSO control) of oxidative stress genes upon CDDO (30 nM) and DEM (100uM) exposure for indicated timepoints. B) NF-κB family member expression (Fold change of control) with and without TNF stimulation is depicted. C) Drug-induced gene expression of oxidative stress target genes with (grey, dashed lines) or without TNF (colored lines and shades) are shown. The expression is visualized as negative deltadelta Ct values compared to DMSO controls. D) The knockdown efficiency of siRNA mediated controls is shown as a Fold Change to DMSO controls. Colors represent drug exposure. E-F) Drug-induced gene expression (Fc to control) is plotted on the x-axis, while the drug-induced gene expression with siRNA mediated knockdown is plotted on the y-axis. The colors represent the pre-exposure drugs. The y=x line shows that the knockdown has no effect on the drug-induced gene expression. All data is the average of three independent experiments and errorbars or shade reflects standard deviation.

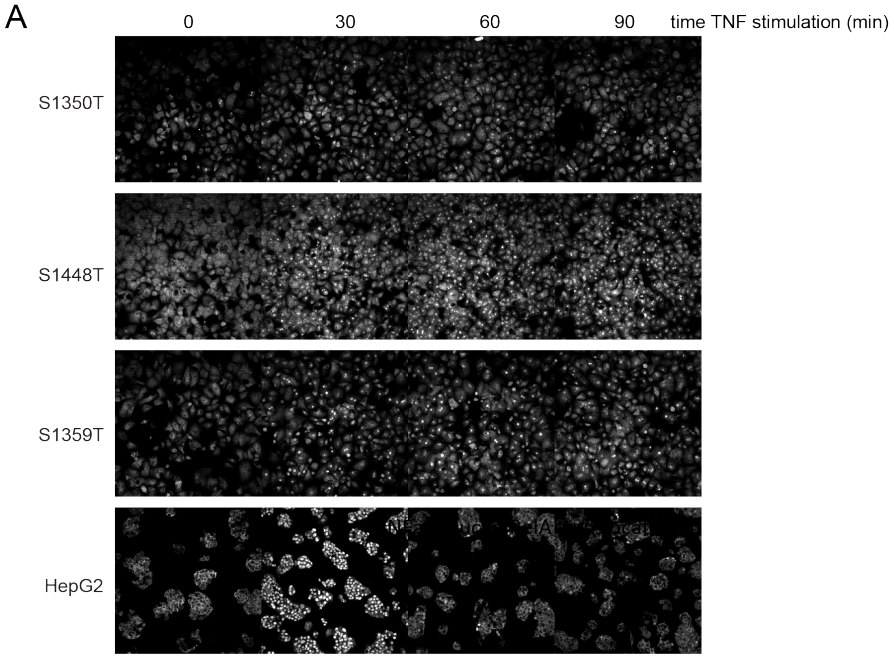

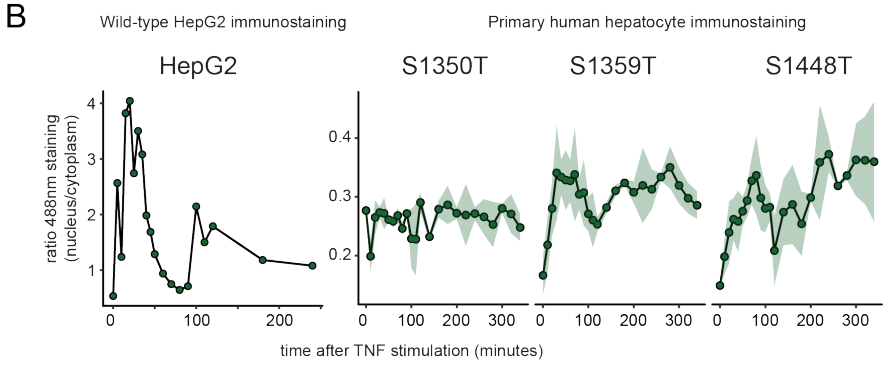

C

Donor	Sex	Age	Virus status	Pathology	Medication
S1359T	F	78	negative*	renal cancer	-
S1448T	M	49	negative*	colorectal carcinoma	-
S1350T	M	82	negative*	colorectal carcinoma	-

*CMV status is not available

***Suppl. Fig. 4:* TNFα-induced RelA translocation in primary human hepatocyte** A) Immunofluorescence images of TNFα stimulated hepatocytes. The numbers correspond to the donors. Cells were stimulated with 10 ng/mL TNF for indicated timepoints. B) Quantification of immunofluorescence image. The ratio of GFP signal in the nucleus/cytoplasm ratio has been depicted. Green shading depicts standard deviation of 2 separate wells. C) Table with donor information of primary human hepatocytes.

A

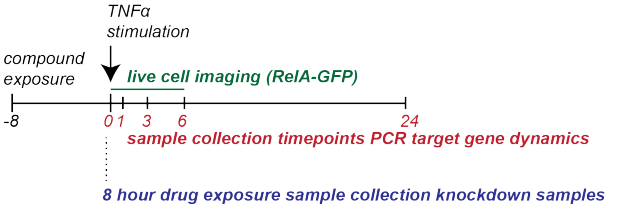

Bi

How do drugs affect TNFα-induced NF-κB oscillation and target gene expression?

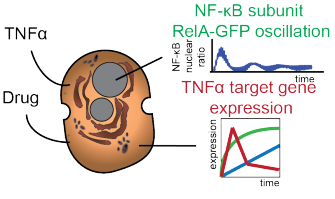

Key messages:
Drug exposure can delay TNFα-induced NF-κB oscillation

Drug exposure can enhance dynamic TNFα-induced target gene expression
- not dependent on NF-κB oscillation delay
- not associated with a specific dynamic or functional cluster of target genes

Bii

How do drugs affect TNFα-independent TNFα target gene expression?

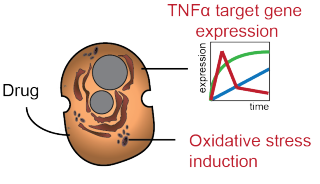

Key messages:
Drug exposure does induce TNFα target gene induction
- including strong immune modulators (e.g. IL8 and CCL5)

Some drug-induced TNFα target gene expression is strongly correlated to oxidative stress induction
- including NF-κB family members (e.g. RelB and NFKB2)

Biii

How do NF-κB family members regulate drug-induced TNFα target gene expression?

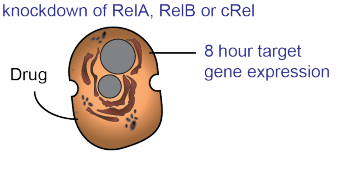

Key messages:
Drug-induced TNFα target gene expression is modulated by all NF-κB family members
- cRel and RelB inhibit IL8 and CCL5 expression
- Most drug-induced gene expression is RelA dependent
- Drug-induced RelB expression is not RelA dependent

Suppl. Fig. 5: **Overview of experimental design and key results** A) Time schedule and experimental design. Colors refer to different experimental designs Bi, ii, iii) Overview of key messages per research question. The figures respresent a schematic overview of experimental design. The colors of the text refer to the time schedule used in these experiments.

Chapter 5

Identification of TNF receptor signaling pathway components that regulate hepatotoxic drug/TNFα-induced synergistic apoptosis

Highlights

- Combined TNFα and carbamazepine, diclofenac, griseofulvin, colchicine and valproic acid exposure induce synergistic apoptosis
- Synergistic compound/TNFα-induced apoptosis is regulated by both generic and compound-specific mechanisms
- The compound-induced onset of adaptive stress responses is strongly correlated with the modulation of TNFα synergism by several candidate genes (e.g PHF5A, CRK7, A20 and CARD12)

This chapter is based on a manuscript in preparation:

Suzanna Huppelschoten[1], Matthijs Vlasveld[1], Steven Wink[1], Steven Hiemstra[1], Janna Klip[1], Wouter den Hollander[1], Casper Roosenstein[1], Lisa Fredriksson[1], Bob van de Water[1,]

Identification of TNF receptor signaling pathway components that regulate hepatotoxic drug/TNFα-induced synergistic apoptosis

[1]Division of Toxicology, Leiden Academic Centre for Drug Research, Leiden University, Leiden, The Netherlands

TNFα stimulation of hepatocytes generally induces cell survival. However, when cellular homeostasis is skewed by drug exposure, the outcome of TNFα stimulation might incline towards cytotoxicity. The mechanistic understanding of this interaction remains largely elusive. Previously we demonstrated TNFα-induced apoptotic synergy with carbamazepine and diclofenac exposure. In this study, we assessed the role of 182 TNFR signaling pathway components on carbamazepine/TNFα-induced apoptosis. We identified 19 genes that upon knockdown inhibit apoptosis, including EP300, CUL1, CARD12, CYLD and RAPSN, and 5 genes that upon knockdown promote apoptosis, including FBXW11, MAP2K7 and PHF5A. We evaluated 124 drugs with drug-induced liver injury liability for TNFα synergism and reveal that colchicine, griseofulvin and valproic acid synergistically enhance TNFα-induced apoptosis. Both A20 (TNFAIP3) and PHF5A were genuine protective genes against TNFα-induced apoptosis upon carbamazepine, diclofenac, valproic acid, griseofulvin and colchicine treatment. Mechanistically most similar, diclofenac and valproic acid TNFα-induced synergistic apoptosis was strongly modulated by knockdown of known apoptotic regulators as CYLD, A20 and CASP8, but also by novel regulators including PHF5A and CARD12. The modulation of apoptosis by PHF5A, CRK7 (CDK12), A20 and CARD12 is strongly correlated to the onset of different branches of oxidative stress and DNA damage response signaling. We anticipate that our study provides improved mechanistic understanding of DILI compound/TNFα-mediated hepatotoxicity and that genetic polymorphisms in the identified candidate genes may define individual susceptibility towards DILI.

Keywords: drug-induced liver injury, TNFα, TNFα-induced apoptosis, TNFα synergism, cellular stress responses

Introduction

The enigmatic TNFα signaling pathway has been a field of extensive research for several decades. This has led to the development of successful clinical use of specific anti-TNFα drugs in various inflammatory disease settings. Idiosyncratic drug-induced liver injury (DILI) is a rare and at the moment unpredictable adverse drug response. One of the current hypotheses on the mechanism of idiosyncratic DILI implicates an activating immune response, acting as danger signal in combination with intracellular drug responses[208]. These combined immune and drug responses could synergistically lead to enhanced cytotoxicity. Indeed, several rodent models showed synergism between otherwise non-toxic doses of LPS and drugs with hepatotoxic liabilities. For trovafloxacin, this synergism was dependent on TNFα[11]. For diclofenac/LPS synergism, the severity of hepatotoxic symptoms was associated to the TNFα expression[99]. *In vitro*, TNFα synergism has been observed in human HepG2 and HepaRG cell lines as well as primary human hepatocytes[16,41,43,130]. Further mechanistic studies indicate that for diclofenac synergistic toxicity, MAPK signaling plays an important role in TNFα synergism in HepG2 cells[14]. This has been confirmed for more drugs, including for trovafloxacin toxicity in primary human hepatocytes[130].

Interestingly, also the succesfull anti-TNFα biologicals have been associated with an increased risk on DILI[139]. This underlines the urgency for more mechanistic understanding of the TNFα signaling pathway in the context of DILI liabilities.

TNFα binding to the TNFR induces formation of the TNF receptor complex, recruiting TRADD, TRAF2, RIP1, A20, the LUBAC complex and TAK1. TAK1 activates MAPK signaling and the IKK complex. IKK activity drives phosphorylation of IκBα, marking it for proteosomal degradation. IκBα's dissociation of the cytoplasmic NF-κB causes it to translocate into the nucleus and activate gene transcription[20]. The spatio-temporal nuclear translocation dynamics of NF-κB are currently considered as one of the critical determinants of target gene expression[26,27]. Target genes include other NF-κB family members as well as members of the IκB family, thus mediating negative feedback responses on TNFR signaling and ultimate biological outcome[289]. Moreover, other target genes are part of the apoptosis regulatory machinery, thereby defining susceptibility for the onset of cell death[17,20]. So far it remains unclear how the various molecules that modulate the TNFR signaling pathway define DILI compound/ TNFα hepatotoxicity.

Carbamazepine is one of the strongest TNFα synergistic drugs that we have studied[16]. The anti-epileptic drug is widely prescribed and induces severe hepatitis in a small subset of patients. The induction of cholestatic and hepatocellular injury occurs in similar rates, but hepatocellular injury is correlated to a negative outcome[290]. Around 30% of the carbamazepine-induced liver injury patients develop an immunoallergic reaction, suggesting involvement of the adaptive immune system[290]. Indeed, very strong HLA allele associations have been found in carbamazepine-induced skin injury. However, these were not detected in patients suffering from carbamazepine-induced liver injury[53]. Carbamazepine has a complex metabolic profile, producing several reactive metabolites and upregulating the expression of several CYPs both *in vitro* and in patients[291,292]. Surprisingly, a low dose of carbamazepine upregulates CYP expression in HepG2 cells as well, already within 24 hours of culture[293]. Only recently rodent models for carbamazepine-induced liver injury have been developed, using high repeated dosing regimens in the mouse and BSO-depleted GSH levels in the rat. In both mice and rat models metabolic capacity and proinflammatory cytokine levels were increased. In the rat, depletion of Kupffer cells decreased proinflammatory cytokine expression and carbamazepine toxicity[294–296]. This suggests that Kupffer cell-produced proinflammatory cytokines are involved in carbamazepine-induced hepatotoxicity. We have used carbamazepine exposure to further understand the interplay between DILI compounds and TNFα in cytotoxic outcome.

Here we systematically determined the role of individual components of the TNFR and related Toll-like receptor (TLR) signaling pathway in modulating drug/TNFα cytotoxicity. We focused on carbamazepine/TNFα-induced apoptosis in our primary screen, later extending these results to a larger panel of TNFα synergistic DILI compounds. We defined 24 genes that modulate DILI carbamazepine/TNFα synergistic apoptosis effects. This includes known modulators of NF-κB activation such as IKBKG (IKKγ or NEMO) and TNFAIP3 (A20) as well as novel players, such as CARD12 (Ipaf, NLRC4) and PHF5A.

Drug-specific and generic candidate gene functions were correlated to several drug-induced stress responses. Our results provide a refined mechanistic understanding of the different TNFR signaling pathway components that control DILI compound-induced adversity outcome.

Material and Methods

Cells and reagents

HepG2 cells were acquired from ATCC (clone HB8065). The cells were maintained and exposed to the various chemicals in DMEM high glucose supplemented with 10% (v/v) FBS, 25 U/mL penicillin and 25 µg/mL streptomycin. The cells were used between passage 5 and 20. For the compound screen, all reference compound (diclofenac, carbamazepine and DMSO) were acquired from Sigma-Aldrich and freshly dissolved in DMSO. The DILI compound library was a kind gift from the Weida Tong, NCTR-FDA. All compounds were dissolved in DMSO, except for metformin, fluphenazine, buthionine sulfoxamine, bromoethlyamine (all PBS), acetaminophen and phenobarbital (all DMEM). All compounds are listed in Suppl. Table 2 together with their respective cmax values. TNFα was acquired from R&D Systems (Abingdon, UK). For the siRNA knockdown experiments, the compounds were resolved fresh from stock in DMSO to a 500-fold DMSO dilution at the intended concentration. Valproic acid was dissolved directly into the medium and spiked with DMSO (final concentration 0.2% v/v). Recombinant AnnexinV labeled with Alexa633 (AnV) was prepared in house as described before[42]. All siRNAs were purchased at Dharmacon GE Healthcare (Lafayette, US). All sequences are listed in Suppl. Table 1.

siRNA screens

Cells were plated and transfected with INTERFERin (Polyplus Transfection) in a 96-well plate. Transfection medium was changed 16-24 hours after transfection. Approximately 72 hours after transfection, the cells were exposed to compounds for 8 hours. For the primary screen, the cells were stimulated with TNFα (1:20 dilution, final concentration 10 ng/mL) and directly live imaged for 24 hours with a BD Pathway TM 855 microscope (Becton Dickinson). For the deconvolution screen and further DILI compound/siRNA experiments, the cells were stimulated with TNFα and imaged for the first time point (t1) on a Nikon TiE2000 confocal laser microscope; after incubation for 24 hours, another image was taken (t24). For an overview of the time scale, see Suppl. Fig 4.

Compound screen

Cells were seeded in 384-well plates and exposed to 24 hours compound, after which the cells were imaged. Next, culture medium (vehicle control) or TNFα (1:10 dilution, final concentration 10 ng/mL) was added and cells were further cultured for another 24 hours, after which the cells were again imaged. Nuclei were stained with Hoechst for live cell imaging, PI and AnnexinV-633 were used to measure cell death. Cell death was quantified using Cell Profiler and R (see image analysis). To calculate the synergistic value, the conditions exposed to TNFα and compound (TNFα + compound) in the same well were

subtracted from the sum of the single exposures in different wells (TNFα) + (compound); (a) + (b) – (a + b) = synergistic value. The synergistic compounds selected for further research did not increase AnV or PI values under compound conditions and did not show increased PI staining upon TNFα exposure. Significance was calculated by Anova and subsequent t-tests with correction for multiple testing with the "fdr" option in the stats package in R[220].

BAC-GFP cell stress reporters

We used BAC-GFP cellular stress reporter data for oxidative stress, ER stress, DNA damage and heat shock response. All data for the BAC-GFP reporter cell lines and DILI compound treatments has been collected previously (Hollander *et al.*, manuscript in preparation). In short, the GFP-reporter cell lines were generated as described previously [44] and maintained in culture as wild-type HepG2 cells. Cells were plated in 384-well plates and exposed for 24 hours. Cells were then imaged with a Nikon TiE2000 confocal laser microscope and analysed as described previously[44]. For this analysis, the mean value of control stimulation (DMSO vehicle 0.2%) was calculated. All cells with GFP levels above this value were counted and a fraction above 1* or 2* mean was calculated.

Image analysis

AnV and propidium iodide (PI) staining was analysed using CellProfiler version 2.1.1[158]. Nuclei were segmented using an in-house watershed module. AnV was imaged using an open pinhole, allowing detection of all AnV staining in a larger focal plane. The total image area positive for AnV and nuclei was measured. For PI, the staining segmentation was masked with the nuclear staining and then measured. Segmentation images were stored for control and data was stored as HDF5 file. The apoptosis is expressed as a fold change over control; general cell death is expressed as percentage PI positive nuclei.

Data analysis

Data analysis and quality control was performed using the in house developed R package H5CellProfiler (Wink *et al.* 2017, manuscript in preparation). Data was further managed with R, using packages plyr, dplyr, tidyr and reshape2[217,218]. For the primary screen, the z-score was calculated. All knockdowns that altered synergism more than 1 z-score value or less than -1 z-score value were included in the validation screen. For the validation screen, the siRNA-mediated knockdowns that altered expression more than 3 times the standard deviation of the control were considered a hit. Hits were considered a candidate gene when more than 2 single siRNA's were a hit in the same direction and the smartpool was also acting in the same direction. Data visualization was performed with ImageJ and R, using the package ggplot[219].

Statistics

Data is the mean of three independent experiments, unless stated different. Significance has been calculated using two-sided t-test with a Welch approximation of the variance,

adjusting the p-value for the false discovery rate as indicated in the figures. A p-value < 0.05 = *, p-value < 0.01 = ** and a p-value < 0.001 = ***.

Results

Identification of TNFR signaling components that regulate DILI compound/TNFα synergy towards apoptosis

To determine both the general and compound specific TNFα signaling pathway components that are involved in compound/TNFα-induced synergistic cell death, we performed a siRNA-mediated knockdown screen. The siRNA library consisted of 163 genes involved in TNFα/Toll-like receptor signaling pathways (see Suppl. Table 1). Carbamazepine was used as exemplary DILI compound for primary screening, since it gives strong synergy with TNFα, inducing apoptosis[16]. HepG2 cells were exposed to carbamazepine for 8 hours and next stimulated with TNFα for 24 hours (Fig. 1A, Suppl. Fig. 4). Live cell imaging revealed 15 genes that affected carbamazepine/TNFα-induced cytotoxicity (Fig. 1D and Suppl. Fig. 1A). In addition, a previously large systematic siRNA screen targeting kinases, ubiquitin editing enzymes and TNFα/Toll-like receptor signaling components identified 19 genes that affect TNFα-induced NF-κB nuclear translocation dynamics (Herpers *et al.* 2017, manuscript in preparation). For validation screening we used early time point (1st hour; siRNA and 8 hours carbamazepine effect) and endpoint measurements (24 hours; carbamazepine and 24 hours TNFα effect) (Fig. 1A and 1C). We validated the knockdown effect of 24 candidate genes on carbamazepine/TNFα-induced synergistic cytotoxicity (Fig. 1E). Knockdown of control caspase-8 and TNF receptor (TNFRSF1A), but also CUL1 and CYLD were among the strongest protectors, while knockdown of PHF5A, FBWX11, TNFAIP3 and IKBKG were the strongest enhancers of carbamazepine/TNFα-induced apoptosis.

Fig. 1: **siRNA screen to detect known TNFR/TLR signaling genes involved in carbamazepine/TNFα synergism** A-B) Overview of experimental setups of the primary and validation screen. C) Representative images and quantification of mock conditions and siRNA-mediated control knockdowns. D) Primary screen data as standard score (Z-score). A Z-score > 1 and < -1 indicates more than a standard deviation difference of the mean and is considered a hit, indicated in red. E) siRNA knockdown effects in carbamazepine/TNFα treated cells were normalized to mock. Visualized are the stacked values of the hits from the primary screen, that also did meet the requirements of the validation screen and were marked as validated candidate gene. Green reflects values lower than, and red reflects values higher than mock minus or plus 3 times the standard deviation of mock. All data is the mean of three independent experiments, error bars reflecting standard deviation.

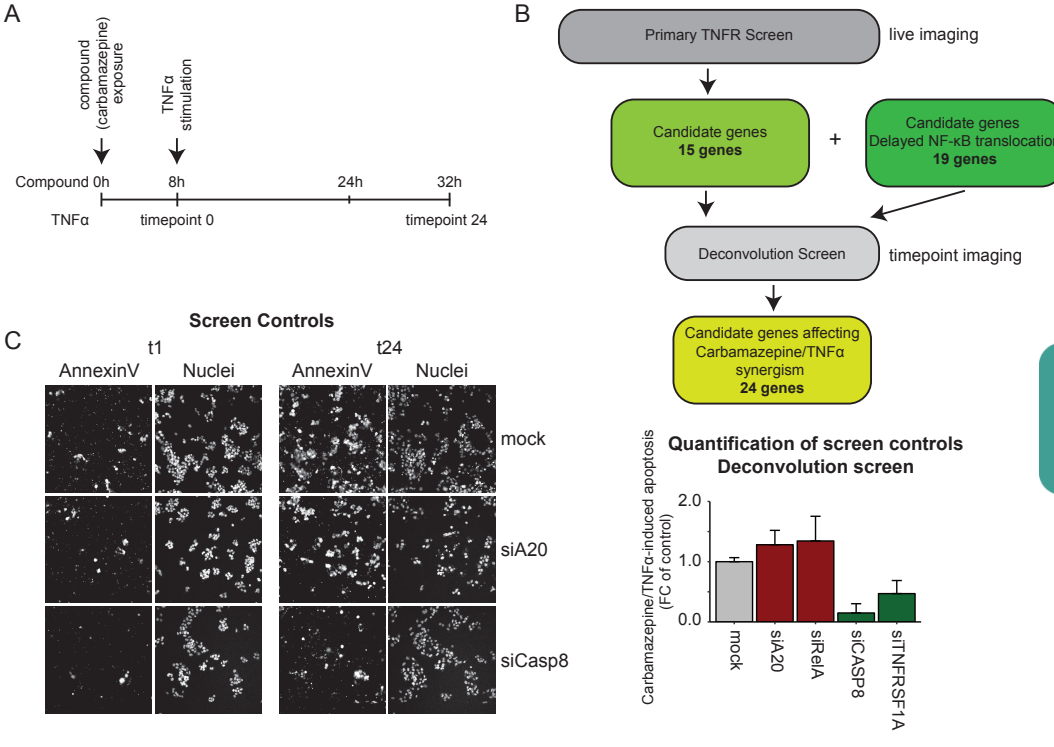
A
compound (carbamazepine) exposure
TNFα stimulation
Compound 0h
8h
24h
32h
TNFα
timepoint 0
timepoint 24
B
Primary TNFR Screen
live imaging
Candidate genes
15 genes
+
Candidate genes
Delayed NF-κB translocation
19 genes
Deconvolution Screen
timepoint imaging
Candidate genes affecting
Carbamazepine/TNFα
synergism
24 genes
C
Screen Controls
t1
t24
AnnexinV
Nuclei
AnnexinV
Nuclei
mock
siA20
siCasp8
Quantification of screen controls
Deconvolution screen
Carbamazepine/TNFα-induced apoptosis
(FC of control)
2.0
1.0
0.0
mock
siA20
siRelA
siCASP8
siTNFRSF1A
D
Primary Screen
Standard Score (z-values)
3
2
1
0
−1
−2
hit
mock
sample
mock
163 siRNA's
E
Validated candidate genes
Singles and smartpool effects stacked
Carbamazepine/TNFα-induced apoptosis
(FC of control; stacked)
10.0
7.5
5.0
2.5
0.0
apoptosis-inducing knockdown
apoptosis-reducing knockdown
no significant effect knockdown
siCASP8
siEP300
siTNFRSF1A
siCUL1
siCARD12
siCYLD
siRAPSN
siTRIM50
siADCK2
siUFD1L
siMAP3K14
siUCHL1
siCDK12
siNFKBIB
siTRIM8
siTNFRSF18
siRBX1
siPIK3R3
siTNFRSF11A
siMAP2K7
siTNFAIP3
siIKBKG
siFBXW11
siPHF5A

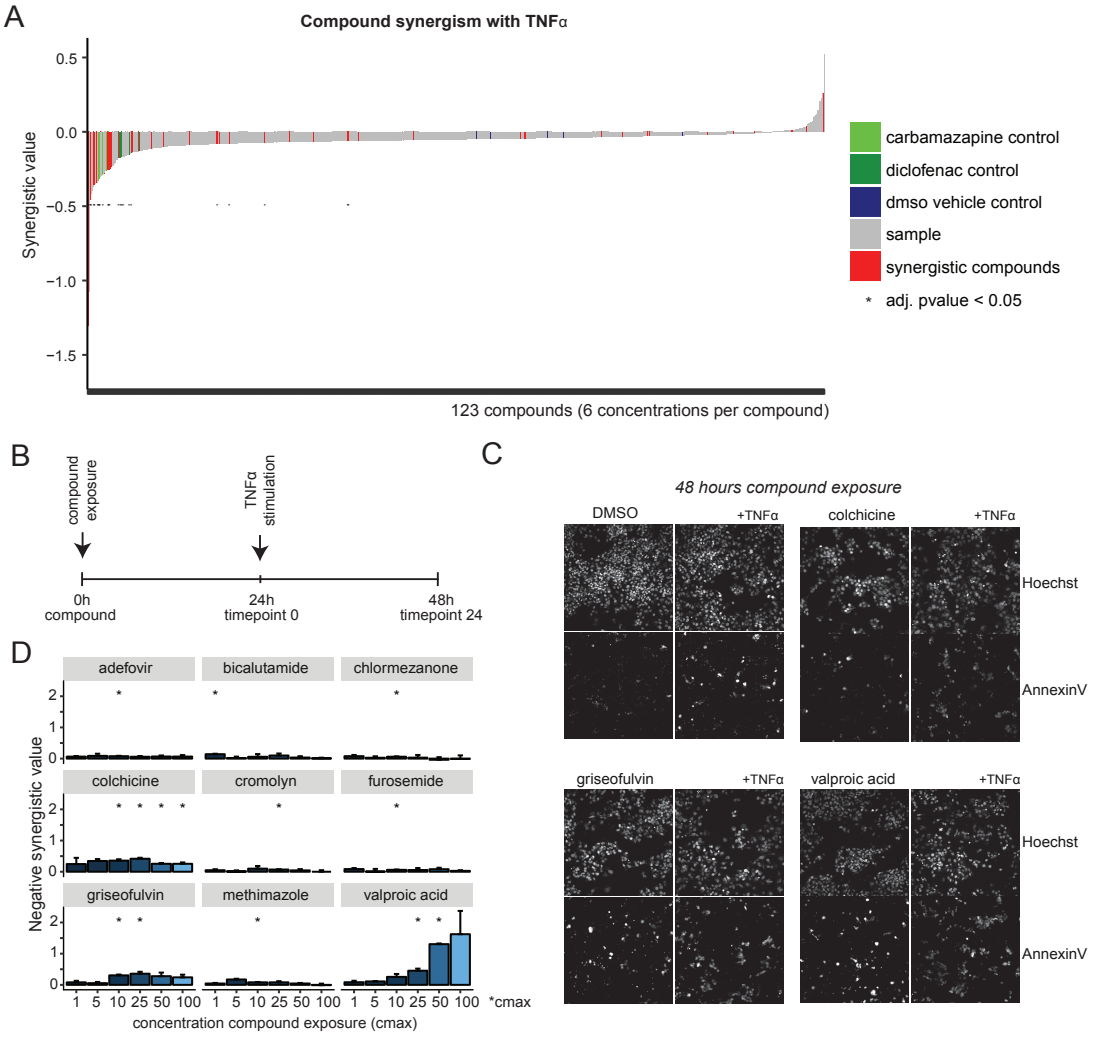

Fig. 2: **DILI compounds that synergize with TNFα towards apoptosis.** Synergism has been calculated by subtracting the conditions exposed to TNFα and compound (TNFα + compound) in the same well from the sum of the single exposures in different wells (TNFα) + (compound). Compound (single exposure) + TNFα (single exposure) - Compound + TNFα (double exposure) = synergistic value. A) An overview of the synergistic value of the compounds in combination with TNFα exposure compared to the cell death induced by compound and TNFα single exposures. Vehicle control DMSO is blue, positive controls are green and all concentrations of compounds that induce significant synergism are red. The concentrations on which there are significant effects of these compounds are indicated with asterixes. B) An overview of the experimental setup of the synergism screen. C) Example images of the compounds chosen from the significantly synergistic compounds in D. Hoechst staining and AnnexinV staining reflects nuclear and apoptosis staining respectively. D) Data of compounds of which at least 1 concentration was significantly synergistic and PI negative. All data is the mean of three independent experiments, error bars reflect standard deviation and * indicates an adjusted p-value < 0.05.

Identification of DILI compounds that synergize with TNFα

To further investigate the signaling components that mediate generic drug/TNFα synergistic effects, we assessed other DILI compounds that could synergize with TNFα. For this, HepG2 cells were exposed for 24 hours to each of 124 DILI compounds at 6 different concentrations and subsequently stimulated with TNFα or control medium (Fig. 2B, Suppl. Table 2). After 48 hours, cell death in compound/TNFα and compound-only treated conditions was determined and synergistic values were calculated (Fig. 2A). Nine DILI compounds showed significant synergistic apoptosis, combined with not significant PI staining. For colchicine, griseofulvin and valproic acid synergism this occurred in a (partially) dose-dependent fashion (Fig. 2C and 2D). At the concentration of 25*cmax, all three compounds did induce significant synergistic apoptosis; this concentration was used for further experiments (Fig. 2D).

TNFR signaling components that generally affect DILI compound/TNFα synergy

We hypothesized that candidate genes that modulate carbamazepine/TNFα synergism could be general TNFα signaling components that define DILI compound/TNFα synergism. To test this, we assessed the effect of siRNA-mediated knockdown of the candidate genes for other synergistic compounds. As we and others have shown diclofenac/TNFα synergistic apoptosis in HepG2 cells, we also included diclofenac[16,42]. After a pre-exposure of 8 hours the accumulation of cell death markers before and after 24 hr TNFα stimulation was determined by time point imaging, in a similar way as the carbamazepine validation screen (Fig. 1A and Suppl. Fig. 4). Quantification of the AnV labeling indicated DILI compound/TNFα-induced apoptosis (Fig.3A).

Most of the candidate gene knockdowns did not affect DILI compound treatment alone; only TNFRSF1A and PHF5A knockdown compared to mock treatment caused a modest increase of apoptosis for all DILI compounds (Suppl. Fig. 2). For all compounds tested, TNFα-induced synergism could be induced by knockdown of A20 (TNFAIP3) (Fig. 3A and 3B). Unexpectedly, our control siRNA against caspase 8 (CASP8) did not protect against colchicine/TNFα-induced synergism (Fig. 3A and 3B), implying that colchicine-mediated TNFα-induced apoptosis has a diverging mechanism independent of TNFR-mediated caspase-8 activation. Interestingly, most candidate genes that upon knockdown enhanced carbamazepine/TNFα-induced synergism, showed a similar response for the other DILI compound/TNFα synergisms (Fig. 3C). The effect level of knockdown of the different candidate genes was compound-specific. For example griseofulvin showed modest effects, in contrast to valproic acid which showed major enhancement of its already high levels of synergism (Fig. 3B). For the candidate genes that upon knockdown inhibited apoptosis, diverse effects were observed for the different DILI compound/TNFα treatments. Strikingly, whereas knockdown of the candidate genes did generally protect against griseofulvin/TNFα-induced cell death, it did induce extra colchicine/TNFα-induced synergistic apoptosis (Fig. 3C).

Knockdown of TNFAIP3 (A20), PHF5A, MAP2K7, IKBKG, CYLD and TNFRSF1A (TNFR) showed the same effect direction for all DILI compounds (Fig. 3Cii), making these genes generic modulators of the drug/TNFα signaling interaction. Since TNFRSF1A (TNFR), A20, CYLD and IKBKG are extremely well-characterized modulators of TNFR signaling, this indicates that the observed compound/TNFα synergistic apoptosis is based on TNFα-induced cell death[141].

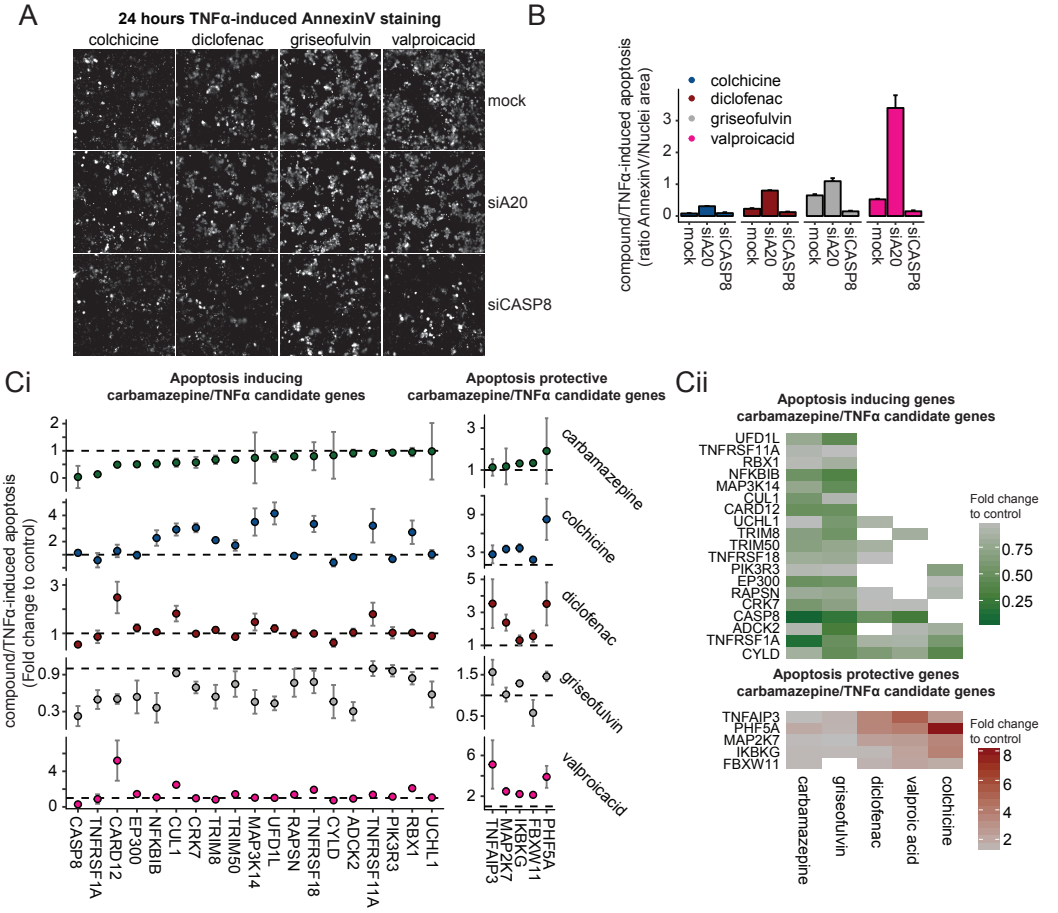

Fig. 3: **Knockdown of TNFα signaling pathway component effects diverge between TNFα synergism by different compound** A) Representative images of AnV staining upon 32 hr of compound exposure together with 24 hours of TNFα stimulation. B) Quantification of the AnV response in A, visualized as AnV/Nuclei area. Ci) Control-normalized values of synergistic apoptosis (AnV/Nuclei) upon knockdown. Cii) Heatmaps of the control-normalized values of synergistic genes in carbamazepine/TNFα-induced synergistic apoptosis. The color reflects the control-normalized effect of the knockdown. All data is the mean of three independent experiments, error bars reflecting standard deviation.

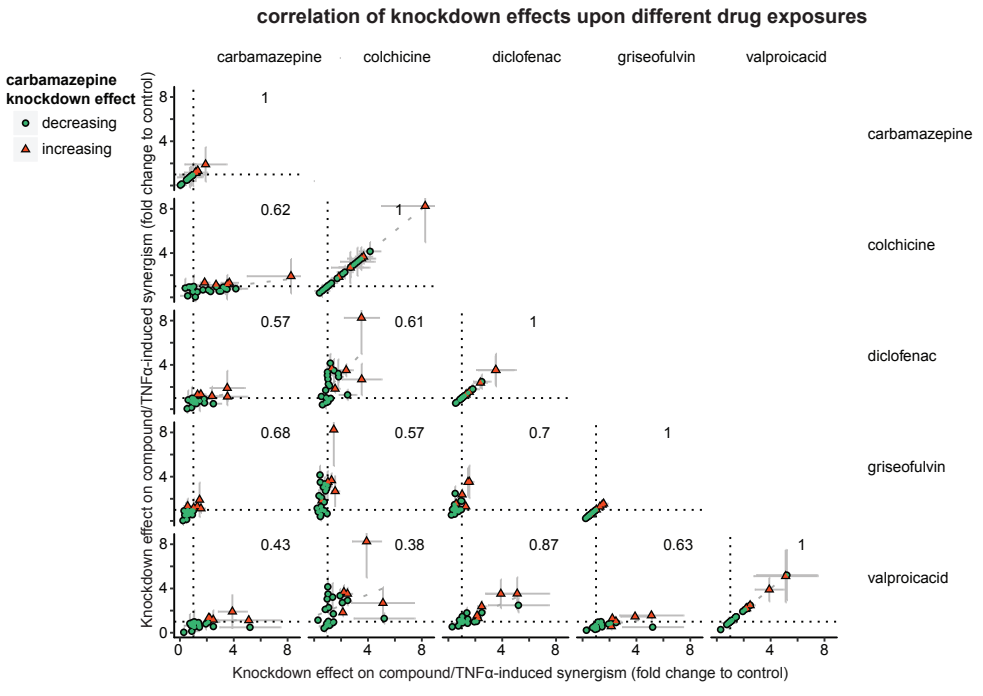

Fig. 4: **DILI compound specific candidate gene effects on TNFα synergism** Knockdown effects of candidate genes on synergistic apoptosis have been plotted compound versus compound. The Pearson correlation coefficient has been calculated and is displayed in the graphs in text. The colors and shapes reflect the effect of the knockdown in the carbamazepine/TNFα condition. Green (round) are carbamazepine/TNFα synergism inhibiting knockdowns, red (triangle) are carbamazepine/TNFα synergism enhancing knockdowns. All data is the mean of three independent experiments, error bars reflecting standard deviation.

Next, we determined which compounds demonstrate the highest similarity for facilitating TNFα-induced apoptosis, based on the effects of the respective knockdowns. Therefore, we correlated the compound/TNFα synergism effects between the different compounds. Interestingly, valproic acid/TNFα synergism showed strongest correlation with diclofenac and only a modest correlation with carbamazepine (Fig. 4). In general, all compound knockdown effects did correlate mildly with each other, suggesting involvement of both general and compound-specific TNFα pathway characteristics in all drug/TNFα synergism responses.

Association with DILI compound/TNFα synergy mechanisms with cellular stress response activation

To interpret the function of candidate genes in compound-specific interaction with TNFα, we studied specific compound-induced cellular stress responses. In another study we mapped the activation of cellular stress responses using BAC-GFP HepG2 reporter cell lines. SRXN1 and HMOX1 are target genes of Nrf2, and their expression is regulated by oxidative

stress; p21 and BTG2 are both regulated by p53 activity and represent DNA damage; BiP and CHOP are activated upon ER stress; and HSPA1B is a heat shock family member and its expression is regulated by HSF1 and activated during protein unfolding[135,297–299]. Exposure to carbamazepine, colchicine, diclofenac, griseofulvin and valproic acid for 24 hours induced unique stress response activation profiles of one or more reporters (Suppl. Fig. 3). The strongest responses were observed for SRXN1-GFP, p21-GFP, CHOP-GFP and HSPA1B-GFP reporters. BTG2-GFP and HMOX1-GFP showed some mild responses. BiP-GFP levels were hardly increased and even showed a dose-dependent decrease for some compounds (Suppl. Fig. 3).

To link these stress response profiles to the effect of knockdown in DILI compound/TNFα synergism, we correlated the stress response induction to the effects of the knock down of the candidate genes. A high positive correlation with a stress response means that as the stress response shows more activation by a certain compound, the synergism with this compound and TNFα is stronger under knockdown condition. In contrast, a negative correlation indicates that the knockdown-induced protection against compound/TNFα synergism is stronger when a particular cellular stress reponse is higher. A strong positive or negative correlation suggests that the function of this candidate gene in compound/TNFα synergism is associated to the compound-induced stress response. In both cases, this could lead to altered TNFα-induced apoptosis.

Strikingly, we observed a pattern of two alternating stress response profiles that correlate strongly with the synergistic effect of knockdown of different candidate genes. The effects of knockdown of one candidate gene group correlates with the expression of SRXN1 and P21 (CASP8, CRK7, CUL1, MAP2K7, MAP3K14, NFKBIB, PHF5A, TNFRSF11, TNFRSF18, TRIM8, and UFD1L) and others with HMOX1 and BTG2 (CARD12, PIK3R3, RAPSN, and TNFAIP3; see Fig. 5B). This suggests that although correlated to the same stress responses (oxidative stress and DNA damage), at least two major, different branches of these stress responses attribute to the synergistic DILI compound/TNFα cytotoxicity. An schematic overview of this study can be found in Suppl. Fig. 4.

Fig. 5: **Correlation of compound effects on TNFα synergism with DILI compound-induced stress responses** A) Compound-induced stress responses are plotted versus the compound/TNFα synergism effects per siRNA. Colors reflect different compounds. A linear relation is plotted with the 95% confidence interval as grey shaded area. B) The Pearson's correlation coefficient is calculated of the conditions shown in A. Correlations higher than 0.6 and lower than -0.6 are colored green and orange respectively. All data is the mean of three independent experiments.

Genes regulating hepatotoxic drug/TNFα-induced synergistic apoptosis

A

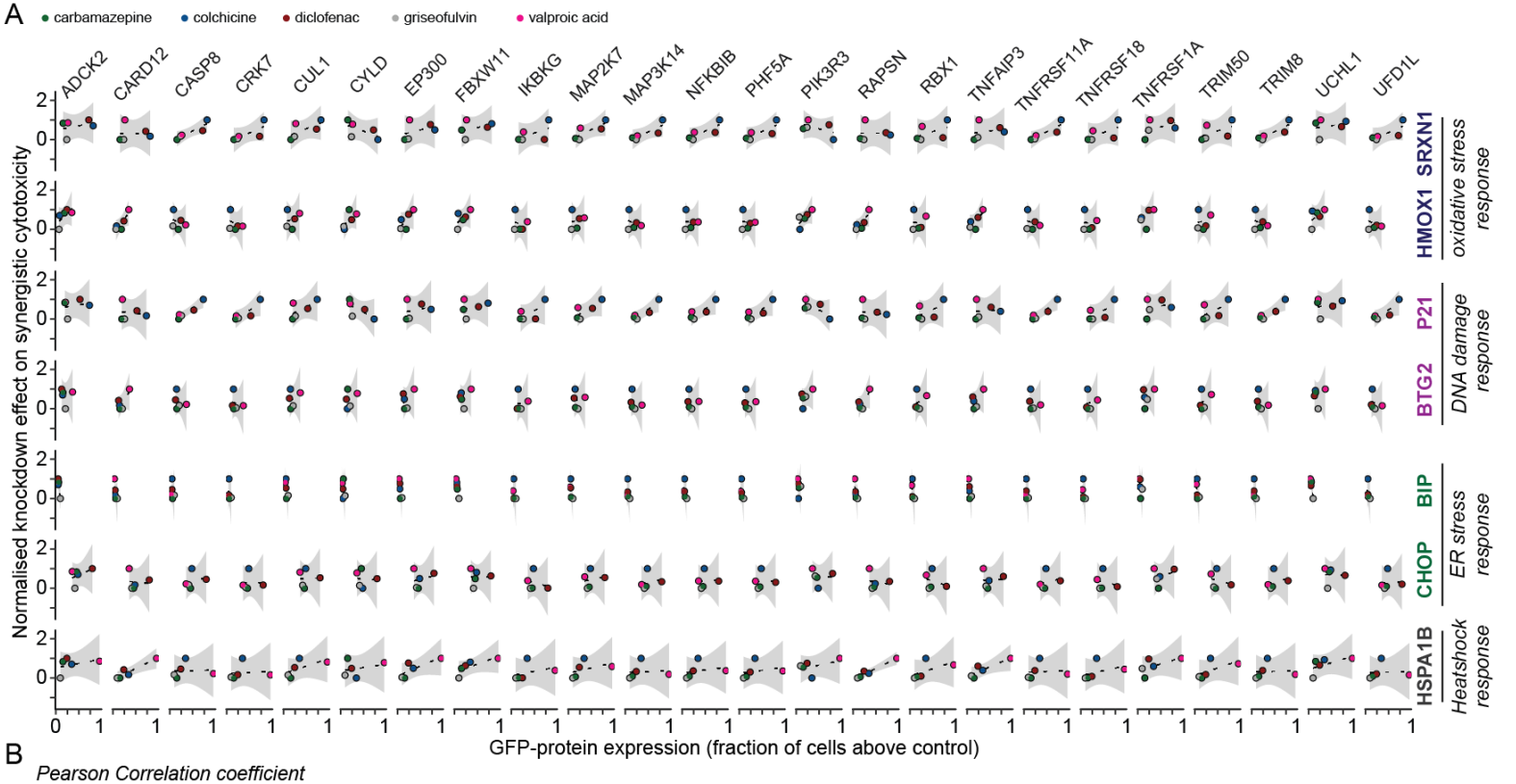

B

Pearson Correlation coefficient

Compound-induced stress responses and the effect of knockdown on compound/TNFα-induced apoptosis

correlation > 0.6 correlation < -0.6

	adck2	card12	casp8	crk7	cul1	cyld	ep300	fbxw11	ikbkg	map2k7	map3k14	nfkbib	phf5a	pik3r3	rapsn	rbx1	tnfaip3	tnfrsf11a	tnfrsf18	tnfrsf1a	trim50	trim8	uchl1	ufd1l
SRXN1	0.34	0.01	0.91	0.77	0.68	-0.61	0.41	0.37	0.58	0.82	0.85	0.82	0.79	-0.55	-0.01	0.50	0.24	0.89	0.61	0.45	0.53	0.88	0.25	0.78
HMOX1	0.68	0.87	-0.34	-0.39	0.21	0.72	0.73	0.65	-0.20	0.11	-0.29	-0.12	-0.15	0.78	0.85	0.05	0.77	-0.29	-0.13	0.52	0.08	-0.28	0.56	-0.35
P21	0.22	-0.14	0.96	0.87	0.65	-0.69	0.24	0.29	0.68	0.80	0.92	0.86	0.84	-0.72	-0.14	0.56	0.09	0.94	0.69	0.28	0.57	0.94	0.22	0.87
BTG2	-0.06	0.77	-0.32	-0.24	0.26	0.29	0.48	0.36	0.06	0.00	-0.33	-0.15	-0.12	0.62	0.80	0.27	0.64	-0.30	0.09	0.41	0.32	-0.35	0.18	-0.30
BIP	-0.90	-0.72	-0.31	-0.31	-0.66	-0.38	-0.79	-0.98	-0.44	-0.69	-0.43	-0.55	-0.53	-0.13	-0.75	-0.60	-0.73	-0.40	-0.49	-0.47	-0.59	-0.43	-0.94	-0.37
CHOP	0.44	-0.08	0.26	0.01	0.03	-0.10	0.23	0.01	-0.24	0.20	0.18	0.12	0.06	-0.01	-0.17	-0.29	0.06	0.22	-0.20	0.32	-0.25	0.23	-0.03	0.06
HSPA1B	0.39	0.94	0.04	0.09	0.63	0.29	0.80	0.78	0.36	0.45	0.07	0.27	0.28	0.46	0.97	0.59	0.88	0.09	0.41	0.61	0.62	0.06	0.60	0.07

Discussion

In the current study we have systematically determined DILI compounds that synergize with TNFα and several individual signaling components of the TNFR/TLR signaling pathways that are required in this process. Out of 124 DILI compounds we observed strongest synergistic activity for valproic acid, griseofulvin, and colchine. Out of in total 182 candidate genes involved in TNFR/TLR signaling we identified 24 genes that are genuinely involved in DILI compound/TNFα synergy. Of the generic TNFα toxicity regulators, TNFAIP3 (A20) and PHF5A are strongly involved in suppressing TNFα-mediated cell death, while TNFRSF1A (TNF receptor), CYLD and ACDK2 are generally involved in promoting TNFα-induced apoptosis. In addition, we detected several genes that affected TNFα synergy in a more or less compound-specific manner. Altogether, our data suggest that drugs synergize with TNFα towards cytotoxicity in both compound specific and general ways. Given the overall involvement of inflammatory responses in DILI, we anticipate that screening for TNFα synergy would be relevant in DILI liability assessment. Also, mechanistic insight in generic compound/TNFα synergism regulators could be directly used to increase test sensitivity, for instance by using TNFAIP3 or PHF5A knockout/diminished expression cell lines.

Our data indicate a very strong synergistic interaction between valproic acid and TNFα-mediated pro-apoptotic signaling in liver cells. Hepatotoxicity of the anti-epileptic, HDAC inhibiting drug valproic acid is so far mainly associated with its metabolites and the onset of mitochondrial injury[290]. Indeed, valproic acid-induced liver toxicity is most of the time dose-dependent and not idiosyncratic. This argues against an important role of proinflammatory signaling in the etiology of valproic acid-induced liver inury. However, rare cases of severe idiosyncratic acute liver injury have been detected and their etiology is currently unkown[290,300]. *In vitro*, valproic acid synergizes towards apoptosis with TNFα exposure in U937 cells[301] and induces mitochondrial dysfunction in HepG2 cells[302]. Lymphocytes exposed to a dose range of valproic acid secrete TNFα in a dose-dependent fashion[303]. We show that valproic acid/TNFα synergy is remarkable similar to the much better characterized diclofenac/TNFα synergy. The strong correlation suggests a similar mechanism by which these compounds affect TNFα signaling outcome.

Here, we demonstrate that valproic acid/TNFα synergy towards apoptosis is fully dependent on caspase 8 and can be very strongly enhanced by knockdown of CARD12, TNFAIP3 (A20) and PHF5A. Of these, knockdown of CARD12 and TNFAIP3 effects were strongly associated with the onset of the stress response reflected by HMOX1, BTG2 and HSPA1B upregulation (Fig. 5). Diclofenac and valproic acid differ greatly in their stress reporter activation profile (Suppl. Fig. 3), in stark contrast to the high similarity in drug/TNFα cytotoxic synergism. This suggests that TNFα synergism is not fully determined by the drug-induced cellular stress response pathways, but relies on drug-induced alterations in the TNFα pathway itself. The exact interaction between the candidate genes and valproic acid or diclofenac-induced stress response activation warrants further research.

Griseofulvin is an antifungal agent that inhibits fungal replication and microtubule formation. Very rare cases of hepatotoxicity have been related to griseofulvin use[304]. *In vivo* rat experiments showed mild liver injury upon repeated griseofulvin exposure with inflammation and leukocyte infiltration[305]. In this study, we show for the first time that griseofulvin synergizes with TNFα towards apoptosis and that candidate gene knockdown in general inhibits this synergism. Griseofulvin does not induce many cellular stress responses, making the drug-induced liver injury hazard, although very low, unexpected. The synergistic TNFα/griseofulvin hepatotoxicity *in vitro* provides insight into griseofulvin-induced liver injury in humans.

The anti-gout therapy colchicine was also detected as synergistically inducing TNFα-induced apoptosis. Colchicine binds to the alpha and beta subunit of tubulin, has a weak anti-inflammatory effect and disturbs many cellular signaling pathways in various cell types. Colchicine-induced toxicity is uncommon, but when it occurs it is severe and is characterized by multi-organ toxicity[306]. In a study using precision-cut liver slices, super-pharmacological exposures with cholchicine (2.5 – 5 mM) did induce transcriptomic changes that correctly classified colchicine toxicity as a necrotic damage inducing compound. These changes included upregulation of genes involved in the heatshock, ER stress, oxidative stress responses and lipid metabolism[133]. Indeed, we also see upregulation of oxidative stress response (SRXN1), in combination with upregulation of the DNA damage response (p21) by colchicine exposure (Suppl. Fig. 3). Knockdown of candidate genes in colchicine/TNFα treated cells in general enhance the synergistic response (Fig. 3). This effect is a stark contrast to the generally inhibiting effect of candidate gene knockdown in griseofulvin/TNFα-induced toxicity.. Interestingly, we show that colchicine/TNFα-induced toxicity is not caspase-8 dependent. This is similar to the well-characterized synergistically trovafloxacin/TNFα-induced apoptosis. Trovafloxacin induces strong p21 activation and cell death via caspase 9 activation[120]. More research is necessary to show if colchicine and trovafloxacin induce TNFα toxicity in a similar manner.

Unexpectedly, CHOP expression does not show correlation with the effect of candidate gene knockdown on compound/TNFα-induced apoptosis. Previously, we have shown that CHOP expression is necessary for carbamazepine and diclofenac-mediated TNFα-induced apoptosis[16]. However, CHOP induction is a relatively late event in the process of apoptosis and our candidate genes are acting more upstream in the compound/TNFα interaction. In addition, we did not see strong concentration-dependent effects on CHOP induction by compounds other than diclofenac and carbamazepine, which suggests strong compound-specific effects (Suppl. Fig. 3).

Inhibited expression of some candidate genes affected compound/TNFα synergism very strongly. For instance, knockdown of the key inflammasome subunit CARD12 (Ipaf, NLRC4) induced strong effects upon most DILI compound/TNFα conditions. Such a role of CARD12 has not been described previously.

CARD12 is involved in IL1β processing[307]. Also knockdown of TNFAIP3 (A20) strongly promoted DILI compound/TNFα synergistic apoptosis, as expected. Both siCARD12 and siA20 effects correlated with a similar cellular stress response profile, including the induction of HMOX1, BTG2, HSPA1B and the reduction of BIP expression (Fig. 5B). *In vivo,* both proteins activate regenerative or protective responses upon liver damage upon carbon tetrachloride or partial hepatectomy[141,308,309]. *In vitro,* CARD12 is a target gene of p53 activity while A20 regulates the expression of p21, independently of p53 activity[309,310]. However, A20 knockout has no effect on LPS-induced CARD12 inflammasome formation in macrophages[311]. As the function of A20 and CARD12 are likely very cell type and context dependent, it would be very interesting to see their role and interaction in drug and TNFα -treated hepatocytes.

The strongest enhancer of synergistic compound/TNFα-induced apoptosis determined in this study is knockdown of PHF5A. The overall function of PHF5A is not well-described. PHF5A is essential for maintaining pluripotency in different types of stem cells by regulating Ser2 phosphorylation of RNA polymerase II and thereby inducing transcriptional elongation of certain gene targets[312]. Interestingly, CRK7 (CDK12), another candidate gene modulating TNFα responses detected in this study, is has a similar function. CRK7 also regulates Ser2 RNA polymerase II phosphorylation, regulating the expression of DNA damage and oxidative stress target genes[198,199]. We assessed that effects of both siCRK7 and siPHF5A on compound/TNFα-induced cytotoxicity correlate strongly with SRXN1-GFP and p21-GFP induction, two stress responses induced by almost all our compounds at varying levels (Suppl. Fig. 3). Therefore, we anticipate that PHF5A, similar to CRK7, regulates transcriptional elongation and is a novel regulator of specific subsets of stress-regulated target genes, including SRXN1 and P21. We show that CRK7 and PHF5A knockdown have opposite effects on compound/TNFα synergism. This suggests that both PHF5A and CRK7 regulate separate subsets of Nrf2 and p53 target gene expression. The subsequent different activity of these adaptive cellular stress responses could well lead to the partially opposing effects upon PHF5A and CRK7 knockdown on synergistic compound/TNFα-induced cytotoxicity.

The TNFα signaling pathway has long been an area of great interest and anti-TNFα therapies are a great improvement in the treatment of many immune-related diseases. However, their efficacy cannot always be predicted or explained. Furthermore, TNFα inhibitors have been associated with an increased risk on drug-induced liver injury[139]. In addition, excessive TNFα signaling is implicated in many liver disease states. To be able to treat inflammation driven diseases, an improved understanding of the TNFα signaling pathway in a cell and context specific manner is essential. In this study, we identified critical modulators of TNFα-mediated hepatocyte death, including PHF5A, CRK7 (CDK12), TNFAIP3 (A20) and CARD12. We anticipate this will contribute to alternative therapeutic approaches for treatment of TNFα-dependent inflammatory disease states, including adverse drug reactions.

Acknowledgements

This work was supported by the Innovative Medicine Initiative MIP-DILI project (Grant agreement No. 115336) and the European Union's **Horizon 2020** research and innovation programme EU-ToxRisk project (grant agreement No 681002)

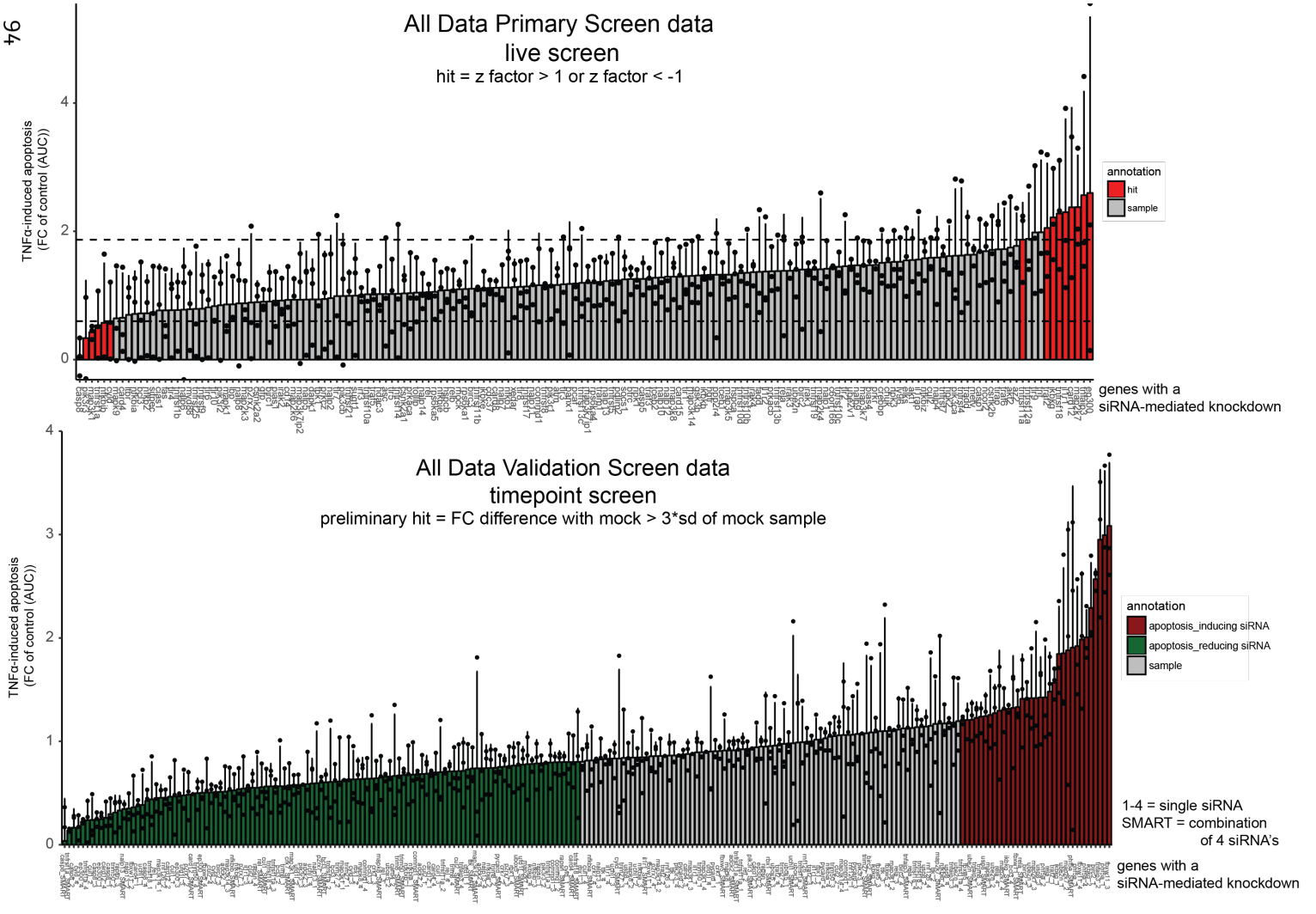
All Data Primary Screen data
live screen
hit = z factor > 1 or z factor < -1
TNFα-induced apoptosis
(FC of control (AUC))
annotation
hit
sample
genes with a
siRNA-mediated knockdown
All Data Validation Screen data
timepoint screen
preliminary hit = FC difference with mock > 3*sd of mock sample
TNFα-induced apoptosis
(FC of control (AUC))
annotation
apoptosis_inducing siRNA
apoptosis_reducing siRNA
sample
1-4 = single siRNA
SMART = combination
of 4 siRNA's
genes with a
siRNA-mediated knockdown

Suppl. Fig. 1: **Data of the primary and validation siRNA screen** A) Visualization of the control-normalized visualization of all data. Mean are reflected as bar graphs and separate experiments as black dots. Hits with a Z-score of higher than 1 or lower than -1 are visualized in red. B) Control-normalized data, of which the mean is reflected as bar graphs and separate experiments as black dots. Hits that alter synergism with more than 3 times the standard deviation of mock control are red and green for increasing and decreasing apoptosis respectively. All data is the mean of three independent experiments and error bars reflect the standard deviation

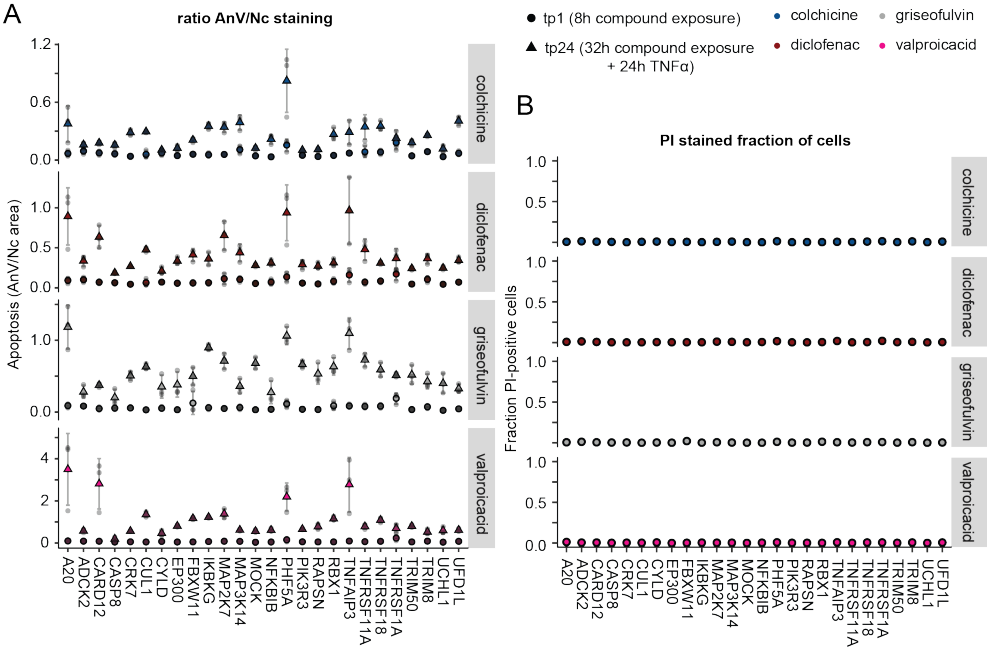

Suppl. Fig. 2: **Effect of knockdowns on DILI compound cytotoxicity** A) Apoptosis reflected as non-normalized AnV/Nuclei ratios. Different compounds are visualized in different colors. B) PI staining is shown as the fraction of cells that is considered PI positive. Different compounds are visualized in different colors. All data is the mean of three independent experiments.

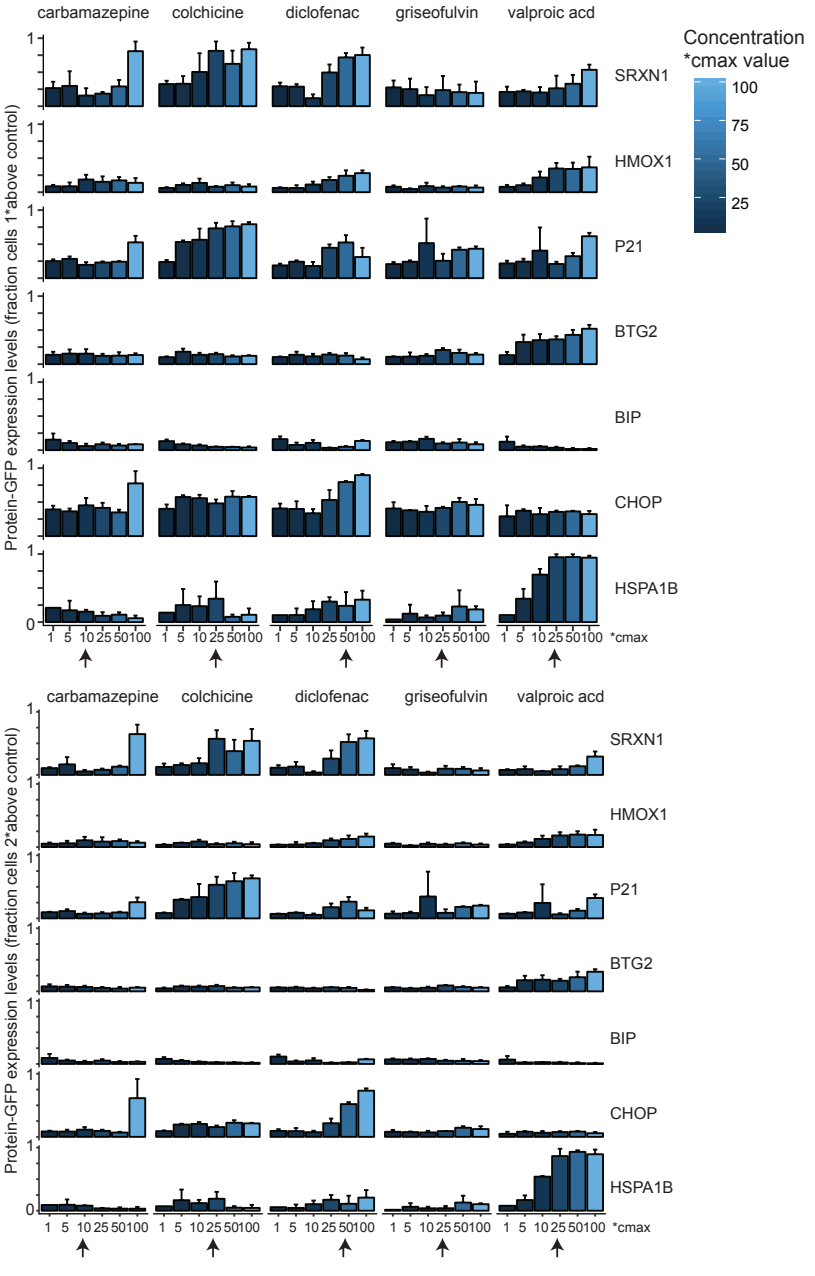

Suppl. Fig. 3: **DILI compound-induced cellular stress responses** The fraction of cells that has GFP levels higher than 1*mean (upper panel) or 2*mean (lower panel) of the control condition at 24 hours of exposure is visualized in bar graphs. Color reflects the concentration of exposure. All data is the mean of three independent experiments and error bars reflect standard deviation.

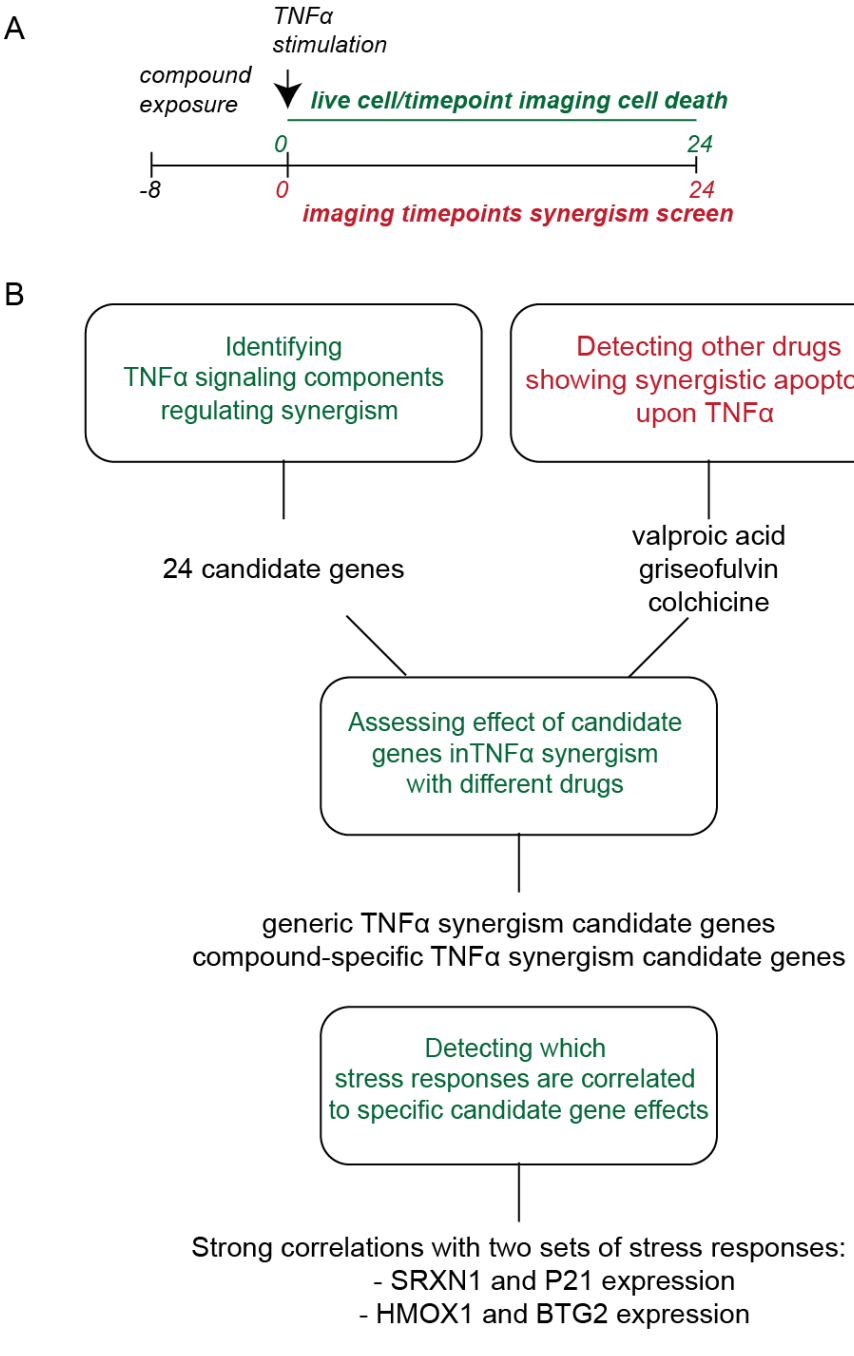

Suppl. Fig. 4: **Schematic overview of experimental design and key results** A) Overview of time lines in different experimental designs (indicated by colors). B) Experimental workflow of this study. Colored text refers back to time schedules in A

Supplementary Tables

Gene Symbol	Pool Number	Duplex Number	Gene Id	Accession Number	Gene Symbol	Pool Number	Duplex Number	Gene Id	Accession Number
AKT1	M-003000-03	D-003000-05	207	NM_001014431	MAP3K1	M-003575-02	D-003575-02	4214	NM_005921
AKT1	M-003000-03	D-003000-07	207	NM_001014431	MAP3K1	M-003575-02	D-003575-04	4214	NM_005921
AKT1	M-003000-03	D-003000-22	207	NM_001014431	MAP3K1	M-003575-02	D-003575-05	4214	NM_005921
AKT1	M-003000-03	D-003000-08	207	NM_001014431	MAP3K1	M-003575-02	D-003575-03	4214	NM_005921
AKT2	M-003001-02	D-003001-05	208	NM_001626	MAP3K14	M-003580-04	D-003580-10	9020	NM_003954
AKT2	M-003001-02	D-003001-21	208	NM_001626	MAP3K14	M-003580-04	D-003580-11	9020	NM_003954
AKT2	M-003001-02	D-003001-07	208	NM_001626	MAP3K14	M-003580-04	D-003580-12	9020	NM_003954
AKT2	M-003001-02	D-003001-08	208	NM_001626	MAP3K14	M-003580-04	D-003580-26	9020	NM_003954
ASC	M-004378-01	D-004378-03	29108	NM_013258	MAP3K5	M-003584-02	D-003584-01	4217	NM_005923
ASC	M-004378-01	D-004378-04	29108	NM_013258	MAP3K5	M-003584-02	D-003584-04	4217	NM_005923
ASC	M-004378-01	D-004378-05	29108	NM_013258	MAP3K5	M-003584-02	D-003584-09	4217	NM_005923
ASC	M-004378-01	D-004378-01	29108	NM_013258	MAP3K5	M-003584-02	D-003584-03	4217	NM_005923
ATM	M-003201-04	D-003201-28	472	NM_138292	MAP3K7	M-003790-06	D-003790-17	6885	NM_145333
ATM	M-003201-04	D-003201-27	472	NM_138292	MAP3K7	M-003790-06	D-003790-31	6885	NM_145333
ATM	M-003201-04	D-003201-29	472	NM_138292	MAP3K7	M-003790-06	D-003790-16	6885	NM_145333
ATM	M-003201-04	D-003201-30	472	NM_138292	MAP3K7	M-003790-06	D-003790-18	6885	NM_145333
AZ2	M-014092-00	D-014092-03	64343	NM_022461	MAP3K7IP1	M-004770-02	D-004770-02	10454	NM_153497
AZ2	M-014092-00	D-014092-04	64343	NM_022461	MAP3K7IP1	M-004770-02	D-004770-03	10454	NM_153497
AZ2	M-014092-00	D-014092-01	64343	NM_022461	MAP3K7IP1	M-004770-02	D-004770-18	10454	NM_153497
AZ2	M-014092-00	D-014092-02	64343	NM_022461	MAP3K7IP1	M-004770-02	D-004770-01	10454	NM_153497
BCL3	M-003874-02	D-003874-12	602	NM_005178	MAP3K7IP2	M-004771-01	D-004771-02	23118	NM_015093
BCL3	M-003874-02	D-003874-10	602	NM_005178	MAP3K7IP2	M-004771-01	D-004771-03	23118	NM_015093
BCL3	M-003874-02	D-003874-11	602	NM_005178	MAP3K7IP2	M-004771-01	D-004771-17	23118	NM_015093
BCL3	M-003874-02	D-003874-09	602	NM_005178	MAP3K7IP2	M-004771-01	D-004771-04	23118	NM_015093
BIRC1	M-004389-02	D-004389-01	4671	NM_022892	MAP3K8	M-003511-03	D-003511-07	1326	NM_005204
BIRC1	M-004389-02	D-004389-04	4671	NM_022892	MAP3K8	M-003511-03	D-003511-08	1326	NM_005204
BIRC1	M-004389-02	D-004389-05	4671	NM_022892	MAP3K8	M-003511-03	D-003511-10	1326	NM_005204
BIRC1	M-004389-02	D-004389-02	4671	NM_022892	MAP3K8	M-003511-03	D-003511-09	1326	NM_005204
BIRC2	M-004390-02	D-004390-08	329	NM_001166	MAPK1	M-003555-04	D-003555-01	5594	NM_138957
BIRC2	M-004390-02	D-004390-10	329	NM_001166	MAPK1	M-003555-04	D-003555-04	5594	NM_138957
BIRC2	M-004390-02	D-004390-09	329	NM_001166	MAPK1	M-003555-04	D-003555-03	5594	NM_138957
BIRC2	M-004390-02	D-004390-11	329	NM_001166	MAPK1	M-003555-04	D-003555-09	5594	NM_138957
BIRC3	M-004099-02	D-004099-02	330	NM_001165	MAPK9	M-003505-02	D-003505-05	5601	NM_002752
BIRC3	M-004099-02	D-004099-08	330	NM_001165	MAPK9	M-003505-02	D-003505-09	5601	NM_002752
BIRC3	M-004099-02	D-004099-09	330	NM_001165	MAPK9	M-003505-02	D-003505-06	5601	NM_002752
BIRC3	M-004099-02	D-004099-10	330	NM_001165	MAPK9	M-003505-02	D-003505-07	5601	NM_002752
BTRC	M-003463-01	D-003463-02	8945	NM_033939	MEFV	M-011081-00	D-011081-01	4210	NM_000243
BTRC	M-003463-01	D-003463-04	8945	NM_033939	MEFV	M-011081-00	D-011081-02	4210	NM_000243
BTRC	M-003463-01	D-003463-01	8945	NM_033939	MEFV	M-011081-00	D-011081-04	4210	NM_000243
BTRC	M-003463-01	D-003463-03	8945	NM_033939	MEFV	M-011081-00	D-011081-03	4210	NM_000243
C6ORF166	M-031863-00	D-031863-02	55122	NM_018064	MYD88	M-004769-01	D-004769-02	4615	NM_002468
C6ORF166	M-031863-00	D-031863-01	55122	NM_018064	MYD88	M-004769-01	D-004769-04	4615	NM_002468
C6ORF166	M-031863-00	D-031863-03	55122	NM_018064	MYD88	M-004769-01	D-004769-01	4615	NM_002468
C6ORF166	M-031863-00	D-031863-04	55122	NM_018064	MYD88	M-004769-01	D-004769-03	4615	NM_002468
CARD12	M-004396-00	D-004396-01	58484	NM_021209	NALP1	M-004423-02	D-004423-05	22861	NM_001033053
CARD12	M-004396-00	D-004396-02	58484	NM_021209	NALP1	M-004423-02	D-004423-02	22861	NM_001033053
CARD12	M-004396-00	D-004396-04	58484	NM_021209	NALP1	M-004423-02	D-004423-04	22861	NM_001033053
CARD12	M-004396-00	D-004396-03	58484	NM_021209	NALP1	M-004423-02	D-004423-03	22861	NM_001033053
CARD15	M-003464-01	D-003464-02	64127	NM_022162	NALP10	M-019113-01	D-019113-01	338322	NM_176821
CARD15	M-003464-01	D-003464-02	64127	NM_022162	NALP10	M-019113-01	D-019113-03	338322	NM_176821
CARD15	M-003464-01	D-003464-04	64127	NM_022162	NALP10	M-019113-01	D-019113-02	338322	NM_176821
CARD15	M-003464-01	D-003464-07	64127	NM_022162	NALP10	M-019113-01	D-019113-04	338322	NM_176821
CARD4	M-004398-00	D-004398-03	10392	NM_006092	NALP11	M-009033-01	D-009033-01	204801	NM_145007
CARD4	M-004398-00	D-004398-04	10392	NM_006092	NALP11	M-009033-01	D-009033-02	204801	NM_145007
CARD4	M-004398-00	D-004398-02	10392	NM_006092	NALP11	M-009033-01	D-009033-04	204801	NM_145007
CARD4	M-004398-00	D-004398-01	10392	NM_006092	NALP11	M-009033-01	D-009033-03	204801	NM_145007
CARD8	M-004454-00	D-004454-04	22900	NM_014959	NALP12	M-015092-00	D-015092-01	91662	NM_033297
CARD8	M-004454-00	D-004454-02	22900	NM_014959	NALP12	M-015092-00	D-015092-03	91662	NM_033297
CARD8	M-004454-00	D-004454-01	22900	NM_014959	NALP12	M-015092-00	D-015092-04	91662	NM_033297
CARD8	M-004454-00	D-004454-03	22900	NM_014959	NALP12	M-015092-00	D-015092-02	91662	NM_033297
CASP1	M-004401-03	D-004401-18	834	NM_033295	NALP13	M-018073-01	D-018073-03	126204	NM_176810
CASP1	M-004401-03	D-004401-03	834	NM_033295	NALP13	M-018073-01	D-018073-02	126204	NM_176810
CASP1	M-004401-03	D-004401-02	834	NM_033295	NALP13	M-018073-01	D-018073-01	126204	NM_176810
CASP1	M-004401-03	D-004401-05	834	NM_033295	NALP13	M-018073-01	D-018073-04	126204	NM_176810
CASP5	M-004405-01	D-004405-02	838	NM_004347	NALP14	M-019075-01	D-019075-02	338323	NM_176822
CASP5	M-004405-01	D-004405-03	838	NM_004347	NALP14	M-019075-01	D-019075-03	338323	NM_176822
CASP5	M-004405-01	D-004405-05	838	NM_004347	NALP14	M-019075-01	D-019075-04	338323	NM_176822
CASP5	M-004405-01	D-004405-04	838	NM_004347	NALP14	M-019075-01	D-019075-01	338323	NM_176822
CD14	M-011121-02	D-011121-18	929	NM_001040021	NALP2	M-020253-01	D-020253-01	55655	NM_017852
CD14	M-011121-02	D-011121-03	929	NM_001040021	NALP2	M-020253-01	D-020253-03	55655	NM_017852
CD14	M-011121-02	D-011121-02	929	NM_001040021	NALP2	M-020253-01	D-020253-02	55655	NM_017852
CD14	M-011121-02	D-011121-04	929	NM_001040021	NALP2	M-020253-01	D-020253-04	55655	NM_017852
CDC37	M-003231-01	D-003231-07	11140	NM_007065	NALP4	M-015351-01	D-015351-03	147945	NM_134444
CDC37	M-003231-01	D-003231-06	11140	NM_007065	NALP4	M-015351-01	D-015351-01	147945	NM_134444
CDC37	M-003231-01	D-003231-05	11140	NM_007065	NALP4	M-015351-01	D-015351-04	147945	NM_134444
CDC37	M-003231-01	D-003231-08	11140	NM_007065	NALP4	M-015351-01	D-015351-02	147945	NM_134444
CHUK	M-003473-02	D-003473-05	1147	NM_001278	NALP5	M-019146-01	D-019146-01	126206	NM_153447
CHUK	M-003473-02	D-003473-04	1147	NM_001278	NALP5	M-019146-01	D-019146-03	126206	NM_153447
CHUK	M-003473-02	D-003473-07	1147	NM_001278	NALP5	M-019146-01	D-019146-02	126206	NM_153447
CHUK	M-003473-02	D-003473-06	1147	NM_001278	NALP5	M-019146-01	D-019146-04	126206	NM_153447
CIAS1	M-017367-00	D-017367-01	114548	NM_004895	NALP6	M-015334-00	D-015334-01	171389	NM_138329
CIAS1	M-017367-00	D-017367-04	114548	NM_004895	NALP6	M-015334-00	D-015334-04	171389	NM_138329
CIAS1	M-017367-00	D-017367-02	114548	NM_004895	NALP6	M-015334-00	D-015334-03	171389	NM_138329
CIAS1	M-017367-00	D-017367-03	114548	NM_004895	NALP6	M-015334-00	D-015334-02	171389	NM_138329
COMMD1	M-007264-01	D-007264-03	150684	NM_152516	NALP7	M-016890-01	D-016890-01	199713	NM_206828
COMMD1	M-007264-01	D-007264-01	150684	NM_152516	NALP7	M-016890-01	D-016890-02	199713	NM_206828
COMMD1	M-007264-01	D-007264-02	150684	NM_152516	NALP7	M-016890-01	D-016890-04	199713	NM_206828
COMMD1	M-007264-01	D-007264-04	150684	NM_152516	NALP7	M-016890-01	D-016890-03	199713	NM_206828
CREBBP	M-003477-02	D-003477-19	1387	NM_001079846	NALP8	M-019472-00	D-019472-01	126205	NM_176811
CREBBP	M-003477-02	D-003477-20	1387	NM_001079846	NALP8	M-019472-00	D-019472-04	126205	NM_176811
CREBBP	M-003477-02	D-003477-18	1387	NM_001079846	NALP8	M-019472-00	D-019472-02	126205	NM_176811
CREBBP	M-003477-02	D-003477-21	1387	NM_001079846	NALP8	M-019472-00	D-019472-03	126205	NM_176811
CSNK2A1	M-003475-03	D-003475-01	1457	NM_177560	NALP9	M-019254-00	D-019254-02	338321	NM_176820
CSNK2A1	M-003475-03	D-003475-24	1457	NM_177560	NALP9	M-019254-00	D-019254-04	338321	NM_176820
CSNK2A1	M-003475-03	D-003475-02	1457	NM_177560	NALP9	M-019254-00	D-019254-01	338321	NM_176820
CSNK2A1	M-003475-03	D-003475-23	1457	NM_177560	NALP9	M-019254-00	D-019254-03	338321	NM_176820
CSNK2A2	M-004752-00	D-004752-04	1459	NM_001896	NCOR2	M-020145-02	D-020145-03	9612	NM_001077261
CSNK2A2	M-004752-00	D-004752-03	1459	NM_001896	NCOR2	M-020145-02	D-020145-01	9612	NM_001077261
CSNK2A2	M-004752-00	D-004752-01	1459	NM_001896	NCOR2	M-020145-02	D-020145-04	9612	NM_001077261
CSNK2A2	M-004752-00	D-004752-02	1459	NM_001896	NCOR2	M-020145-02	D-020145-05	9612	NM_001077261
CSNK2B	M-007679-00	D-007679-03	1460	NM_001320	NFKB1	M-003520-01	D-003520-02	4790	NM_003998
CSNK2B	M-007679-00	D-007679-01	1460	NM_001320	NFKB1	M-003520-01	D-003520-01	4790	NM_003998
CSNK2B	M-007679-00	D-007679-02	1460	NM_001320	NFKB1	M-003520-01	D-003520-03	4790	NM_003998
CSNK2B	M-007679-00	D-007679-04	1460	NM_001320	NFKB1	M-003520-01	D-003520-04	4790	NM_003998
CUL2	M-007277-00	D-007277-01	8453	NM_003591	NFKB2	M-003918-02	D-003918-02	4791	NM_002502
CUL2	M-007277-00	D-007277-04	8453	NM_003591	NFKB2	M-003918-02	D-003918-01	4791	NM_002502
CUL2	M-007277-00	D-007277-02	8453	NM_003591	NFKB2	M-003918-02	D-003918-18	4791	NM_002502
CUL2	M-007277-00	D-007277-03	8453	NM_003591	NFKB2	M-003918-02	D-003918-03	4791	NM_002502
CYLD	M-004609-01	D-004609-04	1540	NM_001042355	NFKBIA	M-004765-00	D-004765-01	4792	NM_020529
CYLD	M-004609-01	D-004609-03	1540	NM_001042355	NFKBIA	M-004765-00	D-004765-04	4792	NM_020529
CYLD	M-004609-01	D-004609-02	1540	NM_001042355	NFKBIA	M-004765-00	D-004765-02	4792	NM_020529
CYLD	M-004609-01	D-004609-04	1540	NM_001042355	NFKBIA	M-004765-00	D-004765-03	4792	NM_020529
DAPK1	M-004417-03	D-004417-02	1612	NM_004938	NFKBIB	M-015757-00	D-015757-02	4793	NM_001001716
DAPK1	M-004417-03	D-004417-21	1612	NM_004938	NFKBIB	M-015757-00	D-015757-01	4793	NM_001001716
DAPK1	M-004417-03	D-004417-04	1612	NM_004938	NFKBIB	M-015757-00	D-015757-03	4793	NM_001001716

Suppl. Table 1

DAPK1	M-004417-03	D-004417-07	1612	NM_004938	NFKBIB	M-015757-00	D-015757-04	4793	NM_001001716
ELKS	M-010942-00	D-010942-03	23085	NM_015064	NFKBIE	M-004766-01	D-004766-03	4794	NM_004556
ELKS	M-010942-00	D-010942-01	23085	NM_015064	NFKBIE	M-004766-01	D-004766-04	4794	NM_004556
ELKS	M-010942-00	D-010942-02	23085	NM_015064	NFKBIE	M-004766-01	D-004766-01	4794	NM_004556
ELKS	M-010942-00	D-010942-04	23085	NM_015064	NFKBIE	M-004766-01	D-004766-02	4794	NM_004556
EP300	M-003486-04	D-003486-10	2033	NM_001429	NFKBIZ	M-013497-01	D-013497-01	64332	NM_001005474
EP300	M-003486-04	D-003486-01	2033	NM_001429	NFKBIZ	M-013497-01	D-013497-02	64332	NM_001005474
EP300	M-003486-04	D-003486-02	2033	NM_001429	NFKBIZ	M-013497-01	D-013497-03	64332	NM_001005474
EP300	M-003486-04	D-003486-03	2033	NM_001429	NFKBIZ	M-013497-01	D-013497-04	64332	NM_001005474
FADD	M-003800-03	D-003800-02	8772	NM_003824	NGFR	M-009340-02	D-009340-05	4804	NM_002507
FADD	M-003800-03	D-003800-19	8772	NM_003824	NGFR	M-009340-02	D-009340-04	4804	NM_002507
FADD	M-003800-03	D-003800-01	8772	NM_003824	NGFR	M-009340-02	D-009340-06	4804	NM_002507
FADD	M-003800-03	D-003800-04	8772	NM_003824	NGFR	M-009340-02	D-009340-19	4804	NM_002507
FAS	M-003776-04	D-003776-01	355	NM_152876	P2RX7	M-003728-01	D-003728-01	5027	NM_002562
FAS	M-003776-04	D-003776-21	355	NM_152876	P2RX7	M-003728-01	D-003728-03	5027	NM_002562
FAS	M-003776-04	D-003776-20	355	NM_152876	P2RX7	M-003728-01	D-003728-05	5027	NM_002562
FAS	M-003776-04	D-003776-02	355	NM_152876	P2RX7	M-003728-01	D-003728-04	5027	NM_002562
GSK3B	M-003010-03	D-003010-08	2932	NM_002093	PANX1	M-018253-00	D-018253-01	24145	NM_015368
GSK3B	M-003010-03	D-003010-05	2932	NM_002093	PANX1	M-018253-00	D-018253-02	24145	NM_015368
GSK3B	M-003010-03	D-003010-06	2932	NM_002093	PANX1	M-018253-00	D-018253-03	24145	NM_015368
GSK3B	M-003010-03	D-003010-09	2932	NM_002093	PANX1	M-018253-00	D-018253-04	24145	NM_015368
HDAC3	M-003496-02	D-003496-02	8841	NM_003883	PCAF	M-005055-00	D-005055-04	8850	NM_003884
HDAC3	M-003496-02	D-003496-01	8841	NM_003883	PCAF	M-005055-00	D-005055-03	8850	NM_003884
HDAC3	M-003496-02	D-003496-03	8841	NM_003883	PCAF	M-005055-00	D-005055-01	8850	NM_003884
HDAC3	M-003496-02	D-003496-04	8841	NM_003883	PCAF	M-005055-00	D-005055-02	8850	NM_003884
HSPCA	M-005186-02	D-005186-01	3320	NM_005348	PDLIM2	M-010731-02	D-010731-01	64236	NM_198042
HSPCA	M-005186-02	D-005186-02	3320	NM_005348	PDLIM2	M-010731-02	D-010731-04	64236	NM_198042
HSPCA	M-005186-02	D-005186-05	3320	NM_005348	PDLIM2	M-010731-02	D-010731-14	64236	NM_198042
HSPCA	M-005186-02	D-005186-03	3320	NM_005348	PDLIM2	M-010731-02	D-010731-02	64236	NM_198042
HSPCB	M-005187-02	D-005187-05	3326	NM_007355	PIAS1	M-008167-01	D-008167-05	8554	NM_016166
HSPCB	M-005187-02	D-005187-01	3326	NM_007355	PIAS1	M-008167-01	D-008167-01	8554	NM_016166
HSPCB	M-005187-02	D-005187-02	3326	NM_007355	PIAS1	M-008167-01	D-008167-02	8554	NM_016166
HSPCB	M-005187-02	D-005187-18	3326	NM_007355	PIAS1	M-008167-01	D-008167-03	8554	NM_016166
IKBKB	M-003503-03	D-003503-01	3551	NM_001556	PIAS4	M-006445-00	D-006445-01	51588	NM_015897
IKBKB	M-003503-03	D-003503-03	3551	NM_001556	PIAS4	M-006445-00	D-006445-04	51588	NM_015897
IKBKB	M-003503-03	D-003503-04	3551	NM_001556	PIAS4	M-006445-00	D-006445-02	51588	NM_015897
IKBKB	M-003503-03	D-003503-02	3551	NM_001556	PIAS4	M-006445-00	D-006445-03	51588	NM_015897
IKBKE	M-003723-02	D-003723-06	9641	NM_014002	PIK3CA	M-003018-03	D-003018-25	5290	NM_006218
IKBKE	M-003723-02	D-003723-03	9641	NM_014002	PIK3CA	M-003018-03	D-003018-07	5290	NM_006218
IKBKE	M-003723-02	D-003723-04	9641	NM_014002	PIK3CA	M-003018-03	D-003018-08	5290	NM_006218
IKBKE	M-003723-02	D-003723-07	9641	NM_014002	PIK3CA	M-003018-03	D-003018-24	5290	NM_006218
IKBKG	M-003767-02	D-003767-01	8517	NM_001099856	PIK3CB	M-003019-02	D-003019-09	5291	NM_006219
IKBKG	M-003767-02	D-003767-04	8517	NM_001099856	PIK3CB	M-003019-02	D-003019-05	5291	NM_006219
IKBKG	M-003767-02	D-003767-03	8517	NM_001099856	PIK3CB	M-003019-02	D-003019-06	5291	NM_006219
IKBKG	M-003767-02	D-003767-02	8517	NM_001099856	PIK3CB	M-003019-02	D-003019-07	5291	NM_006219
IL1R1	M-005188-00	D-005188-04	3554	NM_000877	PIK3R1	M-003020-04	D-003020-26	5295	NM_181504
IL1R1	M-005188-00	D-005188-01	3554	NM_000877	PIK3R1	M-003020-04	D-003020-10	5295	NM_181504
IL1R1	M-005188-00	D-005188-03	3554	NM_000877	PIK3R1	M-003020-04	D-003020-27	5295	NM_181504
IL1R1	M-005188-00	D-005188-02	3554	NM_000877	PIK3R1	M-003020-04	D-003020-11	5295	NM_181504
IL1R2	M-007960-01	D-007960-05	7850	NM_004633	PIK3R2	M-003021-03	D-003021-07	5296	NM_005027
IL1R2	M-007960-01	D-007960-01	7850	NM_004633	PIK3R2	M-003021-03	D-003021-26	5296	NM_005027
IL1R2	M-007960-01	D-007960-03	7850	NM_004633	PIK3R2	M-003021-03	D-003021-05	5296	NM_005027
IL1R2	M-007960-01	D-007960-02	7850	NM_004633	PIK3R2	M-003021-03	D-003021-08	5296	NM_005027
IL1RAP	M-003504-00	D-003504-02	3556	NM_002182	PIK3R3	M-019546-00	D-019546-01	8503	NM_003629
IL1RAP	M-003504-00	D-003504-04	3556	NM_002182	PIK3R3	M-019546-00	D-019546-04	8503	NM_003629
IL1RAP	M-003504-00	D-003504-01	3556	NM_002182	PIK3R3	M-019546-00	D-019546-02	8503	NM_003629
IL1RAP	M-003504-00	D-003504-03	3556	NM_002182	PIK3R3	M-019546-00	D-019546-03	8503	NM_003629
IRAK1	M-004760-03	D-004760-04	3654	NM_001569	PPP2R4	M-005214-01	D-005214-01	5524	NM_178003
IRAK1	M-004760-03	D-004760-07	3654	NM_001569	PPP2R4	M-005214-01	D-005214-02	5524	NM_178003
IRAK1	M-004760-03	D-004760-01	3654	NM_001569	PPP2R4	M-005214-01	D-005214-04	5524	NM_178003
IRAK1	M-004760-03	D-004760-03	3654	NM_001569	PPP2R4	M-005214-01	D-005214-17	5524	NM_178003
IRAK2	M-004761-01	D-004761-03	3656	NM_001570	PRKACA	M-004649-01	D-004649-17	5566	NM_207518
IRAK2	M-004761-01	D-004761-17	3656	NM_001570	PRKACA	M-004649-01	D-004649-03	5566	NM_207518
IRAK2	M-004761-01	D-004761-04	3656	NM_001570	PRKACA	M-004649-01	D-004649-01	5566	NM_207518
IRAK2	M-004761-01	D-004761-01	3656	NM_001570	PRKACA	M-004649-01	D-004649-02	5566	NM_207518
IRAK3	M-004762-00	D-004762-03	11213	NM_007199	PRKACB	M-004650-00	D-004650-04	5567	NM_002731
IRAK3	M-004762-00	D-004762-04	11213	NM_007199	PRKACB	M-004650-00	D-004650-02	5567	NM_002731
IRAK3	M-004762-00	D-004762-01	11213	NM_007199	PRKACB	M-004650-00	D-004650-03	5567	NM_002731
IRAK3	M-004762-00	D-004762-02	11213	NM_007199	PRKACB	M-004650-00	D-004650-01	5567	NM_002731
IRAK4	M-003302-01	D-003302-02	51135	NM_016123	PRKCZ	M-003526-04	D-003526-10	5590	NM_002744
IRAK4	M-003302-01	D-003302-05	51135	NM_016123	PRKCZ	M-003526-04	D-003526-12	5590	NM_002744
IRAK4	M-003302-01	D-003302-01	51135	NM_016123	PRKCZ	M-003526-04	D-003526-11	5590	NM_002744
IRAK4	M-003302-01	D-003302-06	51135	NM_016123	PRKCZ	M-003526-04	D-003526-13	5590	NM_002744
IRF3	M-006875-02	D-006875-01	3661	NM_001571	PRKR	M-003527-00	D-003527-02	5610	NM_002759
IRF3	M-006875-02	D-006875-03	3661	NM_001571	PRKR	M-003527-00	D-003527-04	5610	NM_002759
IRF3	M-006875-02	D-006875-04	3661	NM_001571	PRKR	M-003527-00	D-003527-01	5610	NM_002759
IRF3	M-006875-02	D-006875-05	3661	NM_001571	PRKR	M-003527-00	D-003527-03	5610	NM_002759
LBP	M-010128-00	D-010128-01	3929	NM_004139	REL	M-004768-01	D-004768-03	5966	NM_002908
LBP	M-010128-00	D-010128-02	3929	NM_004139	REL	M-004768-01	D-004768-04	5966	NM_002908
LBP	M-010128-00	D-010128-04	3929	NM_004139	REL	M-004768-01	D-004768-01	5966	NM_002908
LBP	M-010128-00	D-010128-03	3929	NM_004139	REL	M-004768-01	D-004768-02	5966	NM_002908
LTBR	M-008023-01	D-008023-02	4055	NM_002342	RELA	M-003533-02	D-003533-03	5970	NM_021975
LTBR	M-008023-01	D-008023-03	4055	NM_002342	RELA	M-003533-02	D-003533-04	5970	NM_021975
LTBR	M-008023-01	D-008023-04	4055	NM_002342	RELA	M-003533-02	D-003533-05	5970	NM_021975
LTBR	M-008023-01	D-008023-05	4055	NM_002342	RELA	M-003533-02	D-003533-18	5970	NM_021975
LY96	M-020298-00	D-020298-01	23643	NM_015364	RELB	M-004767-02	D-004767-04	5971	NM_006509
LY96	M-020298-00	D-020298-02	23643	NM_015364	RELB	M-004767-02	D-004767-01	5971	NM_006509
LY96	M-020298-00	D-020298-04	23643	NM_015364	RELB	M-004767-02	D-004767-05	5971	NM_006509
LY96	M-020298-00	D-020298-03	23643	NM_015364	RELB	M-004767-02	D-004767-18	5971	NM_006509
MAP2K3	M-003509-03	D-003509-04	5606	NM_002756	RIPK1	M-004445-02	D-004445-04	8737	NM_003804
MAP2K3	M-003509-03	D-003509-05	5606	NM_002756	RIPK1	M-004445-02	D-004445-05	8737	NM_003804
MAP2K3	M-003509-03	D-003509-02	5606	NM_002756	RIPK1	M-004445-02	D-004445-06	8737	NM_003804
MAP2K3	M-003509-03	D-003509-06	5606	NM_002756	RIPK1	M-004445-02	D-004445-03	8737	NM_003804
MAP2K4	M-003574-02	D-003574-03	6416	NM_003010	RIPK2	M-003602-02	D-003602-02	8767	NM_003821
MAP2K4	M-003574-02	D-003574-05	6416	NM_003010	RIPK2	M-003602-02	D-003602-04	8767	NM_003821
MAP2K4	M-003574-02	D-003574-06	6416	NM_003010	RIPK2	M-003602-02	D-003602-01	8767	NM_003821
MAP2K4	M-003574-02	D-003574-01	6416	NM_003010	RIPK2	M-003602-02	D-003602-03	8767	NM_003821
MAP2K6	M-003967-01	D-003967-01	5608	NM_002758	RIPK3	M-003534-01	D-003534-02	11035	NM_006871
MAP2K6	M-003967-01	D-003967-17	5608	NM_002758	RIPK3	M-003534-01	D-003534-01	11035	NM_006871
MAP2K6	M-003967-01	D-003967-04	5608	NM_002758	RIPK3	M-003534-01	D-003534-03	11035	NM_006871
MAP2K6	M-003967-01	D-003967-03	5608	NM_002758	RIPK3	M-003534-01	D-003534-04	11035	NM_006871
MAP2K7	M-004016-01	D-004016-04	5609	NM_145185	RPS6KA1	M-003025-04	D-003025-12	6195	NM_001006665
MAP2K7	M-004016-01	D-004016-06	5609	NM_145185	RPS6KA1	M-003025-04	D-003025-07	6195	NM_001006665
MAP2K7	M-004016-01	D-004016-05	5609	NM_145185	RPS6KA1	M-003025-04	D-003025-06	6195	NM_001006665
MAP2K7	M-004016-01	D-004016-02	5609	NM_145185	RPS6KA1	M-003025-04	D-003025-08	6195	NM_001006665

Suppl. Table 1

Gene Symbol	Pool Number	Duplex Number	Gene Id	Accession Number
RPS6KA4	M-004664-01	D-004664-01	8986	NM_001006944
RPS6KA4	M-004664-01	D-004664-03	8986	NM_001006944
RPS6KA4	M-004664-01	D-004664-04	8986	NM_001006944
RPS6KA4	M-004664-01	D-004664-02	8986	NM_001006944
RPS6KA5	M-004665-02	D-004665-04	9252	NM_182398
RPS6KA5	M-004665-02	D-004665-06	9252	NM_182398
RPS6KA5	M-004665-02	D-004665-01	9252	NM_182398
RPS6KA5	M-004665-02	D-004665-19	9252	NM_182398
SITPEC	M-010826-00	D-010826-03	51295	NM_016581
SITPEC	M-010826-00	D-010826-01	51295	NM_016581
SITPEC	M-010826-00	D-010826-02	51295	NM_016581
SITPEC	M-010826-00	D-010826-04	51295	NM_016581
SOCS1	M-011511-04	D-011511-09	8651	NM_003745
SOCS1	M-011511-04	D-011511-07	8651	NM_003745
SOCS1	M-011511-04	D-011511-08	8651	NM_003745
SOCS1	M-011511-04	D-011511-23	8651	NM_003745
SUGT1	M-012877-00	D-012877-03	10910	NM_006704
SUGT1	M-012877-00	D-012877-04	10910	NM_006704
SUGT1	M-012877-00	D-012877-02	10910	NM_006704
SUGT1	M-012877-00	D-012877-01	10910	NM_006704
TBK1	M-003788-02	D-003788-07	29110	NM_013254
TBK1	M-003788-02	D-003788-02	29110	NM_013254
TBK1	M-003788-02	D-003788-01	29110	NM_013254
TBK1	M-003788-02	D-003788-06	29110	NM_013254
TCEB1	M-010541-01	D-010541-06	6921	NM_005648
TCEB1	M-010541-01	D-010541-01	6921	NM_005648
TCEB1	M-010541-01	D-010541-02	6921	NM_005648
TCEB1	M-010541-01	D-010541-05	6921	NM_005648
TCEB2	M-012376-02	D-012376-07	6923	NM_207013
TCEB2	M-012376-02	D-012376-20	6923	NM_207013
TCEB2	M-012376-02	D-012376-01	6923	NM_207013
TCEB2	M-012376-02	D-012376-21	6923	NM_207013
TIRAP	M-004713-02	D-004713-03	114609	NM_148910
TIRAP	M-004713-02	D-004713-04	114609	NM_148910
TIRAP	M-004713-02	D-004713-02	114609	NM_148910
TIRAP	M-004713-02	D-004713-18	114609	NM_148910
TLR1	M-008086-01	D-008086-17	7096	NM_003263
TLR1	M-008086-01	D-008086-01	7096	NM_003263
TLR1	M-008086-01	D-008086-04	7096	NM_003263
TLR1	M-008086-01	D-008086-03	7096	NM_003263
TLR10	M-008087-01	D-008087-03	81793	NM_001017388
TLR10	M-008087-01	D-008087-02	81793	NM_001017388
TLR10	M-008087-01	D-008087-04	81793	NM_001017388
TLR10	M-008087-01	D-008087-01	81793	NM_001017388
TLR2	M-005120-03	D-005120-09	7097	NM_003264
TLR2	M-005120-03	D-005120-06	7097	NM_003264
TLR2	M-005120-03	D-005120-07	7097	NM_003264
TLR2	M-005120-03	D-005120-08	7097	NM_003264
TLR3	M-007745-00	D-007745-01	7098	NM_003265
TLR3	M-007745-00	D-007745-04	7098	NM_003265
TLR3	M-007745-00	D-007745-03	7098	NM_003265
TLR3	M-007745-00	D-007745-02	7098	NM_003265
TLR4	M-008088-01	D-008088-02	7099	NM_138554
TLR4	M-008088-01	D-008088-03	7099	NM_138554
TLR4	M-008088-01	D-008088-01	7099	NM_138554
TLR4	M-008088-01	D-008088-04	7099	NM_138554
TLR5	M-008089-01	D-008089-01	7100	NM_003268
TLR5	M-008089-01	D-008089-02	7100	NM_003268
TLR5	M-008089-01	D-008089-04	7100	NM_003268
TLR5	M-008089-01	D-008089-17	7100	NM_003268
TLR6	M-005156-01	D-005156-02	10333	NM_006068
TLR6	M-005156-01	D-005156-03	10333	NM_006068
TLR6	M-005156-01	D-005156-05	10333	NM_006068
TLR6	M-005156-01	D-005156-01	10333	NM_006068
TLR7	M-004714-01	D-004714-02	51284	NM_016562
TLR7	M-004714-01	D-004714-03	51284	NM_016562
TLR7	M-004714-01	D-004714-01	51284	NM_016562
TLR7	M-004714-01	D-004714-04	51284	NM_016562
TLR8	M-004715-01	D-004715-04	51311	NM_138636
TLR8	M-004715-01	D-004715-02	51311	NM_138636
TLR8	M-004715-01	D-004715-01	51311	NM_138636
TLR8	M-004715-01	D-004715-03	51311	NM_138636
TLR9	M-004066-01	D-004066-02	54106	NM_017442
TLR9	M-004066-01	D-004066-04	54106	NM_017442
TLR9	M-004066-01	D-004066-05	54106	NM_017442
TLR9	M-004066-01	D-004066-03	54106	NM_017442
TNFAIP3	M-009919-00	D-009919-03	7128	NM_006290
TNFAIP3	M-009919-00	D-009919-04	7128	NM_006290
TNFAIP3	M-009919-00	D-009919-01	7128	NM_006290
TNFAIP3	M-009919-00	D-009919-02	7128	NM_006290
TNFRSF10A	M-008090-02	D-008090-15	8797	NM_003844
TNFRSF10A	M-008090-02	D-008090-16	8797	NM_003844
TNFRSF10A	M-008090-02	D-008090-06	8797	NM_003844
TNFRSF10A	M-008090-02	D-008090-17	8797	NM_003844
TNFRSF10B	M-004448-00	D-004448-01	8795	NM_003842
TNFRSF10B	M-004448-00	D-004448-02	8795	NM_003842
TNFRSF10B	M-004448-00	D-004448-03	8795	NM_003842
TNFRSF10B	M-004448-00	D-004448-04	8795	NM_003842
TNFRSF10C	M-008091-00	D-008091-01	8794	NM_003841
TNFRSF10C	M-008091-00	D-008091-02	8794	NM_003841
TNFRSF10C	M-008091-00	D-008091-03	8794	NM_003841
TNFRSF10C	M-008091-00	D-008091-04	8794	NM_003841
TNFRSF10D	M-008092-01	D-008092-03	8793	NM_003840
TNFRSF10D	M-008092-01	D-008092-05	8793	NM_003840
TNFRSF10D	M-008092-01	D-008092-01	8793	NM_003840
TNFRSF10D	M-008092-01	D-008092-02	8793	NM_003840
TNFRSF11A	M-008093-01	D-008093-01	8792	NM_003839
TNFRSF11A	M-008093-01	D-008093-04	8792	NM_003839
TNFRSF11A	M-008093-01	D-008093-05	8792	NM_003839
TNFRSF11A	M-008093-01	D-008093-06	8792	NM_003839
TNFRSF11B	M-008094-01	D-008094-01	4982	NM_002546
TNFRSF11B	M-008094-01	D-008094-04	4982	NM_002546
TNFRSF11B	M-008094-01	D-008094-02	4982	NM_002546
TNFRSF11B	M-008094-01	D-008094-03	4982	NM_002546
TNFRSF12A	M-010661-01	D-010661-04	51330	NM_016639
TNFRSF12A	M-010661-01	D-010661-05	51330	NM_016639
TNFRSF12A	M-010661-01	D-010661-03	51330	NM_016639
TNFRSF12A	M-010661-01	D-010661-01	51330	NM_016639
TNFRSF13B	M-008095-00	D-008095-01	23495	NM_012452
TNFRSF13B	M-008095-00	D-008095-02	23495	NM_012452
TNFRSF13B	M-008095-00	D-008095-04	23495	NM_012452
TNFRSF13B	M-008095-00	D-008095-03	23495	NM_012452
TNFRSF13C	M-013424-00	D-013424-01	115650	NM_052945
TNFRSF13C	M-013424-00	D-013424-02	115650	NM_052945
TNFRSF13C	M-013424-00	D-013424-03	115650	NM_052945
TNFRSF13C	M-013424-04	D-013424-04	115650	NM_052945
TNFRSF14	M-008096-00	D-008096-02	8764	NM_003820
TNFRSF14	M-008096-00	D-008096-03	8764	NM_003820
TNFRSF14	M-008096-00	D-008096-04	8764	NM_003820
TNFRSF14	M-008096-00	D-008096-01	8764	NM_003820
TNFRSF17	M-011217-02	D-011217-01	608	NM_001192
TNFRSF17	M-011217-02	D-011217-04	608	NM_001192
TNFRSF17	M-011217-02	D-011217-03	608	NM_001192
TNFRSF17	M-011217-02	D-011217-18	608	NM_001192
TNFRSF18	M-006449-02	D-006449-05	8784	NM_148901
TNFRSF18	M-006449-02	D-006449-06	8784	NM_148901
TNFRSF18	M-006449-02	D-006449-07	8784	NM_148901
TNFRSF18	M-006449-02	D-006449-17	8784	NM_148901
TNFRSF19	M-008098-00	D-008098-01	55504	NM_018647
TNFRSF19	M-008098-00	D-008098-02	55504	NM_018647
TNFRSF19	M-008098-00	D-008098-04	55504	NM_018647
TNFRSF19	M-008098-00	D-008098-03	55504	NM_018647
TNFRSF1A	M-005197-00	D-005197-02	7132	NM_001065
TNFRSF1A	M-005197-00	D-005197-03	7132	NM_001065
TNFRSF1A	M-005197-00	D-005197-04	7132	NM_001065
TNFRSF1A	M-005197-00	D-005197-01	7132	NM_001065
TNFRSF1B	M-003934-00	D-003934-02	7133	NM_001066
TNFRSF1B	M-003934-00	D-003934-01	7133	NM_001066
TNFRSF1B	M-003934-00	D-003934-03	7133	NM_001066
TNFRSF1B	M-003934-00	D-003934-04	7133	NM_001066
TNFRSF21	M-004450-01	D-004450-02	27242	NM_014452
TNFRSF21	M-004450-01	D-004450-05	27242	NM_014452
TNFRSF21	M-004450-01	D-004450-01	27242	NM_014452
TNFRSF21	M-004450-01	D-004450-04	27242	NM_014452
TNFRSF25	M-004449-02	D-004449-16	8718	NM_001039664
TNFRSF25	M-004449-02	D-004449-14	8718	NM_001039664
TNFRSF25	M-004449-02	D-004449-15	8718	NM_001039664
TNFRSF25	M-004449-02	D-004449-17	8718	NM_001039664
TNFRSF4	M-008100-00	D-008100-02	7293	NM_003327
TNFRSF4	M-008100-00	D-008100-04	7293	NM_003327
TNFRSF4	M-008100-00	D-008100-03	7293	NM_003327
TNFRSF4	M-008100-00	D-008100-01	7293	NM_003327
TNFRSF5	M-008101-02	D-008101-02	958	NM_152854
TNFRSF5	M-008101-02	D-008101-04	958	NM_152854
TNFRSF5	M-008101-02	D-008101-01	958	NM_152854
TNFRSF5	M-008101-02	D-008101-05	958	NM_152854
TNFRSF7	M-008103-01	D-008103-03	939	NM_001242
TNFRSF7	M-008103-01	D-008103-02	939	NM_001242
TNFRSF7	M-008103-01	D-008103-01	939	NM_001242
TNFRSF7	M-008103-01	D-008103-04	939	NM_001242
TNFRSF8	M-008104-01	D-008104-03	943	NM_152942
TNFRSF8	M-008104-01	D-008104-04	943	NM_152942
TNFRSF8	M-008104-01	D-008104-17	943	NM_152942
TNFRSF8	M-008104-01	D-008104-02	943	NM_152942
TNFRSF9	M-008105-02	D-008105-04	3604	NM_001561
TNFRSF9	M-008105-02	D-008105-19	3604	NM_001561
TNFRSF9	M-008105-02	D-008105-05	3604	NM_001561
TNFRSF9	M-008105-02	D-008105-06	3604	NM_001561
TOLLIP	M-016930-01	D-016930-01	54472	NM_019009
TOLLIP	M-016930-01	D-016930-17	54472	NM_019009
TOLLIP	M-016930-01	D-016930-02	54472	NM_019009
TOLLIP	M-016930-01	D-016930-04	54472	NM_019009
TRADD	M-004452-01	D-004452-02	8717	NM_003789
TRADD	M-004452-01	D-004452-04	8717	NM_003789
TRADD	M-004452-01	D-004452-01	8717	NM_003789
TRADD	M-004452-01	D-004452-03	8717	NM_003789
TRAF2	M-005198-00	D-005198-02	7186	NM_021138
TRAF2	M-005198-00	D-005198-04	7186	NM_021138
TRAF2	M-005198-00	D-005198-01	7186	NM_021138
TRAF2	M-005198-00	D-005198-03	7186	NM_021138
TRAF3	M-005252-02	D-005252-03	7187	NM_003300
TRAF3	M-005252-02	D-005252-21	7187	NM_003300
TRAF3	M-005252-02	D-005252-01	7187	NM_003300
TRAF3	M-005252-02	D-005252-04	7187	NM_003300
TRAF5	M-006568-01	D-006568-01	7188	NM_001033910
TRAF5	M-006568-01	D-006568-02	7188	NM_001033910
TRAF5	M-006568-01	D-006568-04	7188	NM_001033910
TRAF5	M-006568-01	D-006568-03	7188	NM_001033910
TRAF6	M-004712-00	D-004712-02	7189	NM_004620
TRAF6	M-004712-00	D-004712-03	7189	NM_004620
TRAF6	M-004712-00	D-004712-01	7189	NM_004620
TRAF6	M-004712-00	D-004712-04	7189	NM_004620
TRAM1	M-018676-01	D-018676-02	23471	NM_014294
TRAM1	M-018676-01	D-018676-03	23471	NM_014294
TRAM1	M-018676-01	D-018676-04	23471	NM_014294
TRAM1	M-018676-01	D-018676-01	23471	NM_014294
TRIF	M-012833-02	D-012833-02	148022	NM_182919
TRIF	M-012833-02	D-012833-04	148022	NM_182919
TRIF	M-012833-02	D-012833-01	148022	NM_182919
TRIF	M-012833-02	D-012833-21	148022	NM_182919
UBE2N	M-003920-01	D-003920-04	7334	NM_003348
UBE2N	M-003920-01	D-003920-02	7334	NM_003348
UBE2N	M-003920-01	D-003920-05	7334	NM_003348
UBE2N	M-003920-01	D-003920-01	7334	NM_003348
UBE2V1	M-010064-03	D-010064-21	7335	NM_001032288
UBE2V1	M-010064-03	D-010064-23	7335	NM_001032288
UBE2V1	M-010064-03	D-010064-02	7335	NM_001032288
UBE2V1	M-010064-03	D-010064-22	7335	NM_001032288
XEDAR	M-008044-01	D-008044-06	60401	NM_021783
XEDAR	M-008044-01	D-008044-05	60401	NM_021783
XEDAR	M-008044-01	D-008044-07	60401	NM_021783
XEDAR	M-008044-01	D-008044-08	60401	NM_021783

Suppl. Table 1

compound	cmax (µM)	compound	cmax (µM)	compound	cmax (µM)	compound	cmax (µM)
acarbose	0,15	dexamethasone	0,224	indomethacin	5,59	phenytoin	21,72
acetaminophen	139	dextromethorphan HBr	0,022	isoniazid	76,56	pioglitazone	2,946
adefovir	0,085	diclofenac	10,1	isoproterenol	2,02	prednisolone	0,68
allopurinol	13,81	didanosine	9,83	kanamycin	60,1	primaquine	0,615
altretamine	3,76	diethylmaleate	NA	ketoconazole	6,59	primidone	4,67
amiodarone	0,807	digoxin	0,003	ketorolac	3,53	procyclidine	0,404
amoxicillin	22,3	diltiazem	0,356	labetalol	2,68	propranolol	0,201
azathioprine	0,34	disulfiram	5,4	maprotiline	0,18	propylthiouracil	9,1
benzbromarone	4,339	DMSO	0,2	mebendazole	0,13	ranitidine	1,79
betaine	940	edrophonium	60,2	meclizine	0,026	ribavirin	2,61
bicalutamide	1,97	enalapril	0,4	mercaptopurine	0,48	rifampicin	15
bosentan	7,4	entacapone	3,93	metformin	7,78	simvastatin	0,082
bromfenac	17,96	epinephrine	0,002	methimazole	2,62	succinylcholine	137,74
buspirone	0,016	erythromycin	11	methotrexate	0,77	sulindac	31,985
busulfan	0,277	ethambutol	24,47	methyldopa	18,94	tacrolimus	0,037
captopril	8,882	etodolac	68,49	metoprolol	0,56	tamoxifen	0,162
carbamazepine	50,79	etoposide	NA	mexiletine	3,83	terbinafine	4
chloramphenicol	46,36	famotidine	0,308	moxisylyte	0,16	thapsigargin	NA
chlormezanone	10,59	fenofibrate	4,1	naproxen	0,2	thioridazine	0,55
chlorpromazine	0,94	fenoprofen	58,2	nefazodone	3,95	ticlopidine	8,075
chlorpropamide	130,1	fialuridine	1	neomycin	0,44	tnfα	NA
cimetidine	11,89	fluoxetine	0,05	nifedipine	0,43	tolbutamide	233,03
ciprofloxacin	6,58	flurbiprofen	57,32	nimesulide	21,082	tolcapone	21,99
clofibrate	470	folic acid	0,043	nitrofurantoin	6	trazodone	5,056
clotrimazole	0,087	furosemide	3,29	nizatidine	4	troglitazone	6,39
clozapine	2,44	ganciclovir	4,62	ofloxacin	9,96	valproic acid	243, 08
colchicine	0,016	glimepiride	1,12	omeprazole	4,7	verapamil	0,5
cyclosporin A	0,2	griseofulvin	4,54	oxytetracycline	3,26	warfarin	4,86
dacarbazine	20,64	haloperidol	0,005	paroxetine	0,061	ximelagatran	0,3
danazol	0,109	hydroxyzine	0,27	perhexiline	2,16	zafirlukast	1,21
dantrolene	7,9	imipramine	0,29	phenobarbital	145,5	zimelidine	0,267

Suppl. Table 2

Chapter 6

High content live cell imaging of the dynamics of multiple adaptive stress response pathways enables assessment of drug-induced liver injury liabilities

Highlights

- DILI compound exposure induces specific adaptive stress reporter activation with distinct time dynamics and magnitude
- Quantitative data analysis and hierarchical clustering reveals both mechanistic and predictive inshight into mechanisms of toxicity
- Feature selection and SVM classification show predictive power of a diverse and complex set of biologically interpretable features

This chapter is based on a manuscript in preparation:

Steven Wink[1,2], Steven Hiemstra[1,2], Suzanna Huppelschoten[1,2], Janna Klip[1], Bob van de Water[1]

High content live cell imaging of the dynamics of multiple adaptive stress response pathways enables assessment of drug-induced liver injury (DILI) liabilities

[1]*Division of Toxicology, Leiden Academic Centre for Drug Research, Leiden University, Leiden, The Netherlands*
[2]*These authors contributed equally*

Drug-induced liver injury remains a major concern during drug development. There is an urgent need for improved mechanistic understanding and prediction of DILI liabilities from *in vitro* approaches. Previously, we have reported a high content live cell microscopy platform containing mechanism-based fluorescent protein toxicity pathway reporters to detect cellular stress responses reflecting primary human hepatocyte drug responses. Here, we have systematically evaluated the application of integrated stress pathway target gene activation of four key adaptive stress pathways: oxidative stress, ER stress, DNA damage stress and inflammatory stress. More than 118 FDA-labeled drugs in 5 concentrations based on human plasma maximum concentration levels were screened for reporter activation, using live cell confocal imaging. Quantitative data analysis revealed activation of single or multiple reporters by most drugs in a concentration and time dependent manner. Hierarchical clustering of time course dynamics and refined single cell analysis allowed the allusion of key events in toxicity. Concentration response modeling was performed to calculate benchmark concentrations (BMCs). Extracted temporal dynamic parameters and BMCs were used to assess the predictive power of sublethal adaptive stress pathway activation. Although cellular adaptive responses were activated by non-DILI and severe-DILI compounds alike, dynamic behavior and lower BMCs of pathway activation were sufficiently distinct between these compound classes as shown by unsupervised hierarchical clustering and their combined high correct classification. The high level detailed temporal and concentration-dependent dynamics of adaptive stress pathway activation by exposure with compounds with DILI liabilities add to the overall understanding and prediction of drug-induced liver toxicities

Keywords: Drug-induced liver injury, live cell imaging, adaptive stress response pathways, machine learning

Introduction

Despite major efforts to understand and predict drug-induced liver injury (DILI), unpredicted liver failure upon drug use remains an important problem both in the clinic and during drug development[313]. In general, various chemical, genetic, and life style factors can contribute to the development of DILI. To be able to improve prediction of DILI liabilities of new molecular entities it is essential to understand how currently known compounds induce injury. Of most interest are the idiosyncratic DILI compounds, inducing unpredicted results at a normal dose, and only in a very small group of patients.

Gene expression analysis has contributed significantly to our understanding of DILI[314,315] . This has led to the identification of specific signaling pathways that are activated during DILI and are possibly predictive for chemical-induced liver injury. Key among these are classic stress responses activated to maintain cellular homeostasis, including the oxidative stress response, the ER stress response and the DNA damage response[314], together with inflammatory stress[208]. We have established fluorescent protein reporter

hepatoma cell lines using bacterial artificial chromosome (BAC) GFP tagging, that capture each of these four pathways using SRXN1, CHOP, p21 and ICAM1 as biomarkers[44].

For the oxidative stress pathway we have established a SRXN1-GFP reporter[44]. Parent compounds or their metabolites can oxidize, reduce or alkylate cellular components, thereby directly inducing oxidative stress or indirectly for example via disruption of essential mitochondrial functioning. The activation of transcription factor Nrf2 together with AP1 is dependent on the redox sensor Kelch-like ECH-associated protein 1 (Keap1), and induces expression of antioxidants among which the small redox protein (SRXN1)[316,317]. SRXN1, conserved in all eukaryotes, is best characterized for its ATP-dependent reduction of the hyperoxidized form of peroxiredoxin[317]. Peroxiredoxin (Prx) is an enigmatic protein, its reversible inactivation caused by its own substrate. However, it is hypothesized that SRXN1 activity is the essential switch between Prx either acting as chaperone of the intracellular messenger peroxides and its usual peroxidase function, protecting the cell against oxidative damage[317]. Furthermore, deglutathionylation of s-glutathionylated cysteins by SRXN1 has been shown to be essential for the functioning of phosphatases[318]. *In vivo* studies show that in the liver, upregulation of SRXN1 via Nrf2 activation, upon either cadmium-induced heavy metal stress and Pyrazole exposure or alcohol-induced CYP2E1 related toxicity, is vital for protection against fulminant oxidative stress and subsequent organ failure[319–321].

To monitor ER stress we have established a CHOP-GFP reporter[44]. ER stress is a protective response upon the accumulation of untranslated proteins in the endoplasmic reticulum (ER). This can be induced by compound or metabolite-induced disruption of for example N-linked glycosylation, disulfide bond formation, transport of folded proteins from the ER, protein folding, calcium homeostasis, or ER stress response components itself. The outcome of the compound-induced ER stress response, cell survival or cell death, is dependent both on the strength and duration of the response[322]. Upon ER stress, three classical signaling pathways are activated via the sensor proteins PKR-like ER kinase (PERK), activating transcription factor 6 (Atf6), and inositol-requiring enzyme 1 (Ire1). Activation of PERK leads to arrested protein translation by phosphorylation of the eukaryotic transcription factor 2, in order to diminish the flux of unfolded proteins into the ER. Permitted translation of activating transcription factor 4 (Atf4) and results in the specific expression of ER function-related proteins and the transcription factor C/EBP homologous protein (CHOP). Activation of the Ire1 and Atf6 pathways can also induce CHOP expression, although with lower efficiency[323]. CHOP activity induces or represses the expression and function of many proteins, including proapoptotic proteins like Bcl-X, BAX and caspase3, and the suppression of antiapoptotic proteins as Bcl2. In the liver, CHOP expression is not conclusively linked to protection or increased drug-induced injury. *In vitro* as well as *in vivo* studies have detected CHOP induction upon drug exposure, however, at this moment a causal relationship with cell death or protection against cell death cannot be drawn[324].

DNA damage can be monitored by a fluorescent protein reporter for the p53 downstream target gene p21, as shown previously[44]. The cellular protective response upon DNA damage induces cell cycle arrest and subsequent senescence, to prevent genomic

instability during replication. DNA damage can be induced either directly by chemical mutagens, usually electrophiles that directly interact with DNA and form covalent bonds, or indirectly by the formation of ROS that can interact with DNA[135]. The key transcription factor p53 is activated upon DNA damage and induces expression of its many target genes, among which is p21[325]. The best-characterized function of p21 is its effective inhibition of cyclin-dependent kinases (CDK), which halts the progression of the cell cycle in the G1 or G2/M phase. Localization of p21 has been found both in the nucleus and the cytoplasm, reflecting different roles in both cell cycle arrest and antiapoptosis signaling respectively[326]. In the liver, *in vivo* studies show upregulated p21 nuclear expression upon drug exposure, mostly via p53 activation[327,328].

Finally, a fluorescent reporter for ICAM1 allows the monitoring of the cytokine-mediated activation of NF-κB signaling[28]. Besides intrinsic drug qualities as dose and lipophilicity, several host factors have been described to be involved in the development of idiosyncratic DILI. Among these, inflammatory processes have been known to be detrimental in the process of liver injury, but are also known to be essential for recovery after injury[208]. Inflammatory cytokine excretion firstly activates and recruits innate as well as adaptive immune cells, and secondly activates the hepatocytes and non-parenchymal cells themselves. In *in vivo* studies, the production of proinflammatory cytokine TNFα upon lipopolysaccharide exposure in combination with drugs is strongly suggested to increase toxicity[10]. TNFα stimulation of endothelial cells as hepatocytes has been known to induce both adaptive, pro-survival, and adverse, pro-death, cellular signaling. The activation of the key transcription factor nuclear factor kB (NF-κB) ensures the expression of several pro-survival genes, but also enhances the proinflammatory gene expression[20]. One of the proinflammatory genes induced by NF-κB activation is intercellular adhesion molecule 1 (ICAM1). ICAM1 is expressed at the membrane of TNFα-activated hepatocytes, aiding in the adherence and transendothelial migration of leukocytes from the blood stream[329]. ICAM1 is widely used as a marker for inflammation and ICAM1 expression is also increased upon inflammation in the liver[330].

Given the central role of the above pathways in liver injury and DILI specifically, our objective was to evaluate the application of our panel of target gene BAC-GFP reporter cell lines that represent these four major adaptive stress response pathways to predict DILI liability. Previously, we demonstrated that the BAC-GFP reporters allow the quantification of the chemical-induced stress responses similar to primary human hepatocytes[44]. Here we systematically determined the application of the BAC GFP-SRXN1, GFP-CHOP, GFP-p21 and GFP-ICAM1 reporters for the assessment of DILI using a set of 118 FDA-labeled drugs with DILI drug label classification. The concentration- and time-dependent GFP responses were determined in association with several cytotoxicity parameters. In this study, we provide quantitative information of the dynamic adaptive stress response activation for all 118 drugs allowing detailed mode-of-action assessment. Mechanism-based temporal dynamic data together with concentration response modeling was used for prediction of DILI outcome.

Materials and methods

Cell culture

Human hepatoma HepG2 cells were acquired from ATCC (clone HB8065). HepG2 SRXN1, DDIT3 (CHOP), CDKN1A (p21) and ICAM1 BAC GFP reporter cell lines were generated and characterized as described previously[44]. HepG2 BAC-GFP reporters were maintained and exposed to drugs in DMEM high glucose supplemented with 10% (v/v) FBS, 25 U/mL penicillin and 25 µg/mL streptomycin. The cell lines were used between passage 5 and 25. For live cell imaging, the cells were seeded in Greiner black µ-clear 384 wells plates, at 8,000 cells per well.

Reagents

All reference compound chemicals were acquired from Sigma-Aldrich and freshly dissolved in DMSO; except for metformin, fluphenazine, buthionine sulfoxamine, bromoethlyamine (all PBS), acetaminophen and phenobarbital (all DMEM). TNFα was acquired from R&D Systems (Abingdon, UK). DILI compounds were a kind gift from the Dr. Weida Tong, NCTR-FDA[331]. All compounds were maintained as 500-fold stock such that final treatments did not exceed 0.2 % v/v DMSO.

Microscopy

Accumulation of GFP levels, propidium iodide (PI) and Hoechst staining was monitored using a Nikon TiE2000 confocal laser microscope (lasers: 540nm, 488nm and 408nm), equipped with an automated stage and perfect focus system at 37 degrees Celsius with humidified atmosphere and 5% CO_2/air mixture. Prior to imaging at 20x magnification, HepG2 cells were loaded for 45 minutes with 100 ng/mL $Hoechst_{33342}$ to visualize the nuclei, upon which the Hoechst-containing medium was washed away to avoid Hoechst phototoxicity[332] and replaced with medium containing PI to monitor cell death. Each 384-well plate contained one reporter cell line, which was exposed to all the compounds used in the screen at one certain concentration (1, 5, 10, 50 or 100 C-max); for each concentration at least two replicates were imaged per reporter cell line. For the ICAM1-GFP reporter experiments, cells were first exposed for 8 hours to compound only. Next, TNFα was added to all wells, up to a final concentration of 10 ng/mL, which diluted the compound concentration ten times. Upon TNFα exposure, imaging was started.

Reporter response quantification

Quantitative image analysis was performed with CellProfiler version 2.1.1[158] with an in house developed CellProfiler module implementing the watershed masked algorithm for segmentation[44,159]. Image analysis results were stored as HDF5 files. Data analysis, quality control and graphics was performed using the in house developed R package h5CellProfiler (manuscript in preparation). For each reporter hourly intensity levels of the GFP signal, the nuclear $Hoechst_{33342}$ intensity levels and at 24 hours the PI staining were measured at the single cell level. In addition cell numbers, nuclei size and cell speed were measured.

Data analysis

GFP intensity cell population means were calculated. In addition, for each plate the cell population mean GFP intensity of the DMSO treated cells was calculated to determine background control values. Per plate, the single cells that had values above the 2X mean, 3X mean were counted. For ICAM1, the background control values consisted of DMSO conditions treated with TNFα, and the single cells with values above, as well as below background values were counted. Due to the non-symmetric distribution of ICAM1 cell population GFP intensities, the interquartile range (IQR) was used to count the number of cells 1.5X, 2X and 3X above and below the TNFα IQR control values (Suppl. Fig. 1). To account for PI background staining noise the PI segmentations were masked by a 2 pixel dilated nuclei. The area of these nuclei and the PI objects were divided to obtain a PI/nuclei ratio. These ratios were filtered to be at least 10 % of the cell size and following this procedure each cell was either flagged as alive or dead in the final time point of the 24 live imaging session. PI positive fraction were normalized to DMSO (or TNFα for ICAM1) by subtracting the control PI positive fractions. Linear regression was applied with time as independent variable to quantify treatment effects on a plate to plate basis of cell speed, nuclear size, $Hoechst_{33342}$ nuclear intensity cell numbers. The slope coefficient mean over all plates was used to obtain a compound-concentration specific summary feature. All summary features were scaled between 0 and 1 with the formula $(x\text{-}x_{min_replicate}) / (x_{max_replicate} - x_{min_replicate})$, with the exception of 1) the cell count features which were scaled between 0 and 1 by calculating cell fractions and 2) the ICAM1-GFP intensity features which were scaled between -1 and 1 to account for up or down regulation of the TNFα-induced ICAM1 expression (Suppl. Fig. 1).

Concentration response data transformation and Benchmark Concentration (BMC) modeling

The maximum values over time of the scaled intensity levels and positive GFP fractions were selected for the concentration response curves. These values were fit to a 4 parameter log-logistic model using the drc package[333]. BMC values were calculated as the concentration at which +0.25 (and – 0.25 for ICAM1) absolute increase from the initial response values occurred (Fig. 4A). The replicate means of the maximum over-time features were calculated for each compound-concentration preceding unsupervised hierarchical clustering. For the time courses (Fig. 3) natural cubic splines with 8 degrees of freedom were fit after which 24 discrete equidistant time points were selected to calculate per-time point replicate means. The time course hierarchical clustering was performed by first calculating Manhattan-based distances between all time course vectors. The mean Manhattan-based distances over all reporters were used as inputs for the Ward-based clustering. This ensured the temporal dynamics were also clustered appropriately.

Data representation

All HCI data representations were generated or modified with Illustrator CS6, Fiji, ggplot2[219], the `aheatmap` function of the NMF package[334].

Severe vs non-Severe DILI prediction with Support vector machine

FDA DILI-annotation was used as 'ground truth' with non-DILI (n=16), less-severe DILI (n=36) and ambiguous DILI (n=12) grouped as `nonSevere DILI` and severe-DILI (n=54) as `severe DILI` resulting in a two-classification problem. Features were obtained by time dynamic feature extraction of time courses using functional data analysis using the in house developed R-package `celloscillate` and the BMC and cmax normalized BMC values (Fig. 6). Feature selection and SVM model tuning was performed in an 200 times iterative process with randomly selected 80/20 – equal class distributed training/test set procedure. The training phase included a first feature selection step using a Kolmogorov-Smirnov test for equal distributions between the two classes followed by pair-wise correlation filter step (>0.8 or <-08). After the feature selection step the training phase. The second step in the training phase consisted of the SVM model tuning with 10 repeats of 10-fold cross-validation. The test phase on 20% of the compounds was performed using the selected features and tuned SVM model. Reported prediction results are the average of the 200 test-set runs (Fig. 6), the ROC distribution of the test-runs are displayed in Fig. 6A. Hierarchical clustering of the 20 selected features (Fig. 6) correspond to the features selected >150 times through the 200 iterations.

Gene expression analysis

CEL files were downloaded from the Open TG-GATEs database: "Toxicogenomics Project and Toxicogenomics Informatics Project under CC Attribution-Share Alike 2.1 Japan" http://dbarchive.biosciencedbc.jp/en/open-tggates/desc.html and analyzed as described previously[44].

Statistics

For statistical significance of all time courses first linear interpolation was applied for each separate time course using the `approx` function from the R-stats package to obtain 100 equal discretized time points for each replicate. The high number of linear interpolations was required to retain the original noise in the time course data. Following this step, a one-way ANOVA for functional data method was applied using the `anova.onefactor` function of the R-package fda.usc to determine significant difference in time-curves compared to DMSO for SRXN1/CHOP/p21 or TNFα for ICAM1. Multiple testing correction was applied using the fdr-method (Benjamini & Hochberg). SRXN1/CHOP/p21 were assessed for significant upregulation and ICAM1 for significant down- or up-regulation. For the log-BMC values a linear model with the BMC as explanatory and C-max as explanatory variable was fit as null-model. The null-model was compared in an anova to a model containing DILI-class as additional additive explanatory variable. The models were compared in an anova for significant effect of DILI-class. For the C-max normalized BMC a Welch two-sample t-test was performed between the severe and non-severe DILI groups.

Results

High content adaptive stress response screen with DILI compounds

To assess the application of adaptive stress response pathway activation for the assessment of DILI liabilities we screened 123 compounds, of which 118 with known DILI liabilities (Fig. 1 and Table 1). As an adaptive stress response read-out, HepG2 BAC-GFP reporter cell lines for oxidative stress (SRXN1-GFP), DNA damage (p21-GFP), ER-stress (CHOP-GFP) and inflammatory cytokine signaling stress (ICAM1-GFP) were used ([28] and see Suppl. Fig. 2). Stress response activation following drug exposure was monitored with live cell confocal microscopy for a period of 24 hours. The time-resolved single cell data was quantified using an established image analysis pipeline[44]. For labeling DILI compounds we used the FDA DILI labeling, which labels drugs either as no-DILI-concern, ambiguous DILI-concern, less-DILI concern or most-DILI-concern[335]. Most-DILI-concern drugs are highly associated with DILI and represent multiple specialist verified cases of DILI. Less-DILI-concern drugs represent few verified cases of DILI. If drugs are suspected to cause most- or less-DILI-concern, but the presented cases cannot be conclusively validated by experts, drugs received the ambiguous DILI-concern label. No-DILI-concern drugs are on the market for decades and are never associated with DILI. In order to separate out clear examples of DILI, we made two classes: non-severe and severe DILI, where the most-DILI-concern drugs are in the severe DILI group and all others are in the non-severe DILI group. In addition, we included FDA labeling in eight separate classes of hepatotoxicity ranging from no hepatotoxicity to fatal hepatotoxicity (Table 1). The screen also included control reference compounds included negative controls (DMSO and medium) and positive controls (i.e. DNA damage inducers, alkylating agents, ER stress inducers etc.) (Table 1 and Fig. 2).

Single cell analysis allows fine tuning of sensitivity versus dynamic range of BAC-GFP reporter responses

All reporters were exposed to five concentrations: 1, 5, 10, 50 and 100 C-max followed by automated live cell imaging and multiparametric image analysis (Fig. 1). C-max values and drug metabolite formation were obtained either from FDA or from literature (see Table 1). For all images single cell analysis was performed to extract a diverse set of quantitative data, including GFP reporter activity, cell number and cytotoxicity (Suppl. Fig. 1). SRXN1-GFP, p21-GFP and CHOP-GFP reporter single cell data was used to derive quantitative data for four different determinants of reporter activity: intensity, fraction of cells with GFP intensity levels above control values. All ICAM1-GFP reporter drug exposures were primed with TNFα exposure; likewise, ICAM1-GFP shows a gradual increase over 24 hour time period in the vehicle control. Therefore drug treatment can lead to an up- or downregulation of the ICAM1-GFP response. Systematic evaluation of these descriptors for the least and strongest responding compound for each individual reporter allowed fine tuning of the sensitivity versus the dynamic range (Fig. 2).

For example, based on the SRXN1-GFP intensity over the single cell population chlorpromazine would not have been defined as positive in the SRXN1-GFP reporter cell line, because only in a small proportion of cells that contain a higher level of SRXN1-GFP the signal was detected. Yet, the GFP_pos.2m and GFP_pos.3m responses of chlorpromazine were more sensitive descriptors that also allowed evaluation of the time course dynamics. Similar observations were made for nitrofurantoin and clozapine for the CHOP-GFP and p21-GFP reporters, respectively. However for strong inducers of oxidative stress (diethylmaleate; DEM), UPR (thapsigargin) and DNA damage (etoposide), GFP mean intensity already allowed detection of the reporter responses, while GFP_pos.2m caused an early saturation, thereby lowering the information value of the temporal dynamics. Further, well-known inflammatory stress modulating compounds diclofenac (DCLF) and azathioprine (AZA) showed inhibiting and enhancing modulatory effects on ICAM1-GFP, respectively.

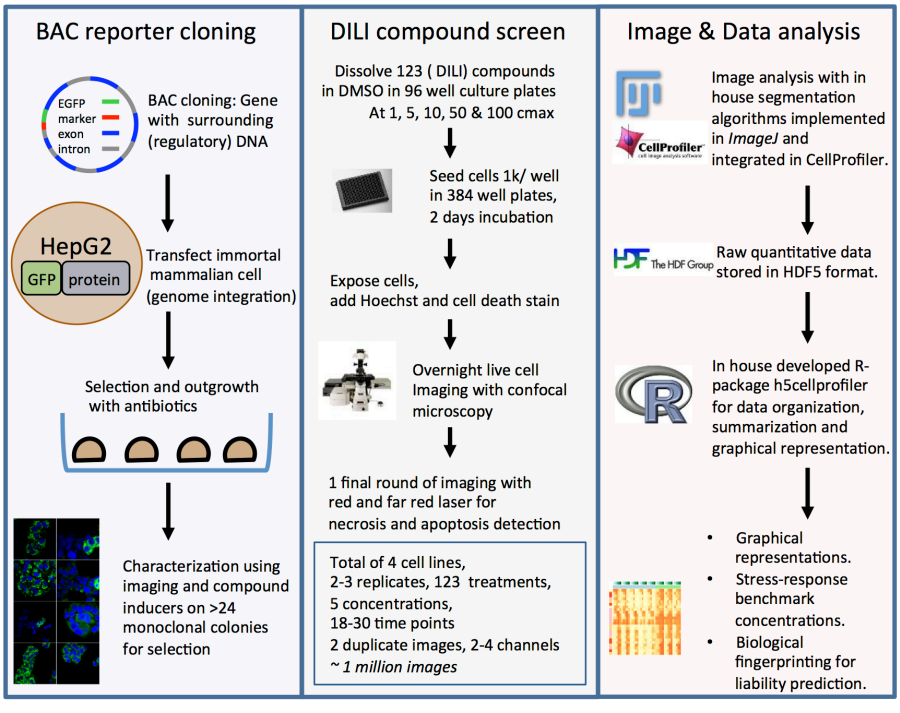

Fig. 1: **BAC cloning, BAC reporter DILI screen and analysis pipeline** Left panel) BAC cloning technology is used to maintain endogenously regulated reporter protein levels and regulation. Monoclonal reporter selection from a high number of clones to ensure endogenous response to positive control stimuli and suitability of reporter for imaging. Middle panel) High content live cell screen of 123 compound at 1, 5, 10, 50 and 100 C-max at 2 or 3 replicates. Right panel) Image and data analysis is performed with CellProfiler/Fiji and R, respectively. Some in-house tools were developed in CellProfiler and R to assist in the quality and analysis of the large data output.

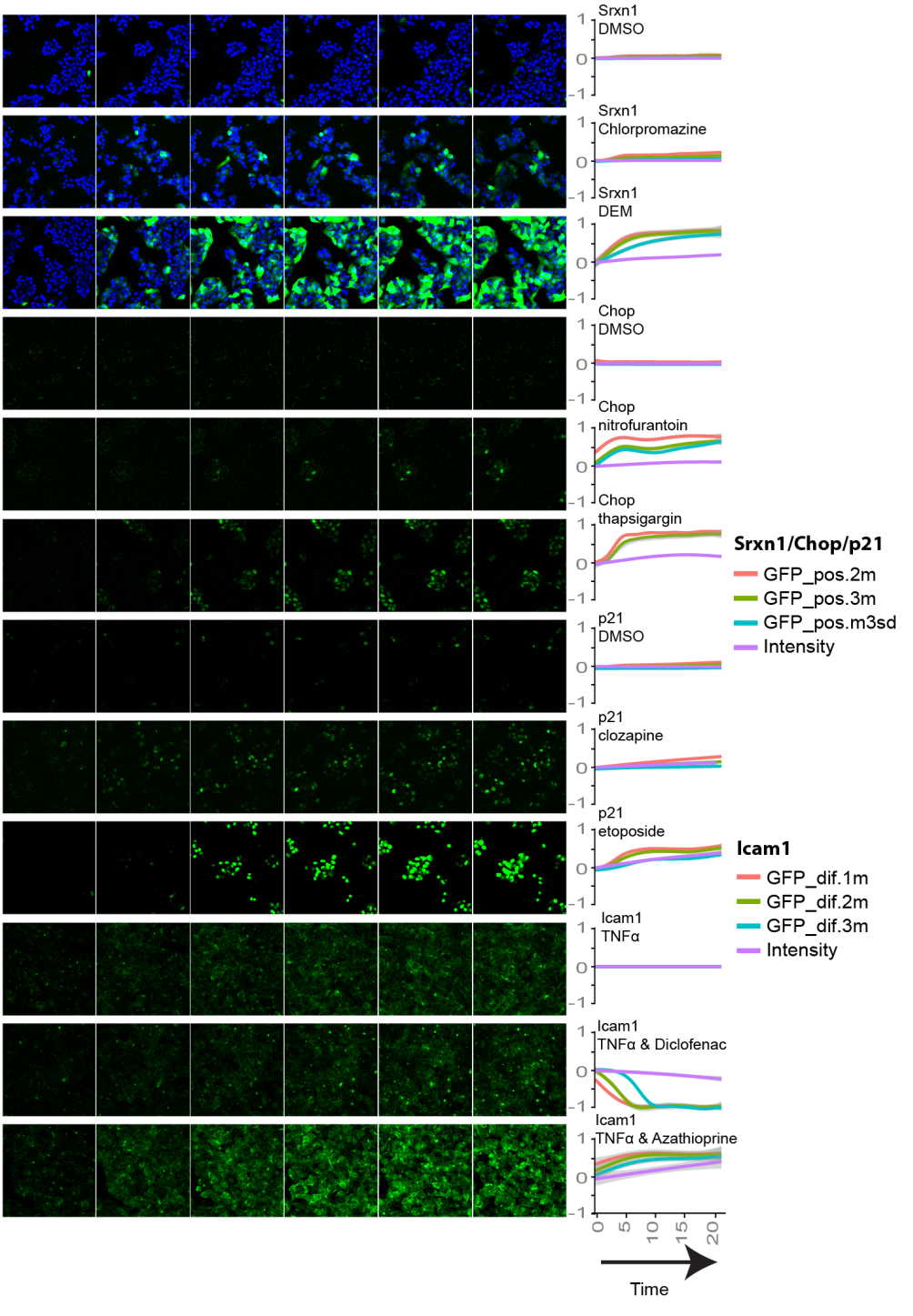
Srxn1
DMSO
Srxn1
Chlorpromazine
Srxn1
DEM
Chop
DMSO
Chop
nitrofurantoin
Chop
thapsigargin
p21
DMSO
p21
clozapine
p21
etoposide
Icam1
TNFα
Icam1
TNFα & Diclofenac
Icam1
TNFα & Azathioprine
1
0
−1
0
5
10
15
20
Time
Srxn1/Chop/p21
GFP_pos.2m
GFP_pos.3m
GFP_pos.m3sd
Intensity
Icam1
GFP_dif.1m
GFP_dif.2m
GFP_dif.3m
Intensity

***Fig. 2*: Dynamics of SRXN1-GFP, CHOP-GFP, p21-GFP and ICAM1-GFP reporter activation** Left panel) Time lapse images of the reporters exemplifying the importance of single cell analysis which allows fine tuning sensitivity versus dynamic range of BAC-reporter read-out. Right panel) Quantification of GFP signal of the SRXN1-GFP, p21-GFP and CHOP-GFP reporters from a control, a weak reporter-activating compound and a strong reporter-activating compound. For ICAM1-GFP the TNFα control was accompanied by a compound which induced the TNFα induced response and by a compound which reduced the TNFα response. Intensity, GFP_pos.2m, GFP_pos.3m and GFP_pos.m3sd are shown for SRXN1-GFP, CHOP-GFP and p21-GFP. For ICAM1-GFP, Intensity, GFP_dif.1m, GFP_dif.2m and GFP_dif.3m are shown.

DILI compounds show specific reporter activation with distinct time dynamics and magnitude

For evaluation of the reporter activation for the entire compound screen GFP_pos.2m was selected as the most sensitive initial readout. The GFP_pos.2m time courses were used to calculate the mean of the replicates for SRXN1-GFP, CHOP-GFP, p21-GFP and ICAM1-GFP reporter responses for all compounds (Fig. 3A and Suppl. Fig. 3). Some compounds showed a response in all four reporters, where ICAM1-GFP can be increased or decreased due to compound exposure. Methyldopa (MD) for example shows an increase in SRXN1-GFP, CHOP-GFP and p21-GFP and a clear decrease in ICAM1-GFP. Mercaptopurine (6MP) induced all four reporters. The data also allowed discrimination of specific time dynamics of stress pathway activation. Thus, for nimesulide (NMS), rifampicin (RFP) and oxytetracycline (OXY) an initial CHOP-GFP response at 100x C-max and a delayed SRXN1-GFP response was observed. In contrast, for the azathioprine (AZA), colchicine (CLC) and dacarbazine (DTIC) an SRXN1-GFP response was followed by CHOP-GFP, eluding to the primary mode of action or type of cellular stress. As a next step we performed hierarchical clustering of the time courses from all 118 compounds representing the reporter activities from all BAC-GFP reporter cell lines (Suppl. Fig. 4). We observed a cluster with strong modulation of stress responses containing mostly the higher C-max treatment conditions (Fig. 3B). This highly active cluster showed an overrepresentation of severe DILI drugs as well as more severe classes of hepatotoxicity (liver necrosis, acute liver failure and fatal hepatotoxicity). Clusters with activation of all four reporters were present, with ICAM1-GFP either up- or downregulated. p21-GFP did show few responses and did not contribute much to the DILI compound clustering. The time response clearly demonstrated the dynamics of the various stress response programs and allowed discrimination between primary stress type and subsequent secondary responses. Strikingly, suppression by DILI compounds of the cytokine-induced ICAM1-GFP expression was highly correlated with activation of the CHOP-GFP reporter, which in a few cases was co-occurring with SRXN1-GFP activation. In conclusion, time resolved clustering results in marked clustering of time dynamics and contributes to mode of action identification.

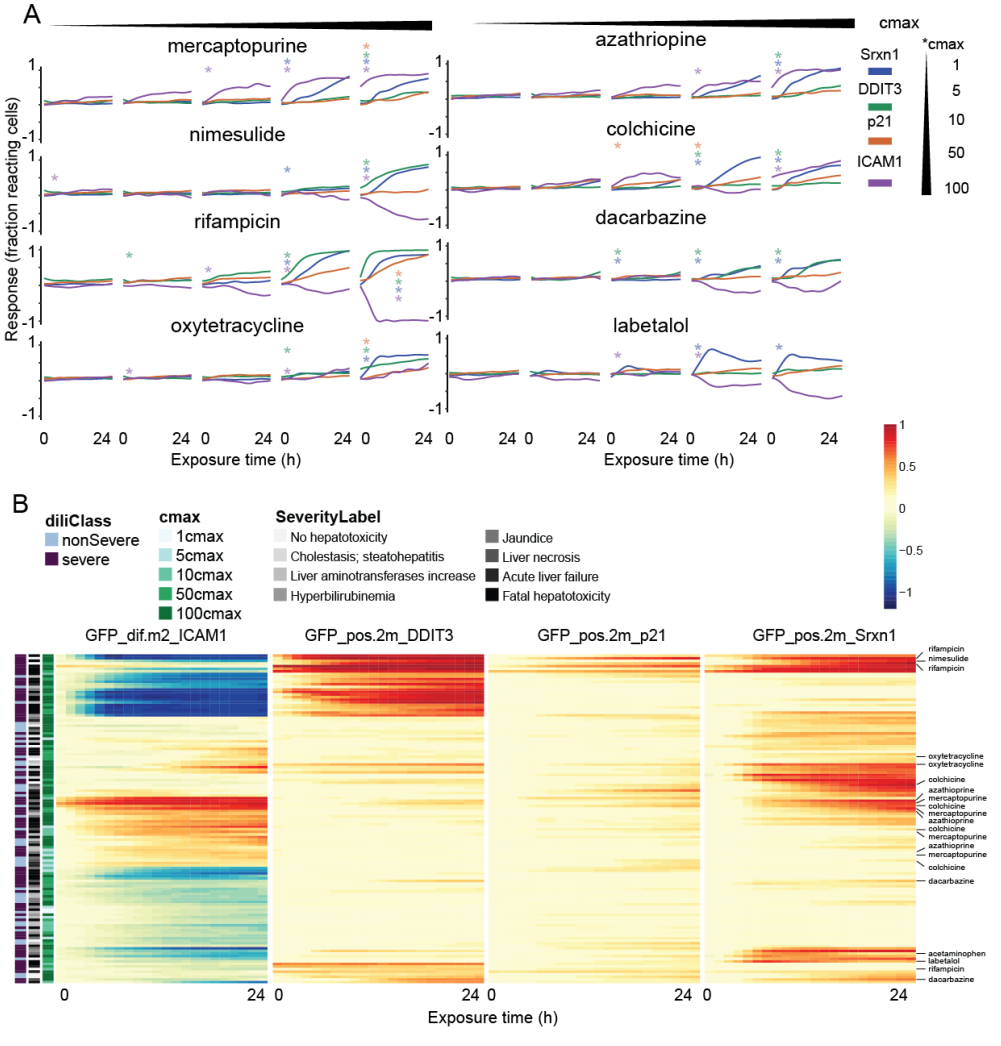

***Fig.3*: Time dynamics of a subset of the screened drugs** A) GFP responses over time of GFP_pos.2m of SRXN1-GFP, CHOP-GFP and p21-GFP and of GFP_dif.2m of ICAM1-GFP. Statistics are performed as described in the material and methods section and represent *<0.01 with the corresponding color to dissect between the different reporter lines. B) Zoom of hierarchical clustering of time dynamic responses. Red is an upregulation and blue is a downregulation. On the left the severe/non-severe (purple) and the hepatotoxicity class (grey) labeling are indicated as well as the C-max values (green).

Clustering of compounds concentration relationships reveals strong clustering towards severe DILI

Next, we summarized time course data by extracting the time point at which the reporter expression reached a peak response using the various quantitative GFP reporter activity descriptors as well as cytotoxicity measurements, including PI and cell number. Hierarchical clustering revealed one large non activate cluster (compound names in red) and one activated group divided over three clusters (compound names in green, blue and purple) (Fig.4). The purple cluster is marked by an increase in SRXN1-GFP, CHOP-GFP and (for some compounds) p21-GFP in combination with a decrease in ICAM1-GFP. The blue cluster is characterized by a strong increase in CHOP-GFP and cytotoxicity and a strong decrease in ICAM1-GFP, also in lower concentrations. In the green cluster SRXN1-GFP and ICAM1-GFP both show a clear increase. Most severe drugs are in one of the activated clusters, as well as the black and dark grey hepatotoxicity classes. The C-max value for magnitude of activation could be discerned through the column wise increasing C-max level and corresponding maximum response level and increased sensitivity features within each reporter, respectively. For example, the fatal hepatotoxicity compound mercaptopurine showed a relatively strong activation of both the oxidative and inflammatory stress pathways, yet, the point-of-departure for inflammatory stress was at a lower Cmax than for the onset of oxidative stress. In contrast, the fatal hepatotoxicity compound ketoconazole showed no SRXN1-GFP response at the intensity feature level but only at the more sensitive GFP positive cell counts starting earliest at 50 C-max and as the primary and only stress-type. Thus, the current high content data analysis revealed the value of measuring quantitative adaptive stress responses for the different DILI classes with a clear distinction in primary stress responses for individual DILI compounds.

Benchmark concentrations reveal low point of departure for SRXN1-GFP and CHOP-GFP in the severe DILI group

Based on the concentration response curves extracted from the peak response in GFP_pos.2m (SRXN1-GFP, CHOP-GFP and p21-GFP) and GFP_dif.m2 (ICAM1-GFP) we were able to calculate the benchmark concentration (BMC) (Fig. 5A). We defined the BMC as the concentration where at least 25% of the cells reach the two times average threshold of the control values.

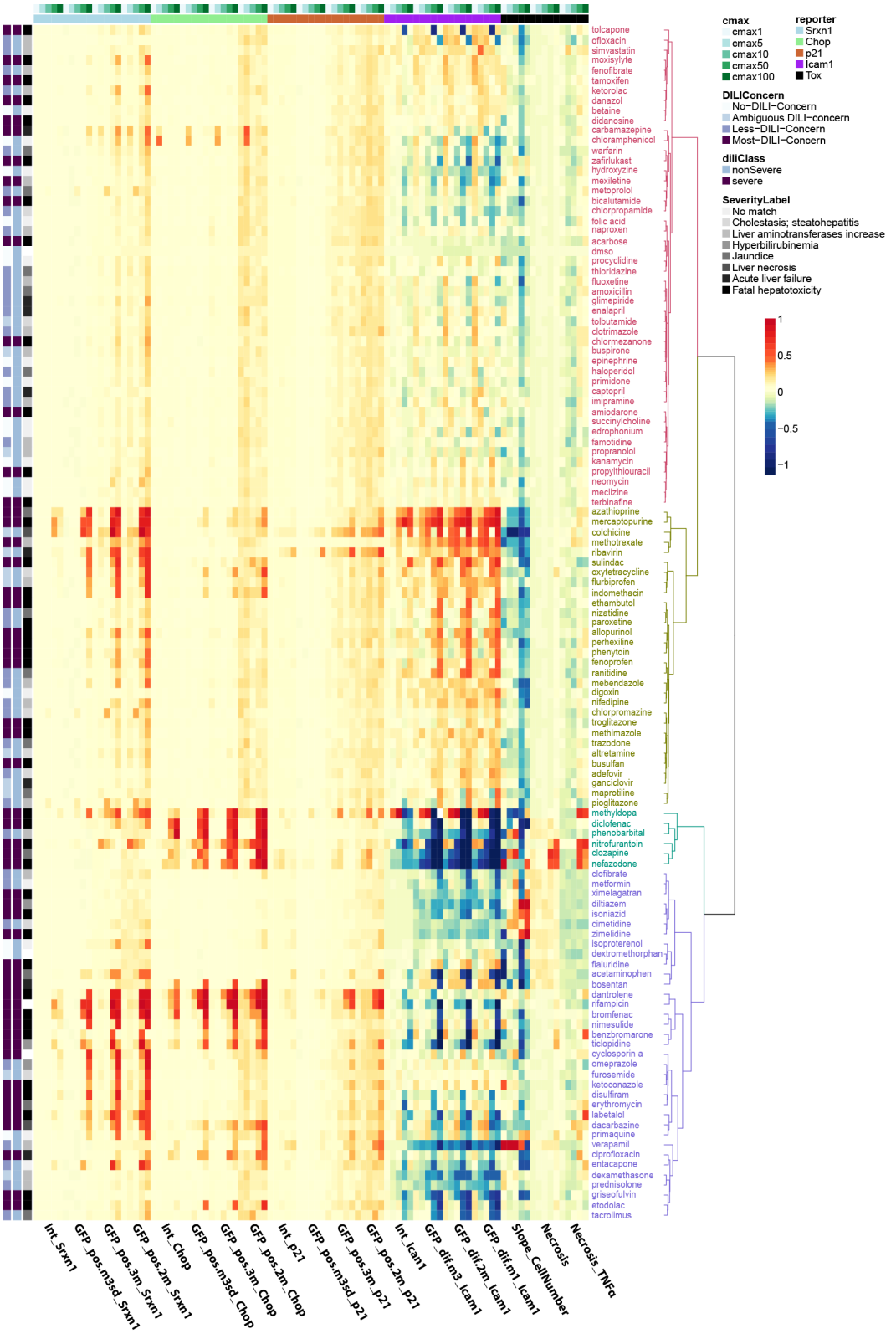
cmax
cmax1
cmax5
cmax10
cmax50
cmax100
reporter
Srxn1
Chop
p21
Icam1
Tox
DILIConcern
No−DILI−Concern
Ambiguous DILI−concern
Less−DILI−Concern
Most−DILI−Concern
diliClass
nonSevere
severe
SeverityLabel
No match
Cholestasis; steatohepatitis
Liver aminotransferases increase
Hyperbilirubinemia
Jaundice
Liver necrosis
Acute liver failure
Fatal hepatotoxicity
1
0.5
0
−0.5
−1
tolcapone
ofloxacin
simvastatin
moxisylyte
fenofibrate
tamoxifen
ketorolac
danazol
betaine
didanosine
carbamazepine
chloramphenicol
warfarin
zafirlukast
hydroxyzine
mexiletine
metoprolol
bicalutamide
chlorpropamide
folic acid
naproxen
acarbose
dmso
procyclidine
thioridazine
fluoxetine
amoxicillin
glimepiride
enalapril
tolbutamide
clotrimazole
chlormezanone
buspirone
epinephrine
haloperidol
primidone
captopril
imipramine
amiodarone
succinylcholine
edrophonium
famotidine
propranolol
kanamycin
propylthiouracil
neomycin
meclizine
terbinafine
azathioprine
mercaptopurine
colchicine
methotrexate
ribavirin
sulindac
oxytetracycline
flurbiprofen
indomethacin
ethambutol
nizatidine
paroxetine
allopurinol
perhexiline
phenytoin
fenoprofen
ranitidine
mebendazole
digoxin
nifedipine
chlorpromazine
troglitazone
methimazole
trazodone
altretamine
busulfan
adefovir
ganciclovir
maprotiline
pioglitazone
methyldopa
diclofenac
phenobarbital
nitrofurantoin
clozapine
nefazodone
clofibrate
metformin
ximelagatran
diltiazem
isoniazid
cimetidine
zimelidine
isoproterenol
dextromethorphan
fialuridine
acetaminophen
bosentan
dantrolene
rifampicin
bromfenac
nimesulide
benzbromarone
ticlopidine
cyclosporin a
omeprazole
furosemide
ketoconazole
disulfiram
erythromycin
labetalol
dacarbazine
primaquine
verapamil
ciprofloxacin
entacapone
dexamethasone
prednisolone
griseofulvin
etodolac
tacrolimus
Int_Srxn1
GFP_pos.m3sd_Srxn1
GFP_pos.3m_Srxn1
GFP_pos.2m_Srxn1
Int_Chop
GFP_pos.m3sd_Chop
GFP_pos.3m_Chop
GFP_pos.2m_Chop
Int_p21
GFP_pos.m3sd_p21
GFP_pos.3m_p21
GFP_pos.2m_p21
Int_Icam1
GFP_dif.m3_Icam1
GFP_dif.2m_Icam1
GFP_dif.m1_Icam1
Slope_CellNumber
Necrosis
Necrosis_TNFα

***Fig.4*: Hierarchical clustering of peak GFP response in tims** Hierarchical clustering of responses of intensity and count related GFP responses in dose response fashion. Cell death measurements cell number and PI staining are in the right bar. On the left side DILI labeling is depicted in three bars: severe/non-severe, DILI-concern labeling and hepatotoxicity class labeling. Compound names are colored based on the clustering.

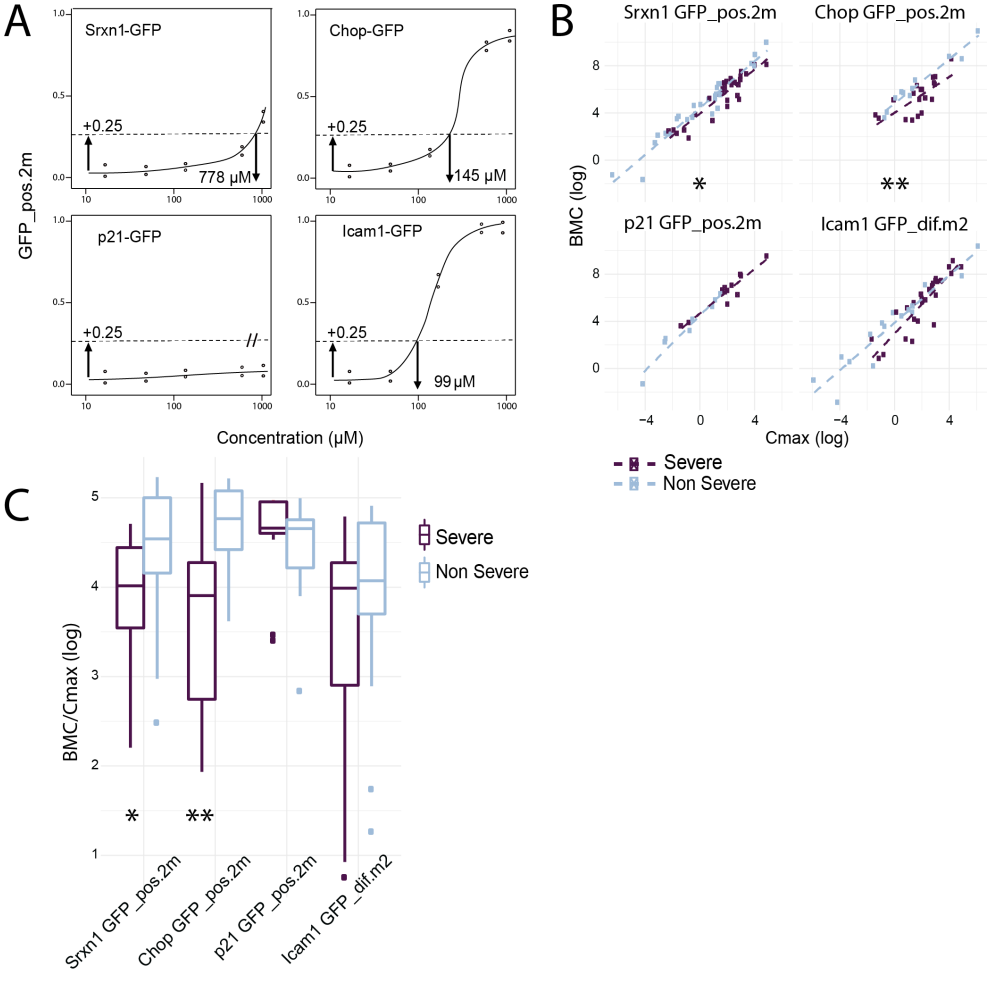

***Fig. 5:* Benchmark concentration (BMC) versus the absolute C-max values per reporter** A) Explanation of how we extract BMC from the fitted dose ranges from different GFP reporters. B) For each reporter the absolute BMC (y-axis) is plotted against the absolute C-max (x-axis), each dot represents a compound which reached the 0.25 threshold. Purple indicates a severe DILI drug, Light blue indicates a non-severe drug; * = $p<0.05$ and ** = $p<0.01$. C) The BMC is divided by the absolute C-max value per compound and represented in the severe/non-severe DILI classes and per reporter; * = $p<0.05$ and ** = $p<0.01$.

A) Obtaining time dynamic features with functional data analysis

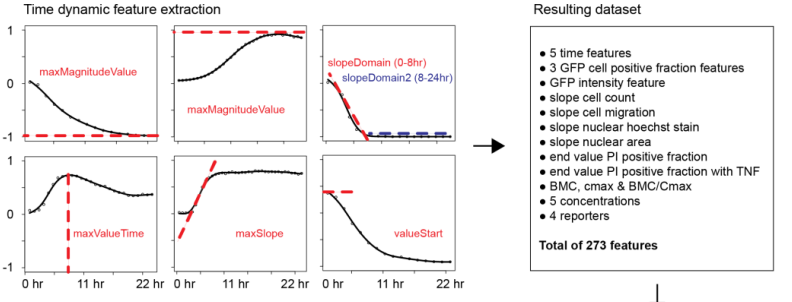

B) Feature selection and Unsupervised Clustering

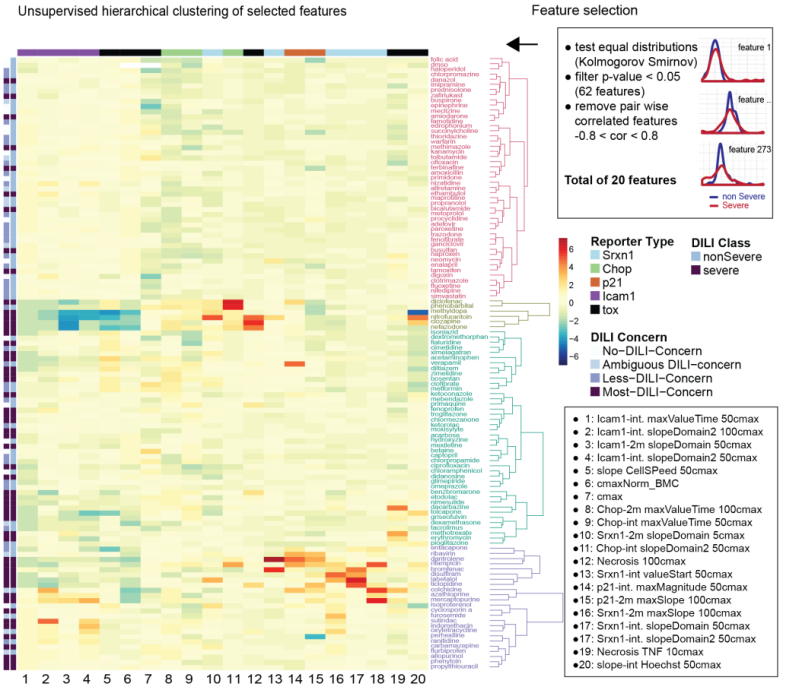

C) Assessing predictive power severe vs non-severe DILI with Support Vector Machine classification

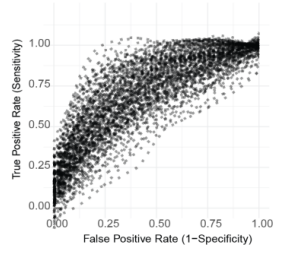

80/20 train/test set prediction validation
Median values after 200 runs:

Balanced Accuracy	0.67
Sensitivity	0.60
Specificity	0.75

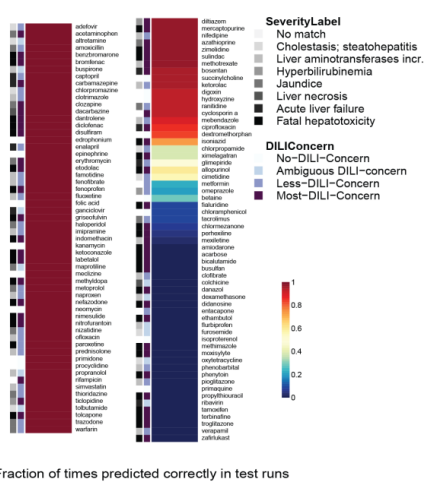

Fig. 6: **Prediction of severe versus non-severe DILI groups.**A) Explanation of temporal feature extraction. B) Feature selection by Kolmogorov Smirnov test and pairwise correlation filter. Followed by unsupervised hierarchical clustering of the most often selected features from the 200 feature selection iterations. C) ROC curves from 200 test data runs and average prediction results (left); Fraction of correct prediction for each drug

This BMC can function as an indicator for the point of departure for further risk assessment modeling. The C-max values for the screened compounds show a large concentration range which ranges from 1.7 nM to 0.94 mM. To correct for this difference we plotted the BMC against the absolute C-max value (Fig. 5B) and we divided the BMC by the absolute C-max (Fig. 5C). After this correction, we are able to observe a lower BMC in SRXN1-GFP, CHOP-GFP and ICAM1-GFP for severe DILI drugs, compared to non-severe drugs. In SRXN1-GFP and CHOP-GFP this difference is statistically significant ($p < 0.001$ for CHOP & $p < 0.05$ for SRXN1 for both methods), indicating severe DILI drugs have a lower point of departure and are therefore more potent to induce adaptive stress responses.

Feature selection and SVM classification show predictive power of a diverse and complex set of biologically interpretable features

Time dynamic features and BMC values were extracted as described in the material and methods section (Fig. 6). The resultant table of 273 variables corresponding to the total set of features and 118 observations corresponding to the compounds was subjected to machine learning to asses temporal stress pathway activation and concentration–response relations for predictive power and feature importance.

Feature selection and support vector machine (SVM) model tuning was performed over 200 iterations of random training/test dataset sampling (Suppl. Fig. 1), as described in detail in the material and methods. The features selected more than 150 times in the 200 iterations were subjected to unsupervised hierarchical clustering (Fig. 6B). Interestingly a diverse set of features, encompassing all reporters, BMC, C-max and also toxicity features including cell death with TNFα at 10 C-max, cell death at 100 C-max and cell speed at 50 C-max. Early and late slope features from the reporters seem to be preferred over the max magnitude values. The resulting clustering with these features shows 3 dominant clusters with enriched severe DILI compounds (purple, blue and green clusters, Fig. 6B).

The 200 independent test-set prediction validations with the tuned SVM model resulted in an average ROC of 0.73 (Fig. 6C, left panel) and a sensitivity of 0.60 and specificity of 0.75 with ‘positive’ being the severe-DILI group. Over the 200 runs the correct prediction rates for each compound was calculated (Fig. 6C, right panel), clearly a subset of 30 compounds have some uncertainty as to being predicted correctly. The remaining compounds are all either predicted correctly, or predicted falsely. No enrichment for DILI-class can be seen for these prediction rates.

.

Discussion

Here we investigated the integrated application of a panel of four adaptive stress response BAC reporters in high content high throughput screening as a method for DILI liability assessment. We focused on adaptive stress pathway signaling as these defense programs are a universal theme in all life forms and respond before the onset of overt toxicity. We monitored four downstream target genes for oxidative stress (Srnx1), ER-stress/UPR (CHOP), DNA damage (p21) and inflammation (ICAM1); these are selective targets for these pathways. Using CellProfiler and R-package h5CellProfiler we quantified all images and summarized the responses in a time- and concentration dependent relationship. Concentration information was used to extract the benchmark concentration for each compound-reporter combination. This revealed significant changes between the severe and non-severe DILI classes for SRXN1-GFP and p21-GFP. Furthermore, a non-significant yet similar trend was observed for ICAM1-GFP. To perform detailed analysis on the contribution of time and concentration based features to DILI classification, we extracted 20 features and assed these data for predictive power using support vector machine approaches. Using these features we are able to classify severe versus non-severe DILI classes with a sensitivity of 60% and a specificity of 75%. We demonstrate how advanced analysis of live-single cell data can provide key information on the concentration-time course reporter responses that can be applied for DILI liability evaluation. We showed that integration of such mode-of-action assessment using different reporters increases our mechanistic understanding of severe DILI concern compounds.

By using adaptive stress response measurements we are able to dissect detailed information on the mode-of-action of different drugs (Fig. 4). Three differently activated clusters are clearly visible. Strikingly, SRXN1-GFP is often not activated without the activation of other responses (CHOP-GFP, ICAM1-GFP). This indicates oxidative stress is either occurring as a secondary effect after cellular stress induction or as a primary cause which also disturbs other systems as protein folding or inflammation[20].Since we also capture the time dependent adaptive stress activation dynamics, we are able to make a distinction between these two possibilities (Fig. 3, Suppl. Fig. 2 and 3). Interestingly, the blue colored compound cluster with strong decrease in ICAM1-GFP show also strong increase in CHOP-GFP, but no or minor activation of SRXN1-GFP, meaning that a specific mode-of-action regulates both the inflammation and the ER-stress pathways. Previously, we demonstrated this dual role for diclofenac[221]. Furthermore, for two other members of this cluster, nefazodone and clozapine, this dual activation has been illustrated before[130,336–338]. An increase in ICAM1-GFP is often accompanied with an increase in SRXN1-GFP (green cluster). Interestingly, also a decrease in cell number is observed in these drugs, indicating a role for ICAM1-GFP in cell cycle arrest. No major increase of p21-GFP is seen for most compounds, this is probably due to the fact that genotoxicity is thoroughly checked during drug development.

The minor role of p21-GFP is especially visible when looking at the benchmark concentration. No difference is observed between the severe and non-severe DILI groups, but this is mainly due to a low amount of compounds (19) that reach the 25% positively

activated cell threshold in p21-GFP. In contrast, SRXN1-GFP, CHOP-GFP and ICAM1-GFP show lower benchmark concentrations at the C-max value, indicating that the severe DILI group are already activating stress responses at lower concentrations. This is especially pronounced in SRXN1-GFP and CHOP-GFP, where the BMCs of the severe DILI group are significantly lower than the BMCs of the non-severe group after C-max correction. For CHOP-GFP this is expected, since CHOP is an important adaptation-adversity-switch in ER stress signaling and therefore activated when the system is more perturbed and closer to cytotoxicity[339]. For SRXN1-GFP this is less obvious since multiple drugs cause oxidative stress, often followed by adaptation[340]. Yet, we are able to distinguish the severe from the non-severe DILI group.

The screen was performed in a time-resolved live single cell setting. To date, toxicity screening efforts using high content imaging have mostly focused on single time point fluorescent dyes or anti-bodies[341] with several real-time based toxicity screening efforts[342]. However, the use of dyes and anti-bodies brings additional noise to already very noisy systems as fixation and anti-body binding are likely additional sources of variability; this is not an issue using our reporter models. With the use of our reporter cell lines biological signaling can be visualized with a high time resolution to more accurately pinpoint the primary mode-of-action in relation to cellular stress. Time course signaling data also greatly benefits computational modeling efforts as these require detailed time and dose response dynamics, this is only feasible using live cell imaging data. Furthermore, we were able to extract features based on this time and dose response dynamics. These features were used in support vector machine approach to assess possible differences in cellular adaptive signaling between less- severe and severe DILI. Due to the limited number of no-DILI compounds (n = 16) and the total of 118 compounds tested we had obtained a limited set of observations for building predictive models. However by combining the less-Severe DILI and ambiguous DILI cases together with the no-DILI compounds we were still able to show significant predictivity with an independent subset of our data not used in the SVM tuning process. This promising result indicates the importance of adaptive signaling dynamics in DILI. However exact pinpointing of key-features remains difficult without a significantly larger dataset containing a more balanced safe versus unsafe labeled compound annotation. We anticipate the development of an ever increasing database containing such detailed signaling based features linked to chemical exposure, i.e. compound specific biological fingerprints, will ultimately aid in the safety evaluation and early (DILI) prediction of new drugs and chemicals.

In addition to screening more DILI related drugs, more adaptive stress response pathways (heat shock response, mitochondrial toxicity, hypoxia) or reporters (Hmox1-GFP, A20-GFP, Btg2-GFP, BiP-GFP) can be screened. Another issue which affected the result of the prediction is labeling of the drugs in different DILI-concern categories. The labeling of these drugs changes over time, making it difficult to establish a balanced set of most-DILI-concern drugs versus no-DILI-concern drugs[331,335]. Separating the most-DILI-concern drugs from all other drugs allows classification, however at a cost of including drugs with ambiguous nature related to DILI-severity. This led to poor prediction of several less-DILI

drugs (glimepiride, cimetidine, metformin, omeprazole, tacrolimus, clofibrate, entacapone, phenobarbital, pioglitazone and verapamil) (Fig. 6C, right panel). Some of them are known to induce adaptive stress responses (verapamil and metformin)[343,344]. In addition, all most-DILI-concern drugs are or have been on the market, meaning they passed toxicity testing stages of drug development. Therefore, when these reporters are to be used in drug development with new chemicals prediction is expected to perform better.

We performed the screen using the HepG2 cell line. Although HepG2 has several advantages for *in vitro* screening (unlimited lifespan, cheap, easy to culture), the major setback is their lack of metabolic capacity. However, several compounds that involve biotransformation-dependent toxicity do show a SRXN1-GFP oxidative stress response (e.g. acetaminophen and sulindac). To test whether there is a concordance between the HepG2 BAC-GFP reporters and the transcript levels in primary human hepatocytes we used the TG-GATES dataset to calculate the correlation of the activity of the reporters genes between TG-GATES and the current BAC-GFP HepG2 DILI screen (Suppl. Fig. 5). This indicates a significant overlap for SRXN1 responses of transcript levels in primary human hepatocyte and BAC-GFP HepG2, indicating a minor role for drug metabolism in the DILI prediction. Still, some of the drugs in the poorly predicted set are supposed to be metabolized (zafirlukast, troglitazone, methimazole, mexilitine). It is noteworthy to mention a large cloud of points exists in the top left (boxed area, Suppl. Fig. 5) demonstrating mainly enhanced SRXN1 protein activation in comparison to PHH transcript levels indicating increased oxidative stress detection sensitivity. Previously, we optimized a HepG2 3D spheroid protocol to enhance liver like properties and to enable chronic exposures[129]. In future research we can test whether this would increase prediction of DILI drugs.

In conclusion, we have shown that BAC-GFP reporter cell lines are a sensitive tool to provide detailed mechanistic information regarding the adaptive stress response activation in a broad compound screening setting using high-content live single cell imaging. Such detailed insights in the perturbations of signaling pathways after chemical exposure provides key information for safety assessment and possibly predictive purposes. We anticipate that our BAC-GFP reporter platform will contribute to the early pre-clinical screening for DILI liabilities and possibly also other chemical safety assessment paradigms.

Acknowledgements

We would to thank Dr. Weida Tong (NCTR, FDA) for providing the DILI compounds and his contribution to this manuscript. This work was financially supported by the Innovative Medicine Initiative MIP-DILI project (Grant agreement No. 115336), the FP7 Seurat-1 program DETECTIVE project (Grant agreement No. 266838), and the European Union's Horizon 2020 EU-ToxRisk project (Grant agreement No. 681002).

compound	cmax (µ	abb.	DILI con.	Severity	Hepa.	Cmax ref.	metab
acarbose	0.15	ACA	Most-DC	sev.	8	FDA	NM
acetaminophen	139	APAP	Most-DC	sev.	5	Xu/O'Brien	YES
adefovir	0.085	ADV	Less-DC	non-sev.	2	Dailymed	NM
allopurinol	13.81	ALLO	Most-DC	sev.	8	FDA	NM
alitretamine	3.76	ALM	Amb.-DC	non-sev.	2	FDA	YES
amiodarone	0.807	AMIO	Most-DC	sev.	8	Xu/O'Brien/Khet.	NM
amoxicillin	22.3	AX	Less-DC	non-sev.	5	FDA	NM
azathioprine	0.34	AZA	Most-DC	sev.	5	FDA	YES
benzbromarone	4.339	BB	Most-DC	sev.	8	FDA	YES
betaine	940	BET	No-DC	non-sev.	1	O'Brien	NM
bicalutamide	1.97	BAT	Most-DC	sev.	8	FDA	YES
bosentan	7.4	BOS	Most-DC	sev.	7	Dawson/Gustaf.	YES
bromfenac	17.96	BFC	Most-DC	sev.	8	FDA	NA
buspirone	0.016	BUS	Amb.-DC	non-sev.	3	FDA	YES
busulfan	0.277	BU	Most-DC	sev.	8	FDA	YES
captopril	8.882	CPL	Less-DC	non-sev.	7	FDA	YES
carbamazepine	50.79	CBZ	Most-DC	sev.	7	Dailymed	NM
chloramphenicol	46.36	CAMP	No-DC	non-sev.	1	Ogutu	NM
chlormezanone	10.59	CMZ	Most-DC	sev.	8	FDA	NA
chlorpromazine	0.94	CPZ	Less-DC	non-sev.	2	Xu	YES
chlorpropamide	130.1	CHL	Less-DC	non-sev.	2	FDA	NM
cimetidine	11.89	CMT	Less-DC	non-sev.	2	Regenthal	YES
ciprofloxacin	6.58	CIPX	Most-DC	sev.	7	FDA	NM
clofibrate	470	CLO	Less-DC	non-sev.	3	O'Brien	YES
clotrimazole	0.087	CTZ	Less-DC	non-sev.	3	FDA	NM
clozapine	2.44	CLZ	Most-DC	sev.	5	Regenthal	YES
colchicine	0.016	CLC	Amb.-DC	non-sev.	6	FDA	YES
cyclosporin A	0.2	CSA	Most-DC	sev.	NA	Dailymed	YES
dacarbazine	20.64	DTIC	Most-DC	sev.	6	FDA	NM
danazol	0.109	DNZ	Most-DC	sev.	8	FDA	NM
dantrolene	7.9	DAN	Most-DC	sev.	8	FDA	YES
dexamethasone	0.224	DXS	Amb.-DC	non-sev.	3	FDA	NM
dextromethorphan HBr	0.022	DXM	No-DC	non-sev.	NA	Xu	NA
diclofenac	10.1	DCF	Most-DC	sev.	8	Gustaf./Regen.	YES
didanosine	9.83	DDL	Most-DC	sev.	8	FDA	NM
diethylmaleate		DEM	control	NA	NA	NA	NA
digoxin	0.003	DIG	No-DC	non-sev.	1	FDA	YES
diltiazem	0.356	DTZ	Most-DC	sev.	4	Patel	YES
disulfiram	5.4	DIS	Most-DC	sev.	8	FDA	YES
DMSO	0.2	DMSO	control	NA	NA	NA	NA
edrophonium	60.2	EDR	No-DC	non-sev.	1	FDA	NA
enalapril	0.4	ENP	Less-DC	non-sev.	7	FDA	YES
entacapone	3.93	ECP	Less-DC	non-sev.	1	Dailymed	YES
epinephrine	0.002	EPI	No-DC	non-sev.	1	FDA	NA
erythromycin	11	ERYC	Most-DC	sev.	5	FDA	NM
ethambutol	24.47	EMB	Most-DC	sev.	8	FDA	NM
etodolac	68.49	ELAC	Most-DC	sev.	8	FDA	YES
etoposide		ETO	control	NA	NA	NA	YES
famotidine	0.308	FAM	Less-DC	non-sev.	3	FDA	YES
fenofibrate	4.1	FF	Less-DC	non-sev.	3	FDA	NM
fenoprofen	58.2	FPF	Most-DC	sev.	8	FDA	YES
fialuridine	1	FIAU	Most-DC	sev.	8	O'Brien	NA
fluoxetine	0.05	FLX	Less-DC	non-sev.	3	Regenthal	YES
flurbiprofen	57.32	FBP	Amb.-DC	non-sev.	3	FDA	YES
folic acid	0.043	FAM	No-DC	non-sev.	1	FDA	YES
furosemide	3.29	FUR	Amb.-DC	non-sev.	2	FDA	YES
ganciclovir	4.62	GCV	Amb.-DC	non-sev.	7	FDA	YES
glimepiride	1.12	GLP	Less-DC	non-sev.	7	FDA	NM
griseofulvin	4.54	GF	Most-DC	sev.	8	FDA	YES
haloperidol	0.005	HDL	Less-DC	non-sev.	5	FDA	YES
hydroxyzine	0.27	HYZ	No-DC	non-sev.	1	FDA	NM
imipramine	0.29	IM	Less-DC	non-sev.	3	FDA	YES

compound	cmax (	abb.	DILI con.	Severity	Hepa.	Cmax ref	metab
indomethacin	5.59	IMN	Most-DC	sev.	8	FDA	YES
isoniazid	76.56	INH	Most-DC	sev.	8	Xu/Regen./Daw.	YES
isoproterenol	2.02	IPR	No-DC	non-sev.	1	Gustafsson	NA
kanamycin	60.1	KM	No-DC	non-sev.	1	Xu	NA
ketoconazole	6.59	KTZ	Most-DC	sev.	8	Khetani	NM
ketorolac	3.53	KTL	Less-DC	non-sev.	3	FDA	NM
labetalol	2.68	LABE	Most-DC	sev.	8	FDA	YES
maprotiline	0.18	MPT	Amb.-DC	non-sev.	5	FDA	NA
mebendazole	0.13	MBZ	Less-DC	non-sev.	3	FDA	NM
meclizine	0.026	MCZ	No-DC	non-sev.	1	FDA	NM
mercaptopurine	0.48	6MP	Most-DC	sev.	8	FDA	YES
metformin	7.78	MF	Less-DC	non-sev.	1	Regenthal	YES
methimazole	2.62	MTZ	Most-DC	sev.	8	FDA	YES
methotrexate	0.77	MXT	Most-DC	sev.	3	Regenthal	NM
methyldopa	18.94	MD	Most-DC	sev.	8	FDA	YES
metoprolol	0.56	MTPL	Less-DC	non-sev.	5	FDA	YES
mexiletine	3.83	MXT	Most-DC	sev.	3	FDA	YES
moxisylyte	0.16	MOX	Most-DC	sev.	8	FDA	NA
naproxen	0.2	NPX	Less-DC	non-sev.	3	Regenthal	YES
nefazodone	3.95	NFZ	Most-DC	sev.	8	Gustaf./Regen./Daw.	YES
neomycin	0.44	NEO	No-DC	non-sev.	1	Hu: in vitro dose	NM
nifedipine	0.43	NFP	Less-DC	non-sev.	3	Wagner	YES
nimesulide	21.082	NMS	Most-DC	sev.	8	FDA	YES
nitrofurantoin	6	NTF	Most-DC	sev.	8	FDA	YES
nizatidine	4	NIZ	Less-DC	non-sev.	5	FDA	YES
ofloxacin	9.96	OFX	Less-DC	non-sev.	3	Dailymed	NM
omeprazole	4.7	OMZ	Less-DC	non-sev.	4	Dailymed	YES
oxytetracycline	3.26	OTC	Amb.-DC	non-sev.	2	FDA	NA
paroxetine	0.061	PXT	Less-DC	non-sev.	8	FDA	YES
perhexiline	2.16	PHX	Most-DC	sev.	8	Xu	NA
phenobarbital	145.5	PBT	Less-DC	non-sev.	3	Schmidt	NM
phenytoin	21.72	PT	Most-DC	sev.	8	Xu et al	YES
pioglitazone	2.946	PGZ	Less-DC	non-sev.	3	Xu/O'Brien	NM
prednisolone	0.68	PRD	Less-DC	non-sev.	3	FDA	NM
primaquine	0.615	PQ	No-DC	non-sev.	1	Xu	NM
primidone	4.67	PRI	No-DC	non-sev.	1	FDA	YES
procyclidine	0.404	PCD	No-DC	non-sev.	1	FDA	NA
propranolol	0.201	PPL	Amb.-DC	non-sev.	3	FDA	YES
propylthiouracil	9.1	PTU	Most-DC	sev.	8	FDA	YES
ranitidine	1.79	RNT	Less-DC	non-sev.	5	FDA	YES
ribavirin	2.61	RBV	Amb.-DC	non-sev.	7	FDA	YES
rifampicin	15	RFP	Most-DC	sev.	NA	Dailymed	YES
simvastatin	0.082	SVN	Less-DC	non-sev.	3	FDA	YES
succinylcholine	137.74	SUCCS	No-DC	non-sev.	1	FDA	NA
sulindac	31.985	SUL	Most-DC	sev.	8	FDA	YES
tacrolimus	0.037	TAC	Less-DC	non-sev.	5	Dailymed	YES
tamoxifen	0.162	TMX	Most-DC	sev.	8	Xu	YES
terbinafine	4	TRB	Most-DC	sev.	8	FDA	NM
thapsigargin		TG	control	NA	NA	NA	NA
thioridazine	0.55	TDZ	Less-DC	non-sev.	5	Ravic	YES
ticlopidine	8.075	TPD	Most-DC	sev.	4	FDA	YES
tnfα		TNF	control	NA	NA	NA	NA
tolbutamide	233.03	TOLB	Amb.-DC	non-sev.	2	FDA	NM
tolcapone	21.99	TC	Most-DC	sev.	8	Dailymed	YES
trazodone	5.056	TZ	Less-DC	non-sev.	5	FDA	YES
troglitazone	6.39	TRG	Most-DC	sev.	8	Xu/Khetani	YES
verapamil	0.5	VRP	Less-DC	non-sev.	3	Regenthal	NM
warfarin	4.86	WAR	Less-DC	non-sev.	5	FDA	NM
ximelagatran	0.3	XML	Most-DC	sev.	8	Keisu	NA
zafirlukast	1.21	ZFL	Most-DC	sev.	8	FDA	YES
zimelidine	0.267	ZMI	Most-DC	sev.	8	Gustafsson	NA

Table 1: Test compound set Alphabetically sorted list of screened compounds in this study including their c-max values, abbreviations, DILI-concern labeling, severity class, hepatotoxicity class (1 = no hepatotoxicity, 2 = cholestasis/steatohepatitis, 3 = liver aminotransferases increase, 4 = hyperbilirubumenia, 5 = jaundice, 6 = liver necrosis, 7 = acute liver failure, 8 = fatal hepatotoxicity), C-max reference and metabolic potential based on the livertox.nih.gov database (YES = compound is metabolized, NM = compound is not metabolized, NA = not available in the database).

Supplementary Figures

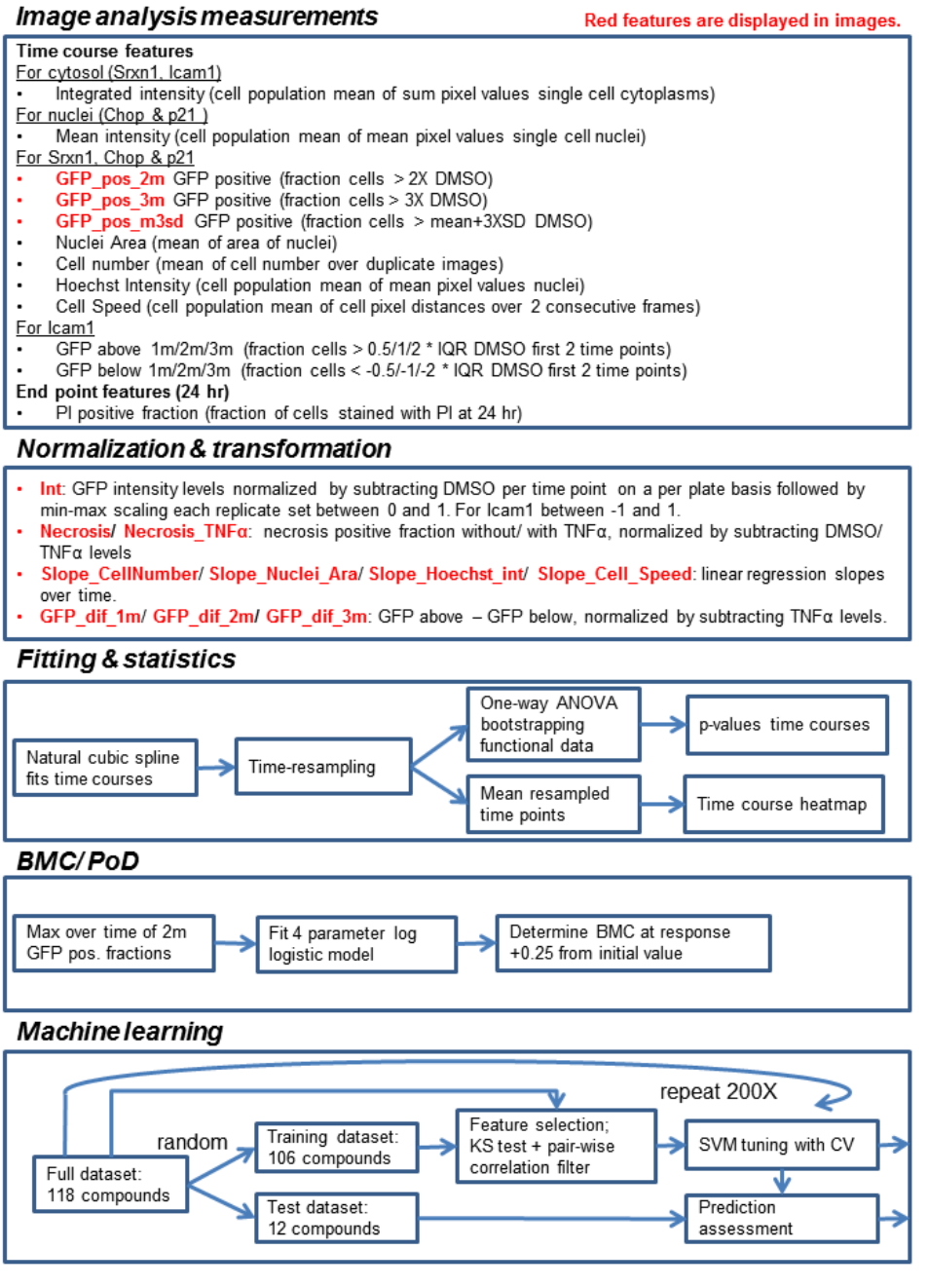

Suppl. Fig. 1: **Data analysis workflow** The features in red are displayed in the figures of the results section.

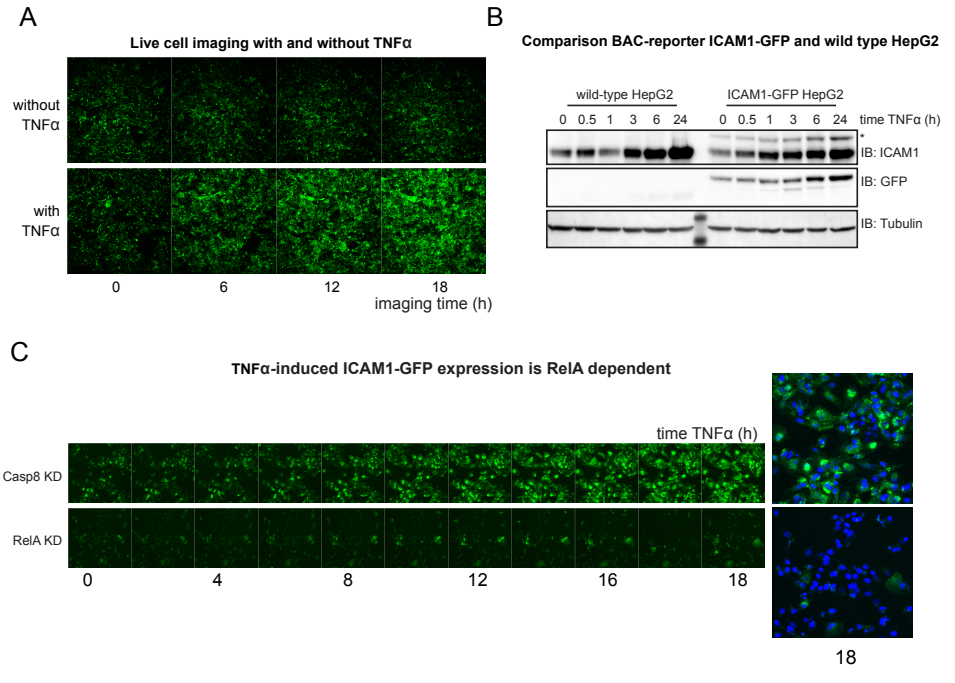

Suppl. Fig. 2: **ICAM1-GFP characterization** A) Time lapse images with and without TNFα. B) Comparison BAC-GFP ICAM1-GFP and wildtype HepG2 with western blotting after induction with TNFα and stained with ICAM1, GFP and tubulin antibodies. C) Time lapse images of ICAM1-GFP after knock down of caspase 8 and NF-κB subunit RelA and TNFα exposure.

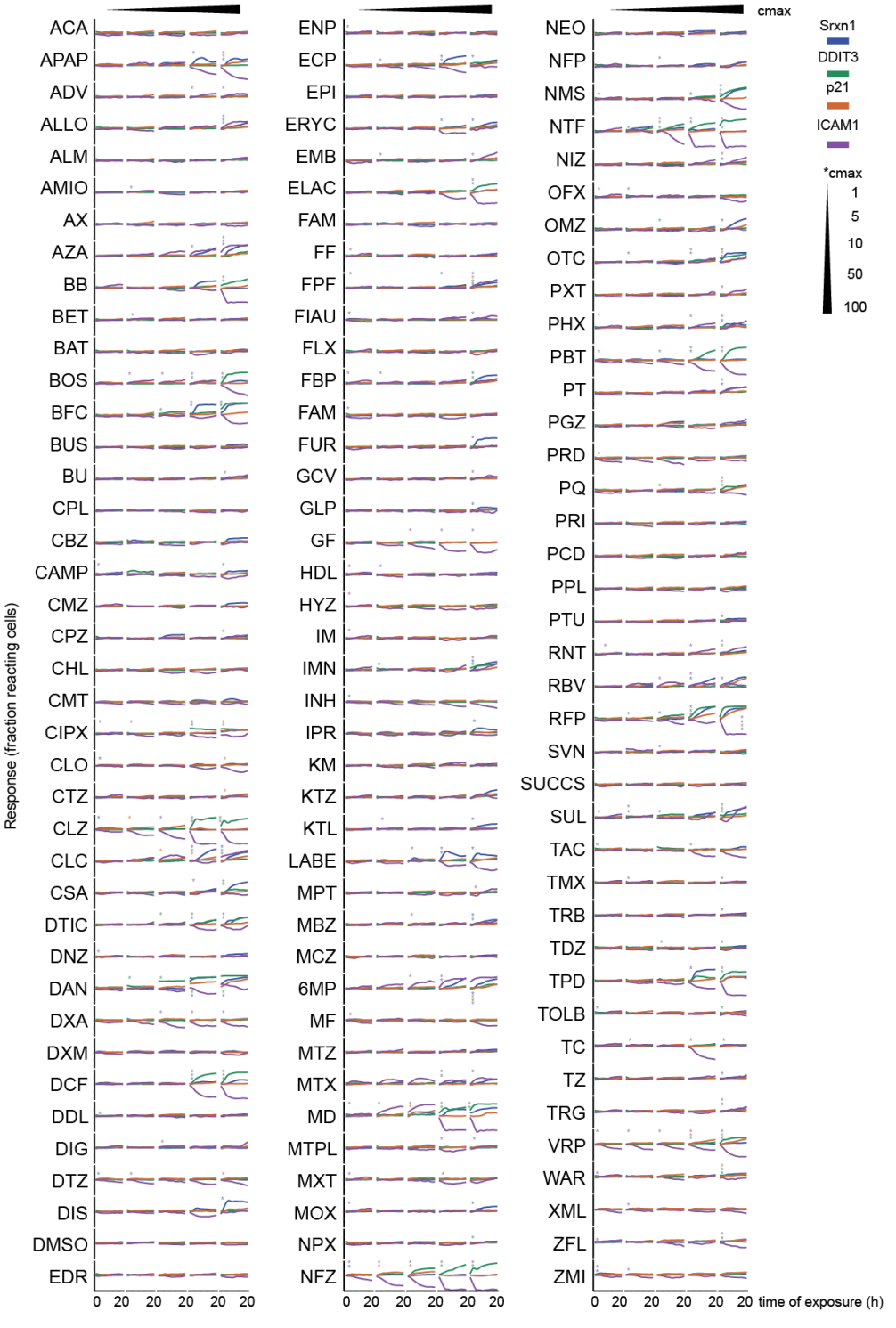

Suppl. Fig. 3: **Time course graphs of all treatments and concentrations.** For all compounds the reporter activity is shown for GFP_pos.2m (SRXN1-GFP, CHOP-GFP and p21-GFP) and GFP_dif.m2 (ICAM1-GFP). Statistics were performed as described in the material and methods section: * = p<0.01

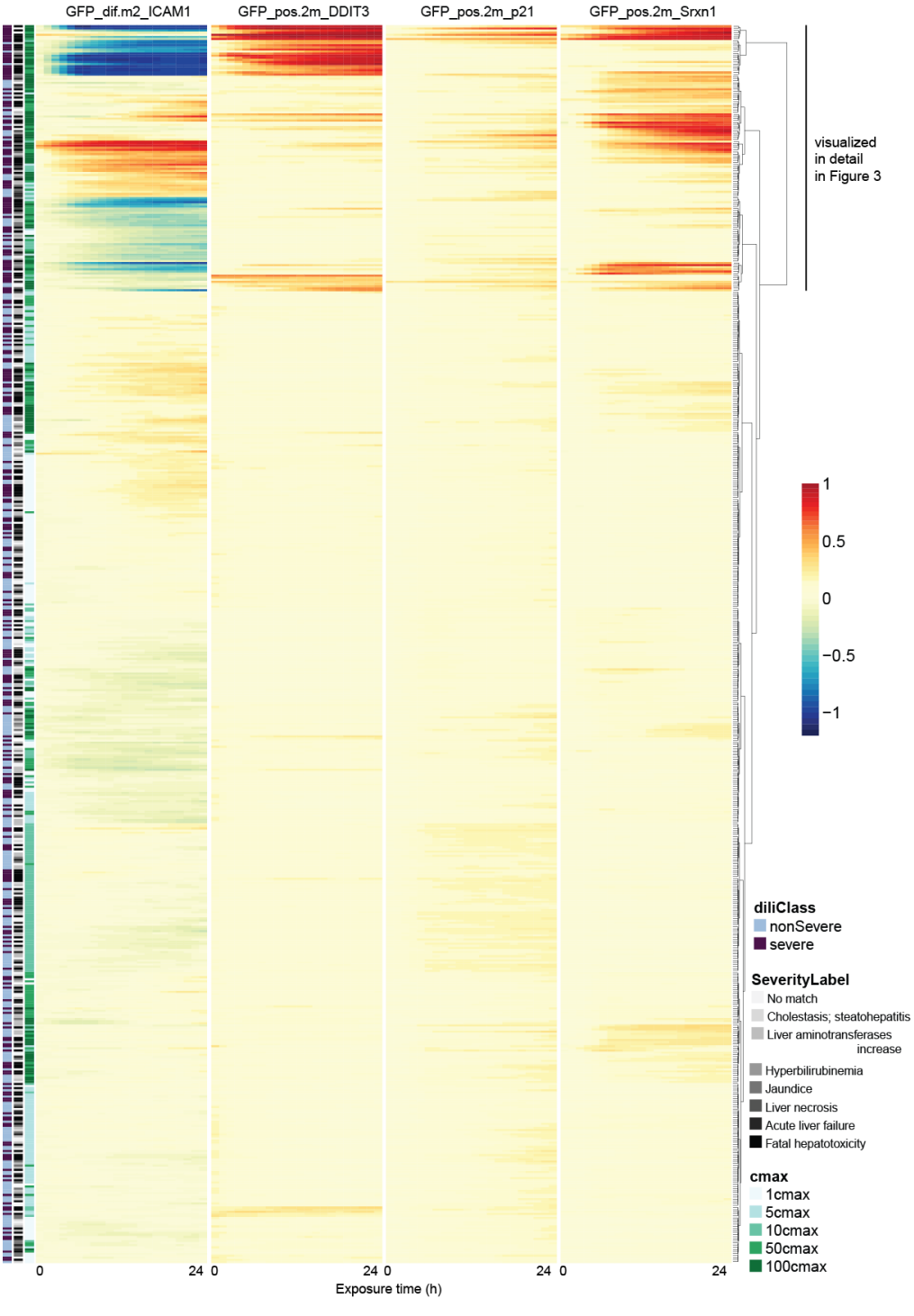

Suppl. Fig. 4: **Hierarchical clustering of time course summarized in a heatmap.** Red depicts an upregulation and blue a downregulation. On the left the severe/non-severe (purple) and the hepatotoxicity class (grey) labeling are indicated as well as the C-max values (green)..

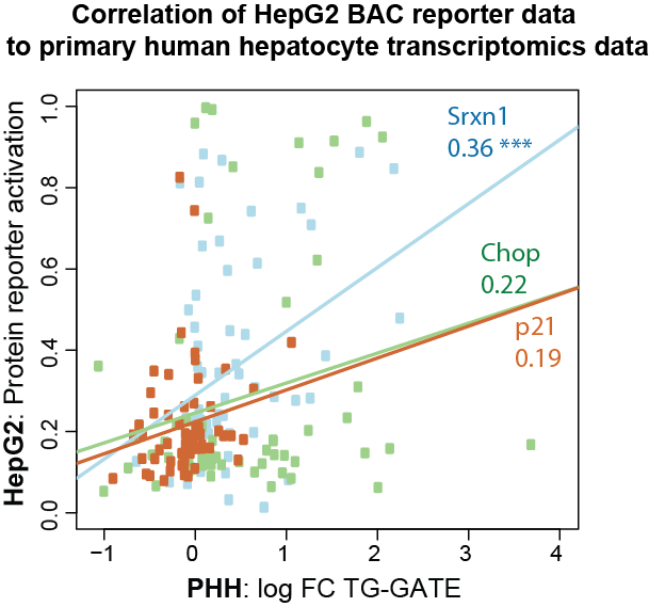

Suppl. Fig. 5: **Correlation of TG GATES primary human hepatocytes transcript levels versus BAC-HepG2 SRXN1-GFP (blue), CHOP-GFP (green) and p21-GFP (red)** BAC-GFP reporter values are plotted against the TG-GATES fold changes, correlation has been depicted next to the graph. Boxed cloud depicts BAC-GFP reporter activated compounds only. Correlation has been calculated using 61 degrees of freedom, *** = pvalue < 0.005.

Chapter 7

Discussion and future perspective

Highlights

- The importance of inflammatory stress on the etiology of drug-induced liver injury is increasingly recognized
- Current *in vitro* models do not capture hepatocyte specific immune signaling
- In this thesis, I report both mechanistic insight into hepatocyte specific immune signaling and application for prediction modeling

Idiosyncratic DILI remains an important problem in drug development and safety assessment, since it is difficult to predict DILI liability. Inflammatory stress is considered as an important host factor involved in DILI[208]. Several *in vivo* and *in vitro* models show that inflammatory stress induced by pathogenic or sterile inflammation decreases the toxicity threshold of certain drugs, as discussed in **Chapter 2**[8,16,41,72]. Toxicity is correlated to TNFα levels for diclofenac/LPS-induced hepatotoxicity, and for trovafloxacin proven to be TNFα and TNFR dependent[11,99]. At this moment, several mechanisms of TNFα-induced cell death in different cell types have been recognized[20]. Also drug-induced cell death mechanisms have been extensively investigated, implicating activation of cellular adaptive stress responses as one of the key events[135]. In this thesis, I focused on drug-induced cellular stress responses and their relation to TNFα-induced hepatotoxicity. The interaction between these cellular stress responses and TNFα signaling has been studied previously, by us and others[15,16,43,345].

Although significant studies on drugs and inflammatory stress have shown that drug/cytokine interaction play an important role in DILI, we do not know how drugs interact with signaling downstream of the TNF receptor complex. Furthermore, it has been suggested that the activation of NF-κB and its target genes play an important role in TNFα-induced cytotoxicity[17,42]. The precise process and role of NF-κB activation in drug/TNF-induced hepatotoxicity is unknown. Moreover, it has been shown that also other TNFα-induced pathways play roles in inducing a synergistic drug/TNF apoptosis, including MAP kinases[14]. Drug/TNFα synergistic toxicity has been detected in both PHHs and HepG2 cultures[16,41,120]. In the studies that are presented in this thesis, we thrived to characterize drug-induced skewed TNFα signaling in HepG2 cells (**Chapter 3-5)**. Furthermore, in **Chapter 6** we used our inflammatory stress reporter in addition to our previously characterized fluorescent reporter platform to predict drug-induced liver injury hazard[44].

TNFα-induced NF-κB signaling

One of the best-characterized results of TNFα stimulation is the nuclear translocation of the RelA subunit of the NF-κB protein family. Previously, our lab has shown that this translocation phenotype can be disrupted by diclofenac pre-exposure[42]. To investigate how this phenotype is induced, we generated a stable CMV-driven RelA-GFP reporter. In **Chapter 3**, we used this reporter cell line for live cellular imaging-based siRNA screening, to determine signaling molecules that are involved in the creation of the typical oscillatory phenotype. We focused mainly on the role of kinases and ubiquitinases, both under control as well as drug-exposed conditions. As expected, we determined that various genes that are involved in ubiquitination processes play an essential role in TNFα-induced NF-κB activation[144]. Intriguingly, many candidate genes that delayed the oscillatory phenotype upon knockdown did not increase the toxicity upon drug exposure only, but decreased the cytotoxic potential of TNFα/diclofenac exposure. This underlines the complex relationship between NF-κB activation and cytotoxicity. We identified knockdown of UFD1L and CDK12 (CRK7) as strong inhibitors of the cytotoxic response and delaying RelA translocation under control and drug exposure conditions. Interestingly, CDK12, but not UFD1L knockdown did

increase the TNFα-induced A20 expression massively. UFD1L had already been described as part of the proteosomal targeting complex of IκBα[182]. However, we show here that UFD1L is not involved in IκBα breakdown in TNFα-stimulated HepG2 cells. This emphasizes the importance of cell type specific experiments and cautions against drawing conclusions based on literature in different cell types. CDK12 is known as RNA pol II kinase that phosphorylates Ser2 on the C-terminal domain, leading to improved elongation of RNA transcripts. Remarkably, CDK12 is specifically involved in the induction of stress-induced gene sets, for example upon oxidative and DNA damage stress[198,199]. Here, we suggest that CDK12 is also involved in NF-κB-mediated transcriptional programs. Whether diclofenac/TNFα cytotoxicity is induced by generally skewed CDK12-mediated gene expression or via specific CDK12-mediated inhibition of A20 expression requires more research. As CDK12 is involved in oxidative stress, inflammatory stress and DNA-damage responses, it is a most promising candidate gene to study in relation to iDILI. Especially since CDK12 knockout/knockdown affects gene transcription efficiency only during stress responses[199], CDK12 polymorphisms could form a genetic basis in which certain individuals could be more sensitive to specific drug-induced stress responses.

As shown in **Chapter 3**, delayed TNFα-induced RelA nuclear translocation is not always associated with increased drug/TNFα cytotoxicity. To determine the physiological effects of drug-delayed RelA responses, we tested compound effects on TNFα-induced RelA translocation, target gene induction and cytotoxicity in **Chapter 4**. The compounds chosen were part of the training compound set defined by IMI MIP-DILI[212], plus carbamazepine, a drug we studied extensively previously[16]. Of these compounds, some delayed TNFα-induced translocation (metformin, nefazodone, diclofenac, tolcapone, troglitazone, carbamazepine), while others did not (acetaminophen, flucloxacillin, pioglitazone and entacapone). To investigate TNFα target gene induction, we chose 45 target genes and determined the effect of drug exposure on their TNFα-induced expression kinetics. In general, drug exposure increased TNFα-induced expression of most target genes, not related to a specific kinetic or functional group of target genes. In addition, this increase was not defined by drug-induced delayed TNFα-induced RelA nuclear translocation.

As expected, TNFα-induced target genes that regulate oxidative stress, including SLC7A11, SOD2 and MAFF, were enhanced upon concurrent drug exposure. However, also proinflammatory cytokine and chemokine signaling target genes, including CCL20, IL8, CXCL3, CSF2, CSF3 and CCL5, were generally increased upon combined drug/TNFα exposure compared to TNFα exposure only. The increased expression of these cytokines could influence nearby liver cell populations, but also hepatocytes in an autocrine feedback loop. While the induction of inflammatory molecules has been studied in several experimental models including KCs and other resident immune cells, the excretion by hepatocytes has not been well characterized. In addition, we determined that expression of transcription regulating proteins including IER3, ELF3 and NFKB2 were increased upon drug exposure. The increased expression of these transcription factors complicates the

overall expected physiological outcome, since the hepatocyte-specific role of these transcription factors is currently not entirely clear[263,346].

In other models, combined drug/inflammatory regulator exposure was often directed at KC activation. Direct co-exposure with drug/LPS of human liver slices generally decreased the overall proinflammatory cytokine secretion[113], which was not entirely similar to the results in mouse liver slices[112]. However, as resident immune cells are present in this model, it is likely that the proinflammatory modulator production is at a different scale compared to hepatocyte only produced cytokines. Indeed, no increased cytokine secretion upon compound-only exposure was detectable in mouse or human slices[112,113], in contrast to our results. In a rat KC study, drug-treated KCs increased proinflammatory gene expression upon LPS stimulation, in contrast to LPS stimulation alone[347]. This is more similar to our result in hepatocytes. However, these contradictory outcomes show that it is difficult to extrapolate results between species and models.

It becomes more and more accepted that also hepatocytes are involved in immune regulation on organ and systemic levels[58]. Mice hepatocyte-specific knockout of A20 seem healthy when unchallenged, whit only slightly increased chronic inflammation levels in the liver. However, when challenged with LPS, LPS-induced NF-κB-dependent responses, including expression of IL6 and CCL2 expression are severely enhanced[192]. Thus, altered hepatocyte NF-κB signaling can enhance liver wide inflammatory responses. Therefore, we anticipate that enhanced TNFα-induced NF-κB target gene expression upon drug exposure as shown in this manuscript, could have severe physiological results.

Drug-induced NF-κB signaling

In **Chapter 4** we show that drug exposure by itself also induces TNFα target gene induction in HepG2 cells. Although this induction is partially regulated by RelB and cREL, the induction of target gene expression mainly depends on RelA expression. Interestingly, IL8 (CXCL8) and CCL5 are well-described chemokines, recruiting macrophages and neutrophils (Fig.1). Macrophage and neutrophil recruitment is considered a key event in the etiology of drug-induced liver injury[116,235]. By our knowledge, the regulation of these target genes by drug-induced activity of the whole NF-κB family in hepatocytes has not been described before.

Here, we show that drug-induced RelB expression is independent of RelA transcriptional activity and is strongly associated, and thus likely induced, by oxidative stress. The role of the non-canonical pathway in liver injury is not well characterized, although key protein MAP3K14 (NIK) activity aggravates (TNFα-mediated) liver injury *in vivo*[348,349]. In addition, inhibition of MAP3K14 decreased oxidative stress generation[349]. Indeed, in **Chapter 5** we show that knockdown of MAP3K14 affects drug/TNFα synergism in a drug-specific way. This effect correlates with drug-induced SRXN1 induction. Intriguingly, intricate connections between the classical (RelA) and alternative (RelB) NF-κB pathways exist, also upon TNFα exposure[21,350]. MAP3K14 activity and RelB are not interacting directly, but via several intermediate signalling proteins. Therefore, these results

do not define whether the effect of MAP3K14 knockdown on drug/ TNFα synergism is related to RelB involvement.

Interestingly, Willy *et al*. did also see a NF-κB target gene induction response upon palmitic acid exposure of HepG2 cells, leading to increased cytotoxicity. The cytotoxicity was dependent on the activation of CHOP via IRAK2, which lead to expression of inflammatory regulators, including IL8 and TNFα itself. While IL8 was mainly involved in macrophage recruitment, the CHOP-mediated secretion of TNFα was essential for palmitic acid cytotoxicity. Importantly, this response was not seen in primary mouse hepatocytes, underlining the species-specific regulation of NF-κB activation[345]. Here, we describe drug-induced regulation of NF-κB target gene induction as well. Although we previously and in this thesis showed that CHOP is activated by several drug exposures[16], we do not anticpate CHOP-mediated cytokine secretion. Our drugs are not cytotoxic upon drug only exposure and could not induce detectable TNFα mRNA expression upon drug exposure (data not shown). Therefore, we assume that there is no TNFα excretion by our HepG2 cells upon exposure of drugs alone. However, we anticipate that the increased secretion of inflammatory regulators as we have detected, demonstrate a subtle modulation of the inflammatory response upon drug exposure *in vivo*.

Drug/TNFα-induced cytotoxicity

Already a decade ago, the groups of Roth and Ganey were one of the first to describe synergistic responses in rodents upon low doses drug and LPS[8,72]. Since then, they and others have developed several models to detect inflammatory stress and drug synergistic hepatotoxicity. Roth and colleagues have also demonstrated that TNFα is an essential cytokine in the LPS/drug-induced liver injury *in vivo*[11]. We and others have shown that HepG2 cells also show TNFα/drug synergistic cell death[42,120]. This synergistic cell death is dependent on CHOP expression, MAPK function and the regulation of general protein translation machinery components[14,16]. However, it is still unknown how TNFα stimulation can interact with drug-induced cellular stress responses to increase cytotoxicity. In this thesis we studied both regulators of TNFα-induced RelA nuclear translocation in **Chapter 3** and regulators TNFα/drug synergism in **Chapter 5**. Synergistic cell death seems not strictly correlated with a delayed RelA translocation phenotype, as knockdown of candidate genes can both delay TNFα-induced RelA translocation and inhibit cytotoxicity. Therefore, in **Chapter 5**, we studied several candidate genes that affected TNFα/drug synergistic toxicity with different drug exposures. We detected both generic and compound specific characteristics of the candidate gene effects. Strong generic TNFα/drug synergistic toxicity regulators (A20 and PHF5A) increased cytotoxicity upon knockdown. This knowledge could be used in the development of sensitive safety testing approaches to detect inflammatory cytotoxicity.

The correlation between candidate gene effects under diclofenac and valproic acid exposure suggests a similar mechanism of TNFα toxicity. However, the compound-induced stress responses show stark differences. In conclusion, there must be other, yet unknown,

mechanisms involved in both valproic acid and diclofenac toxicity that synergize with TNFα signaling and affect our candidate gene function.

The effect of candidate gene knockdown on drug/TNFα toxicity was correlated to the drug-induced onset of several stress responses. This effect was most strongly seen with two separate branches of oxidative stress and the DNA damage response (SRXN1/P21 and HMOX1/BTG2). Both branches of these stress responses interact with TNFα and NF-κB signaling differently, according to literature[19,121,351]. Remarkably, both the oxidative stress and DNA damage response are related to target gene expression regulated by candidate gene CDK12 (CRK7)[198,199].

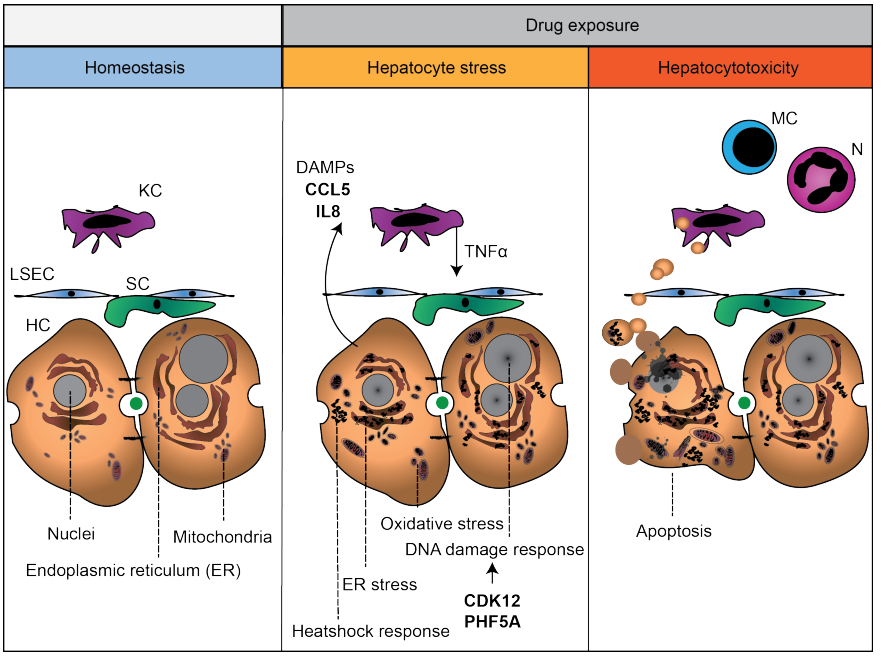

Fig. 1: Overview of drug-induced mechanisms Hepatocytes exposed to drugs induce several responses. In the first panel, hepatocytes are in homeostasis. In the second panel, drugs induce the activation of cellular stress responses. This includes swollen or perturbed mitochondria, increased levels of unfolded/misfolded proteins inside and outside of the endoplasmic reticulum and DNA damage occurring. CDK12 and PHF5A start elongating mRNA transcripts of specific stress-related target genes. The hepatocytes start producing damage associated molecular patterns (DAMPs) and chemokines, including CCL5 and IL8 (as described in this thesis). The DAMPs activate the Kupffer cell, which start to produce high amounts of proinflammatory cytokines, including TNFα. The chemokines start attracting immune cells, including monocytes and neutrophils. In the last panel, the TNFα in combination with the drug-induced responses has led to increased levels of hepatocyte apoptosis. Specific cell types and responses are indicated. KC is Kupffer cell, LSEC is liver sinusoidal endothelial cell, SC is stellate cell, HC is hepatocyte. DAMPs are damage associated molecular patterns. MC is monocyte, N is neutrophil.

This protein function of CDK12 is similar to the RNA pol II Ser2 kinase function of PHF5A, the strongest generic regulator of drug/TNFα toxicity in our study. We determined that the drug/TNFα toxicity effect of both kinases correlated strongly with the SRXN1/P21 branch of stress responses. We anticipate that both CDK12 and PHF5A are essential regulators of drug/TNFα toxicity in hepatocytes and control specific stress-induced transcription programs (Fig.1).

Assessing TNFα signaling in toxicity screening approaches

As discussed in **Chapter 2**, screening approaches that involve addition of TNFα can add valuable information for safety assessment. In **Chapter 6**, we applied a high throughput approach in which we used the previously described BAC-GFP HepG2 reporter platform[44], complemented with the ICAM1-GFP cell line and manual addition of TNFα. Addition of the TNFα-treated ICAM1 reporter increased the mechanistic and predictive power of our stress response reporter platform. The effects of drug exposure on TNFα-induced ICAM1 expression reflects some of the distortion of the inflammatory stress response in hepatocytes by the drug *in vivo*. Clusters of compounds that decrease or increase TNFα-induced ICAM1 expression concurrent with SRXN1 and/or CHOP expression indicate diverse toxicity mechanisms. Furthermore, we show that severe DILI compounds did in general increase adaptive stress responses at a lower exposure concentration than non-severe DILI compounds. Time dynamic, single cell features were distracted for support vector machine-based prediction of liver injury liability. To our best knowledge, this is the first time that high density dynamic temporal data for actual toxicity screening and prediction approaches is used. We anticipate that the detection of more adaptive stress responses, tested with and without inflammatory mediators, will increase the predictive power during *in vitro* safety assessment approaches.

As described in **Chapter 5**, separate branches of individual adaptive stress response pathway correlated strongly with the effects of individual candidate gene knockdowns on drug/TNFα synergism. Therefore, we anticipate that the inclusion of more reporters of the same stress response pathways also improves predictive power. Furthermore we recommend the optimization of the cellular model, for instance by 3D culture, co-culture or the use of stem-cell derived hepatocytes/primary human hepatocytes. To improve the detection of drug-induced immune-related toxicity, culture methods of all of these models should be adjusted to improve the resemblance to liver immunotolerant environment[1]. Furthermore, we anticipate that including hepatocyte-produced pro- and anti-inflammatory factors detection methods in early drug discovery toxicity screening increases the predictive power of *in vitro* safety assessment.

Conclusion and future perspectives

In this thesis I describe the drug-induced perturbations of TNFα signaling in HepG2 cells. The findings in this thesis report several novel processes and candidate genes that were not previously implicated in drug-induced liver injury (some are summarized in Fig. 1). Overall, the importance of inflammatory stress and its detection in

drug toxicity screens for safety assessment is emphasized. The findings in this thesis can be used to develop better predictive models for drug toxicity in early drug development. Furthermore, the knowledge that specific genes are involved in drug/TNFα interactions may, in the end, lead to more specific prescription practice in a personalized medicine approach.

The HepG2 cell line is still one of the most widely used *in vitro* methods in predictive toxicology to test hepatocyte toxicity. The detection of inflammation-induced drug hepatotoxicity is usually not incorporated in the early *in vitro* studies and only detected in animal studies. To lower animal burden and increase early detection of drug-interaction with inflammatory stress signaling pathways, we hypothesized in this thesis that HepG2 cells could be used as an adequate model to study inflammatory stress and drug toxicity. The outcome of these studies show that HepG2 cells are able to reflect many inflammatory signaling characteristics and can be used in predictive screening approaches.

The development of both inflammatory hepatocyte-only and co-culture models would increase our knowledge on inflammatory signaling in the liver substantially. Although primary hepatocytes are currently unsuitable for studying inflammatory signaling[37], evolving isolation and culture methods could increase the usability of this cell type. Furthermore, the development of induced pluripotent stem cells holds the most promising possibilities in the future, for both toxicity testing and personalized medicine strategies. This thesis contributes to the development of inflammatory stress models in the current, but also future testing approaches and clinical practice.

Appendix

References
Abbreviations
Nederlandse samenvatting
List of publications
About the author

References

1. Godoy, P. *et al.* Recent advances in 2D and 3D in vitro systems using primary hepatocytes, alternative hepatocyte sources and non-parenchymal liver cells and their use in investigating mechanisms of hepatotoxicity, cell signaling and ADME. *Arch Toxicol* **87,** 1315–1530 (2013).
2. LeCluyse, E. L., Witek, R. P., Andersen, M. E. & Powers, M. J. Organotypic liver culture models: meeting current challenges in toxicity testing. *Crit. Rev. Toxicol.* **42,** 501–48 (2012).
3. Weiskirchen, R. & Tacke, F. Cellular and molecular functions of hepatic stellate cells in inflammatory responses and liver immunology. *Hepatobiliary Surg Nutr* **3,** 344–363 (2014).
4. Knolle, P. A. & Wohlleber, D. Immunological functions of liver sinusoidal endothelial cells. *Cell. Mol. Immunol.* (2016). doi:10.1038/cmi.2016.5
5. Nguyen-Lefebvre, A. T. & Horuzsko, A. Kupffer Cell Metabolism and Function. *J Enzym. Metab* **1,** (2015).
6. Knolle, P. A. Staying local-antigen presentation in the liver. *Curr Opin Immunol* **40,** 36–42 (2016).
7. Roth, A. D. & Lee, M.-Y. Idiosyncratic drug-induced liver injury (IDILI): Mechanisms and predictive assays. *Biomed. Res. Int.* **2017,** In Press (2016).
8. Deng, X. *et al.* Modest inflammation enhances diclofenac hepatotoxicity in rats: role of neutrophils and bacterial translocation. *J. Pharmacol. Exp. Ther.* **319,** 1191–1199 (2006).
9. Zou, W. *et al.* Sulindac metabolism and synergy with tumor necrosis factor-alpha in a drug-inflammation interaction model of idiosyncratic liver injury. *J. Pharmacol. Exp. Ther.* **331,** 114–121 (2009).
10. Shaw, P. J. *et al.* Trovafloxacin enhances TNF-induced inflammatory stress and cell death signaling and reduces TNF clearance in a murine model of idiosyncratic hepatotoxicity. *Toxicol. Sci.* **111,** 288–301 (2009).
11. Shaw, P. J., Ganey, P. E. & Roth, R. A. Tumor necrosis factor alpha is a proximal mediator of synergistic hepatotoxicity from trovafloxacin/lipopolysaccharide coexposure. *J. Pharmacol. Exp. Ther.* **328,** 62–68 (2009).
12. Kegel, V. *et al.* Subtoxic Concentrations of Hepatotoxic Drugs Lead to Kupffer Cell Activation in a Human In Vitro Liver Model: An Approach to Study DILI. *Mediat. Inflamm* **2015,** 640631 (2015).
13. Brenner, C., Galluzzi, L., Kepp, O. & Kroemer, G. Decoding cell death signals in liver inflammation. *J. Hepatol.* **59,** 583–594 (2013).
14. Maiuri, A. R. *et al.* Cytotoxic Synergy Between Cytokines and NSAIDs Associated With Idiosyncratic Hepatotoxicity Is Driven by Mitogen-Activated Protein Kinases. *Toxicol. Sci.* **146,** 265–280 (2015).
15. Maiuri, A. R., Breier, A. B., Turkus, J. D., Ganey, P. E. & Roth, R. A. Calcium Contributes to the Cytotoxic Interaction Between Diclofenac and Cytokines. *Toxicol. Sci.* **149,** 372–384 (2016).
16. Fredriksson, L. *et al.* Drug-induced endoplasmic reticulum and oxidative stress responses independently sensitize toward TNFalpha-mediated hepatotoxicity. *Toxicol. Sci.* **140,** 144–159 (2014).
17. Liu, H., Lo, C. R. & Czaja, M. J. NF-??B inhibition sensitizes hepatocytes to TNF-induced apoptosis through a sustained activation of JNK and c-Jun. *Hepatology* **35,** 772–778 (2002).
18. Kamata, H. *et al.* Reactive oxygen species promote TNF??-induced death and sustained JNK activation by inhibiting MAP kinase phosphatases. *Cell* **120,** 649–661 (2005).
19. Blaser, H., Dostert, C., Mak, T. W. & Brenner, D. TNF and ROS Crosstalk in Inflammation. *Trends Cell Biol.* **26,** 249–261 (2016).
20. Brenner, D., Blaser, H. & Mak, T. W. Regulation of tumour necrosis factor signalling: live or let die. *Nat Rev Immunol* **15,** 362–374 (2015).
21. Cildir, G., Low, K. C. & Tergaonkar, V. Noncanonical NF-??B Signaling in Health and Disease. *Trends Mol. Med.* **22,** 414–429 (2016).
22. Smale, S. T. Dimer-specific regulatory mechanisms within the NF-kappaB family of transcription factors. *Immunol. Rev.* **246,** 193–204 (2012).
23. Hoffmann, A., Levchenko, A., Scott, M. L. & Baltimore, D. The IkappaB-NF-kappaB signaling module: temporal control and selective gene activation. *Science (80-.).* **298,** 1241–1245 (2002).
24. Werner, S. L. *et al.* Encoding NF-kappaB temporal control in response to TNF: distinct roles for the negative regulators IkappaBalpha and A20. *Genes Dev.* **22,** 2093–2101 (2008).
25. Nelson, D. E. *et al.* Oscillations in NF-kappaB signaling control the dynamics of gene expression. *Science (80-.).* **306,** 704–708 (2004).
26. Ashall, L. *et al.* Pulsatile stimulation determines timing and specificity of NF-kappaB-dependent transcription. *Science (80-.).* **324,** 242–246 (2009).
27. Zambrano, S., De Toma, I., Piffer, A., Bianchi, M. E. & Agresti, A. NF-kappaB oscillations translate into functionally related patterns of gene expression. *Elife* **5,** e09100 (2016).
28. Tian, B., Nowak, D. E. & Brasier, A. R. A TNF-induced gene expression program under oscillatory NF-kappaB control. *BMC Genomics* **6,** 137 (2005).
29. Courtois, G. & Gilmore, T. D. Mutations in the NF-kappaB signaling pathway: implications for human disease. *Oncogene* **25,** 6831–6843 (2006).
30. Lin, C. & Khetani, S. R. Advances in Engineered Liver Models for Investigating Drug-Induced Liver Injury. *Biomed Res. Int.* **2016,** (2016).
31. Rose, K. A., Holman, N. S., Green, A. M., Andersen, M. E. & Lecluyse, E. L. Co-culture of Hepatocytes and Kupffer Cells as an in Vitro Model of Inflammation and Drug-Induced Hepatotoxicity. *J. Pharm. Sci.* **105,** 950–964 (2016).
32. Nguyen, T. V *et al.* Establishment of a hepatocyte-kupffer cell coculture model for assessment of proinflammatory cytokine effects on metabolizing enzymes and drug transporters. *Drug Metab. Dispos.* **43,** 774–785 (2015).

33. Beggs, K. M., Fullerton, A. M., Miyakawa, K., Ganey, P. E. & Roth, R. A. Molecular mechanisms of hepatocellular apoptosis induced by trovafloxacin-tumor necrosis factor-alpha interaction. *Toxicol. Sci.* **137,** 91–101 (2014).
34. Zhang, L. *et al.* TRAF2 exerts opposing effects on basal and TNFα-induced activation of the classic IKK complex in hematopoietic cells in mice. *J. Cell Sci.* **129,** 1455–1467 (2016).
35. Wewering, F. *et al.* Characterization of chemical-induced sterile inflammation in vitro: application of the model compound ketoconazole in a human hepatic co-culture system. *Arch Toxicol* (2016). doi:10.1007/s00204-016-1686-y
36. Sison-Young, R. L. *et al.* Comparative Proteomic Characterization of 4 Human Liver-Derived Single Cell Culture Models Reveals Significant Variation in the Capacity for Drug Disposition, Bioactivation, and Detoxication. *Toxicol. Sci.* **147,** 412–424 (2015).
37. Godoy, P. *et al.* Gene network activity in cultivated primary hepatocytes is highly similar to diseased mammalian liver tissue. *Arch. Toxicol.* **90,** 2513–2529 (2016).
38. Jigorel, E., Le Vee, M., Boursier-Neyret, C., Parmentier, Y. & Fardel, O. Differential regulation of sinusoidal and canalicular hepatic drug transporter expression by xenobiotics activating drug-sensing receptors in primary human hepatocytes. *Drug Metab. Dispos.* **34,** 1756–1763 (2006).
39. Hewitt, N. J. & Hewitt, P. Phase I and II enzyme characterization of two sources of HepG2 cell lines. *Xenobiotica.* **34,** 243–256 (2004).
40. Sison-Young, R. L. *et al.* A multicenter assessment of single-cell models aligned to standard measures of cell health for prediction of acute hepatotoxicity. *Arch. Toxicol.* **91,** 1–16 (2016).
41. Cosgrove, B. D. *et al.* Synergistic drug-cytokine induction of hepatocellular death as an in vitro approach for the study of inflammation-associated idiosyncratic drug hepatotoxicity. *Toxicol. Appl. Pharmacol.* **237,** 317–330 (2009).
42. Fredriksson, L. *et al.* Diclofenac inhibits tumor necrosis factor-alpha-induced nuclear factor-kappaB activation causing synergistic hepatocyte apoptosis. *Hepatology* **53,** 2027–2041 (2011).
43. Herpers, B. *et al.* Activation of the Nrf2 response by intrinsic hepatotoxic drugs correlates with suppression of NF-kappaB activation and sensitizes toward TNFalpha-induced cytotoxicity. *Arch Toxicol* **90,** 1163–1179 (2016).
44. Wink, S., Hiemstra, S., Herpers, B. & van de Water, B. High-content imaging-based BAC-GFP toxicity pathway reporters to assess chemical adversity liabilities. *Arch. Toxicol.* 1–17 (2016). doi:10.1007/s00204-016-1781-0
45. Reuben, A., Koch, D. G. & Lee, W. M. Drug-induced acute liver failure: results of a U.S. multicenter, prospective study. *Hepatology* **52,** 2065–2076 (2010).
46. Bjornsson, E. S., Bergmann, O. M., Bjornsson, H. K., Kvaran, R. B. & Olafsson, S. Incidence, presentation, and outcomes in patients with drug-induced liver injury in the general population of Iceland. *Gastroenterology* **144,** 1419–25, 1425-3-20 (2013).
47. Senior, J. R. Evolution of the Food and Drug Administration approach to liver safety assessment for new drugs: current status and challenges. *Drug Saf.* **37 Suppl 1,** S9-17 (2014).
48. Gregory, B., Larson, A. M., Reisch, J., Lee, W. M. & Acute Liver Failure Study, G. Acetaminophen dose does not predict outcome in acetaminophen-induced acute liver failure. *J Investig Med* **58,** 707–710 (2010).
49. Larson, A. M. *et al.* Acetaminophen-induced acute liver failure: results of a United States multicenter, prospective study. *Hepatology* **42,** 1364–1372 (2005).
50. Lee, W. M. Drug-induced acute liver failure. *Clin Liver Dis* **17,** 575–86, viii (2013).
51. Björnsson, E. S. Epidemiology and Risk Factors for Idiosyncratic Drug-Induced Liver Injury. *Semin Liver Dis* **34,** 115–122 (2014).
52. Kim, S. H. & Naisbitt, D. J. Update on Advances in Research on Idiosyncratic Drug-Induced Liver Injury. *Allergy Asthma Immunol Res* **8,** 3–11 (2016).
53. Yip, V. L., Alfirevic, A. & Pirmohamed, M. Genetics of immune-mediated adverse drug reactions: a comprehensive and clinical review. *Clin Rev Allergy Immunol* **48,** 165–175 (2015).
54. Giefing-Kroll, C., Berger, P., Lepperdinger, G. & Grubeck-Loebenstein, B. How sex and age affect immune responses, susceptibility to infections, and response to vaccination. *Aging Cell* **14,** 309–321 (2015).
55. Cho, J. *et al.* Sex bias in experimental immune-mediated, drug-induced liver injury in BALB/c mice: suggested roles for Tregs, estrogen, and IL-6. *PLoS One* **8,** e61186 (2013).
56. Takamoto, S., Nakamura, K., Yoneda, M. & Makino, I. Gender-related differences in concanavalin A-induced liver injury and cytokine production in mice. *Hepatol Res* **27,** 221–229 (2003).
57. Tian, Z., Chen, Y. & Gao, B. Natural killer cells in liver disease. *Hepatology* **57,** 1654–1662 (2013).
58. Crispe, I. N. Hepatocytes as Immunological Agents. *J. Immunol.* **196,** 17–21 (2016).
59. Dara, L., Liu, Z. X. & Kaplowitz, N. Mechanisms of adaptation and progression in idiosyncratic drug induced liver injury, clinical implications. *Liver Int* **36,** 158–165 (2016).
60. Crispe, I. N. Immune tolerance in liver disease. *Hepatology* **60,** 2109–2117 (2014).
61. Soares, J. B., Pimentel-Nunes, P., Roncon-Albuquerque, R. & Leite-Moreira, A. The role of lipopolysaccharide/toll-like receptor 4 signaling in chronic liver diseases. *Hepatol Int* **4,** 659–672 (2010).
62. Nakamoto, N. & Kanai, T. Role of toll-like receptors in immune activation and tolerance in the liver. *Front Immunol* **5,** 221 (2014).
63. Liu, Z. J. *et al.* Up-regulation of IRAK-M is essential for endotoxin tolerance induced by a low dose of lipopolysaccharide in Kupffer cells. *J. Surg. Res.* **150,** 34–39 (2008).
64. Uhrig, A. *et al.* Development and functional consequences of LPS tolerance in sinusoidal endothelial cells of the liver. *J. Leukoc. Biol.* **77,** 626–633 (2005).
65. Carotti, S., Guarino, M. P., Vespasiani-Gentilucci, U. & Morini, S. Starring role of toll-like receptor-4

activation in the gut-liver axis. *World J Gastrointest Pathophysiol* **6,** 99–109 (2015).
66. Zhang, S. *et al.* Pretreatment of lipopolysaccharide (LPS) ameliorates D-GalN/LPS induced acute liver failure through TLR4 signaling pathway. *Int J Clin Exp Pathol* **7,** 6626–6634 (2014).
67. Sano, T. *et al.* Protective effect of lipopolysaccharide preconditioning in hepatic ischaemia reperfusion injury. *HPB* **12,** 538–545 (2010).
68. Sharifnia, T. *et al.* Hepatic TLR4 signaling in obese NAFLD. *Am J Physiol Gastrointest Liver Physiol* **309,** G270-8 (2015).
69. Bjornsson, E. S. Hepatotoxicity by Drugs: The Most Common Implicated Agents. *Int J Mol Sci* **17,** (2016).
70. Knoop, K. A., McDonald, K. G., Kulkarni, D. H. & Newberry, R. D. Antibiotics promote inflammation through the translocation of native commensal colonic bacteria. *Gut* **65,** 1100–1109 (2016).
71. Lu, J., Jones, A. D., Harkema, J. R., Roth, R. A. & Ganey, P. E. Amiodarone exposure during modest inflammation induces idiosyncrasy-like liver injury in rats: role of tumor necrosis factor-alpha. *Toxicol. Sci.* **125,** 126–133 (2012).
72. Shaw, P. J., Hopfensperger, M. J., Ganey, P. E. & Roth, R. A. Lipopolysaccharide and trovafloxacin coexposure in mice causes idiosyncrasy-like liver injury dependent on tumor necrosis factor-alpha. *Toxicol. Sci.* **100,** 259–266 (2007).
73. Buchweitz, J. P., Ganey, P. E., Bursian, S. J. & Roth, R. A. Underlying endotoxemia augments toxic responses to chlorpromazine: is there a relationship to drug idiosyncrasy? *J. Pharmacol. Exp. Ther.* **300,** 460–467 (2002).
74. Bikhazi, A. B. *et al.* Kinetics of lipopolysaccharide clearance by Kupffer and parenchyma cells in perfused rat liver. *Comp Biochem Physiol C Toxicol Pharmacol* **129,** 339–348 (2001).
75. Mimura, Y., Sakisaka, S., Harada, M., Sata, M. & Tanikawa, K. Role of hepatocytes in direct clearance of lipopolysaccharide in rats. *Gastroenterology* **109,** 1969–1976 (1995).
76. Fox, E. S., Thomas, P. & Broitman, S. A. Comparative studies of endotoxin uptake by isolated rat Kupffer and peritoneal cells. *Infect Immun* **55,** 2962–2966 (1987).
77. Scott, M. J. & Billiar, T. R. Beta2-integrin-induced p38 MAPK activation is a key mediator in the CD14/TLR4/MD2-dependent uptake of lipopolysaccharide by hepatocytes. *J. Biol. Chem.* **283,** 29433–29446 (2008).
78. Chen, C. *et al.* Lipopolysaccharide stimulates p62-dependent autophagy-like aggregate clearance in hepatocytes. *Biomed Res Int* **2014,** 267350 (2014).
79. Liu, S. *et al.* Role of toll-like receptors in changes in gene expression and NF-kappa B activation in mouse hepatocytes stimulated with lipopolysaccharide. *Infect Immun* **70,** 3433–3442 (2002).
80. Saad, B., Frei, K., Scholl, F. A., Fontana, A. & Maier, P. Hepatocyte-derived interleukin-6 and tumor-necrosis factor alpha mediate the lipopolysaccharide-induced acute-phase response and nitric oxide release by cultured rat hepatocytes. *Eur J Biochem* **229,** 349–355 (1995).
81. Shedlofsky, S. I., Israel, B. C., McClain, C. J., Hill, D. B. & Blouin, R. A. Endotoxin administration to humans inhibits hepatic cytochrome P450-mediated drug metabolism. *J Clin Invest* **94,** 2209–2214 (1994).
82. Aitken, A. E., Richardson, T. A. & Morgan, E. T. Regulation of drug-metabolizing enzymes and transporters in inflammation. *Annu Rev Pharmacol Toxicol* **46,** 123–149 (2006).
83. Christmas, P. Role of Cytochrome P450s in Inflammation. *Adv Pharmacol* **74,** 163–192 (2015).
84. Deng, M. *et al.* Lipopolysaccharide clearance, bacterial clearance, and systemic inflammatory responses are regulated by cell type-specific functions of TLR4 during sepsis. *J. Immunol.* **190,** 5152–5160 (2013).
85. Tsung, A. *et al.* The nuclear factor HMGB1 mediates hepatic injury after murine liver ischemia-reperfusion. *J. Exp. Med.* **201,** 1135–1143 (2005).
86. Izuishi, K. *et al.* Cutting edge: high-mobility group box 1 preconditioning protects against liver ischemia-reperfusion injury. *J. Immunol.* **176,** 7154–7158 (2006).
87. Nace, G. W. *et al.* Cellular-specific role of toll-like receptor 4 in hepatic ischemia-reperfusion injury in mice. *Hepatology* **58,** 374–387 (2013).
88. Kopydlowski, K. M. *et al.* Regulation of macrophage chemokine expression by lipopolysaccharide in vitro and in vivo. *J. Immunol.* **163,** 1537–1544 (1999).
89. Hoshino, K. *et al.* Cutting edge: Toll-like receptor 4 (TLR4)-deficient mice are hyporesponsive to lipopolysaccharide: evidence for TLR4 as the Lps gene product. *J. Immunol.* **162,** 3749–3752 (1999).
90. Peters, T., Karck, U. & Decker, K. Interdependence of tumor necrosis factor, prostaglandin E2, and protein synthesis in lipopolysaccharide-exposed rat Kupffer cells. *Eur J Biochem* **191,** 583–589 (1990).
91. Jaeschke, H., Williams, C. D., Ramachandran, A. & Bajt, M. L. Acetaminophen hepatotoxicity and repair: the role of sterile inflammation and innate immunity. *Liver Int* **32,** 8–20 (2012).
92. Mao, S. A., Glorioso, J. M. & Nyberg, S. L. Liver regeneration. *Transl Res* **163,** 352–362 (2014).
93. Aithal, G. P. & Day, C. P. Nonsteroidal anti-inflammatory drug-induced hepatotoxicity. *Clin Liver Dis* **11,** 563–75, vi–vii (2007).
94. Schmeltzer, P. A. *et al.* Liver injury from nonsteroidal anti-inflammatory drugs in the United States. *Liver Int* **36,** 603–609 (2016).
95. Banks, A. T., Zimmerman, H. J., Ishak, K. G. & Harter, J. G. Diclofenac-associated hepatotoxicity: analysis of 180 cases reported to the Food and Drug Administration as adverse reactions. *Hepatology* **22,** 820–827 (1995).
96. Daly, A. K. *et al.* Genetic susceptibility to diclofenac-induced hepatotoxicity: contribution of UGT2B7, CYP2C8, and ABCC2 genotypes. *Gastroenterology* **132,** 272–281 (2007).
97. de Abajo, F. J., Montero, D., Madurga, M. & Garcia Rodriguez, L. A. Acute and clinically relevant drug-induced liver injury: a population based case-control study. *Br J Clin Pharmacol* **58,** 71–80 (2004).
98. Al-Attrache, H. *et al.* Differential sensitivity of metabolically competent and non-competent HepaRG cells to

apoptosis induced by diclofenac combined or not with TNF-alpha. *Toxicol. Lett.* **258,** 71–86 (2016).
99. Ramm, S. & Mally, A. Role of drug-independent stress factors in liver injury associated with diclofenac intake. *Toxicology* **312C,** 83–96 (2013).
100. Hammond, T. G. *et al.* Mass spectrometric characterization of circulating covalent protein adducts derived from a drug acyl glucuronide metabolite: multiple albumin adductions in diclofenac patients. *J. Pharmacol. Exp. Ther.* **350,** 387–402 (2014).
101. Zhang, Y. *et al.* Diclofenac and Its Acyl Glucuronide: Determination of In Vivo Exposure in Human Subjects and Characterization as Human Drug Transporter Substrates In Vitro. *Drug Metab. Dispos.* **44,** 320–328 (2016).
102. Aithal, G. P. *et al.* Hepatic adducts, circulating antibodies, and cytokine polymorphisms in patients with diclofenac hepatotoxicity. *Hepatology* **39,** 1430–1440 (2004).
103. Wu, Y., Farrell, J., Pirmohamed, M., Park, B. K. & Naisbitt, D. J. Generation and characterization of antigen-specific CD4+, CD8+, and CD4+CD8+ T-cell clones from patients with carbamazepine hypersensitivity. *J Allergy Clin Immunol* **119,** 973–981 (2007).
104. Berson, A. *et al.* Possible role of HLA in hepatotoxicity. An exploratory study in 71 patients with drug-induced idiosyncratic hepatitis. *J. Hepatol.* **20,** 336–342 (1994).
105. Pirmohamed, M., Naisbitt, D. J., Gordon, F. & Park, B. K. The danger hypothesis--potential role in idiosyncratic drug reactions. *Toxicology* **181–182,** 55–63 (2002).
106. Curtsinger, J. M., Johnson, C. M. & Mescher, M. F. CD8 T cell clonal expansion and development of effector function require prolonged exposure to antigen, costimulation, and signal 3 cytokine. *J. Immunol.* **171,** 5165–5171 (2003).
107. Foureau, D. M. *et al.* Comparative analysis of portal hepatic infiltrating leucocytes in acute drug-induced liver injury, idiopathic autoimmune and viral hepatitis. *Clin Exp Immunol* **180,** 40–51 (2015).
108. Metushi, I. G., Hayes, M. A. & Uetrecht, J. Treatment of PD-1 mice with amodiaquine and anti-CTLA4 leads to liver injury similar to idiosyncratic liver injury in patients. *Hepatology* (2014). doi:10.1002/hep.27549
109. Metushi, I. G. *et al.* Development of a novel mouse model of amodiaquine-induced liver injury with a delayed onset. *J Immunotoxicol* **12,** 1–14 (2014).
110. Deng, X. *et al.* Gene expression profiles in livers from diclofenac-treated rats reveal intestinal bacteria-dependent and -independent pathways associated with liver injury. *J. Pharmacol. Exp. Ther.* **327,** 634–644 (2008).
111. Ramm, S. *et al.* Application of a discovery to targeted LC-MS proteomics approach to identify deregulated proteins associated with idiosyncratic liver toxicity in a rat model of LPS/diclofenac co-administration. *Toxicology* **331,** 100–111 (2015).
112. Hadi, M., Chen, Y., Starokozhko, V., Merema, M. T. & Groothuis, G. M. Mouse precision-cut liver slices as an ex vivo model to study idiosyncratic drug-induced liver injury. *Chem Res Toxicol* **25,** 1938–1947 (2012).
113. Hadi, M. *et al.* Human precision-cut liver slices as an ex vivo model to study idiosyncratic drug-induced liver injury. *Chem Res Toxicol* **26,** 710–720 (2013).
114. Wu, J. *et al.* Toll-like receptor-induced innate immune responses in non-parenchymal liver cells are cell type-specific. *Immunology* **129,** 363–374 (2010).
115. Fisher, J. E. *et al.* Role of Kupffer cells and toll-like receptor 4 in acetaminophen-induced acute liver failure. *J. Surg. Res.* **180,** 147–155 (2013).
116. Krenkel, O., Mossanen, J. C. & Tacke, F. Immune mechanisms in acetaminophen-induced acute liver failure. *Hepatobiliary Surg Nutr* **3,** 331–343 (2014).
117. Wallach, D. The cybernetics of TNF: Old views and newer ones. *Semin Cell Dev Biol* **50,** 105–114 (2016).
118. Wu, F. L. *et al.* Targeting endoplasmic reticulum stress in liver disease. *Expert Rev Gastroenterol Hepatol* (2016). doi:10.1080/17474124.2016.1179575
119. Xiu, F., Catapano, M., Diao, L., Stanojcic, M. & Jeschke, M. G. Prolonged Endoplasmic Reticulum-Stressed Hepatocytes Drive an Alternative Macrophage Polarization. *Shock* **44,** 44–51 (2015).
120. Beggs, K. M. *et al.* Trovafloxacin-induced replication stress sensitizes HepG2 cells to tumor necrosis factor-alpha-induced cytotoxicity mediated by extracellular signal-regulated kinase and ataxia telangiectasia and Rad3-related. *Toxicology* **331,** 35–46 (2015).
121. Muralidharan, S. & Mandrekar, P. Cellular stress response and innate immune signaling: integrating pathways in host defense and inflammation. *J. Leukoc. Biol.* **94,** 1167–1184 (2013).
122. Gomez-Lechon, M. J., Tolosa, L. & Donato, M. T. Metabolic activation and drug-induced liver injury: in vitro approaches for the safety risk assessment of new drugs. *J Appl Toxicol* (2015). doi:10.1002/jat.3277
123. Jiang, J., Wolters, J. E., van Breda, S. G., Kleinjans, J. C. & de Kok, T. M. Development of novel tools for the in vitro investigation of drug-induced liver injury. *Expert Opin Drug Metab Toxicol* **11,** 1523–1537 (2015).
124. Andersson, T. B., Kanebratt, K. P. & Kenna, J. G. The HepaRG cell line: a unique in vitro tool for understanding drug metabolism and toxicology in human. *Expert Opin Drug Metab Toxicol* **8,** 909–920 (2012).
125. Jetten, M. J., Kleinjans, J. C., Claessen, S. M., Chesne, C. & van Delft, J. H. Baseline and genotoxic compound induced gene expression profiles in HepG2 and HepaRG compared to primary human hepatocytes. *Toxicol Vitr.* **27,** 2031–2040 (2013).
126. Hart, S. N. *et al.* A comparison of whole genome gene expression profiles of HepaRG cells and HepG2 cells to primary human hepatocytes and human liver tissues. *Drug Metab. Dispos.* **38,** 988–994 (2010).
127. Kamalian, L. *et al.* The utility of HepG2 cells to identify direct mitochondrial dysfunction in the absence of cell death. *Toxicol Vitr.* **29,** 732–740 (2015).
128. Van den Hof, W. F. *et al.* Classification of hepatotoxicants using HepG2 cells: A proof of principle study.

Chem Res Toxicol **27,** 433–442 (2014).
129. Ramaiahgari, S. C. *et al.* A 3D in vitro model of differentiated HepG2 cell spheroids with improved liver-like properties for repeated dose high-throughput toxicity studies. *Arch Toxicol* **88,** 1083–1095 (2014).
130. Cosgrove, B. D. *et al.* Cytokine-associated drug toxicity in human hepatocytes is associated with signaling network dysregulation. *Mol Biosyst* **6,** 1195–1206 (2010).
131. Zinchenko, Y. S., Schrum, L. W., Clemens, M. & Coger, R. N. Hepatocyte and kupffer cells co-cultured on micropatterned surfaces to optimize hepatocyte function. *Tissue Eng* **12,** 751–761 (2006).
132. Messner, S., Agarkova, I., Moritz, W. & Kelm, J. M. Multi-cell type human liver microtissues for hepatotoxicity testing. *Arch Toxicol* **87,** 209–213 (2013).
133. Vatakuti, S., Pennings, J. L., Gore, E., Olinga, P. & Groothuis, G. M. Classification of Cholestatic and Necrotic Hepatotoxicants Using Transcriptomics on Human Precision-Cut Liver Slices. *Chem Res Toxicol* **29,** 342–351 (2016).
134. Sampaziotis, F., Segeritz, C. P. & Vallier, L. Potential of human induced pluripotent stem cells in studies of liver disease. *Hepatology* **62,** 303–311 (2015).
135. Wink, S. *et al.* Quantitative High Content Imaging of Cellular Adaptive Stress Response Pathways in Toxicity for Chemical Safety Assessment. *Chem. Res. Toxicol.* (2014). doi:10.1021/tx4004038
136. Luedde, T. & Schwabe, R. F. NF-kappaB in the liver--linking injury, fibrosis and hepatocellular carcinoma. *Nat Rev Gastroenterol Hepatol* **8,** 108–118 (2011).
137. Wullaert, A., van Loo, G., Heyninck, K. & Beyaert, R. Hepatic tumor necrosis factor signaling and nuclear factor-kappaB: effects on liver homeostasis and beyond. *Endocr. Rev.* **28,** 365–386 (2007).
138. Hayden, M. S., West, A. P. & Ghosh, S. NF-kappaB and the immune response. *Oncogene* **25,** 6758–6780 (2006).
139. French, J. B., Bonacini, M., Ghabril, M., Foureau, D. & Bonkovsky, H. L. Hepatotoxicity Associated with the Use of Anti-TNF-alpha Agents. *Drug Saf.* **39,** 199–208 (2015).
140. Micheau, O. & Tschopp, J. Induction of TNF receptor I-mediated apoptosis via two sequential signaling complexes. *Cell* **114,** 181–190 (2003).
141. Lork, M., Verhelst, K. & Beyaert, R. CYLD, A20 and OTULIN deubiquitinases in inflammation and cell death, so similar yet so different. *Cell Death Differ.* (2016).
142. Ma, A. & Malynn, B. A. A20: linking a complex regulator of ubiquitylation to immunity and human disease. *Nat Rev Immunol* **12,** 774–785 (2012).
143. Catrysse, L., Vereecke, L., Beyaert, R. & van Loo, G. A20 in inflammation and autoimmunity. *Trends Immunol* **35,** 22–31 (2014).
144. Kupka, S., Reichert, M., Draber, P. & Walczak, H. Formation and removal of poly-ubiquitin chains in the regulation of tumor necrosis factor-induced gene activation and cell death. *FEBS J* **283,** 2626–2639 (2016).
145. Halsey, T. A., Yang, L., Walker, J. R., Hogenesch, J. B. & Thomas, R. S. A functional map of NFkappaB signaling identifies novel modulators and multiple system controls. *Genome Biol* **8,** R104 (2007).
146. Chew, J. *et al.* WIP1 phosphatase is a negative regulator of NF-kappaB signalling. *Nat. Cell Biol.* **11,** 659–666 (2009).
147. Li, S., Wang, L., Berman, M. A., Zhang, Y. & Dorf, M. E. RNAi screen in mouse astrocytes identifies phosphatases that regulate NF-kappaB signaling. *Mol. Cell* **24,** 497–509 (2006).
148. Zemirli, N., Pourcelot, M., Dogan, N., Vazquez, A. & Arnoult, D. The E3 ubiquitin ligase RNF121 is a positive regulator of NF-kappaB activation. *Cell Commun Signal* **12,** 72 (2014).
149. Metzig, M. *et al.* An RNAi screen identifies USP2 as a factor required for TNF-α-induced NF-κB signaling. *Int. J. Cancer* **129,** 607–618 (2011).
150. Fraser, B., Maranchuk, R. A. & Foley, E. A High-Content RNAi Screen Identifies Ubiquitin Modifiers That Regulate TNF-Dependent Nuclear Accumulation of NF-kappaB. *Front Immunol* **5,** 322 (2014).
151. Olarerin-George, A. O., Anton, L., Hwang, Y. C., Elovitz, M. A. & Hogenesch, J. B. A functional genomics screen for microRNA regulators of NF-kappaB signaling. *BMC Biol* **11,** 19 (2013).
152. Hao, S. & Baltimore, D. The stability of mRNA influences the temporal order of the induction of genes encoding inflammatory molecules. *Nat. Immunol.* **10,** 281–288 (2009).
153. Tian, B., Nowak, D. E., Jamaluddin, M., Wang, S. & Brasier, A. R. Identification of direct genomic targets downstream of the nuclear factor-kappaB transcription factor mediating tumor necrosis factor signaling. *J. Biol. Chem.* **280,** 17435–17448 (2005).
154. Lee, R. E., Walker, S. R., Savery, K., Frank, D. A. & Gaudet, S. Fold change of nuclear NF-kappaB determines TNF-induced transcription in single cells. *Mol. Cell* **53,** 867–879 (2014).
155. Bartfeld, S. *et al.* High-throughput and single-cell imaging of NF-kappaB oscillations using monoclonal cell lines. *BMC Cell Biol* **11,** 21 (2010).
156. Di, Z. *et al.* Automated analysis of NF-kappaB nuclear translocation kinetics in high-throughput screening. *PLoS One* **7,** e52337 (2012).
157. Hendriks, G. *et al.* The ToxTracker assay: novel GFP reporter systems that provide mechanistic insight into the genotoxic properties of chemicals. *Toxicol. Sci.* **125,** 285–298 (2012).
158. Kamentsky, L. *et al.* Improved structure, function and compatibility for CellProfiler: modular high-throughput image analysis software. *Bioinformatics* **27,** 1179–1180 (2011).
159. Yan, K. & Verbeek, F. J. Segmentation for High-Throughput Image Analysis: Watershed Masked Clustering. in *Leveraging Applications of Formal Methods, Verification and Validation. Applications and Case Studies: 5th International Symposium, ISoLA 2012, Heraklion, Crete, Greece, October 15-18, 2012, Proceedings, Part II* (eds. Margaria, T. & Steffen, B.) 25–41 (Springer Berlin Heidelberg, 2012). doi:10.1007/978-3-642-34032-1_4
160. Puigvert, J. C., de Bont, H., van de Water, B. & Danen, E. H. High-throughput live cell imaging of apoptosis.

Curr. Protoc. Cell Biol. **Chapter 18,** Unit 18 10 1-13 (2010).
161. Zhang, S. Q., Kovalenko, A., Cantarella, G. & Wallach, D. Recruitment of the IKK signalosome to the p55 TNF receptor: RIP and A20 bind to NEMO (IKKgamma) upon receptor stimulation. *Immunity* **12,** 301–311 (2000).
162. Takami, Y. *et al.* Ubiquitin carboxyl-terminal hydrolase L1, a novel deubiquitinating enzyme in the vasculature, attenuates NF-kappaB activation. *Arter. Thromb Vasc Biol* **27,** 2184–2190 (2007).
163. Karim, R. *et al.* Human papillomavirus (HPV) upregulates the cellular deubiquitinase UCHL1 to suppress the keratinocyte's innate immune response. *PLoS Pathog* **9,** e1003384 (2013).
164. Guo, R. W., Yang, L. X., Wang, H., Liu, B. & Wang, L. Angiotensin II induces matrix metalloproteinase-9 expression via a nuclear factor-kappaB-dependent pathway in vascular smooth muscle cells. *Regul Pept* **147,** 37–44 (2008).
165. Rompe, F. *et al.* Direct angiotensin II type 2 receptor stimulation acts anti-inflammatory through epoxyeicosatrienoic acid and inhibition of nuclear factor kappaB. *Hypertension* **55,** 924–931 (2010).
166. Pandey, A., Goru, S. K., Kadakol, A., Malek, V. & Gaikwad, A. B. Differential regulation of angiotensin converting enzyme 2 and nuclear factor-kappaB by angiotensin II receptor subtypes in type 2 diabetic kidney. *Biochimie* **118,** 71–81 (2015).
167. Zhu, L. *et al.* Activation of angiotensin II type 2 receptor suppresses TNF-alpha-induced ICAM-1 via NF-small ka, CyrillicB: possible role of ACE2. *Am J Physiol Hear. Circ Physiol* **309,** H827-34 (2015).
168. Gorska, M. M. *et al.* MK2 controls the level of negative feedback in the NF-kappaB pathway and is essential for vascular permeability and airway inflammation. *J. Exp. Med.* **204,** 1637–1652 (2007).
169. Lee, M. H., Mabb, A. M., Gill, G. B., Yeh, E. T. & Miyamoto, S. NF-kappaB induction of the SUMO protease SENP2: A negative feedback loop to attenuate cell survival response to genotoxic stress. *Mol. Cell* **43,** 180–191 (2011).
170. Shembade, N. & Harhaj, E. W. Regulation of NF-kappaB signaling by the A20 deubiquitinase. *Cell. Mol. Immunol.* **9,** 123–130 (2012).
171. Alexaki, V. I. *et al.* B-cell maturation antigen (BCMA) activation exerts specific proinflammatory effects in normal human keratinocytes and is preferentially expressed in inflammatory skin pathologies. *Endocrinology* **153,** 739–749 (2012).
172. Lee, D. F. *et al.* KEAP1 E3 ligase-mediated downregulation of NF-kappaB signaling by targeting IKKbeta. *Mol. Cell* **36,** 131–140 (2009).
173. Placke, T., Kopp, H. G. & Salih, H. R. Glucocorticoid-induced TNFR-related (GITR) protein and its ligand in antitumor immunity: functional role and therapeutic modulation. *Clin Dev Immunol* **2010,** 239083 (2010).
174. Tan, P. *et al.* Recruitment of a ROC1-CUL1 ubiquitin ligase by Skp1 and HOS to catalyze the ubiquitination of I kappa B alpha. *Mol. Cell* **3,** 527–533 (1999).
175. Suzuki, H. *et al.* Homodimer of two F-box proteins betaTrCP1 or betaTrCP2 binds to IkappaBalpha for signal-dependent ubiquitination. *J. Biol. Chem.* **275,** 2877–2884 (2000).
176. Israel, A. The IKK complex, a central regulator of NF-kappaB activation. *Cold Spring Harb Perspect Biol* **2,** a000158 (2010).
177. Zarnegar, B., Yamazaki, S., He, J. Q. & Cheng, G. Control of canonical NF-kappaB activation through the NIK-IKK complex pathway. *Proc. Natl. Acad. Sci. U. S. A.* **105,** 3503–3508 (2008).
178. Tan, J. *et al.* Inhibition of NFkappaB by activated c-Jun NH2 terminal kinase 1 acts as a switch for C2C12 cell death under excessive stretch. *Apoptosis* **14,** 764–770 (2009).
179. Zha, J. *et al.* The Ret finger protein inhibits signaling mediated by the noncanonical and canonical IkappaB kinase family members. *J. Immunol.* **176,** 1072–1080 (2006).
180. Li, Q. *et al.* Tripartite motif 8 (TRIM8) modulates TNFalpha- and IL-1beta-triggered NF-kappaB activation by targeting TAK1 for K63-linked polyubiquitination. *Proc. Natl. Acad. Sci. U. S. A.* **108,** 19341–19346 (2011).
181. Tomar, D., Sripada, L., Prajapati, P., Singh, R. & Singh, A. K. Nucleo-cytoplasmic trafficking of TRIM8, a novel oncogene, is involved in positive regulation of TNF induced NF-kappaB pathway. *PLoS One* **7,** e48662 (2012).
182. Li, J. M., Wu, H., Zhang, W., Blackburn, M. R. & Jin, J. The p97-UFD1L-NPL4 protein complex mediates cytokine-induced IkappaBalpha proteolysis. *Mol. Cell. Biol.* **34,** 335–347 (2014).
183. Kaikkonen, M. U. *et al.* Remodeling of the enhancer landscape during macrophage activation is coupled to enhancer transcription. *Mol. Cell* **51,** 310–325 (2013).
184. Kovalenko, A. *et al.* The tumour suppressor CYLD negatively regulates NF-kappaB signalling by deubiquitination. *Nature* **424,** 801–805 (2003).
185. Urbanik, T. *et al.* CYLD deletion triggers nuclear factor-kappaB-signaling and increases cell death resistance in murine hepatocytes. *World J Gastroenterol* **20,** 17049–17064 (2014).
186. Burke, M. A. & Bothwell, M. p75 neurotrophin receptor mediates neurotrophin activation of NF-kappa B and induction of iNOS expression in P19 neurons. *J Neurobiol* **55,** 191–203 (2003).
187. Gewurz, B. E. *et al.* Genome-wide siRNA screen for mediators of NF-kappaB activation. *Proc. Natl. Acad. Sci. U. S. A.* **109,** 2467–2472 (2012).
188. Li, S. *et al.* Regulation of virus-triggered signaling by OTUB1- and OTUB2-mediated deubiquitination of TRAF3 and TRAF6. *J. Biol. Chem.* **285,** 4291–4297 (2010).
189. Schweitzer, K., Bozko, P. M., Dubiel, W. & Naumann, M. CSN controls NF-kappaB by deubiquitinylation of IkappaBalpha. *EMBO J.* **26,** 1532–1541 (2007).
190. Chilà, R., Guffanti, F. & Damia, G. Role and therapeutic potential of CDK12 in human cancers. *Cancer Treat. Rev.* **50,** 83–88 (2016).
191. Stratford, J. K. *et al.* Genetic and pharmacological inhibition of TTK impairs pancreatic cancer cell line growth by inducing lethal chromosomal instability. (2017).

192. Catrysse, L. *et al.* A20 prevents chronic liver inflammation and cancer by protecting hepatocytes from death. *Cell Death Dis.* **7,** e2250 (2016).
193. Arvelo, M. B. *et al.* A20 protects mice from D-galactosamine/lipopolysaccharide acute toxic lethal hepatitis. *Hepatology* **35,** 535–543 (2002).
194. Tay, S. *et al.* Single-cell NF-kappaB dynamics reveal digital activation and analogue information processing. *Nature* **466,** 267–271 (2010).
195. Bartkowiak, B. & Greenleaf, A. L. Expression, purification, and identification of associated proteins of the full-length hCDK12/CyclinK complex. *J. Biol. Chem.* **290,** 1786–1795 (2015).
196. Bowman, E. A. & Kelly, W. G. RNA polymerase II transcription elongation and Pol II CTD Ser2 phosphorylation: A tail of two kinases. *Nucleus* **5,** 224–236 (2014).
197. Bosken, C. A. *et al.* The structure and substrate specificity of human Cdk12/Cyclin K. *Nat Commun* **5,** 3505 (2014).
198. Blazek, D. *et al.* The Cyclin K/Cdk12 complex maintains genomic stability via regulation of expression of DNA damage response genes. *Genes Dev.* **25,** 2158–72 (2011).
199. Li, X., Chatterjee, N., Spirohn, K., Boutros, M. & Bohmann, D. Cdk12 Is A Gene-Selective RNA Polymerase II Kinase That Regulates a Subset of the Transcriptome, Including Nrf2 Target Genes. *Sci Rep* **6,** 21455 (2016).
200. Amir-Zilberstein, L. *et al.* Differential regulation of NF-kappaB by elongation factors is determined by core promoter type. *Mol. Cell. Biol.* **27,** 5246–5259 (2007).
201. Diamant, G., Amir-Zilberstein, L., Yamaguchi, Y., Handa, H. & Dikstein, R. DSIF restricts NF-kappaB signaling by coordinating elongation with mRNA processing of negative feedback genes. *Cell Rep.* **2,** 722–731 (2012).
202. Buchberger, A., Schindelin, H. & H??nzelmann, P. Control of p97 function by cofactor binding. *FEBS Lett.* **589,** 2578–2589 (2015).
203. Bug, M. & Meyer, H. Expanding into new markets--VCP/p97 in endocytosis and autophagy. *J. Struct. Biol.* **179,** 78–82 (2012).
204. Riemer, A. *et al.* The p97-Ufd1-Npl4 ATPase complex ensures robustness of the G2/M checkpoint by facilitating CDC25A degradation. *Cell Cycle* **13,** 919–927 (2014).
205. Chen, M., Gutierrez, G. J. & Ronai, Z. A. Ubiquitin-recognition protein Ufd1 couples the endoplasmic reticulum (ER) stress response to cell cycle control. *Proc. Natl. Acad. Sci. U. S. A.* **108,** 9119–9124 (2011).
206. Antoniades, C. G., Berry, P. A., Wendon, J. A. & Vergani, D. The importance of immune dysfunction in determining outcome in acute liver failure. *J. Hepatol.* **49,** 845–861 (2008).
207. Funk, C. & Roth, A. Current limitations and future opportunities for prediction of DILI from in vitro. *Arch. Toxicol.* **91,** 131–142 (2017).
208. Chen, M., Suzuki, A., Borlak, J., Andrade, R. J. & Lucena, M. I. Drug-induced liver injury: Interactions between drug properties and host factors. *J. Hepatol.* **63,** 503–514 (2015).
209. Huppelschoten, S. & van de Water, B. Drug-Induced Liver Injury and TNFα Signaling: From In Vivo Understanding to In Vitro Testing Approaches. *Appl. Vitr. Toxicol.* **0,** 1–10 (2016).
210. Hayden, M. S. & Ghosh, S. NF-kappaB, the first quarter-century: remarkable progress and outstanding questions. *Genes Dev.* **26,** 203–234 (2012).
211. Lawrence, T. The Nuclear Factor NF- B Pathway in Inflammation. *Cold Spring Harb. Perspect. Biol.* **1,** a001651–a001651 (2009).
212. Dragovic, S. *et al.* Evidence-based selection of training compounds for use in the mechanism-based integrated prediction of drug-induced liver injury in man. *Arch Toxicol* (2016). doi:10.1007/s00204-016-1845-1
213. Hao, S. & Baltimore, D. RNA splicing regulates the temporal order of TNF-induced gene expression. *Proc. Natl. Acad. Sci.* **110,** 11934–11939 (2013).
214. Wu, C. *et al.* Evaluation of potential reference genes for qRT-PCR studies in human hepatoma cell lines treated with TNF- a. 780–786 (2013). doi:10.1093/abbs/gmt072.Advance
215. Cicinnati, V. R. *et al.* Validation of putative reference genes for gene expression studies in human hepatocellular carcinoma using real-time quantitative. **12,** 1–12 (2008).
216. Fekete-drimusz, N., Manns, M. P., Vondran, F. W. R., Riedel, G. & Ru, U. An Extended D CT-Method Facilitating Normalisation with Multiple Reference Genes Suited for Quantitative RT-PCR Analyses of Human Hepatocyte-Like Cells. **9,** 2–6 (2014).
217. Wickham, H. & Francois, R. dplyr: A Grammar of Data Manipulation. *R Packag. version 0.4.2.* 3 (2015).
218. Wickham, H. Reshaping Data with the \pkgreshape Package. *J. Stat. Softw.* **21,** 1–20 (2007).
219. Wickham, H. ggplot2:Elegant Graphics for Data Analysis. *J. Stat. Softw.* **31,** 1–3 (2009).
220. R Development Core Team. *R: A Language and Environment for Statistical Computing*. **2,** (2008).
221. Fredriksson, L. *et al.* Drug-induced endoplasmic reticulum and oxidative stress responses independently sensitize toward TNF??-mediated hepatotoxicity. *Toxicol. Sci.* **140,** 144–159 (2014).
222. Igarashi, Y. *et al.* Open TG-GATEs: a large-scale toxicogenomics database. *Nucleic Acids Res* **43,** D921-7 (2015).
223. Kannan, M. B., Solovieva, V. & Blank, V. The small MAF transcription factors MAFF, MAFG and MAFK: current knowledge and perspectives. *Biochim Biophys Acta* **1823,** 1841–1846 (2012).
224. Li, S. *et al.* The Role of Oxidative Stress and Antioxidants in Liver Diseases. *Int. J. Mol. Sci.* **16,** 26087–124 (2015).
225. Wang, Y., Singh, R., Lefkowitch, J. H., Rigoli, R. M. & Czaja, M. J. Tumor necrosis factor-induced toxic liver injury results from JNK2-dependent activation of caspase-8 and the mitochondrial death pathway. *J. Biol. Chem.* **281,** 15258–15267 (2006).

226. Ventura, J. J., Cogswell, P., Flavell, R. A., Baldwin, A. S. & Davis, R. J. JNK potentiates TNF-stimulated necrosis by increasing the production of cytotoxic reactive oxygen species. *Genes Dev.* **18,** 2905–2915 (2004).
227. Zhang, R. *et al.* Thioredoxin-2 inhibits mitochondria-located ASK1-mediated apoptosis in a JNK-independent manner. *Circ. Res.* **94,** 1483–1491 (2004).
228. Authier, H. *et al.* IKK phosphorylates RelB to modulate its promoter specificity and promote fibroblast migration downstream of TNF receptors. *Proc. Natl. Acad. Sci. U. S. A.* **111,** 14794–14799 (2014).
229. Jacque, E., Billot, K., Authier, H., Bordereaux, D. & Baud, V. RelB inhibits cell proliferation and tumor growth through p53 transcriptional activation. *Oncogene* (2012). doi:10.1038/onc.2012.282
230. Baud, V. & Collares, D. Post-Translational Modifications of RelB NF-κB Subunit and Associated Functions. *Cells* **5,** 22 (2016).
231. Jacque, E., Tchenio, T., Piton, G., Romeo, P. H. & Baud, V. RelA repression of RelB activity induces selective gene activation downstream of TNF receptors. *Proc. Natl. Acad. Sci. U. S. A.* **102,** 14635–14640 (2005).
232. Fang, L. *et al.* ATM regulates NF-kappaB-dependent immediate-early genes via RelA Ser 276 phosphorylation coupled to CDK9 promoter recruitment. *Nucleic Acids Res* **42,** 8416–8432 (2014).
233. Seldon, M. P. *et al.* Heme oxygenase-1 inhibits the expression of adhesion molecules associated with endothelial cell activation via inhibition of NF-kappaB RelA phosphorylation at serine 276. *J. Immunol.* **179,** 7840–7851 (2007).
234. Derudder, E. *et al.* RelB/p50 dimers are differentially regulated by tumor necrosis factor-α and lymphotoxin-β receptor activation. Critical roles for p100. *J. Biol. Chem.* **278,** 23278–23284 (2003).
235. Marra, F. & Tacke, F. Roles for chemokines in liver disease. *Gastroenterology* **147,** 577–594 e1 (2014).
236. Luo, L. *et al.* RNA interference targeting RelB attenuates liver ischemia/reperfusion injury. *J. Surg. Res.* (2012). doi:10.1016/j.jss.2012.08.032
237. Shen, H. *et al.* Mouse hepatocyte overexpression of NF-kappaB-inducing kinase (NIK) triggers fatal macrophage-dependent liver injury and fibrosis. *Hepatology* **60,** 2065–2076 (2014).
238. Zhou, S. L. *et al.* Overexpression of CXCL5 mediates neutrophil infiltration and indicates poor prognosis for hepatocellular carcinoma. *Hepatology* **56,** 2242–2254 (2012).
239. Oppmann, B. *et al.* Novel p19 protein engages IL-12p40 to form a cytokine, IL-23, with biological activities similar as well as distinct from IL-12. *Immunity* **13,** 715–725 (2000).
240. Mukherjee, A. *et al.* FSTL3 deletion reveals roles for TGF-beta family ligands in glucose and fat homeostasis in adults. *Proc. Natl. Acad. Sci. U. S. A.* **104,** 1348–1353 (2007).
241. Tanino, Y. *et al.* Syndecan-4 regulates early neutrophil migration and pulmonary inflammation in response to lipopolysaccharide. *Am J Respir Cell Mol Biol* **47,** 196–202 (2012).
242. Turer, E. E. *et al.* Homeostatic MyD88-dependent signals cause lethal inflamMation in the absence of A20. *J. Exp. Med.* **205,** 451–464 (2008).
243. Affo, S. *et al.* CCL20 mediates lipopolysaccharide induced liver injury and is a potential driver of inflammation and fibrosis in alcoholic hepatitis. *Gut* **63,** 1782–1792 (2014).
244. Tumanov, A. V *et al.* T cell-derived lymphotoxin regulates liver regeneration. *Gastroenterology* **136,** 694–704 e4 (2009).
245. Hoffmann, A., Natoli, G. & Ghosh, G. Transcriptional regulation via the NF-kappaB signaling module. *Oncogene* **25,** 6706–6716 (2006).
246. Brien, G. *et al.* C-terminal residues regulate localization and function of the antiapoptotic protein Bfl-1. *J. Biol. Chem.* **284,** 30257–30263 (2009).
247. Yang, L. *et al.* ICAM-1 regulates neutrophil adhesion and transcellular migration of TNF-alpha-activated vascular endothelium under flow. *Blood* **106,** 584–592 (2005).
248. Matheny, H. E., Deem, T. L. & Cook-Mills, J. M. Lymphocyte migration through monolayers of endothelial cell lines involves VCAM-1 signaling via endothelial cell NADPH oxidase. *J. Immunol.* **164,** 6550–6559 (2000).
249. Kim, H. J. *et al.* Reverse signaling through the costimulatory ligand CD137L in epithelial cells is essential for natural killer cell-mediated acute tissue inflammation. *Proc. Natl. Acad. Sci. U. S. A.* **109,** E13-22 (2012).
250. Shen, L., Guo, J., Santos-Berrios, C. & Wu, M. X. Distinct domains for anti- and pro-apoptotic activities of IEX-1. *J. Biol. Chem.* **281,** 15304–15311 (2006).
251. Katsuoka, F. *et al.* Genetic evidence that small maf proteins are essential for the activation of antioxidant response element-dependent genes. *Mol. Cell. Biol.* **25,** 8044–8051 (2005).
252. Yamazaki, H., Katsuoka, F., Motohashi, H., Engel, J. D. & Yamamoto, M. Embryonic lethality and fetal liver apoptosis in mice lacking all three small Maf proteins. *Mol. Cell. Biol.* **32,** 808–816 (2012).
253. Stutchfield, B. M. *et al.* CSF1 Restores Innate Immunity After Liver Injury in Mice and Serum Levels Indicate Outcomes of Patients With Acute Liver Failure. *Gastroenterology* **149,** 1896–1909 e14 (2015).
254. Zigmond, E. *et al.* Infiltrating monocyte-derived macrophages and resident kupffer cells display different ontogeny and functions in acute liver injury. *J. Immunol.* **193,** 344–353 (2014).
255. Efsen, E. *et al.* Up-regulated expression of fractalkine and its receptor CX3CR1 during liver injury in humans. *J. Hepatol.* **37,** 39–47 (2002).
256. Pryhuber, G. S. *et al.* Acute tumor necrosis factor-alpha-induced liver injury in the absence of tumor necrosis factor receptor-associated factor 1 gene expression. *Am. J. Pathol.* **166,** 1637–1645 (2005).
257. Pulukuri, S. M. *et al.* RNA interference-directed knockdown of urokinase plasminogen activator and urokinase plasminogen activator receptor inhibits prostate cancer cell invasion, survival, and tumorigenicity in vivo. *J. Biol. Chem.* **280,** 36529–36540 (2005).
258. Gondi, C. S., Kandhukuri, N., Dinh, D. H., Gujrati, M. & Rao, J. S. Down-regulation of uPAR and uPA

activates caspase-mediated apoptosis and inhibits the PI3K/AKT pathway. *Int J Oncol* **31,** 19–27 (2007).
259. Amanzada, A. *et al.* Induction of chemokines and cytokines before neutrophils and macrophage recruitment in different regions of rat liver after TAA administration. *Lab Invest* **94,** 235–247 (2014).
260. Cheng, Z. *et al.* MicroRNA-184 inhibits cell proliferation and invasion, and specifically targets TNFAIP2 in Glioma. *J Exp Clin Cancer Res* **34,** 27 (2015).
261. Zhang, X. *et al.* CXCL10 plays a key role as an inflammatory mediator and a non-invasive biomarker of non-alcoholic steatohepatitis. *J. Hepatol.* **61,** 1365–1375 (2014).
262. Hintermann, E., Bayer, M., Pfeilschifter, J. M., Luster, A. D. & Christen, U. CXCL10 promotes liver fibrosis by prevention of NK cell mediated hepatic stellate cell inactivation. *J Autoimmun* **35,** 424–435 (2010).
263. Li, L. *et al.* Epithelial-specific ETS-1 (ESE1/ELF3) regulates apoptosis of intestinal epithelial cells in ulcerative colitis via accelerating NF-kappaB activation. *Immunol Res* **62,** 198–212 (2015).
264. Longoni, N. *et al.* ETS transcription factor ESE1/ELF3 orchestrates a positive feedback loop that constitutively activates NF-kappaB and drives prostate cancer progression. *Cancer Res* **73,** 4533–4547 (2013).
265. Totzke, G. *et al.* A novel member of the IkappaB family, human IkappaB-zeta, inhibits transactivation of p65 and its DNA binding. *J. Biol. Chem.* **281,** 12645–12654 (2006).
266. Bhattacharya, P. *et al.* GM-CSF: An immune modulatory cytokine that can suppress autoimmunity. *Cytokine* **75,** 261–271 (2015).
267. McDonald, B. *et al.* Intravascular danger signals guide neutrophils to sites of sterile inflammation. *Science (80-.).* **330,** 362–366 (2010).
268. Song, L. *et al.* BCL3 Reduces the Sterile Inflammatory Response in Pancreatic and Biliary Tissues. *Gastroenterology* **150,** 499–512 e20 (2016).
269. Kashatus, D., Cogswell, P. & Baldwin, A. S. Expression of the Bcl-3 proto-oncogene suppresses p53 activation. *Genes Dev.* **20,** 225–235 (2006).
270. Ahmed, S. U. & Milner, J. Basal cancer cell survival involves JNK2 suppression of a novel JNK1/c-Jun/Bcl-3 apoptotic network. *PLoS One* **4,** e7305 (2009).
271. Stock, M. K. *et al.* Met-CCL5 modifies monocyte subpopulations during liver fibrosis regression. *Int J Clin Exp Pathol* **6,** 678–685 (2013).
272. Qiao, H. X. *et al.* JNK activation mediates the apoptosis of xCT-deficient cells. *Biochem. Biophys. Res. Commun.* **370,** 584–588 (2008).
273. Markiewski, M. M. *et al.* C3a and C3b activation products of the third component of complement (C3) are critical for normal liver recovery after toxic injury. *J. Immunol.* **173,** 747–754 (2004).
274. Cresci, G. A., Allende, D., McMullen, M. R. & Nagy, L. E. Alternative complement pathway component Factor D contributes to efficient clearance of tissue debris following acute CCl(4)-induced injury. *Mol Immunol* **64,** 9–17 (2015).
275. Borkham-Kamphorst, E. *et al.* Protective effects of lipocalin-2 (LCN2) in acute liver injury suggest a novel function in liver homeostasis. *Biochim Biophys Acta* **1832,** 660–673 (2013).
276. Kim, M. S., Lee, K. H., Lee, W. M., Jun, J. H. & Kim, D. H. CD44 disruption attenuates murine hepatic ischemia/reperfusion injury. *J Korean Med Sci* **26,** 919–926 (2011).
277. Ramachandran, A., Lebofsky, M., Weinman, S. A. & Jaeschke, H. The impact of partial manganese superoxide dismutase (SOD2)-deficiency on mitochondrial oxidant stress, DNA fragmentation and liver injury during acetaminophen hepatotoxicity. *Toxicol. Appl. Pharmacol.* **251,** 226–233 (2011).
278. Wullaert, A. *et al.* Adenoviral gene transfer of ABIN-1 protects mice from TNF/galactosamine-induced acute liver failure and lethality. *Hepatology* **42,** 381–389 (2005).
279. Augustin, R. The protein family of glucose transport facilitators: It's not only about glucose after all. *IUBMB Life* **62,** 315–333 (2010).
280. Millet, P., McCall, C. & Yoza, B. RelB: an outlier in leukocyte biology. *J. Leukoc. Biol.* **94,** 941–951 (2013).
281. Yokota, S. *et al.* IRF-1 promotes liver transplant ischemia/reperfusion injury via hepatocyte IL-15/IL-15Ralpha production. *J. Immunol.* **194,** 6045–6056 (2015).
282. Eyles, J. L. *et al.* A key role for G-CSF-induced neutrophil production and trafficking during inflammatory arthritis. *Blood* **112,** 5193–5201 (2008).
283. Rainard, P. *et al.* The chemokine CXCL3 is responsible for the constitutive chemotactic activity of bovine milk for neutrophils. *Mol Immunol* **45,** 4020–4027 (2008).
284. Shimizu, Y. *et al.* Activation-independent binding of human memory T cells to adhesion molecule ELAM-1. *Nature* **349,** 799–802 (1991).
285. Tada, Y., Ho, A., Matsuyama, T. & Mak, T. W. Reduced incidence and severity of antigen-induced autoimmune diseases in mice lacking interferon regulatory factor-1. *J. Exp. Med.* **185,** 231–238 (1997).
286. Fulda, S. & Debatin, K. M. IFNgamma sensitizes for apoptosis by upregulating caspase-8 expression through the Stat1 pathway. *Oncogene* **21,** 2295–2308 (2002).
287. Tang, R., Yang, G., Zhang, S., Wu, C. & Chen, M. Opposite effects of interferon regulatory factor 1 and osteopontin on the apoptosis of epithelial cells induced by TNF-alpha in inflammatory bowel disease. *Inflamm Bowel Dis* **20,** 1950–1961 (2014).
288. Soler Palacios, B. *et al.* Macrophages from the synovium of active rheumatoid arthritis exhibit an activin A-dependent pro-inflammatory profile. *J. Pathol.* **235,** 515–526 (2015).
289. Fagerlund, R. *et al.* Anatomy of a negative feedback loop: the case of IkappaBalpha. *J R Soc Interface* **12,** 262 (2015).
290. Björnsson, E. Hepatotoxicity associated with antiepileptic drugs. *Acta Neurol. Scand.* **118,** 281–290 (2008).
291. Pearce, R. E., Lu, W., Wang, Y., Uetrecht, J. P. & Correia, M. A. Pathways of Carbamazepine Bioactivation In Vitro III. The Role of Human Cytochrome P450 Enzymes in the Formation of 2,3-

Dihydroxycarbamazepine. *In Vitro* **36,** 1637–1649 (2009).
292. Oscarson, M. *et al.* Transcriptional profiling of genes induced in the livers of patients treated with carbamazepine. *Clin. Pharmacol. Ther.* **80,** (2006).
293. Usui, T., Saitoh, Y. & Komada, F. Induction of CYP3As in HepG2 cells by several drugs. Association between induction of CYP3A4 and expression of glucocorticoid receptor. *Biol. Pharm. Bull.* **26,** 510–517 (2003).
294. Sasaki, E. *et al.* Pathogenetic analyses of carbamazepine-induced liver injury in F344 rats focused on immune- and inflammation-related factors. *Exp. Toxicol. Pathol.* **68,** 27–38 (2016).
295. Iida, A. *et al.* Carbamazepine-induced liver injury requires CYP3A-mediated metabolism and glutathione depletion in rats. *Drug Metab. Dispos.* **43,** 958–968 (2015).
296. Higuchi, S. *et al.* Metabolic activation and inflammation reactions involved in carbamazepine-induced liver injury. *Toxicol. Sci.* **130,** 4–16 (2012).
297. Origassa, C. S. T. & Câmara, N. O. S. Cytoprotective role of heme oxygenase-1 and heme degradation derived end products in liver injury. *World J. Hepatol.* **5,** 541–549 (2013).
298. Mao, B., Zhang, Z. & Wang, G. BTG2: A rising star of tumor suppressors (Review). *Int. J. Oncol.* **46,** 459–464 (2015).
299. Dayalan Naidu, S. & Dinkova-Kostova, A. T. Regulation of the mammalian heat shock factor 1. *FEBS J.* 1–22 (2017). doi:10.1111/febs.13999
300. Nanau, R. M. & Neuman, M. G. Adverse drug reactions induced by valproic acid. *Clin. Biochem.* **46,** 1323–1338 (2013).
301. Yao, C., Mather, G. G., Stephens, J. R. & Levy, R. H. Cytotoxicity induced by the combination of valproic acid and tumor necrosis factor-α. *Biochem. Pharmacol.* **58,** 455–459 (1999).
302. Komulainen, T. *et al.* Sodium valproate induces mitochondrial respiration dysfunction in HepG2 in vitro cell model. *Toxicology* **331,** 47–56 (2015).
303. Neuman, M. G., Nanau, R. M., Shekh-Ahmad, T., Yagen, B. & Bialer, M. Valproic acid derivatives signal for apoptosis and repair in vitro. *Clin. Biochem.* **46,** 1532–1537 (2013).
304. Kyriakidis, I., Tragiannidis, A., Munchen, S. & Groll, A. H. Clinical hepatotoxicity associated with antifungal agents. *Expert Opin. Drug Saf.* **16,** 1–17 (2016).
305. Khoza, S., Moyo, I. & Ncube, D. Comparative Hepatotoxicity of Fluconazole, Ketoconazole, Itraconazole, Terbinafine, and Griseofulvin in Rats. *J. Toxicol.* **2017,** 1–9 (2017).
306. Finkelstein, Y. *et al.* Colchicine poisoning: the dark side of an ancient drug. *Clin. Toxicol. (Phila).* **48,** 407–14 (2010).
307. Mariathasan, S. *et al.* Differential activation of the inflammasome by caspase-1 adaptors ASC and Ipaf. *Nature* **430,** 213–218 (2004).
308. DeSantis, D. A., Ko, C. W., Wang, L., Lee, P. & Croniger, C. M. Constitutive Activation of the Nlrc4 Inflammasome Prevents Hepatic Fibrosis and Promotes Hepatic Regeneration after Partial Hepatectomy. *Mediators Inflamm.* **2015,** (2015).
309. Longo, C. R. *et al.* A20 protects mice from lethal radical hepatectomy by promoting hepatocyte proliferation via a p21waf1-dependent mechanism. *Hepatology* **42,** 156–164 (2005).
310. Sadasivam, S. *et al.* Caspase-1 activator Ipaf is a p53-inducible gene involved in apoptosis. *Oncogene* **24,** 627–636 (2005).
311. Vande Walle, L. *et al.* Negative regulation of the NLRP3 inflammasome by A20 protects against arthritis. *Nature* **512,** 69–73 (2014).
312. Strikoudis, A. *et al.* Regulation of transcriptional elongation in pluripotency and cell differentiation by the PHD-finger protein Phf5a. *Nat. Cell Biol.* **18,** 1127–1138 (2016).
313. Raschi, E. & Ponti, F. De. Drug- and herb-induced liver injury : Progress , current challenges and emerging signals of post-marketing risk. **7,** 1761–1771 (2015).
314. Laifenfeld, D. *et al.* Utilization of causal reasoning of hepatic gene expression in rats to identify molecular pathways of idiosyncratic drug-induced liver injury. *Toxicol. Sci.* **137,** 234–248 (2014).
315. Raschi, E. & Ponti, F. De. Drug-induced liver injury : Towards early prediction and risk stratification. *World J. Hepatol.* **9,** 30–37 (2017).
316. Espinosa-Diez, C. *et al.* Antioxidant responses and cellular adjustments to oxidative stress. *Redox Biol.* **6,** 183–197 (2015).
317. Jeong, W., Bae, S. H., Toledano, M. B. & Rhee, S. G. Role of sulfiredoxin as a regulator of peroxiredoxin function and regulation of its expression. *Free Radic. Biol. Med.* **53,** 447–456 (2012).
318. Findlay, V. J. *et al.* A novel role for human sulfiredoxin in the reversal of glutathionylation. *Cancer Res.* **66,** 6800–6806 (2006).
319. Wu, K. C., Liu, J. J. & Klaassen, C. D. Nrf2 activation prevents cadmium-induced acute liver injury. *Toxicol. Appl. Pharmacol.* **263,** 14–20 (2012).
320. Bae, S. H. *et al.* Peroxiredoxin III and sulfiredoxin together protect mice from pyrazole-induced oxidative liver injury. *Antioxid. Redox Signal.* **17,** 1351–61 (2012).
321. Bae, S. H. *et al.* Concerted action of sulfiredoxin and peroxiredoxin I protects against alcohol-induced oxidative injury in mouse liver. *Hepatology* **53,** 945–953 (2011).
322. Lafleur, M. a, Stevens, J. L. & Lawrence, J. W. Xenobiotic perturbation of ER stress and the unfolded protein response. *Toxicol. Pathol.* **41,** 235–62 (2013).
323. Li, Y., Guo, Y., Tang, J., Jiang, J. & Chen, Z. New insights into the roles of CHOP-induced apoptosis in ER stress Structure and Properties of C / EBP Homologous Protein Roles of CHOP in ER Stress-Mediated Apoptosis. *Acta Biochim Biophys Sin* **46,** 629–640 (2014).
324. Foufelle, F. & Fromenty, B. Role of endoplasmic reticulum stress in drug-induced toxicity. *Pharmacol. Res.*

Perspect. **4,** e00211 (2016).
325. El-Deiry, W. S. p21(WAF1) mediates cell-cycle inhibition, relevant to cancer suppression and therapy. *Cancer Res.* **76,** 5189–5191 (2016).
326. Ćmielová, J. & Řezáčová, M. Protein and its function based on a subcellular localization. *J. Cell. Biochem.* **112,** 3502–3506 (2011).
327. Bandi, S. *et al.* Perturbations in ataxia telangiectasia mutant signaling pathways after drug-induced acute liver failure and their reversal during rescue of animals by cell therapy. *Am. J. Pathol.* **178,** 161–174 (2011).
328. Yafune, A. *et al.* Expression patterns of cell cycle proteins in the livers of rats treated with hepatocarcinogens for 28 days. *Arch. Toxicol.* **87,** 1141–1153 (2013).
329. Rahman, A. & Fazal, F. Hug tightly and say goodbye: role of endothelial ICAM-1 in leukocyte transmigration. *Antioxid Redox Signal* **11,** 823–839 (2009).
330. Kubes, P. & Mehal, W. Z. Sterile inflammation in the liver. *Gastroenterology* **143,** 1158–1172 (2012).
331. Chen, M. *et al.* FDA-approved drug labeling for the study of drug-induced liver injury. *Drug Discov. Today* **16,** 697–703 (2011).
332. Purschke, M., Rubio, N., Held, K. D. & Redmond, R. W. Phototoxicity of Hoechst 33342 in time-lapse fluorescence microscopy. *Photochem Photobiol Sci* **9,** 1634–1639 (2010).
333. Ritz, C., Baty, F., Streibig, J. C. & Gerhard, D. Dose-Response Analysis Using R. 1–13 (2015). doi:10.1371/journal.pone.0146021
334. Gaujoux, R. & Seoighe, C. A flexible R package for nonnegative matrix factorization. *BMC Bioinformatics* **11,** 367 (2010).
335. Chen, M., Suzuki, A., Thakkar, S., Yu, K. & Hu, C. DILIrank : the largest reference drug list ranked by the risk for developing drug-induced liver injury in humans. **21,** 648–653 (2016).
336. Metwally, B. A. A. M. E. Clozapine-Induced Cardiotoxicity : Role of Oxidative Stress , Tumour Necrosis Factor Alpha and NF- jb. *Cardiovasc. Toxicol.* 355–365 (2015). doi:10.1007/s12012-014-9304-9
337. Ren, Z. *et al.* Endoplasmic Reticulum Stress Induction and ERK1/2 Activation Contribute to Nefazodone-Induced Toxicity in Hepatic Cells. *Toxicol. Sci.* **154,** 368–380 (2016).
338. Lauressergues, E. *et al.* Neuropharmacology Does endoplasmic reticulum stress participate in APD-induced hepatic metabolic dysregulation ? *Neuropharmacology* **62,** 784–796 (2012).
339. Yamaguchi, H. & Wang, H. G. CHOP is involved in endoplasmic reticulum stress-induced apoptosis by enhancing DR5 expression in human carcinoma cells. *J Biol Chem* **279,** 45495–45502 (2004).
340. Osburn, W. O. & Kensler, T. W. Nrf2 signaling: An adaptive response pathway for protection against environmental toxic insults. **659,** 31–39 (2009).
341. Garside, H. *et al.* Evaluation of the use of imaging parameters for the detection of compound-induced hepatotoxicity in 384-well cultures of HepG2 cells and cryopreserved primary human hepatocytes. *Toxicol. Vitr.* **28,** 171–181 (2014).
342. Kim, J. A., Han, E., Eun, C. J., Tak, Y. K. & Song, J. M. Real-time concurrent monitoring of apoptosis, cytosolic calcium, and mitochondria permeability transition for hypermulticolor high-content screening of drug-induced mitochondrial dysfunction-mediated hepatotoxicity. *Toxicol. Lett.* **214,** 175–181 (2012).
343. Quentin, T., Steinmetz, M., Poppe, a. & Thoms, S. Metformin differentially activates ER stress signaling pathways without inducing apoptosis. *J. Cell Sci.* **125,** e1–e1 (2012).
344. Lee, D. H. The hypertension drug , verapamil , activates Nrf2 by promoting p62-dependent autophagic Keap1 degradation and prevents acetaminophen-induced cytotoxicity. **50,** 91–96 (2017).
345. Willy, J. A., Young, S. K., Stevens, J. L., Masuoka, H. C. & Wek, R. C. CHOP links endoplasmic reticulum stress to NF-kappaB activation in the pathogenesis of nonalcoholic steatohepatitis. *Mol Biol Cell* **26,** 2190–2204 (2015).
346. Arlt, A. & Schafer, H. Role of the immediate early response 3 (IER3) gene in cellular stress response, inflammation and tumorigenesis. *Eur J Cell Biol* **90,** 545–552 (2011).
347. Goto, S., Deguchi, J., Nishio, N., Nomura, N. & Funabashi, H. Hepatotoxicants induce cytokine imbalance in response to innate immune system. *J. Toxicol. Sci.* **40,** 389–404 (2015).
348. Boutaffala, L. *et al.* NIK promotes tissue destruction independently of the alternative NF-kappaB pathway through TNFR1/RIP1-induced apoptosis. *Cell Death Differ.* **22,** 2020–2033 (2015).
349. Ren, X. *et al.* A small-molecule inhibitor of NF-κB-inducing kinase (NIK) protects liver from toxin-induced inflammation, oxidative stress, and injury. *FASEB J.* **31,** 711–718 (2017).
350. Lovas, A. *et al.* p100 Deficiency is insufficient for full activation of the alternative NF-kappaB pathway: TNF cooperates with p52-RelB in target gene transcription. *PLoS One* **7,** e42741 (2012).
351. Barzilai, A. & Yamamoto, K. I. DNA damage responses to oxidative stress. *DNA Repair (Amst).* **3,** 1109–1115 (2004).

List of abbreviations

A20, TNFAIP3	Tumor necrosis factor alpha induced protein 3
AnV	AnnexinV
BAC	Bacterial Artifical Chromosome
BMC	Benchmark Concentration
CCL	C-C motif chemokine ligand
CDK12 , CRK7	Cyclin Dependent Kinase 12
CHOP	CCAAT-enhancer-binding proetin homologous protein
CXCL	C-X-C motif chemokine ligand
CYP	cytochrome p450
DC	Dendritic Cell
DCF	diclofenac
DDR	DNA Damage Response
DILI	Drug-Induced Liver Injury
DMSO	dimethylsulfoxide
ER	Endoplasmic Reticulum
GFP	Green Fluorescent Protein
HLA	Human Leukocyte Antigen
HMBG1	High Mobility Group Box 1
ICAM1	Intercellular Adhesion Molecule 1
iDILI	idiosyncratic Drug-Induced Liver Injury
IκBα, NFKBIA	NF-κB Inhibitor alpha
IKK	IκBα kinase
IMI MIP-DILI	Innovative Medicine Initiative Mechanism-based Integrated systems for the Prediction of DILI
JNK	c-Jun N-terminal kinase
KC	Kupffer Cell
LPS	Lipopolysaccharide
LSEC	Liver Sinusoidal Endothelial Cell
MAPK	Mitogen-activated protein kinase
MET	Mouse Embryonic Fibroblast
NF-κB	Nuclear Factor kappa B
NIK	NF-κB inducing kinase
NK	Natural Killer cell
NSAID	nonsteroidal anti-inflammatory drug
OSR	Oxidative Stress Response
PHH	Primary Human Hepatocyte
PI	Propidium Iodide
ROS	Reactive Oxygen Species
siRNA	small interfering RNA
SVM	Support Vector Machine

TLR	Toll-like Receptor
TNFα	Tumor Necrosis Factor alpha
TNFR	TNF receptor
UFD1L	Ubiquitin Fusion Degradation Like 1
UPR	Unfolded Protein Response

Nederlandse samenvatting

Een bekende bijwerking van medicijnen is leverschade (in het engels Drug-Induced Liver Injury, afgekort tot DILI). DILI is de meest voorkomende oorzaak van opname in het ziekenhuis voor acuut leverfalen. De meeste DILI ontstaat door een overdosis, bijvoorbeeld van acetaminophen (paracetamol). Er zijn echter ook medicijnen die bij een normale dosis in een paar patienten DILI veroorzaken. Doordat deze idiosyncratische DILI (iDILI) onafhankelijk is van de dosis en een erg lage incidentie heeft is het lastig te voorspellen welk medicijn iDILI gaat veroorzaken, en in welke patienten. Deze op zichzelf effectieve medicijnen krijgen vaak een “black box warning” (de zwaarste vorm van een waarschuwing in een bijsluiter) en worden minder voorgeschreven aan patienten. Ook worden medicijnen soms van de markt gehaald of in een van de laatste fases van ontwikkeling gestopt. De farmaceutische industrie is erg gemotiveerd om in een vroeg stadium in de ontwikkeling van een nieuw medicijn het risico op iDILI te bepalen. Daarnaast zou de herkenning van personen die gevoelig zijn voor deze bijwerkingen de effectief behandelde patientpopulatie vergroten.

De oorzaak van iDILI is momenteel onbekend. Onderzoek laat zien dat er specifieke interacties zijn tussen de eigenschappen van het medicijn (lipofiliciteit, metabolisme, transport en dosis) en patient-gebonden factoren. De patient-gebonden factoren bestaan onder andere uit variatie in metabole competentie en expressie van transporter eiwitten, (toxicologische) stress responsen, ontstekingsreacties en de mogelijkheid tot herstel na schade. De schade die een medicijn uiteindelijk toebrengt aan de lever is een som van al deze processen.

De meeste medicijnen induceren adaptieve stress responsen in levercellen, die de cel beschermen tegen schade. Als de schade een drempelwaarde bereikt, gaan deze responsen over in het activeren van specifieke celdood programma’s. Stress, celdood, of een infectie kan de lever residente macrofagen activeren. Geactiveerde macrofagen gaan een ontstekingsbevorderend cytokine, TNFα, uitscheiden. De levercel is dan dus blootgesteld aan zowel het medicijn als TNFα.

TNFα is een enigmatisch cytokine. Het kan zowel overleving van de cel bevorderen (via de activatie van transcriptie factor NF-κB) als celdood induceren (via de activatie van caspase 8 of RIPK3). In een gezonde levercel induceert stimulatie met TNFα geen celdood. Echter, als de levercel gestresst is door medicijngebruik kan de balans omslaan en kan TNFα stimulatie leiden tot synergistisch meer celdood.

In dit proefschrift bestuderen we specifieke stress responsen die ontstaan na medicijngebruik, en hoe deze interacteren met TNFα signalering. Voor dit onderzoek gebruiken we een HepG2 levercellijn, die we behandelen met medicijnen en TNFα. In **hoofdstuk 2** vatten we samen wat er op dit moment bekend is over TNFα in iDILI. Als voorbeeldmedicijn gebruiken we diclofenac, waarvan wij en anderen al eerder hebben laten zien dat leverceldood synergistisch verhoogd wordt als levercellen gestimuleerd worden door diclofenac in combinatie met TNFα. We bespreken de mogelijkheden om

inflammatoire stress (zoals TNFα) te gebruiken als test in de ontwikkeling van nieuwe medicijnen.

Zoals eerder gezegd, TNFα induceert NF-κB transcriptie factor activatie en dat leidt tot celgroei en het voortbestaan van de levercel. In **hoofdstuk 3** hebben we de regulering van NF-κB activatie na TNFα stimulatie onderzocht. Hiervoor hebben we aan een onderdeel van NF-κB (RelA) een fluorescent label geplakt, dat we kunnen volgen in levende cellen met confocale microscopie. TNFα stimulatie induceert translocatie van NF-κB vanuit het cytoplasma naar de celkern, waar NF-κB pas actief kan zijn. In de celkern activeert NF-κB de expressie van specifieke genen, waaronder genen die NF-κB uit de kern halen (bijvoorbeeld IκBα) en genen die activatie van het receptor complex negatief beinvloeden (bijvoorbeeld A20). Hierdoor ontstaat een typisch kern/cytoplasma oscillatie patroon. De kwantificatie van dit patroon laat zien dat NF-κB translocatie vertraagd is als levercellen behandeld zijn met diclofenac. Om te bepalen welke eiwitten betrokken zijn in de totstandkoming van het oscillatie patroon en dus NF-κB activatie, hebben we een siRNA screen uitgevoerd. Behandeling met siRNA vermindert de expressie van een specifiek eiwit. Van de 1567 geteste eiwitten bleken uiteindelijk 46 betrokken te zijn bij de regulatie van door TNFα gestimuleerde NF-κB oscillatie. Verlaagde expressie van sommige genen vertraagde NF-κB translocatie, net zoals diclofenac, maar beschermden in het algemeen tegen de synergistische celdood door TNFα en diclofenac of carbamazepine. De verlaagde expressie van een aantal van deze genen had ook een groot effect op de expressie van A20. Een van de sterkste effecten had de RNA polymerase II kinase CDK12. Wij laten hier voor het eerst zien dat CDK12 betrokken is bij de regulering van NF-κB translocatie, A20 expressie en celdood inductie door TNFα stimulatie.

In **hoofdstuk 4** hebben we meerdere, door het MIP-DILI consortium geselecteerde medicijnen getest op hun effect op TNFα signalering in HepG2 cellen. TNFα signalering in HepG2 cellen lijkt veel op de meest gebruikte, niet-immuun cellen voor TNFα onderzoek: muis embryonale fibroblasten (MEFs). We hebben hier aangetoond dat TNFα de expressie van groepen genen induceert die een verschillende kinetiek vertonen: vroege expressie, gemiddelde expressie en late expressie. Dit wordt in HepG2s, net zoals in MEFs, onder andere gereguleerd door splicing; het splitsen van boodschapper RNA moleculen vlak na de transcriptie vanuit het DNA. We zien hier ook dat de functies van de door TNFα geinduceerde genexpressie verschilt in de expressiegroepen. De vroege genexpressie groep bevat meer pro-inflammatoire genen, terwijl de late genexpressie groep nauwelijks pro-inflammatoire genen bevat en bijvoorbeeld meer genen die bekend staan om hun rol in herstel. Blootstelling aan medicijnen verhoogde de TNFα geinduceerde expressie van target genen. Dit was niet direct gecorreleerd aan de mate van synergistische celdood. Wel was het gedeeltelijk gecorreleerd aan de mate van disruptie van NF-κB nucleare translocatie patronen, en dus NF-κB activatie. In een andere interessante observatie bleek dat blootstelling aan medicijnen zonder TNFα al NF-κB (RelA) geinduceerde gen expressie te activeren, waaronder chemokines CCL5 en IL8. Verschillende andere NF-κB transcriptie factor familieleden (RelB, cREL) reguleerden deze expressie. Dit was gedeeltelijk gecorreleerd met de medicijn-geinduceerde activatie van

adaptieve oxidatieve stress responsen. Hiermee tonen we aan dat medicijnen intrinsiek TNFα genexpressie kunnen induceren, onder andere bekende immunomodulatoren in de lever zoals CCL5 (neutrofiel recruterende signaalstof) en IL8 (macrofaag recruterende signaalstof). We laten ook zien dat dit gereguleerd wordt door meerdere eiwitten uit de NF-κB familie en de medicijn geinduceerde oxidatieve stress respons.

In **hoofdstuk 5** hebben we ons geconcentreerd op specifieke compenenten van de TNFα signaleringscascade die bijdragen aan de synergistisch verhoogde medicijn/TNFα celdood. We hebben een kleine siRNA screen gedaan met 184 bekende TNFα signaleringseiweitten. Verlaagde expressie van uiteindelijk 24 genen reguleerde de verhoogde celdood met het anti-epileptische medicijn carbamazepine en TNFα. Een screen met 124 medicijnen in 6 concentraties identificeerde nog 3 andere medicijnen (colchicine, griseofulvine en valproine zuur) die ook in synergie met TNFα celdood veroorzaakten. De 24 genen die carbamazepine/TNFα synergie reguleerden hebben we getest met de andere medicijnen en TNFα. Verlaging van de expressie van de 24 genen en medicijn/TNFα blootstelling liet een wisselend beeld zien. Dit betekent dat er genen zijn die in het algemeen medicijn/TNFαsynergisme reguleren, maar ook dat sommige genen specifieke functies hebben in synergie met een specifiek medicijn. Dit zou kunnen samenhangen met de medicijn-specifieke adaptieve stress responsen die geinduceerd worden. In ons lab gebruiken we een platform van fluorescente cellijnen, waarmee we de activatie van verschillende adaptieve stress responsen kunnen meten met confocale microscopie. De synergistische medicijnen in deze studie activeerden allemaal een aantal van deze stress responsen, en deze activatie was medicijn-specifiek. De activatie van specifieke stress responsen correleerde in veel gevallen met het effect van verminderde genexpressie op TNFα/medicijn synergistische celdood. Dit betekent dat deze genen waarschijnlijk een rol spelen, of beinvloed worden door deze adaptieve stress responsen. Meer inzicht in het functioneren van deze genen zou kunnen leiden tot patientspecifieke behandeling.

Behalve mechanistisch onderzoek hebben we in **hoofdstuk 6** ook de fluorescente cellijnen van verschillende stress responsen gebruikt in een nieuw testsysteem, om te voorspellen welke medicijnen DILI veroorzaken in patienten. De oxidatieve stress respons (SRXN1), endoplasmic reticulum stress respons (CHOP), DNA schade respons (p21) werden blootgesteld aan een set van 118 medicijnen. Om inflammatoire stress te kunnen meten hebben we NF-κB target gen ICAM1 blootgesteld aan zowel de medicijnen als TNFα. Alle responsen zijn gekwantificeerd over tijd en samengebracht in verschillende statistische modellen. We laten zien dat de medicijnen verschillende combinaties van stress responsen activeren. Verder tonen we aan dat de medicijnen die ernstige DILI veroorzaken, in tegenstelling tot diegenen die minder ernstige DILI veroorzaken, bij een lagere absolute concentratie van het medicijn al stress responsen activeren. Uiteindelijk hebben we een automatische selectie van de belangrijkste karakteristieken van over tijd gemeten activatie curves gemaakt. Met deze selectie hebben we machine learning gedaan en konden we voorspellen welke compounds DILI in mensen veroorzaken. Dit konden we met een sensitiviteit en specificiteit van respectievelijk 0,6 en 0,75. In de toekomst kunnen we dit

model gebruiken om zowel mechanistische als voorspellende informatie te verkrijgen over de medicijnen voordat ze in mensen of dieren getest worden.

In **hoofdstuk 7** vat ik de resultaten uit dit proefschrift samen en hoe deze samenhangen met de huidige literatuur. Inflammatoire stress is inmiddels erkend als een belangrijke patientgebonden factor in het onstaan van iDILI. In deze studies laten we zien dat de interacties tussen medicijn geinduceerde responsen en inflammatoire stimuli als TNFα kunnen leiden tot afwijkende genexpressie en synergistische celdood. We hebben verschillende nieuwe eiwitten geidentificeerd (CDK12, PHF5A, CARD12) die een belangrijke rol spelen in medicijn/TNFα geinduceerde signalering en synergistische celdood. We laten ook zien dat blootstelling aan medicijnen zelf bijdraagt aan inflammatoire signalering vanuit levercellen. Dit gebeurt via activatie van de NF-κB familie en daaropvolgende expressie van bekende proinflammatoire signaalstoffen zoals CCL5 en IL8.

De identificatie van patienten met polymorfismen in de in dit proefschrift beschreven genen zou kunnen bedragen aan het uitsluiten van een kleine patientpopulatie waardoor een effectief medicijn weer veilig is voor een grote populatie. Naast een bijdrage aan inzicht in door medicijn en TNFα geinduceerde signaleringscascades in HepG2 cellen, hebben we deze kennis ook toegepast. We hebben een platform opgezet van cellijnen die cellulaire stress responsen detecteren en waarmee nieuwe medicijnen getest kunnen worden in een vroeg stadium van medicijnontwikkeling. In dit proefschrift hebben we dus bijgedragen aan zowel mechanistische kennis van TNFα signalering in levercellen als aan de opbouw van een nieuw fluorescent reporter testsysteem.

List of publications

Drug-Induced Liver Injury and TNFα Signaling: From In Vivo Understanding to In Vitro Testing Approaches
***Huppelschoten, S**. and Water, van de B.*
Applied in Vitro Toxicology, 2016, doi: 10.1089/aivt.2016.0017

High content live cell imaging of the dynamics of multiple adaptive stress response pathways enables assessment of drug-induced liver injury (DILI) liabilities
*Steven Wink[1], Steven Hiemstra[1], **Suzanna Huppelschoten[1],** Janna Klip, Bob van de Water*
[1] **Authors contributed equally**
Manuscript in preparation

Phenotypic screen of TNFα-mediated NF-κB nuclear translocation dynamics reveals CDK12 as suppressor of anti-apoptotic signaling and A20 expression
*Bram Herpers[1], Lisa Fredriksson[1], **Suzanna Huppelschoten[1]**, Giulia Benedetti, Zi Di, Matthijs Vlasveld, Janna Klip, Sylvia Lé Dévedec, Hans de Bont, John Meerman, Marjo de Graauw and Bob van de Water*
[1] **Authors contributed equally**
Manuscript in preparation

Drugs with liver toxicity liability enhance both TNFα-induced and intrinsically drug-induced inflammatory target gene expression
***Suzanna Huppelschoten**, Steven Wink, Wanda van der Stel, Anke Essing, Cécile Parmentier, Lysiane Richert, Bob van de Water*
Manuscript in preparation

Identification of TNF receptor signaling pathway components that regulate hepatotoxic drug/TNFα-induced synergistic apoptosis
***Suzanna Huppelschoten**, Matthijs Vlasveld, Steven Wink, Steven Hiemstra, Janna Klip, Wouter den Hollander, Casper Roosenstein, Lisa Fredriksson, Bob van de Water*
Manuscript in preparation

Model-based identification of TNFα-induced IKKβ- and IκBα-mediated regulation of NFκB signal transduction as a tool to quantify the impact of Drug-Induced Liver Injury compounds
*Angela Oppelt[1], Daniel Kaschek[1], **Suzanna Huppelschoten**, Rowena Sison-Young, Fang Zhang, Marie Buck-Wiese, Franziska Herrmann, Sebastian Malkusch, Carmen L. Krüger, Mara Meub[5], Benjamin Merkt, Lea Zimmermann, Mike Heilemann, Bob van de Water, Christopher E. Goldring, Jens Timmer, Ursula Klingmüller*
[1] Authors contributed equally
Submitted to Nature Systems Biology and Applications (August 2017)

Trovafloxacin induces aberrant early NF-κB inhibitor synthesis leading to disruption of TNF-mediated p65 translocation *in vivo* and *in vitro*
*G.Giustarini, **S.Huppelschoten,** A. Oppelt, L. Kruijssen, B. van de Water, U. Klingmuller, R.Pieters*
Manuscript in preparation

Quantitative High Content Imaging of Cellular Adaptive Stress Response Pathways in Toxicity for Chemical Safety Assessment
*Wink Steven, Hiemstra Steven, **Huppelschoten Suzanna,** Danen Erik, Niemeijer Marije, Hendriks Giel, Vrieling Harry, Herpers Bram, Water Bob van de*
Chemical Research in Toxicology, 2014. doi: 10.1021/tx4004038

Vaccine-induced tumor necrosis factor-producing T cells synergize with cisplating to promote tumor cell death
*Tetje C. van der Sluijs, Suzanne van Duikeren, **Suzanna Huppelschoten,** Ekaterina S. Jordanova, Elham Beyranvand Nejad, Arjen Sloots, Louis Boon, Vincent THBM Smit, Marij JP Welters, Ferry Ossendorp, Bob van de Water, Ramon Arens, Sjoerd H. van der Burg, Cornelis J.M. Melief*
Clinical Cancer Research, 2015, doi: 10.1158/1078-0432.CCR-14-2142

FOXP3 can modulate TAL1 transcriptional activity through interaction with LMO2
*Fleskens, V., Mokry, M., van der Leun, A.M., **Huppelschoten, S.**, Pals, C., Peeters, J., Coenen, S., Cardoso, B.A., Barata, J.T., van Loosdregt, J., Coffer, P.J.*
Oncogene, 2016, doi: 10.1038/onc.2015.481

About the author

Suzanna Huppelschoten was born in Zeist, the Netherlands, on the 8th of December 1987. At the Christelijk Lyceum Zeist she obtained her VWO diploma with a major in Natuur en Gezondheid (Nature and Health), with as extra subject Latin. Her final thesis was on Basal cell carcinoma. She completed her bachelor and master studies Biomedical Science at the Utrecht University. During her master program *Immunity and Infection* she studied Foxp3 regulation in regulatory T cells in the lab of Paul Coffer in Utrecht. The results of this study were used in a publication in Oncogene. Her second internship was in the group lead by Vasilis Koronakis in Cambridge. There she studied the role of SET and pp32 in Salmonella infection. In her literature thesis she summarised the recent knowledge on latency of HIV in resting T cells, under supervision of Theo Geijtenbeek. Upon acquiring her masters degree, she started with her PhD project *Systems biology of cytokine signaling in drug-induced liver injury* at the Leiden Academic Centre for Drug Research, University of Leiden, under supervision of Bob van de Water. Upon completing her PhD project she started traveling. Currently, she is sailing on European waters.